

Electrical and Control Aspects of Offshore Wind Farms II (Erao II)

Volume 1: Dynamic models of wind farms

J.T.G. Pierik (ECN) S.W.H. de Haan (TUD)

J. Morren (TUD) E.J T.G. van Engelen (ECN)

E.J. Wiggelinkhuizen (ECN)
CN) J. Bozelie (Neg-Micon)

June 2004

Distribution

Novem:		VTT:	
J. 't Hooft	1 - 5	B. Lemstrom	28
TUD:		NREL:	
J. Morren	6	Y-H. Wan	29
S.W.H. de Haan	7 – 11	E. Muljadi	30
P. Bauer	12		
		Ineti:	
TenneT:		A. Lopez Estanquero	31
W. Kling	13	The Eopez Estanquero	51
J. Bozelie	14	University College	
		Dublin:	
Kema:		A. Mullane	32
R. de Groot	15	M. O'Malley	33
P. Vaessen	16	Wi. O Waney	33
1. Vaessen	10	UMIST:	
Essent:		N. Jenkins	2.4
H. Slootweg	17		34
C. Houben	18	O. Anaya-Lara	35
C. Houben	10	Undra Ouchaa	
Continuon:		Hydro Quebec:	26
	19	R. Gagnon	36
M. Bongaerts	19	ECN	
Margan		ECN:	
Nuon:	20	A.B.M. Hoff	37
M. van Riet	20	C.A.M. van der Klein	38
37 361		W.C. Sinke	39
Neg-Micon:		G.J.H. van Nes	40
A. Winnemuller	21	G. Peppink	41
		H.J.M. Beurskens	42
ICE:		L.W.M.M. Rademakers	43
J.C. Montero	22	H. Snel	44
R. Jimenez	23	B.H. Hendriks	45
		G.P. Corten	46
Sintef:		E.J. Wiggelinkhuizen	47
J.O. Tande	24	B.H. Bulder	48
		P. Schaak	49
Chalmers:		P. Heskes	50
O. Carlson	25	P. Lako	51
T. Thiringer	26	T.J. de Lange	52
	20	T.G. van Engelen	53
Risoe:		E.L. van der Hooft	54
P. Soerensen	27	J.T.G. Pierik	55
1. SUCICIISCII	21	ECN Wind Energy Archive	
		ECN Central Archive	70

ABSTRACT

To investigate dynamic interaction of wind farms and the electrical grid, dynamic models of wind farms are needed. These models are not available however. The objective of the Erao-2 project has been (1) to develop these models, (2) to demonstrate their use by evaluating wind farms with different types of electrical systems and (3) to design and demonstrate controllers that can cope with grid code requirements.

Four types of wind farm models have been developed based on different types of turbines:

- Constant Speed Stall turbine with directly coupled Induction Generator (CSS-IG);
- Constant Speed Stall turbine with Cluster Controlled induction generator operating in variable speed mode (CSS-CC);
- Variable Speed Pitch turbine with Doubly-Fed Induction Generator (VSP-DFIG);
- Variable Speed Pitch turbine with Permanent Magnet generator and full converter (VSP-PM).

For each type of wind farm, three cases have been evaluated:

- normal operation including flicker production;
- response to a grid frequency dip;
- · response to a grid voltage dip.

For the wind farms which are able to support grid voltage or grid frequency, controllers for these purposes have been developed and demonstrated.

Results and conclusions

The response of a wind farm to a grid frequency dip strongly depends on the presence of a converter. A full converter, in the CSS-CC and VSP-PM wind farms, decouples the turbines from the disturbance. But also the system with a partial converter (VSP-DFIG) is hardly affected by the frequency dip. The constant speed wind farm (CSS-IG) on the other hand has serious problems with a frequency dip and the corresponding voltage dip.

The constant speed wind farm can stay connected during the voltage dips that have been applied. The high amount of reactive power that is required by this wind farm during a voltage disturbances can be problematic. The Cluster Controlled wind farm (CSS-CC) can handle voltage dips if a resistor is placed in parallel to the dc-link capacitor and the surplus of energy during the voltage dip is dissipated. Wind farms using doubly-fed induction machines (VSP-DFIG) are the most problematic concept when voltage dips are considered. A solution is to provide a controlled by-pass for the high currents in the rotor. In the variable speed pitch wind farm with permanent magnet generators (VSP-PM) good voltage dip ride-through is achieved.

The constant speed stall controlled wind farm (CSS-IG) can not assist in grid frequency control. The cluster controlled wind farm in the Erao-2 study is based on a stall controlled turbine (CSS-CC). Therefore it can not assist in grid frequency support either. Both variable speed pitch wind farms (VSP-DFIG and VSP-PM) can support grid frequency, which has been demonstrated by simulations.

Only systems with converters are suitable for grid voltage control. The simulations demonstrate the feasibility of voltage control for wind farms with doubly-fed induction generators. There is no large difference between voltage control by wind farms with doubly-fed induction generators and voltage control by the other wind farms with IGBT converters: CSS-CC and VSP-PM.

Recommendation

With the completion of the wind farm models based on individual turbines, verification of models should now have a high priority.

Keywords: wind farm models, wind farm dynamics, electrical systems, fault ride through, grid support

Acknowledgement

Erao-2 is a continuation of the Erao-1 project, in which a steady state (load flow) and economic model for offshore wind farms has been developed [18]. The Erao projects have been supported by the Dutch Agency for Energy and Environment (NOVEM) in the "Programma Duurzame Energie" of the Netherlands, executed by Novem by order of the Ministry of Economic Affairs.

Novem project number: 2020-01-13-10-001

ECN project number: 7.4336

EXECUTIVE SUMMARY

In The Netherlands offshore wind power is on the brink of implementation. Plans exist for two offshore wind farms of about 100 MW, located 12 and 25 km from the coast of the province of North Holland. In 2003 an investigation has been started to quantify the effect of 6000 MW offshore wind power on the high voltage grid. Only the steady state behaviour has been considered, resulting in suggestions for grid reinforcement. This investigation needs to be complemented by a study on the dynamic interaction of wind power and the electrical grid.

Objective of Erao-2

To investigate dynamic interaction of wind farms and the electrical grid, dynamic models of wind farms are needed. These models will be of great help in the evaluation of the behaviour of wind power during normal grid operation as well as during grid faults and in the design of controllers that enable wind farms to support the grid. Dynamic models of wind farms, including the relevant electrical components and sections of the grid, are not available however. The objective of the Erao-2 project is (1) to develop these models, (2) to demonstrate their use by evaluating wind farms with different types of electrical systems and (3) to design and demonstrate controllers that can cope with grid code requirements.

Part 1: Model development

The wind farm models are based on models of electrical components and controllers developed in this project and already existing models of wind, rotor, tower, mechanical drive train and pitch controller. The modelled electrical components and controllers are:

- induction generator
- · doubly-fed induction generator
- permanent magnet generator
- IGBT converter and converter controller
- transformer
- cable
- synchronous generator
- consumer load
- wind farm controller for grid frequency support
- converter controller for grid voltage support

A simple grid model and a model of the flicker meter has also been developed.

An important aspect of dynamic models of electrical systems is computational speed. Electrical transients have very small time constants, resulting in small time steps and long computation time. In Erao-2 special attention has been paid to computational speed. An important increase in speed can be realised by the use of the dq0-transformation, which has been applied to all models of electrical components in the Erao-2 component library.

Volume 1 of this report gives a mathematical derivation of the electrical component models, followed by the implementation of the models in Simulink, a computer program suitable for dynamic simulation. Turbines are modelled by connecting the electrical component models to

ECN-C- -04-050 5

the models of the rotor, tower, mechanical drive train and pitch controller. In the second step, individual turbine models are connected by cable models to produce the wind farm model.

Results and conclusions from model development

Dynamic models of wind farms based on individual turbine models are large and complicated. The number of state variables is high and some of the time constants are small, leading to a relatively long simulation time. The level of detail is high however, which makes these models suitable for the evaluation of wind farm dynamics and wind farm-grid interaction as well as for the design of controllers.

The application of the dq0-transformation significantly reduces the simulation time during normal operation of the wind farm, when transients from electrical switching operation have died out.

Part 2: Model demonstration

The second part of the Erao-2 project demonstrates the use of the developed wind farm models. In a number of case studies, four types of wind farms have been compared. The wind farm types use different turbines and different control methods, viz.:

- Constant Speed Stall turbine with directly coupled Induction Generator (CSS-IG, reference case);
- Constant Speed Stall turbine with Cluster Controlled induction generator operating in variable speed mode (CSS-CC);
- Variable Speed Pitch turbine with Doubly Fed Induction Generator (VSP-DFIG);
- Variable Speed Pitch turbine with Permanent Magnet generator and full converter (VSP-PM).

The layout of a proposed offshore wind farm, the Near Shore Wind farm (NSW), has been taken as reference. The Near Shore Wind Farm is planned in the North Sea near the town of Egmond in The Netherlands. One string of 12 turbines has been modelled with each of the four types of turbines. A simplified grid model has been included to enable simulation of wind farm-grid interaction.

For each type of wind farm, three cases have been evaluated:

- normal operation including flicker production;
- response to a grid frequency dip;
- response to a grid voltage dip.

For the wind farms which are able to support grid voltage or grid frequency, a converter controller or a wind farm controller suitable for this purpose has been developed and demonstrated. Volume 2 of this report describes the case study results.

Results and conclusions from case studies

Normal operation of the wind farms has been simulated by the response to a wind gust. The simulations demonstrated proper operation of the generator and converter models, the converter controllers and proper overall behaviour of the wind farm.

A limited flicker evaluation has been executed. Instantaneous flicker values have been determined over the complete range of operating conditions for the four types of wind farms. Flicker

values of a single turbine have been compared to the values of a string of twelve turbines under the same operating conditions and fictitious grid parameters. The constant speed stall wind farm generates the highest flicker, the flicker production of the wind farms with partial and full converter is lower.

Wind farm response to grid frequency and grid voltage dips

The response of a wind farm to a grid frequency dip (5 Hz, 10 sec) strongly depends on the presence of a converter. A full converter, in the case of the CSS-CC and VSP-PM wind farms decouples the turbines from the disturbance. But also the system with a partial converter (VSP-DFIG) is hardly affected by the frequency dip due to the effective adjustment of the rotor currents by the rotor converter. The constant speed system on the other hand has serious problems with a frequency dip and the corresponding voltage dip: depending on the depth and the conditions at the start of the dip, current, power and reactive power peaks may exceed rated values and may lead to a wind farm shut down.

The farm with constant speed stall turbines and directly connected induction generators (CSS-IG) can stay connected during the voltage dips that have been applied (30%-10 sec, 50%-0.5 sec and 85%-0.2 sec). High currents are flowing during the voltage drop. Due to the high thermal capacity of the induction machine these currents will be no problem. The currents may trigger protective devices in the grid. The high amount of reactive power that is required by the wind farm during a voltage disturbances can be more problematic. When the dip lasts too long this may lead to voltage collapse.

The Cluster Controlled wind farm (CSS-CC) can handle voltage dips if a resistor is placed in parallel to the dc-link capacitor and the surplus of energy during the voltage dip is dissipated.

Wind farms using doubly-fed induction machines (VSP-DFIG) are the most problematic concept when voltage dips are considered. Large currents will flow in the rotor circuits and in the converters. Due to the limited thermal capacity of the power electronic devices in the converters, these currents may destroy the converters. A possible solution is to limit the high currents in the rotor by providing a by-pass over a set of resistors connected to the rotor windings. With these resistors it is possible to survive grid faults without disconnecting the turbine from the grid. One of the case studies demonstrates this solution. Manufacturers of DFIG systems are working on this solution and are making progress in meeting the voltage ride-through requirement.

In the variable speed pitch wind farm with permanent magnet generators (VSP-PM), all the essential parameters can be controlled. Therefore good voltage dip ride-through can be achieved. The power supplied by the generator is reduced by the controllers during the dip. This is required because otherwise the current in the converters or the dc-link voltage becomes too high. To avoid overspeeding the pitch controller is activated.

Wind farms assisting grid frequency or grid voltage

The constant speed stall controlled wind farm (CSS-IG) can not assist in grid frequency control. The cluster controlled wind farm in the Erao-2 study is based on a stall controlled turbine (CSS-CC). It can not control aerodynamic power directly and therefore it can not assist in grid frequency support either.

Both variable speed pitch wind farms (VSP-DFIG and VSP-PM) can be controlled to support grid frequency, which has been demonstrated by simulations. The controller consists of two parts: delta-control to realise a power margin and frequency feed-back to act on a frequency deviation. Since frequency control capability for wind farms implies maintaining a power margin, this feature may not be cost-efficient.

Only systems with converters are suitable for grid voltage control. Different voltage and reac-

tive power control strategies have been investigated for the VSP-DFIG wind farm. It has been shown that it is possible to control the power factor and that the wind farm can follow reactive power setpoints. Two voltage control options have been investigated. In the first option each turbine controls the voltage at its own terminal, in the second option the voltage at the grid connection point is controlled. Droop control has been implemented on each turbine. With this type of control, the wind farm behaviour during voltage deviations is similar to conventional power plant behaviour. The results depend on the X/R ratio of the grid: low X/R ratios require large amounts of reactive power to control the voltage and the wind farm converters are limited in current and thus in reactive power. Nonetheless, the simulations demonstrate the feasibility of voltage control for wind farms with doubly-fed induction generators.

There is no large difference between voltage control by wind farms with doubly-fed induction generators and voltage control by the other wind farms with IGBT converters: CSS-CC and VSP-PM. This has been demonstrated by simulations with a cluster of CSS-CC turbines and a string of VSP-PM turbines. The results are similar to those of the VSP-DFIG wind farm.

Economic evaluation

The load flow program and the database with electrical and economic parameters developed in the Erao-1 project has been used in an economic evaluation of the four wind farm electrical systems. For a wind regime representative of the North Sea, the power production including the electrical losses, has been determined for the layout of the Near Shore Wind farm. This results in the contribution of the electrical system to the Levelised Production Costs (LPC). The VSP-DFIG farm performs best: 1.42 Eurocent/kWh. The CSS-IG farm is of the same magnitude: 1.62 Eurocent/kWh, while the other two farms have relatively expensive electrical systems: 2.60 Eurocent/kWh (VSP-PM) and 4.57 Eurocent/kWh (CSS-CC). The high price for the Cluster Controlled system is caused by the expensive converters.

Recommendations

With the completion of the wind farm models based on individual turbines, verification of models should now have a high priority. The Erao-3 project has been started with model validation as one of the objectives.

For the incorporation of dynamic models of wind farms in models of national grids, the complexity of the wind farm models has to be reduced. Aggregated wind farm models, in which all turbines are represented by a single equivalent model are more suitable for this purpose. However, aggregated models loose the wide range of applicability of the wind farm models based on individual turbine models. It is recommended to develop aggregated wind farm models, tailored to application in power system models. The wind farm models developed in Erao-2 can serve as reference in the development of these aggregated models.

Systems with DC cables to shore have not been included in the Erao-2 case studies. The Erao-2 component library includes all models necessary to investigate DC connections, with the exception of the thyristor converter. This converter however, is a less likely option for the connection of offshore wind farms than the IGBT converter, due to its limited controllability and large footprint. DC connections are currently more expensive than AC, but may offer a number of advantages. It is recommended to include these systems in a future study and for comparison purpose also develop a thyristor converter model.

Symbols		Subscripts	
C	capacitance	a	aerodynamic, phase a
E	electromagnetic force	abc	abc reference frame
f	frequency	b	phase b
G	transfer function	c	phase c
i	current	conv	converter
I	unit matrix	d	d-axis
J	inertia	dc	dc-link
K	constant, transfer function	dq0	dq0 reference frame
L	inductance	e	electrical
N	number of turns	f	field, filter
p	number of pole pairs	g	grid, ground
P	(active) power, instantaneous or average	i	integral
Q	reactive power, instantaneous or average	m	mechanical, mutual
R	resistance	p	proportional
S	Laplace operator	q	q-axis
S	saturation function	r	rotor
T	torque	S	stator
T	transformation matrix	0	zero-sequence component
u	voltage		
V	voltage		
V	Velocity		
W	energy		
X	arbitrary signal		
Z	impedance		
α	bandwidth of control loop		
θ	angle		
au	time constant		
ω	angular velocity		
ψ	flux		

.

CONTENTS

1	Introduction		13	
2	Mat	hematio	cal models of electrical components	16
	2.1	Model	ling in a dq0-reference frame	16
		2.1.1	Introduction	16
		2.1.2	Park Transformation	16
		2.1.3	Modelling of basic components	18
	2.2	Model	s of wind turbine generators	23
		2.2.1	Introduction	23
		2.2.2	Doubly-Fed Induction Machine	24
		2.2.3	Induction machine	29
		2.2.4	Permanent Magnet Synchronous Machine	29
		2.2.5	Converter	31
	2.3	Other	electrical components	40
		2.3.1	Transmission line and cable	40
		2.3.2	Transformer	42
		2.3.3	Grid model	44
	2.4	Zero-s	equence components	46
		2.4.1	Introduction	46
		2.4.2	Zero-sequence components	46
		2.4.3	Star and delta connections	46
		2.4.4	Three-phase transformers	48
		2.4.5	NSW-park ERAO-II	49
3	Mod	lels of w	vind and wind turbine	50
	3.1	Wind 1	model	50
		3.1.1	Longitudinal turbulence model, tower passage and wind shear	50
	3.2	Turbin	e models	52
		3.2.1	Aerodynamic conversion, rotation and torsion	53
		3.2.2	Tower mechanical model	53
		3.2.3	Pitch control and electrical torque setpoint	54
4	Dyn	amic m	odels of wind farms in Simulink	58
	4.1	Consta	ant speed stall controlled wind farm	58
	4.2	Consta	ant speed stall controlled WF with cluster controlled induction machines .	68
	4.3	Variab	le speed pitch controlled WF with doubly fed induction machines	75
	4.4	Variab	le speed pitch controlled WF with permanent magnet machines	86
	4.5	Grid m	nodel	95

Erao II, Volume 1: Dynamic models for wind farms

5 Flicker meter			99	
	5.1	Introduction	99	
	5.2	Flicker meter	02	
	5.3	Implementation in Simulink	03	
	5.4	Testing the flicker meter in Simulink	06	
		5.4.1 Response to calibration input signal	06	
		5.4.2 Response to modulated grid voltage and load step	07	
	5.5	Conclusion	10	
6	Con	clusions and remarks 1	111	
	6.1	Conclusions	11	
	6.2	Remarks	11	
A	Sum	mary of Erao I project	115	
В	Con	tributions to International Conferences 1	116	
	B.1	Nordic Wind Power Conference 2004	16	
	B.2	4th International Workshop on Large Scale Integration of Wind Power and Transmission Networks for Offshore Wind Farms	116	
	B.3	EPE 2003 Toulouse	16	

1 INTRODUCTION

Problem description

Offshore wind farms have to be large to be economical and with the increase of the contribution of wind energy to the electric power production, the interaction between the wind farms and the grid will be an important aspect in the design and planning of wind farms farms [7]. It is essential to ensure that the grid is capable of staying within the operational limits of frequency and voltage for all foreseen combinations of wind power production and consumer loads [19]. A second aspect is to ensure appropriate transient and small signal stability of the grid [22]. Adequate grid control plays an important role but the electrical control and protection of large wind farms is also an important issue.

Large wind farms are a source of fluctuating power and sometimes of reactive power as well. The response of wind farms to voltage and frequency dips is a cause for worry: the farm may shut down instantaneously. The dip itself is a sign of a serious grid control problem, and the problem may become worse if wind power shuts down on a large scale. For conventional power stations the requested behaviour during a grid dip is to stay in operation and supply (reactive) power. This behaviour is prescribed in grid codes. It is likely that large offshore wind farms also have to comply with these rules. In Germany, grid operator E.On Netz already requires specific behaviour of wind farms during dips [12]. Depending on the type of wind turbine, viz. constant or variable speed, and the design of the turbine and wind farm control, a wind farm will have more or less problems to comply with these rules.

Objective of Erao II

In order to investigate the dynamic interaction of wind farms and the electrical grid, dynamic models of wind farms are needed. Dynamic models of wind turbines and wind farms will be of great help in the design and evaluation of the behaviour of wind power during normal grid operation as well as during grid faults. Dynamic models of wind farms, including the relevant electrical components and sections of the grid, are not readily available however. The Erao-2 project has been started with the objective to develop these models and to demonstrate their use by designing controllers to cope with grid code requirements and evaluate different types of electrical systems in wind farms.

Method

An important aspect of dynamic models of wind farms is computational speed. Electrical transients have very small time constants, resulting in small time steps and long computation time. In Erao-2 special attention has been paid to computational speed. An important increase in speed can be realised by the use of the dq0-transformation (also known as Park transformation). This transformation is mainly used in electrical machine theory, in Erao-2 it is applied to all electrical components.

The main characteristics of the simulation models for the electrical components are:

- all electrical components are modelled in dq0-coordinates;
- AC-DC-AC converters are modelled by controlled voltage sources;
- the component models are implemented in Simulink.

Results

The component models developed in the Erao-2 project are listed in table 1.

Table 1: Dynamic models of components of wind farms developed in the Erao-2 project

Mechanical and aerodynamic (turbine):	turbine rotor ¹
•	mechanical drive train ¹
	tower ¹
	rotor effective wind ¹
Electrical (turbine & wind farm):	induction generator
	doubly-fed induction generator
	permanent magnet generator
	voltage source converter
	transformer
	cable
Electrical (grid):	synchronous generator
	frequency and voltage controller
	consumer load
	transformer
	cable
Control (turbine & wind farm):	converter controller
	wind turbine pitch controller ¹
	overall wind farm controller

¹ input from ECN control tool [25]

Volume 1 of this report gives a description of the models. In chapter 2 a description of the Park transformation is given, followed by a derivation of models of different electrical components in the dq0-reference frame. Models of the electrical generators are derived, together with the power electronic converter models. The chapter concludes with a description of models of the other electrical components that are needed and a discussion of the zero-sequence components in the models. Chapter 3 gives a description of the models that has been used for the wind, the turbines, aerodynamic conversion, pitch control, etc. In chapter 4 the Simulink implementation of the four types of wind farms is described. Chapter 5 gives the flicker meter that has been used. The final chapter lists conclusions and remarks and contributions to international conferences can be found in appendices.

Volume 2 of the Erao-2 report the focus is on the use of the four types of wind farm models in a number of case studies. It demonstrates how the models can be used to calculate the flicker contribution of a wind farm, simulate a response to a grid faults and develop wind farm control to support the grid.

Validation

The electrical component models have only been validated partially, viz. by comparing abcmodels with switching converters to dq0-models with controlled voltage source converters
[10], [11]. For extensive testing and validation the Erao-3 project has been started, which
takes part in the IEA Annex XXI (Dynamic models of Wind Farms for Power System Studies).
This Annex is a joint effort of nine countries to set up a database of wind farm measurements
and to use these measurements for validation of dynamic models. The participating countries
are Norway (Coordinator), Sweden, Finland, Denmark, USA, UK, Portugal, Ireland and the
Netherlands. Observing countries are Canada and Ireland.

Future work

In the context of the implementation of large amounts of offshore wind power in the Netherlands [6], a consortium of parties involved in offshore wind power has been formed under the name We@Sea. This group comprises wind farm developers, electricity companies, grid operators, research institutes and universities. We@Sea has defined a number of research activities aiming to resolve the remaining bottlenecks for large scale offshore wind in the Netherlands. One of the activities will be wind farm control, optimalization and the interaction between large offshore wind farms and the grid. ECN and TUD will make the dynamic wind farm models developed in the Erao-2 project available for this project and execute the research together with some of the We@Sea partners.

2 MATHEMATICAL MODELS OF ELECTRICAL COMPONENTS

2.1 Modelling in a dq0-reference frame

2.1.1 Introduction

The models of all electrical components are derived in the dq0-reference system. To obtain these models from the standard abc-models, the Park Transformation is used. The Park transformation (sometimes called Blondel-Park transformation) is well-known from its use in electrical machinery. The electrical signals are transformed to a stationary rotating reference frame. As this stationary frame is chosen to rotate with the grid frequency, all voltages and currents in the dq0-reference frame are constant in steady state situations. Therefore, modelling in the dq0-reference frame is expected to increase the simulation speed significantly, as a variable step-size simulation program can apply a large time step during quasi steady-state phenomena.

In the ERAO-2 project, dynamic models have been derived for: electrical generators (induction generator, doubly-fed induction generator, permanent magnet generator), power electronic converters, transformers, cables, turbine rotor, mechanical drive train and rotor effective wind. All models of electrical components are in the dq0-reference frame.

In this chapter first a description will be given of the way in which models of different electrical components in the dq0-reference frame can be obtained. The model derivation will be shown for two basic components: a three-phase RL line segment and a three-phase shunt capacitance. Next, the models of the electrical generators will be derived, together with the power electronic converter model. In this part also the control of the generators will be described. This is followed by a description of the other electrical component models needed for wind farm models. This chapter concludes with a discussion of the zero-sequence components in the models.

2.1.2 Park Transformation

In the study of power systems, mathematical transformations are often used to decouple variables, to facilitate the solution of difficult equations with time-varying coefficients, or to refer all variables to a common reference frame [13]. Probably the most well-known, is the method of symmetrical components, developed by Fortescue. This transformation is mostly used in its time-independent form and applied to phasors, when it is used in electrical power system studies [15]. Another commonly-used transformation is the Park transformation, which is well-known from the modelling of electrical machines. The Park transformation is instantaneous and can be applied to arbitrary three-phase time-dependent signals. The electrical signals are transformed to a stationary rotating reference frame. As this stationary frame is chosen to rotate with the grid frequency, all voltages and currents in the dq0-reference frame are constant in steady state situations. Therefore, modelling in dq0-domain is expected to increase the simulation speed significantly, as the variable step-size simulation program can apply a large time step during quasi steady state phenomena.

For $\theta_d = \omega_d t + \varphi$, with ω_d angular velocity, t the time and φ initial angle, the Park transformation is given by:

$$[\mathbf{x}_{da0}] = [\mathbf{T}_{da0} (\theta_d)] [\mathbf{x}_{abc}] \tag{1}$$

with:

$$\begin{bmatrix} \mathbf{x}_{dq0} \end{bmatrix} = \begin{bmatrix} x_d \\ x_q \\ x_0 \end{bmatrix}$$
 (2)

and

$$\begin{bmatrix} \mathbf{x}_{abc} \end{bmatrix} = \begin{bmatrix} x_a \\ x_b \\ x_c \end{bmatrix} \tag{3}$$

and with the dq0-transformation matrix \mathbf{T}_{dq0} defined as:

$$\left[\mathbf{T}_{dq0}\left(\theta_{d}\right)\right] = \sqrt{\frac{2}{3}} \begin{bmatrix} \cos\theta_{d} & \cos\left(\theta_{d} - \frac{2\pi}{3}\right) & \cos\left(\theta_{d} + \frac{2\pi}{3}\right) \\ -\sin\theta_{d} & -\sin\left(\theta_{d} - \frac{2\pi}{3}\right) & -\sin\left(\theta_{d} + \frac{2\pi}{3}\right) \\ \frac{1}{\sqrt{2}} & \frac{1}{\sqrt{2}} & \frac{1}{\sqrt{2}} \end{bmatrix}$$
(4)

and its inverse given by:

$$\left[\mathbf{T}_{dq0}\left(\theta_{d}\right)\right]^{-1} = \sqrt{\frac{2}{3}} \begin{bmatrix} \cos\theta_{d} & -\sin\theta_{d} & \frac{1}{\sqrt{2}} \\ \cos\left(\theta_{d} - \frac{2\pi}{3}\right) & -\sin\left(\theta_{d} - \frac{2\pi}{3}\right) & \frac{1}{\sqrt{2}} \\ \cos\left(\theta_{d} + \frac{2\pi}{3}\right) & -\sin\left(\theta_{d} + \frac{2\pi}{3}\right) & \frac{1}{\sqrt{2}} \end{bmatrix}$$
 (5)

The positive q-axis is defined as leading the positive d-axis by $\pi/2$, as can be seen from figure 1. Some additional properties of the Park transformation can be derived. As the transformation is orthogonal:

$$\left[\mathbf{T}_{dq0}\left(\theta_{d}\right)\right] \cdot \left[\mathbf{T}_{dq0}\left(\theta_{d}\right)\right]^{-1} = \left[\mathbf{T}_{dq0}\left(\theta_{d}\right)\right] \cdot \left[\mathbf{T}_{dq0}\left(\theta_{d}\right)\right]^{T} = \left[\mathbf{I}\right]$$
(6)

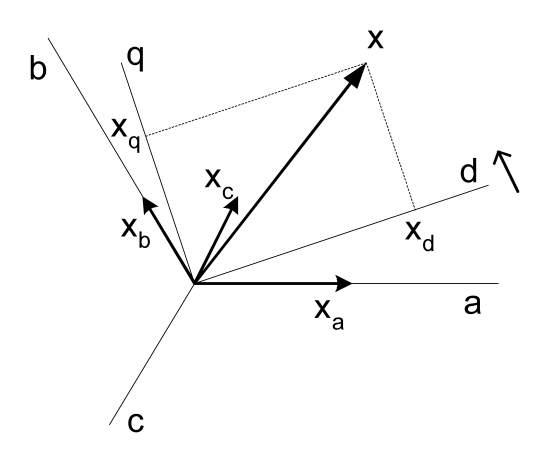


Figure 1: Relationship between abc and dq

With equation 6 it can be shown that the Park transformation conserves power and therefore is a valid transformation. The power conservation principle can then be shown as follows:

$$P(t) = [\mathbf{v}_{abc}]^{T} \cdot [\mathbf{i}_{abc}]$$

$$= \left[[\mathbf{T}_{dq0} (\theta_{d})]^{-1} [\mathbf{v}_{dq0}] \right]^{T} \cdot [\mathbf{T}_{dq0} (\theta_{d})]^{-1} [\mathbf{i}_{dq0}]$$

$$= [\mathbf{v}_{dq0}]^{T} [[\mathbf{T}_{dq0} (\theta_{d})]^{-1}]^{T} \cdot [\mathbf{T}_{dq0} (\theta_{d})]^{-1} [\mathbf{i}_{dq0}]$$

$$= [\mathbf{v}_{dq0}]^{T} [\mathbf{T}_{dq0} (\theta_{d})] \cdot [\mathbf{T}_{dq0} (\theta_{d})]^{-1} [\mathbf{i}_{dq0}]$$

$$= [\mathbf{v}_{dq0}]^{T} \cdot [\mathbf{i}_{dq0}]$$

$$(7)$$

The transformations of (4) and (5) are unitary, as is shown in (6) and conserves power as is shown in equation (7). Note that by replacing the factor $\sqrt{2/3}$ by a factor 2/3 in (4) and (5) the transformation will be amplitude-invariant, implying that the length of the current and voltage vectors in both abc- and dq0-reference frame are the same, however in that case the conservation of power is lost. This amplitude-invariant transformation is mostly used in modelling of electrical machines [15].

The voltages and currents in the dq0-reference frame are constant in steady-state situations. Be aware that also non-fundamental harmonics are correctly transformed as x_a , x_b and x_c are time signals, including all harmonics. In steady state a non-fundamental frequency component with frequency ω_h will appear as a sinusoidal signal with frequency (ω_h - ω_d) in the dq0-domain. The highest frequency that can be represented accurately in the dq0-frame depends on the time step that is used.

With electric machines the d-axis is mostly chosen along the stator flux, which implies that i_q corresponds to real power and i_d to reactive power (see (8)), since ideally $v_d=0$. In general the voltages will be phase shifted with respect to the d-axis which means that active and reactive power cannot be related directly to the d and the q axis component ($v_q \neq 0$). The instantaneous active and reactive power can be obtained directly from the voltages and currents in the dq0-reference system [Aka 84]:

$$P = v_d i_d + v_q i_q$$

$$Q = v_q i_d - v_d i_q$$
(8)

2.1.3 Modelling of basic components

Series RL

In this section the dq0-equations for a three-phase series RL line with ground return, shown in figure 2, will be presented. The dq0-equations for the uniformly transposed line can be obtained by considering the resistive and inductive drops of the *a*-phase equations. The send end voltage with respect to local ground is given by:

$$v_{a1} = R_a i_a + L_a \frac{di_a}{dt} + L_{ab} \frac{di_b}{dt} + L_{ac} \frac{di_c}{dt} + L_{ag} \frac{di_g}{dt} + v_{a2} + v_{g21}$$
(9)

With $v_{g21} = v_{g2} - v_{g1}$.

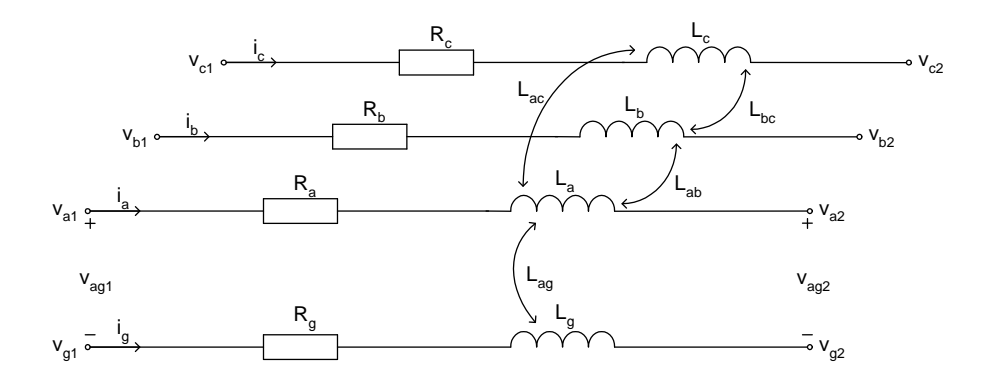


Figure 2: Three-phase RL line with ground return

Using the relation i_g =- $(i_a+i_b+i_c)$, the voltage drops across the three phases of the line can be expressed in matrix form as:

$$[\mathbf{v}_{1,abc}] - [\mathbf{v}_{2,abc}] = [\mathbf{R}] [\mathbf{i}_{abc}] + \frac{d}{dt} [\mathbf{L}] [\mathbf{i}_{abc}]$$
(10)

Where

$$[\mathbf{v}_{1,abc}] = \begin{bmatrix} v_{a1} \\ v_{b1} \\ v_{c1} \end{bmatrix} [\mathbf{v}_{2,abc}] = \begin{bmatrix} v_{a2} \\ v_{b2} \\ v_{c2} \end{bmatrix}$$

$$[\mathbf{R}] = \begin{bmatrix} R_a + R_g & R_g & R_g \\ R_g & R_b + R_g & R_g \\ R_g & R_g & R_c + R_g \end{bmatrix}$$

$$[\mathbf{L}] = \begin{bmatrix} L_a + L_g - 2L_{ag} & L_{ab} + L_g - L_{bg} - L_{ag} & L_{ac} + L_g - L_{cg} - L_{ag} \\ L_{ab} + L_g - L_{ag} - L_{bg} & L_b + L_g - 2L_{bg} & L_{bc} + L_g - L_{cg} - L_{bg} \\ L_{ab} + L_g - L_{ag} - L_{cg} & L_{bc} + L_g - L_{cg} - L_{cg} \end{bmatrix}$$

The equation of the voltage drop across the ground path is:

$$v_{g21} = v_{g2} - v_{g1} = -R_g i_g - L_g \frac{di_g}{dt} - L_{ag} \frac{di_a}{dt} - L_{bg} \frac{di_b}{dt} - L_{cg} \frac{di_c}{dt}$$

$$= R_g (i_a + i_b + i_c) + (L_g - L_{ag}) \frac{di_a}{dt} + (L_g - L_{bg}) \frac{di_b}{dt} + (L_g - L_{cg}) \frac{di_c}{dt}$$
(11)

For a uniformly transposed line, $R_a = R_b = R_c$, $L_{ab} = L_{bc} = L_{ca}$, and $L_{ag} = L_{bg} = L_{cg}$. Letting $L_s = L_a + L_g - 2L_{ag}$, $L_m = L_{ab} + L_g - 2L_{ag} = L_s - L_a + L_{ab}$, $R_s = R_a + R_g$, and $R_m = R_g$, the resistance and inductance matrices simplify to:

and

$$[L] = \begin{bmatrix} L_s & L_m & L_m \\ L_m & L_s & L_m \\ L_m & L_m & L_s \end{bmatrix}$$
 (13)

The dq0-equations for the uniformly transposed line can be obtained by considering the resistive and inductive drops of the a-phase equations. The resistive drop in the a-phase is given by:

$$R_a i_a + R_m \left(i_b + i_c \right) \tag{14}$$

Substituting $i_o = (i_a + i_b + i_c)/3$ to eliminate i_b and i_c , we obtain:

$$(R_s - R_m)i_a + 3R_m i_0 \tag{15}$$

Expressing i_a in terms of the dq0-currents, the resistive drop in the a-phase becomes:

$$(R_s - R_m)\left(i_d \cos \theta_d - i_q \sin \theta_d + i_0\right) + 3R_m i_0 \tag{16}$$

Similarly, for the inductive drop in the a-phase, we have:

$$L_s \frac{di_a}{dt} + L_m \frac{d\left(i_b + i_c\right)}{dt} \tag{17}$$

Eliminating i_b and i_c :

$$(L_s - L_m)\frac{di_a}{dt} + 3L_m\frac{di_0}{dt} \tag{18}$$

Using the inverse dq0-transform of (5) to express i_a in terms of the dq0-currents, the inductive drop in the a-phase becomes:

$$(L_s - L_m)\frac{d}{dt}\left(i_d\cos\theta_d - i_q\sin\theta_d + i_0\right) + 3L_m\frac{di_0}{dt} \tag{19}$$

Knowing that for x=x(t):

$$\frac{d}{dt}\sin x = \cos x \frac{dx}{dt} \tag{20}$$

and

$$\frac{d}{dt}\cos = -\sin x \frac{dx}{dt} \tag{21}$$

(19) can be written as:

$$(L_s - L_m) \left[-i_d \sin \theta_d \frac{d\theta_d}{dt} + \cos \theta_d \frac{di_d}{dt} - i_q \cos \theta_d \frac{d\theta_d}{dt} - \sin \theta_d \frac{di_q}{dt} + \frac{di_0}{dt} \right] + 3L_m \frac{di_0}{dt}$$
 (22)

The dq0-transform can also be applied to the voltage difference $\Delta v_a = v_{a1} - v_{a2}$, resulting in:

$$\Delta v_d \cos \theta_d - \Delta v_q \sin \theta_d + \Delta v_0 \tag{23}$$

Combining (16), (22), and (23), (9) can be written as:

$$\Delta v_d \cos \theta_d - \Delta v_q \sin \theta_d + \Delta v_0 = (R_s - R_m) \left(i_d \cos \theta_d - i_q \sin \theta_d + i_0 \right) + 3R_m i_0 + (L_s - L_m) \left[-i_d \sin \theta_d \frac{d\theta_d}{dt} + \cos \theta_d \frac{di_d}{dt} - i_q \cos \theta_d \frac{d\theta_d}{dt} - \sin \theta_d \frac{di_q}{dt} + \frac{di_0}{dt} \right] + 3L_m \frac{di_0}{dt}$$
(24)

By equating the coefficients of the $\cos\theta_d$, $\sin\theta_d$, and constant terms, we obtain:

$$\Delta v_{d} = (R_{s} - R_{m}) i_{d} + (L_{s} - L_{m}) \frac{di_{d}}{dt} - (L_{s} - L_{m}) i_{q} \frac{d\theta_{d}}{dt}$$

$$\Delta v_{q} = (R_{s} - R_{m}) i_{q} + (L_{s} - L_{m}) \frac{di_{q}}{dt} + (L_{s} - L_{m}) i_{d} \frac{d\theta_{d}}{dt}$$

$$\Delta v_{0} = (R_{s} + 2R_{m}) i_{0} + (L_{s} + 2L_{m}) \frac{di_{0}}{dt}$$
(25)

When the mutual inductances between phases and between phase to ground are zero, that is $L_{ab}=L_{bc}=L_{ca}=0$ and $L_{ag}=L_{bg}=L_{cg}=0$, then $L_{s}=L_{a}+L_{g}$, and $L_{m}=L_{ab}+L_{g}$. With $\omega_{d}=d\theta_{d}/dt$ the final result is:

$$\Delta v_d = R_a i_d + L_a \frac{di_d}{dt} - \omega_d L_a i_q$$

$$\Delta v_q = R_a i_q + L_a \frac{di_q}{dt} + \omega_d L_a i_d$$

$$\Delta v_0 = (R_a + 3R_g) i_0 + (L_a + 3L_g) \frac{di_0}{dt}$$
(26)

The resulting equivalent dq0-circuits are shown in figure 3.

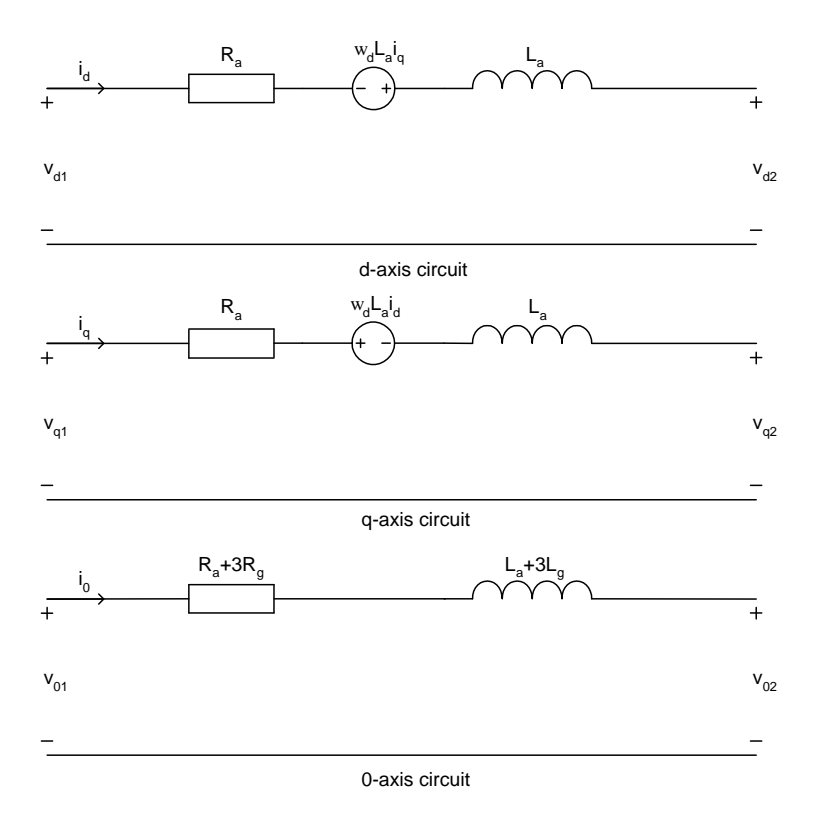


Figure 3: Equivalent dq0-circuit of a series RL line

ECN-C- -04-050 21

Shunt C

The next step is to derive the dq0-equations for the voltage drops across the shunt capacitances of the three-phase line shown in figure 4. Besides the phase to neutral capacitance of the phases, we have also included the mutual capacitances between the phases.

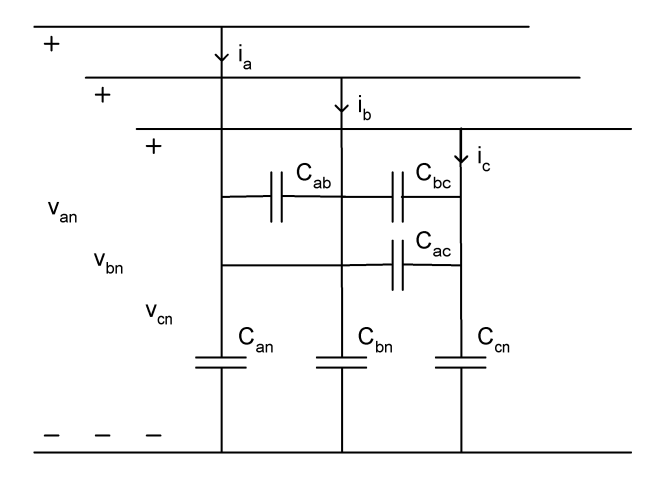


Figure 4: Shunt capacitances of a three-phase line

Let $C_{ab} = C_{bc} = C_{ac} = C_m$, $C_{an} = C_{bn} = C_{cn}$, and $C_s = C_{an} + 2 C_{ab}$. The equation of the *a*-phase current in figure 4 may be expressed as:

$$i_a = C_{an} \frac{d}{dt} v_{an} + C_{ab} \frac{d}{dt} \left(v_{an} - v_{bn} \right) + C_{ac} \frac{d}{dt} \left(v_{an} - v_{cn} \right)$$

$$(27)$$

$$i_a = (C_{an} + C_{ab} + C_{ac})\frac{dv_{an}}{dt} - C_m\frac{dv_{bn}}{dt} - C_m\frac{dv_{cn}}{dt}$$

$$(28)$$

Exchanging the b and c phase voltages with $v_0 = (v_{an} + v_{bn} + v_{cn})/3$ gives:

$$i_a = (C_s + C_m) \frac{dv_{an}}{dt} - 3C_m \frac{dv_0}{dt}$$
 (29)

Applying the dq0-transformation to the current and the voltage of the a-phase we obtain:

$$i_d \cos \theta_d - i_q \sin \theta_d + i_0 = (C_s + C_m) \frac{d}{dt} \left(v_d \cos \theta_d - v_q \sin \theta_d + v_0 \right) - 3C_m \frac{dv_0}{dt}$$
 (30)

In analogy to equations (19) to (25), by equating the coefficients of the $\cos \theta_d$, $\sin \theta_d$, and constant terms, the following set of equations is obtained for the dq0-currents:

$$i_{d} = (C_{s} + C_{m}) \frac{dv_{d}}{dt} - (C_{s} + C_{m}) v_{q} \frac{d\theta_{d}}{dt}$$

$$i_{q} = (C_{s} + C_{m}) \frac{dv_{q}}{dt} + (C_{s} + C_{m}) v_{d} \frac{d\theta_{d}}{dt}$$

$$i_{0} = (C_{s} - 2C_{m}) \frac{dv_{0}}{dt}$$
(31)

When the mutual capacitances between the phases are zero, that is $C_{ab}=C_{bc}=C_{ac}=0$, then $C_m=0$ and $C_s=C_{an}=C$. With $\omega_d=d\theta_d/dt$ the final result is:

$$i_{d} = C \frac{dv_{d}}{dt} - \omega_{d} C v_{q}$$

$$i_{q} = C \frac{dv_{q}}{dt} + \omega_{d} C v_{d}$$

$$i_{0} = C \frac{dv_{0}}{dt}$$
(32)

The resulting equivalent dq0-circuits are shown in figure (6).

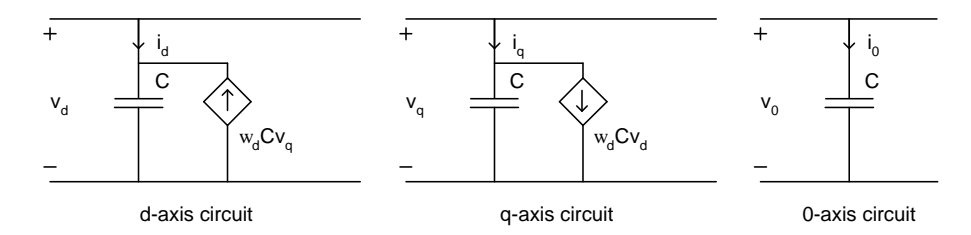


Figure 5: Equivalent dq0-circuits of shunt capacitances of a three-phase line

Summary

The equations for the series resistor, series inductor, and shunt capacitor are derived in the previous sections. The voltage-current relationships for the basic components are summarised in table 2. These reationships can be used to derive models of the different components that are needed. Examples of how this can be done can be found in some of the following sections in which models of transformers and cables are derived.

Under the assumptions that are given during the derivation of the models, i.e. uniformly transposed lines and the mutual inductances/capacitances between phases and phase to ground are zero, the **R**, **L**, and **C** given in the table are equal to the line resistance, line inductance and shunt capacitance.

Three-phase resistor	$\mathbf{R}\left[\mathbf{i}_{dq0} ight]=\left[\mathbf{u}_{dq0} ight]$
Three-phase inductor	$\mathbf{L} \frac{d}{dt} \left[\mathbf{i}_{dq0} \right] + \omega \cdot \mathbf{Y} \cdot \mathbf{L} \cdot \left[\mathbf{i}_{dq0} \right] = \left[\mathbf{u}_{dq0} \right]$
Three-phase capacitor	$\mathbf{C}\frac{d}{dt}\left[\mathbf{u}_{dq0}\right] + \omega \cdot \mathbf{Y} \cdot \mathbf{C} \cdot \left[\mathbf{u}_{dq0}\right] = \left[\mathbf{i}_{dq0}\right]$

$$[\mathbf{R}] = \begin{bmatrix} R_a & 0 & 0 \\ 0 & R_a & 0 \\ 0 & 0 & R_a + 3R_g \end{bmatrix} \qquad [\mathbf{L}] = \begin{bmatrix} L_a & 0 & 0 \\ 0 & L_a & 0 \\ 0 & 0 & L_a + 3R_g \end{bmatrix}$$

$$[\mathbf{C}] = \begin{bmatrix} C & 0 & 0 \\ 0 & C & 0 \\ 0 & 0 & C \end{bmatrix} \qquad [\mathbf{Y}] = \begin{bmatrix} 0 & -1 & 0 \\ 1 & 0 & 0 \\ 0 & 0 & 0 \end{bmatrix}$$

Table 2: Voltage-current relationship in dq0-reference frame for basic components

2.2 Models of wind turbine generators

2.2.1 Introduction

In this section a description will be given of the electrical models that have been developed for the wind turbines that are used in the ERAO-2 project. The section starts with a thorough

ECN-C- -04-050 23

description of the Doubly-Fed Induction Generator (DFIG). The model of an Induction Machine (IM) can easily be derived afterwards. The section continues then with the modelling of the Permanent Magnet Synchronous Machine (PM). At the end of the section a description is given of the converter model that is used for the DFIG and the PM. The converter model is also used for the Cluster-Coupled (CC) park concept.

2.2.2 Doubly-Fed Induction Machine

Introduction

In this section a description will be given of the Doubly-Fed Induction Generator. This type of generator has a converter connected to the rotor windings instead of the stator windings. The advantage is that variable speed operation of the turbine is possible whereas the converter can be much smaller, and therefore also much cheaper. The power rating of the converter is often chosen about 1/3 of the generator rating. A schematic drawing of a wind turbine with Doubly-Fed Induction Generator is shown in figure 6. First a description of the generator model will be given. Afterwards, the controller model will be described.

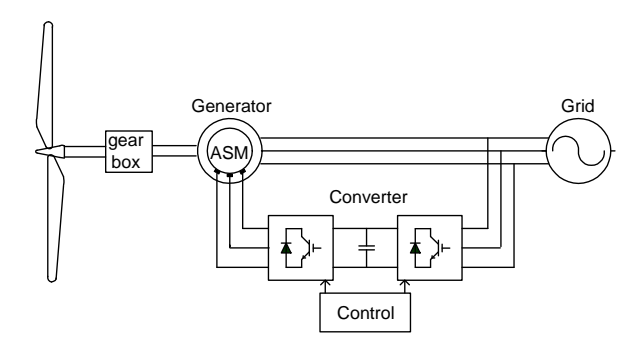


Figure 6: Wind turbine with Doubly-Fed Induction Generator

Generator model

In this section two different models of a doubly-fed induction generator will be developed. The first model includes all dynamic terms whereas in the second model the transient flux terms of the machine are neglected.

A *dq* reference frame is chosen to model the doubly-fed induction generator. The model that is obtained is well known and can be found in literature [23], [13]. The generator convention will be used, which means that the currents are outputs instead of inputs and real power and reactive power have a positive sign when they are fed into the grid. Using the generator convention, the following set of equations results:

$$v_{ds} = -R_s i_{ds} - \omega_s \psi_{qs} + \frac{d\psi_{ds}}{dt}$$

$$v_{qs} = -R_s i_{qs} + \omega_s \psi_{ds} + \frac{d\psi_{qs}}{dt}$$

$$v_{dr} = -R_r i_{dr} - \omega_r \psi_{qr} + \frac{d\psi_{dr}}{dt}$$

$$v_{qr} = -R_r i_{qr} + \omega_r \psi_{dr} + \frac{d\psi_{qr}}{dt}$$
(33)

with

$$\psi_{ds} = -(L_s + L_m) i_{ds} - L_m i_{dr}
\psi_{qs} = -(L_s + L_m) i_{qs} - L_m i_{qr}
\psi_{dr} = -(L_r + L_m) i_{dr} - L_m i_{ds}
\psi_{qr} = -(L_r + L_m) i_{qr} - L_m i_{qs}$$
(34)

with v the voltage [V], R the resistance $[\Omega]$, i the current [A], ω_s and ω_r the stator and rotor electrical angular velocity [rad/s] respectively, L_m the mutual inductance [H], L_s and L_r the stator and rotor leakage inductance [H] respectively and ψ the flux linkage [Vs]. The indices d and q indicate the direct and quadrature axis components of the reference frame and s and r indicate stator and rotor quantities respectively. All voltages, currents and fluxes in (33) and (34) are functions of time.

Sometimes the transients in the fluxes, represented by the derivative terms in equation (33), are neglected. The most important reasons to do this is computational speed during simulations. Another reason is that taking into account the rotor transients would require detailed modelling of the converter [23]. When the transients are neglected, the following set of equations results:

$$v_{ds} = -R_{s}i_{ds} + \omega_{s} ((L_{s} + L_{m}) i_{qs} + L_{m}i_{qr})$$

$$v_{qs} = -R_{s}i_{qs} - \omega_{s} ((L_{s} + L_{m}) i_{ds} + L_{m}i_{dr})$$

$$v_{dr} = -R_{r}i_{dr} + \omega_{r} ((L_{r} + L_{m}) i_{qr} + L_{m}i_{qs})$$

$$v_{qr} = -R_{r}i_{qr} - \omega_{r} ((L_{r} + L_{m}) i_{dr} + L_{m}i_{ds})$$
(35)

The electrical angular velocity of the rotor, ω_r , equals:

$$\omega_r = \omega_s - p\omega_m \tag{36}$$

with p the number of pole pairs [-] and ω_m the mechanical angular velocity [rad/s]. The electrical torque of the generator is given by:

$$T_e = p\left(\psi_{dr}i_{qs} - \psi_{qr}i_{ds}\right) \tag{37}$$

A synchronously rotating d-q reference frame is used with the direct d-axis oriented along the stator flux vector position. In this way a decoupled control between the electrical torque and the rotor excitation current is obtained. This reference frame is rotating with the same speed as the stator voltage and assuming that the stator resistance is negligible, i.e, $R_s \ll \omega_s(L_s + L_m)$, the angle of the stator flux vector can be calculated as:

$$\theta_s = \int \omega_s dt \tag{38}$$

The reference frame of the rotor is rotating with the electrical frequency of the rotor ω_r . The angle of the rotor can be obtained as:

$$\theta_r = \int \omega_r dt = \int (\omega_s - p\omega_m) dt \tag{39}$$

With the dq0-transformation used in (4) the active power delivered by the stator is given by:

$$P_s = v_{ds}i_{ds} + v_{as}i_{as} \tag{40}$$

and the reactive power by:

ECN-C- -04-050 25

$$Q_s = v_{qs}i_{ds} - v_{ds}i_{qs} \tag{41}$$

Due to the chosen reference frame, ψ_{qs} and v_{ds} are zero. Therefore the reactive power and the active power delivered by the stator can be written as:

$$P_s = v_{qs}i_{qs} = v_{qs} \left(\frac{L_m}{L_r + L_m}\right) i_{qr} \tag{42}$$

and:

$$Q_{s} = v_{qs}i_{ds} = \omega_{s} \left(-(L_{s} + L_{m})i_{ds} - L_{m}i_{dr} \right)i_{ds}$$
(43)

As the stator current is equal to the supply current, it can be assumed that it is constant. If the frequency is also constant, the reactive power is proportional to the direct component of the rotor current i_{dr} :

$$Q_s = K_1 + K_2 i_{dr} \tag{44}$$

With constants K_1 and K_2 :

$$K_1 = -\omega_s \left(L_s + L_m \right) i_{ds}^2 \tag{45}$$

and

$$K_2 = -\omega_s L_m i_{ds} \tag{46}$$

Speed and current control of the generator

The electrical and mechanical dynamics of a wind turbine have different time scales. The electrical dynamics are much faster than the mechanical. Therefore, it is possible to control the machine in a cascade structure, as shown in figure 7. The fast electrical dynamics can be controlled in an inner loop and a speed controller can be added in a much slower outer loop.

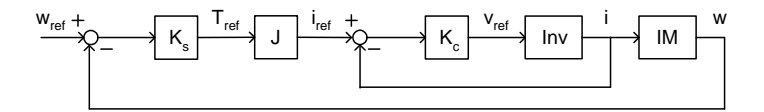


Figure 7: Cascade control; IM=Induction Generator, Inv=Inverter, $K_c=current$ controller, J=inertia of turbine, $K_s=speed$ controller

The internal model control (IMC) principle [21] has been used to design the controllers K_s and K_c . The idea behind internal model control is to reduce the error between the system G(s), and the model of the system $\hat{G}(s)$ by a transfer function K(s). In figure 8 the principle is shown for the current controller.

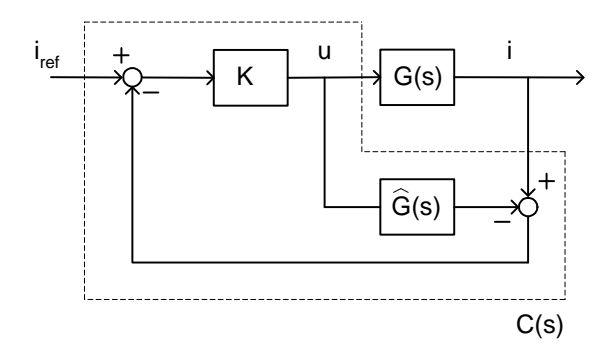


Figure 8: Internal Model Control (IMC): system G(s) and system model $\hat{G}(s)$

One common way of choosing the transfer function K(s) is [5]:

$$K(s) = \left(\frac{\alpha}{s+\alpha}\right)^n G^{-1}(s) \tag{47}$$

where n should be at least one larger than the number of zeros of $\hat{G}(s)$, so that K(s) becomes proper (always converging to zero). The parameter α is a design parameter that is equal to the closed loop bandwidth of the system. The system G(s) should be minimum phase, i.e. it shouldn't contain right half-plane zeros, as these will become unstable under feedback. The controller C(s), inside the dashed line in figure 8, becomes [5]:

$$C(s) = \left(1 - K(s) \hat{G}(s)\right)^{-1} K(s) \tag{48}$$

For a first order system, n=1 is sufficient and the controller becomes then a PI controller. With (48) and $\hat{G}(s) = G(s)$ the controller becomes [5]:

$$C(s) = k_p + \frac{k_i}{s} = \frac{\alpha}{s} G^{-1}(s)$$
(49)

Where k_p is the proportional gain and k_i is the integral gain. The closed loop system with parameters exactly equal to the real parameters becomes:

$$G_{cl}(s) = G(s) K(s) = \frac{\alpha}{s + \alpha}$$
(50)

Since the stator flux is almost fixed to the stator voltage, the flux is practically constant. This implies that the derivative of the stator flux and of the stator magnetizing current are close to zero, and can be neglected [16], [17]. The voltage equations of the rotor which have previously been given in (33) can then be written as:

$$v_{dr} = -R_r i_{dr} - L_r \frac{di_{dr}}{dt} - \omega_r \psi_{qr}$$

$$v_{qr} = -R_r i_{qr} - L_r \frac{di_{qr}}{dt} + \omega_r \psi_{dr}$$
(51)

The last term in both equations causes a cross-relation between the two current components. Reference voltages to obtain the desired currents can be written as [16]:

$$v_{dr}^* = v_{dr}' - \omega_r \psi_{qr} \tag{52}$$

$$v_{qr}^* = v_{qr}' + \omega_r \psi_{dr} \tag{53}$$

ECN-C- -04-050 27

with

$$v'_{dr} = -R_r i_{dr} - L_r \frac{di_{dr}}{dt}$$

$$v'_{qr} = -R_r i_{qr} - L_r \frac{di_{qr}}{dt}$$
(54)

The i_{dr} and i_{qr} errors are processed by a PI controller to give v_{dr} and v_{qr} respectively. To ensure good tracking of these currents, the cross-related flux terms are added to v_{dr} and v_{qr} to obtain the reference voltages. Treating $\omega_r \Psi_{dr}$ and $\omega_r \Psi_{qr}$ as a disturbance, the transfer function from the rotor voltage v_{dr} ' to the rotor current i_{dr} and from the rotor voltage v_{qr} ' to the rotor current i_{qr} is given by:

$$G(s) = \frac{1}{L_r s + R_r} \tag{55}$$

Using the IMC, the current controllers become:

$$C(s) = k_p + \frac{k_i}{s} = \frac{\alpha_c}{s} G^{-1}(s)$$
(56)

Where α_c is the bandwidth of the current control loop, k_p is the proportional gain and k_i is the integral gain. The two gains become [17]:

$$k_p = \alpha_c L_r \tag{57}$$

$$k_i = \alpha_c R_r \tag{58}$$

$$k_i = \alpha_c R_r \tag{58}$$

Speed control:

The rotational speed follows from:

$$\frac{d\omega_m}{dt} = \frac{1}{I} \left(T_m - T_e \right) \tag{59}$$

It is assumed that the current controller is much faster than the speed controller, which implies that for the evaluation of (59) electrical torque is than $T_e = T_{e,ref}$. The reference torque is set to:

$$T_{e,ref} = T_{e,ref'} - B_a \omega_m \tag{60}$$

where B_a is an "active damping torque" [17]. Now the transfer function from rotational speed to electrical torque becomes:

$$G_s(s) = \frac{1}{Js + B_a} \tag{61}$$

Using again the internal model control method, the following gains of the speed controller are obtained:

$$k_{ps} = \alpha_s J$$

$$k_{is} = \alpha_s B_a$$
(62)

$$k_{is} = \alpha_s B_a \tag{63}$$

Where α_s is the desired closed-loop bandwidth of the speed controller. When B_a is chosen to be $B_a = J\alpha_s$ changes in the mechanical torque are damped with the same time constant as the bandwidth of the speed control loop [17].

Converter

As can be seen from figure 6, the Doubly-Fed Induction Generator, has a converter connected to its rotor windings. The generator side converter is used to control the rotor currents of the machine, according to (51)-(58). With this rotor currents, the active power (or indirectly the rotational speed) and reactive power of the machine can be controlled according to (40)-(41). The grid-side converter draws or supplies power to the rotor-side converter and is operated to keep the DC-link voltage constant. A further description of the converter is given in section 2.2.5.

2.2.3 Induction machine

The model of the induction machine can be obtained very easily now, as it is the model of the Doubly-Fed Induction machine, with the rotor windings short-circuited. Equation (33) modifies to:

$$v_{ds} = -R_s i_{ds} - \omega_s \psi_{qs} + \frac{d\psi_{ds}}{dt}$$

$$v_{qs} = -R_s i_{qs} + \omega_s \psi_{ds} + \frac{d\psi_{qs}}{dt}$$

$$0 = -R_r i_{dr} - \omega_r \psi_{qr} + \frac{d\psi_{dr}}{dt}$$

$$0 = -R_r i_{qr} + \omega_r \psi_{dr} + \frac{d\psi_{qr}}{dt}$$
(64)

with

$$\psi_{ds} = -(L_s + L_m) i_{ds} - L_m i_{dr}
\psi_{qs} = -(L_s + L_m) i_{qs} - L_m i_{qr}
\psi_{dr} = -(L_r + L_m) i_{dr} - L_m i_{ds}
\psi_{qr} = -(L_r + L_m) i_{qr} - L_m i_{qs}$$
(65)

To obtain electrical torque and power of the machine, (36)-(43) can be used. In wind turbines the induction machines are normally directly connected to the grid. This means that no converter is needed and that there is no possibility to control the torque directly.

2.2.4 Permanent Magnet Synchronous Machine

Introduction

The next generator type that is often used for wind turbine applications is the permanent magnet synchronous machine. It is especially used in direct-drive wind turbines, which have the advantage that no gearbox is needed, which is favourable with respect to lifetime and maintenance. In this section the basic equations describing the machine behaviour will be given, followed by the way in which controllers can be obtained.

Generator model

Using the generator convention, the stator voltage equations are, in analogy to (33):

$$v_{ds} = -R_s i_{ds} - \omega_s \psi_{qs} - \frac{d\psi_{ds}}{dt}$$

$$v_{qs} = -R_s i_{qs} + \omega_s \psi_{ds} - \frac{d\psi_{qs}}{dt}$$
(66)

with v the voltage [V], R the resistance $[\Omega]$, i the current [A], ω_s the stator electrical angular velocity [rad/s] and ψ the flux linkage [Vs]. The indices d and q indicate the direct and quadrature axis components. All voltages, currents and fluxes in (1) are functions of time.

The flux linkages in (66) can be calculated using the following set of equations:

$$\psi_{ds} = (L_{ds} + L_m) i_{ds} + \Psi_f
\psi_{as} = (L_{as} + L_m) i_{as}$$
(67)

With Ψ_f the excitation flux of the permanent magnets linked with the stator windings, L_m the mutual inductance [H], and L_{ds} and L_{qs} the stator leakage inductances [H].

The electrical torque T_e of the permanent magnet synchronous machine is given by [20]:

$$T_e = p \cdot i_{gs} \left[i_{ds} \left(L_{ds} - L_{gs} \right) + \Psi_f \right] \tag{68}$$

Here p is the number of pole pairs. For a non-salient-pole machine the stator inductances L_{ds} and L_{qs} are approximately equal. This means that the equation becomes:

$$T_e = p i_{as} \Psi_f \tag{69}$$

The stator electrical angular velocity is given by:

$$\omega_s = p\omega_m \tag{70}$$

with ω_m the mechanical angular velocity [rad/s], which can be obtained from:

$$\frac{d\omega_m}{dt} = \frac{1}{J} \left(T_m - T_e \right) \tag{71}$$

with J the inertia constant of the rotor [kg·m²] and T_m and T_e the mechanical and electrical torque [Nm] respectively.

Control of the generator

From the voltage equations in (66) it can be seen that there is a cross relation between the two axes. The d-axis voltage equation has a flux term that depends on the q-axis. Vice-versa the q-axis has a flux term depending on the d-axis. In order to apply independent controllers for the two coordinates the influence of the q-axis on the d-axis-components and vice versa must be eliminated. This can be done by decoupling the two components, in the way shown in figure 9. The faults in the current components can be processed by the (PI) controllers and afterwards the decoupling components should be added to the voltage reference signals.

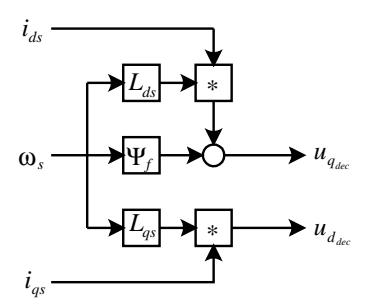


Figure 9: Decoupling of the generator axes

With the decoupling applied, the linear transfer function of i_{ds} to u_{ds} is given by:

$$\frac{i_{ds}\left(s\right)}{u_{ds}\left(s\right)} = \frac{1}{L_{s}s + R_{s}}\tag{72}$$

The proportional and integral constants for the PI-controller can be obtained in the same way as for the doubly-fed induction machine:

$$k_p = \alpha_c L_s \tag{73}$$

$$k_i = \alpha_c R_s \tag{74}$$

$$k_i = \alpha_c R_s \tag{74}$$

With α_c is the bandwidth of the current control loop.

The proportional and integral constants for the speed controller are given by [20]:

$$k_p = \frac{2p^2\psi_f}{J} \tag{75}$$

$$k_p = \frac{2p^2\psi_f}{J}$$

$$k_i = \frac{2p^2\psi_f R_s}{JL_s}$$
(75)

2.2.5 Converter

Introduction

Some of the generators described in the previous sections use a power electronics converter. A description of this converter will be given in this section.

For the doubly-fed induction generator it should be possible to transport power in both directions, and therefore a back-to-back converter consisting of two Voltage Source Converters (VSCs) and a DC link is used. The converter is shown in figure 10. The DC link separates the two Voltage Source Converters, and therefore they can be controlled independent of each other. Therefore, only one converter has to be considered. To obtain sinusoidal line currents, a filter can be placed between the converter and the grid. The phase voltages are referred to the node n. The value of the arbitrary voltage reference node n depends on the circuit configuration. It should not be confused with the neutral. The line voltages can be derived from the phase voltages. For example the voltage v_{ab1} is:

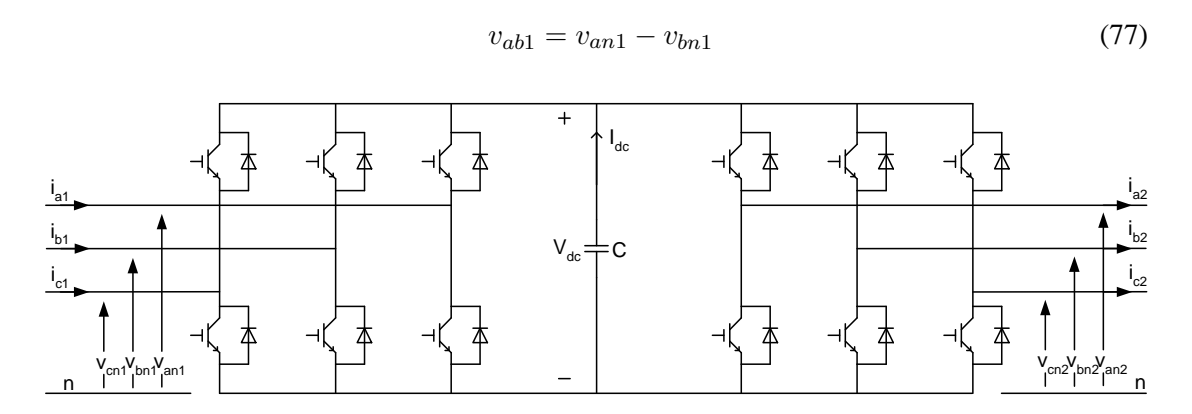


Figure 10: Back-to-back converter

The controller of the converter will be based on a dq0-reference frame, implementing the vector control method. All signals will be constant in steady-state and therefore PI controllers can be used to realise the reference values without steady-state errors. A triangular carrier based Pulse Width Modulation scheme is used to control the switches of the converter. The controller is based on two control loops. The inner loop is a current controller, which get its reference from the outer loop controller, which can be for example a reactive power or torque controller. A block diagram of a PWM converter with a vector controller is shown in figure 11.

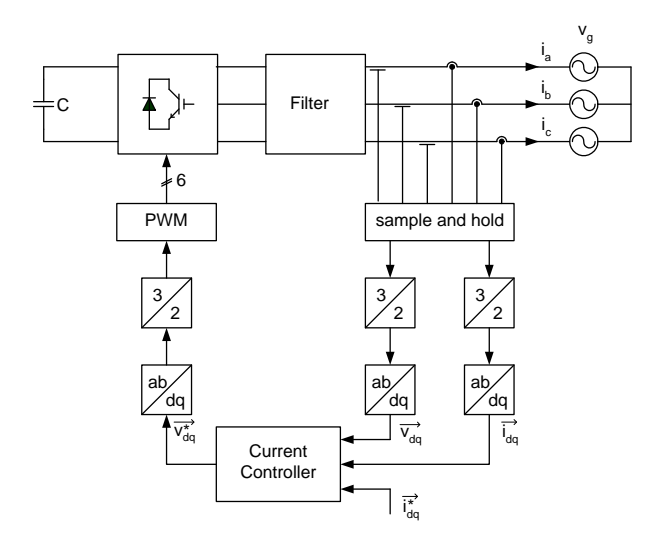


Figure 11: Scheme of PWM Voltage Source Converter with controller

Switching Function Concept

The switching function concept has been used to model the converter [27]. Using this concept, the power conversion circuits are modeled according to their functions, rather than to their circuit topologies. The switching function concept will be described shortly with reference to the circuit configuration of a VSC as shown in figure 12 and the type of voltages that are generated at the AC side. It is well known that with voltage source converters pulsating voltages are generated at the AC side. In figure 15 an example of the voltage V_{an} is shown. This voltage is obtained by alternatively switching the upper and the lower switch in phase a. The ON/OFF

control signals for the switches are generated in some type of Pulse Width Modulator (PWM). An example of the principle of such a modulator is shown in figure 15, where the desired output voltage V_{ref} is compared with a triangular carrier. Whenever $V_{ref} > V_{tri}$ the upper switch is closed, and when $V_{ref} > V_{tri}$, the lower switch is closed. In this way the output waveform has the same shape as the output signal of the comparator. For each phase leg a separate modulator is used, where the reference voltages are displaced over 120 or 240 degrees respectively. The output voltage of a phase can mathematically be described as the product of the logical output signal of the comparator, also called switching function SF_a of phase a, and the DC link voltage [27]:

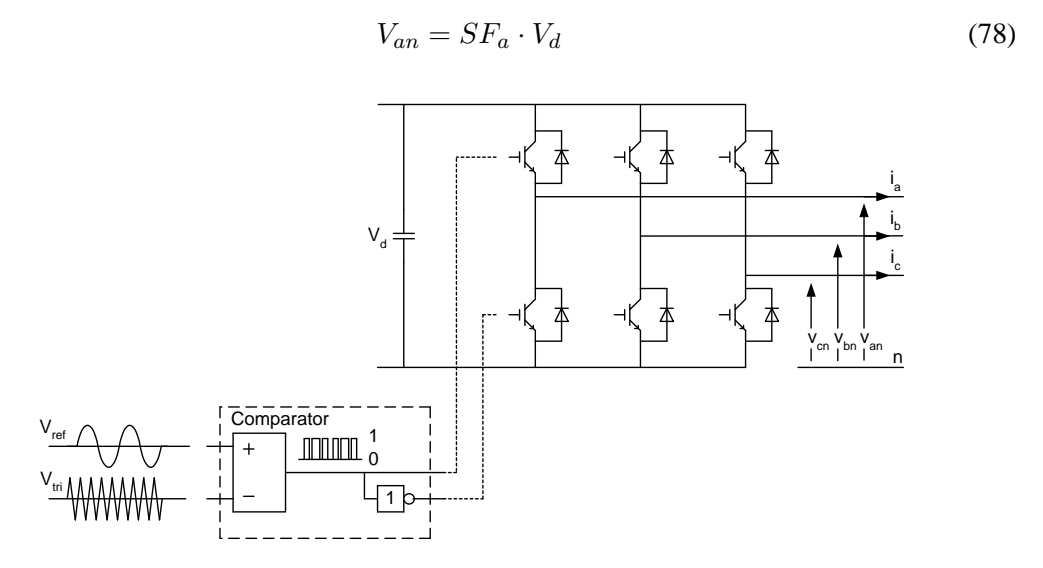


Figure 12: Voltage source converter

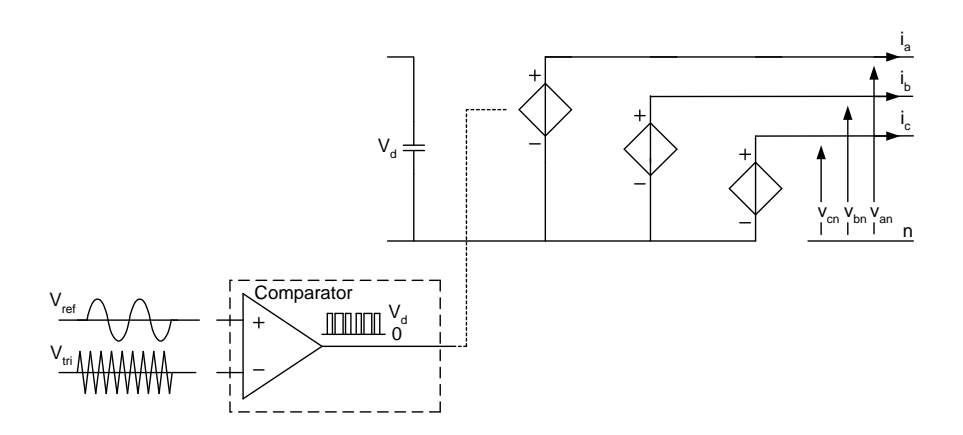


Figure 13: Voltage source converter, switching function equivalent

ECN-C- -04-050 33

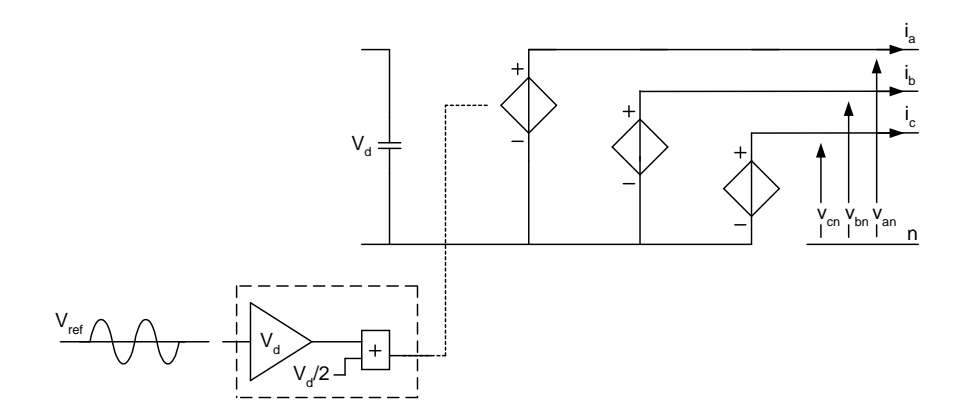


Figure 14: Voltage source converter, sinusoidal voltages equivalent

The voltage V_{an} can also be obtained with the circuit from figure 13, where controllable voltage sources are applied instead of switches in phase legs. The controllable voltage sources are controlled by the same signals as with the phase leg after multiplication by V_d . The mode of figure 13 is obtained then. The switching functions can be expressed as Fourier series.

$$SF = \sum_{n=1}^{\infty} A_n \sin(n\omega t)$$
 (79)

It can be shown that in the lower frequency range the frequency components of $SF \times V_d$ and V_{an} are equal if the frequency of the carrier is sufficiently large [9].

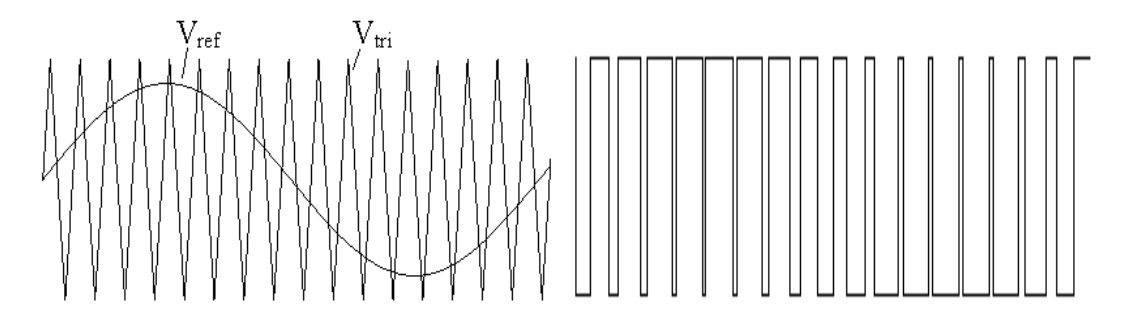


Figure 15: Pulse Width Modulation (l) and switching function (r) for one phase of the voltage source converter

When the complete PWM-operation, or even the switching functions, of the VSC has to be taken into account, the model of the converter becomes complicated, and simulation will become very slow. If the filter is designed well, the higher harmonics that are generated by the switching process will be attenuated. It can be shown that, with a well-designed filter, in the lower frequency range the frequency components of the reference voltage and the practical obtained voltage are equal if the switching frequency is sufficiently large [9]. A further assumption is that the dc-link voltage V_d is constant. In reality this isn't true, causing some higher frequency terms in the output signals. The resulting model is then shown in figure 14. The whole system can then be replaced by a system, creating sinusoidal waveforms, exactly equal to the reference waveforms. One should be aware that this is only valid for frequencies far below the resonance frequency of the filter. In case of a grid-connected converter, with a grid-frequency of 50Hz, this requirement will be met and the model can be used for applica-

tions like voltage regulation, as long as normal grid operation is assumed.

Converter model behaviour during voltage disturbances

It has been explained in the previous section that if the filter is designed well, the higher harmonics that are generated by the switching process will be attenuated. With a well-designed filter, in the lower frequency range the frequency components of the reference voltage and the practical obtained voltage are equal if the switching frequency is sufficiently large, i.e.

$$f_s >> f_0 \tag{80}$$

with f_s the switching frequency and f_0 the fundamental harmonic of the voltage. During fast phenomena the voltage will also have higher harmonic terms and the condition (80) will no longer be valid. When there is no current control or voltage control applied, the harmonics will not be present in the reference voltages and the voltage that is made by the converter is still a good representation of the reference voltage. When control is applied, the reference voltage will also have the higher harmonics in most cases, and the representation between the voltage that is made and the reference voltage isn't correct any longer.

To investigate whether the models based on the switching function concept can be used during disturbances the 'reduced' model has been compared to a reference model. The SimPower-Systems Blockset [8] of Matlab has been used to obtain this reference model of the converter. The 'universal bridge model' with IGBTs has been used. This block of the SimPower Systems Blockset implements a 3-phase bridge converter with 6 IGBT switches with antiparallel diodes. RC-snubber circuits are included in the IGBT-models. Typical parameters such as rise and fall times and voltage drop can be defined in the model. The voltages and currents are measured and transformed to the dq0-reference system. Sample-and-hold circuits are implemented in the measurement loops. The measured voltages and currents are filtered with low-pass filters with a cut-off frequency of 200 Hz. Ordinary PI controllers are used to obtain the desired currents.

The 'reduced' model described in the previous section, has been compared to the 'full' model. A three-phase balanced voltage dip of 70% (the RMS value of the grid voltage is reduced to 30% of its pre-fault voltage) has been simulated. The grid voltage is shown in figure 16. The converter current supplied to the grid is shown in figure 17.

ECN-C- -04-050 35

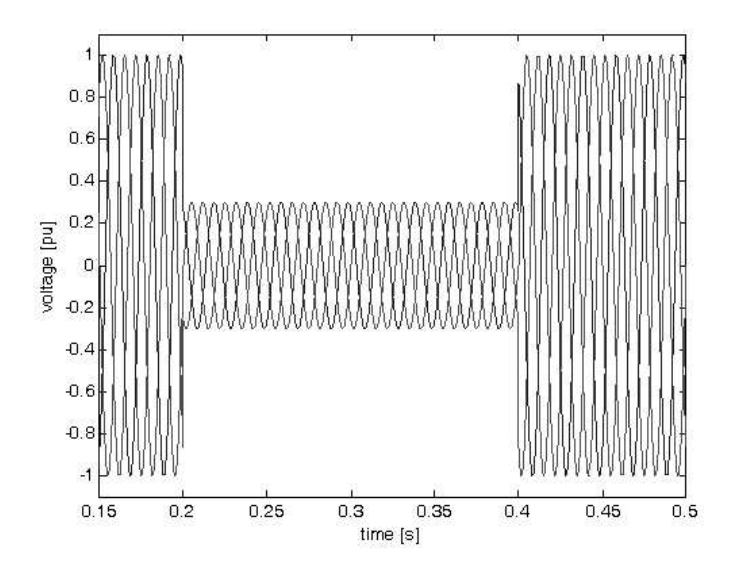


Figure 16: 'Ideal' voltage dip

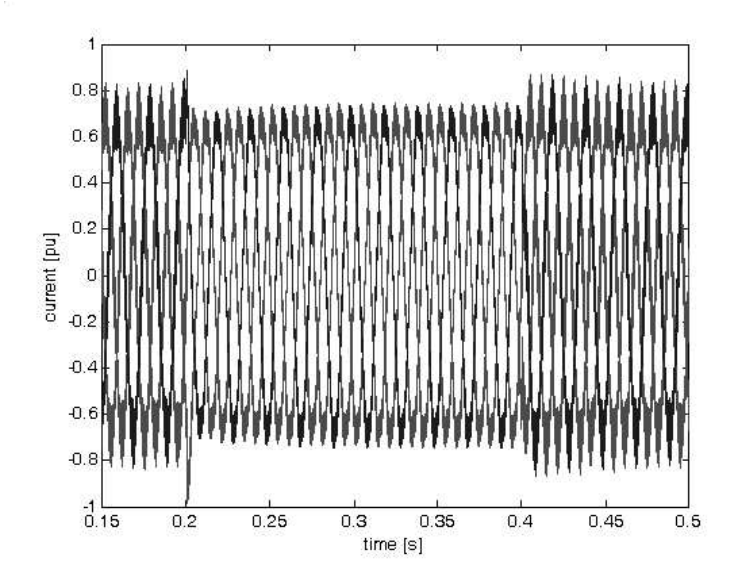


Figure 17: Converter current

The behaviour of the reduced model of the converter has been compared to the behaviour of the full converter. In order to make comparison easier, the currents have been compared in the dq0-reference frame. These current are constant in steady-state situations, which makes it easier to compare them to each other. The *d*-axis current for the reduced and the full model are shown in figure 18: on average the currents of the two models are the same and the initial peaks at the moment of the step in voltage are also equal. The difference is due to the switching of the converter in the full model. When the switching frequency is sufficiently high, these high-frequency terms will be attenuated by a filter. More information on the comparison can be found in [11] and in appendix B.

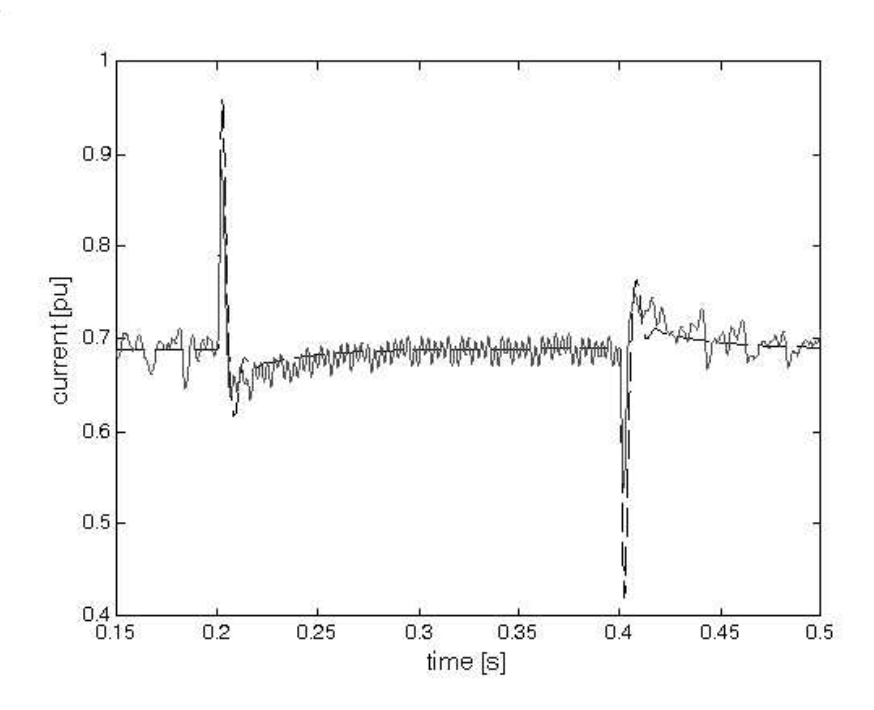


Figure 18: Converter current in d-axis for complete model (solid line) and reduced model (dashed line)

Grid current control

The controllers of the VSC will be obtained with reference to the converter shown in figure 19. A vector-control approach is used for the supply side converter, with a reference frame oriented along the grid voltage vector. Such a reference frame enables independent control of the active and reactive power flowing between the converter and the grid.

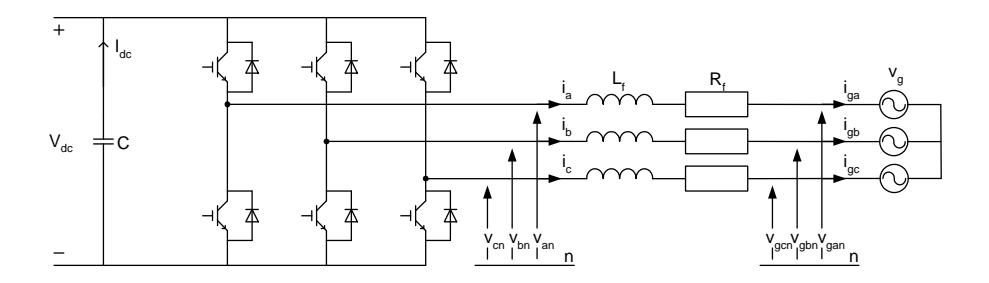


Figure 19: Three-phase full-bridge Voltage Source Converter

Consider the system of figure 19. The voltage balance across the inductors and resistors is:

$$\Delta v_{a} = v_{an} - v_{agn} = L_{f} \cdot \frac{di_{a}}{dt} + R_{f} \cdot i_{a}$$

$$\Delta v_{b} = v_{bn} - v_{bgn} = L_{f} \cdot \frac{di_{b}}{dt} + R_{f} \cdot i_{b}$$

$$\Delta v_{c} = v_{cn} - v_{cgn} = L_{f} \cdot \frac{di_{c}}{dt} + R_{f} \cdot i_{c}$$
(81)

With the Park transformation this equation can be transformed to the dq reference frame:

$$\Delta v_d = R_f i_d + L_f \cdot \frac{di_d}{dt} + \omega_e L_f i_q$$

$$\Delta v_q = R_f i_q + L_f \cdot \frac{di_q}{dt} - \omega_e L_f i_d$$
(82)

The last term in both equations causes a coupling of the two equations, which makes it difficult to control both currents independently. This was also observed in the control of the generator and the same solution can be applied here. The last terms can be considered as a disturbance on the controller. Reference voltages to obtain the desired currents can be written as:

$$\Delta v_d^* = \Delta v_d' + \omega_e L_f i_q$$

$$\Delta v_q^* = \Delta v_q' - \omega_e L_f i_d$$
(83)

with:

$$\Delta v_d' = R_f i_d + L_f \cdot \frac{di_d}{dt}$$

$$\Delta v_g' = R_f i_g + L_f \cdot \frac{di_g}{dt}$$
(84)

Treating the cross-related terms as a disturbance, the transfer function from voltage to current of (84) can be found as (for both the d- and the q-component):

$$G(s) = \frac{1}{L_f s + R_f} \tag{85}$$

A scheme of the controller is given in figure 20.

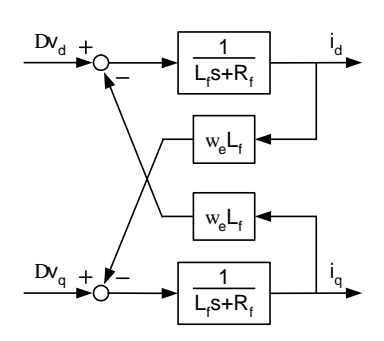


Figure 20: Scheme of current controller

Using the Internal Model Control principle [17] to design the current controllers yields:

$$K(s) = k_p + \frac{k_i}{s} = \frac{\alpha_c}{s} G^{-1}(s)$$
(86)

where α_c is the bandwidth of the current control loop, k_p is the proportional gain and k_i is the integral gain of the controller. The proportional and integral gain become [17]:

$$k_p = \alpha_c L_f; \quad k_i = \alpha_c R_f \tag{87}$$

The active and reactive power delivered by the converter are given by:

$$P = v_{dg}i_d + v_{qg}i_q$$

$$Q = v_{qg}i_d - v_{dg}i_q$$
(88)

with the d-axis of the reference frame along the stator-voltage position, v_q is zero and as long as the supply voltage is constant, v_d is constant. The active and reactive power are proportional to i_d and i_q then.

DC-link controller

The DC-voltage controller is designed by use of feedback linearisation [14].

The capacitor in the dc-link behaves as an energy storage device. Neglecting losses, the time derivative of the stored energy must equal the sum of the instantaneous stator power P_s and grid power P_q :

$$\frac{1}{2}C\frac{d\left(v_{dc}^2\right)}{dt} = P_s - P_g \tag{89}$$

This equation is nonlinear with respect to v_{dc} . To overcome this problem a new state-variable is introduced:

$$W = v_{dc}^2 \tag{90}$$

Substituting this in (89) gives:

$$\frac{1}{2}C\frac{dW}{dt} = P_s - P_g \tag{91}$$

which is linear with respect to *W*. The physical interpretation of this state-variable substitution is that the energy is chosen to represent the dc-link characteristics [14]. With the dq-reference frame of the current controller along the d-axis, (91) can be written as:

$$\frac{1}{2}C\frac{dW}{dt} = P_s - v_d i_d \tag{92}$$

and the transfer function from i_d to W is then found to be:

$$G\left(s\right) = -\frac{2v_d}{sC}\tag{93}$$

As this transfer function has a pole in the origin it will be difficult to control it. An inner feedback loop for active damping will be introduced [14]:

$$i_d = i_d' + G_a W (94)$$

With G_a the active conductance, performing the active damping, and i'_d the reference current provided by the outer control loop, see figure 21. Substituting (94) into (92) gives:

$$\frac{1}{2}C\frac{dW}{dt} = P_s - v_d i_d' - v_d G_a W \tag{95}$$

Which is shown in figure 21. The transfer function from i'_q to W becomes [14]:

$$G'(s) = -\frac{2v_d}{sC + 2v_dG_a} \tag{96}$$

Using the internal model control principle [17] and since (96) is a first-order system, the following controller is proposed:

$$F(s) = \frac{\alpha}{s}G^{\prime - 1}(s) = -\frac{\alpha_d C}{2v_d} - \frac{\alpha_d G_a}{s}$$
(97)

Which is just a PI-controller. A suitable choice will be to make the inner loop as fast as the closed-loop system [14]. When the pole of G'(s) is placed at $-\alpha d$ the following active conductance is obtained:

$$G_a = \frac{\alpha_d C}{2v_d} \tag{98}$$

The PI-controller parameters are then given as [14]:

$$k_p = -\frac{\alpha_d C}{2v_d}, \quad k_i = -\frac{\alpha_d^2 C}{2v_d} \tag{99}$$

The controller is completed by a feedforward term from P_s to i'_q .

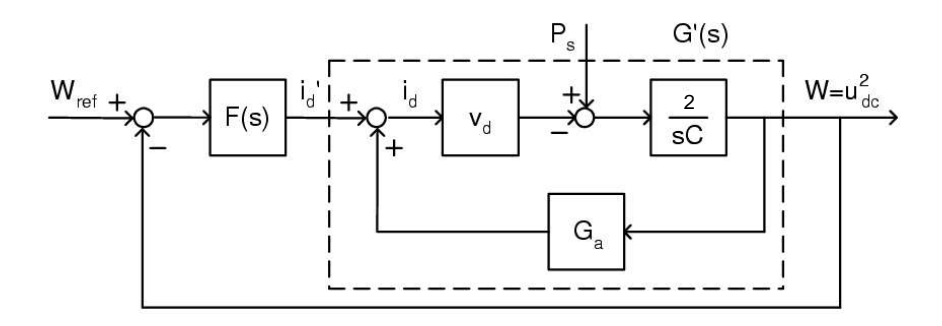


Figure 21: DC-link controller structure

2.3 Other electrical components

Besides the models of the wind turbine generators, models of other electrical components are needed for a complete offshore wind farm model. In this section the models will be derived of the transmission line and cable, the transformer and the grid. Whether zero-sequence components have to be taken into account during the simulations depends on the circuit configuration and will be discussed in section 2.4.2.

2.3.1 Transmission line and cable

The general equations relating voltage and current in a transmission line or cable recognize the fact that all impedances of a transmission line are uniformly distributed along the line. For lines up to about 250 km lumped parameters can be used however [4]. The single-phase equivalent circuit of a lumped line is shown in figure 22.

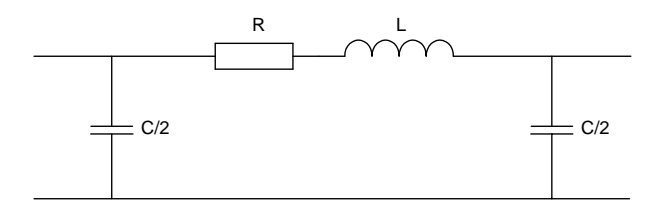


Figure 22: Single-phase equivalent circuit of a transmission line

In the model that will be used, the two shunt capacitances are assumed to be both on one side of the cable segment. The cable model can then be subdivided in two sections: a three-phase shunt capacitor and a three-phase series resistance and inductance. The dq0-models of a three-phase line with shunt capacitors and a three-phase RL line have already been obtained. The voltage across the RL line segment is given in (26) by:

$$\Delta v_{d} = v_{d2} - v_{d1} = R_{a}i_{dl} + L_{a}\frac{di_{dl}}{dt} - \omega L_{a}i_{ql}$$

$$\Delta v_{q} = v_{q2} - v_{q1} = R_{a}i_{ql} + L_{a}\frac{di_{ql}}{dt} + \omega L_{a}i_{dl}$$

$$\Delta v_{0} = v_{02} - v_{01} = (R_{a} + 3R_{g})i_{0} + (L_{a} + 3L_{g})\frac{di_{0}}{dt}$$
(100)

The current through the shunt capacitances is given in (32) by:

$$i_{dc1} = C \frac{dv_{d1}}{dt} - \omega C v_{q1}$$

$$i_{qc1} = C \frac{dv_{q1}}{dt} + \omega C v_{d1}$$

$$i_{0c1} = C \frac{dv_{01}}{dt}$$

$$(101)$$

The resulting cable models for the d-, q-, and θ -axis are shown in figure 23.

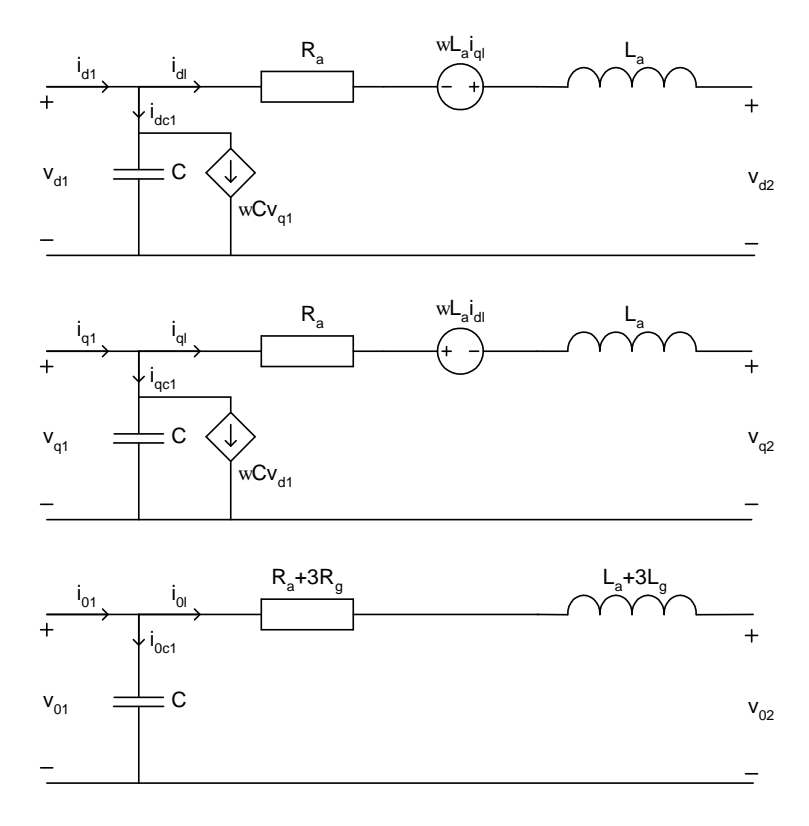


Figure 23: Cable models in dq0-coordinates

To obtain the models, it is assumed that the shield of the cables is grounded, which is true in most cases. The shunt capacitors in the lumped cable model represent the capacitance between cable and shield. The dq0-models obtained for the *RL* circuit assume that a ground return exists. As the cable shield is grounded the ground return exists and the models of figure 23 can be used.

2.3.2 Transformer

The transformer model that has been used will be analysed in this section. A single-phase equivalent circuit of a two-winding transformer is shown in figure 24. Normally the magnetising current i_m is small and can be neglected. The model of figure 24 can then be reduced to the model shown in figure 25, with $R=R_1+a^2R_2$ and $L=L_1+a^2L_2$, with $a=N_1/N_2$.

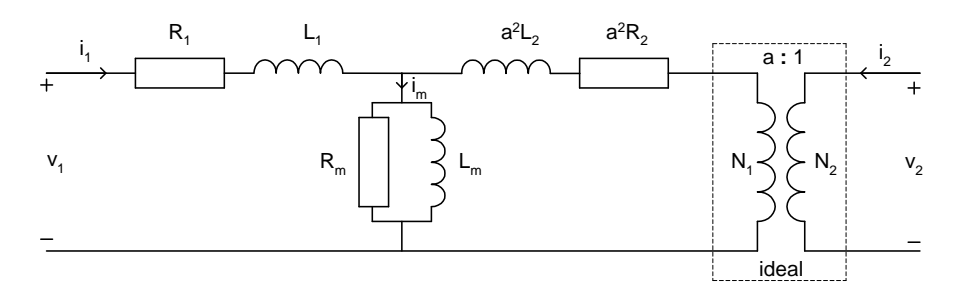


Figure 24: Single-phase equivalent circuit of a transformer

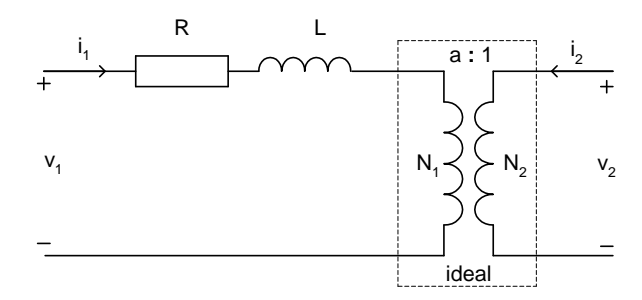


Figure 25: Transformer equivalent circuit with magnetising current neglected

The voltage-current relationship of the single-phase equivalent transformer of figure 25 can be written as:

$$v_1 = Ri_1 + L\frac{di_1}{dt} + av_2 (102)$$

A capacitor has been placed at the primary side of the transformer. The capacitance represents the winding capacitance of the transformer and is primarily needed for numerical reasons. The effect on the results is small. The dq0-models of the transformer are shown in figure 26. The zero-sequence model depends on the type of transformer (star-start, star-delta, etc.). The zero-sequence model represents a star-delta transformer with a ground star connection at the primary side [2].

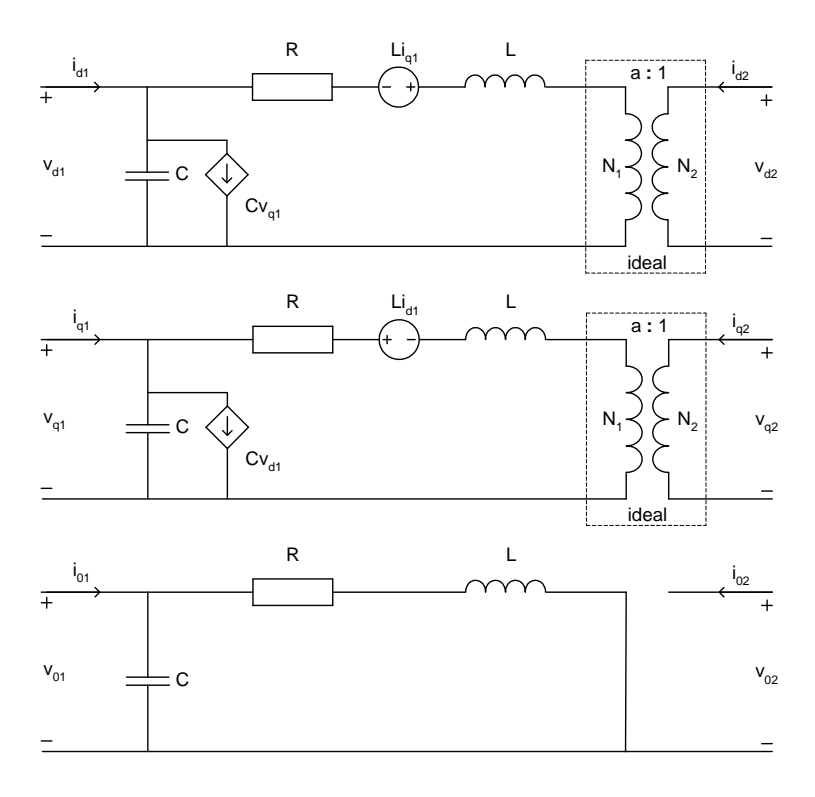


Figure 26: Equivalent transformer model for d, q and zero sequence componenents

2.3.3 Grid model

A simple grid model has been developed to simulate the interaction between a wind farm and the grid and to be able to test the voltage and frequency control capabilities of the different types of wind farms. The main requirement for the grid model is a dynamic behaviour similar to a large high voltage grid. The main component of the grid model is an equivalent synchronous machine, equiped with voltage and frequency control, to represent the dynamic behaviour of the high voltage grid. The synchronous machine model that was chosen is the three winding representation in dq coordinates. Damper windings are not taken into account. The generator convention is adopted:

$$L_d \frac{di_d}{dt} + L_{mf} \frac{di_{fd}}{dt} = -u_d - R_s \cdot i_d - \omega_s \cdot L_q \cdot i_q$$
(103)

$$L_{md}\frac{di_d}{dt} + L_f \frac{di_{fd}}{dt} = u_{fd} - R_{fd} \cdot i_{fd}$$
(104)

$$L_{q} \frac{di_{q}}{dt} = -u_{q} - R_{s}.i_{q} + \omega_{s}.(L_{d}.i_{d} + L_{md}.i_{fd})$$
 (105)

 $\begin{array}{lll} L_d, L_{mf}, L_q, L_{md}, L_f & \text{synchronous machine inductances} \\ R_s, R_{fd} & \text{stator and field winding resistance} \\ i_d, i_q & \text{stator current in d and q axis} \\ u_d, u_q & \text{stator voltage in d and q axis} \\ i_{fd}, u_{fd} & \text{field current and voltage, transposed to stator winding} \\ \omega_s & \text{synchronous machine electrical angular speed} \end{array}$

For the voltage regulator and exciter a type 1 model is used [1] p. 293:

$$\tau_e E_{fd} = -K_e E_{fd} + V_r - S_e E_{fd} \tag{106}$$

$$V_s = \frac{K_f s}{1 + \tau_f s} E_{fd} \tag{107}$$

$$V_r = \frac{K_a}{1 + \tau_f s} V_e \tag{108}$$

$$V_a = \frac{1}{1 + \tau_r s} u_{dq} \tag{109}$$

$$V_e = V_a - V_s \tag{110}$$

 $egin{array}{ll} au_e & ext{exciter time constant} \ E_{fd} & ext{exciter output voltage} \ K_e & ext{exciter constant} \end{array}$

 $egin{array}{ll} V_r & ext{regulator output voltage} \ S_e & ext{exciter saturation function} \ V_e & ext{regulator input voltage} \ V_s & ext{stabilizer output voltage} \ \end{array}$

 K_f, τ_f stabiliser amplification and time constant K_a, τ_a regulator amplification and time constant

 V_a filter output voltage τ_r input filter time constant

The inertia and speed controller of the synchronous machine complete the model:

$$J\frac{d\omega_s}{dt} = T_{mech} - T_{el} \tag{111}$$

$$J\frac{d\omega_s}{dt} = T_{mech} - T_{el}$$

$$T_{mech} = \frac{P_{mech}}{\omega_s}$$

$$P_{mech} = (K_{pw} + \frac{K_{iw}}{s})(\omega_{set} - \omega_s)$$
(111)
(112)

$$P_{mech} = (K_{pw} + \frac{K_{iw}}{s})(\omega_{set} - \omega_s)$$
 (113)

For the connection of the synchronous machine model to the wind farm model, the implementation of the cable model has been modified. In the cable model, used to connect wind turbines in the farm and the farm to the high voltage transformer, the grid side voltage and farm side current are input. To connect the synchronous machine to the wind farm, grid and farm side cable currents are input and the voltages on both sides of the cable are output. This does not affect the mathematical model.

The parameters of the grid model have been chosen to have a fair amount of transient behaviour, not necessarily found in large scale grids. This choice is made to demonstrate the wind farm control capabilities.

2.4 Zero-sequence components

2.4.1 Introduction

A short review of zero-sequence components in voltages and currents will be given here, to see whether short-circuit components can pass through transformers and whether these components have to be taken into account during the modelling of different circuits.

2.4.2 Zero-sequence components

It is proven by Fortescue [3] that each unbalanced system of n related phasors can be resolved into n systems of balanced phasors, called the symmetrical components of the original phasors. According to Fortescue's theorem, three unbalanced phasors of a three-phase system can be resolved into three balanced systems of phasors. A system is balanced when the impedances, voltages and currents in all phases are equal (except for the 120 degrees phase shift of voltages and currents). The first two balanced sets are the positive-sequence and negative-sequence respectively. They consist of three phasors equal in magnitude, displaced from each other by 120 degrees in phase, where the positive-sequence have the same phase sequence as the original phasors and the negative-sequence have the opposite phase sequence. The zero-sequence components consist of three phasors equal in magnitude and with zero phase displacement from each other.

Although Fortescue introduced them as phasors, the symmetrical components can also be written as time-dependent variables [15]. The time-dependent symmetrical components are given by [15]:

$$\begin{bmatrix} u^0 \\ u^+ \\ u^- \end{bmatrix} = \frac{\sqrt{2}}{2} \begin{bmatrix} \underline{\underline{U}}_0 e^{j\omega t} + \underline{\underline{U}}_0^* e^{-j\omega t} \\ \underline{\underline{U}}_1 e^{j\omega t} + \underline{\underline{U}}_1^* e^{-j\omega t} \\ \underline{\underline{U}}_2 e^{j\omega t} + \underline{\underline{U}}_2^* e^{-j\omega t} \end{bmatrix}$$
(114)

with the phasors:

$$\underline{U}_{0} = \frac{1}{\sqrt{3}} \left(\underline{U}_{a} + \underline{U}_{b} + \underline{U}_{c} \right)
\underline{U}_{1} = \frac{1}{\sqrt{3}} \left(\underline{U}_{a} + a\underline{U}_{b} + a^{2}\underline{U}_{c} \right)
\underline{U}_{2} = \frac{1}{\sqrt{3}} \left(\underline{U}_{a} + a^{2}\underline{U}_{b} + a\underline{U}_{c} \right)$$
(115)

where $a=\exp\left(j\frac{2\pi}{3}\right)$. In literature the time-dependent components are usually expressed as u^0 , u^+ , u^- , while the steady-state phasors are written as $\underline{U}_0,\underline{U}_1,\underline{U}_2$ [15].

2.4.3 Star and delta connections

The windings of a three-phase transformer are always connected in a certain way. The two most important types are the star connection and the delta connection, shown in figure 27 (a) and (b) respectively. These two configurations will first be considered in more detail.

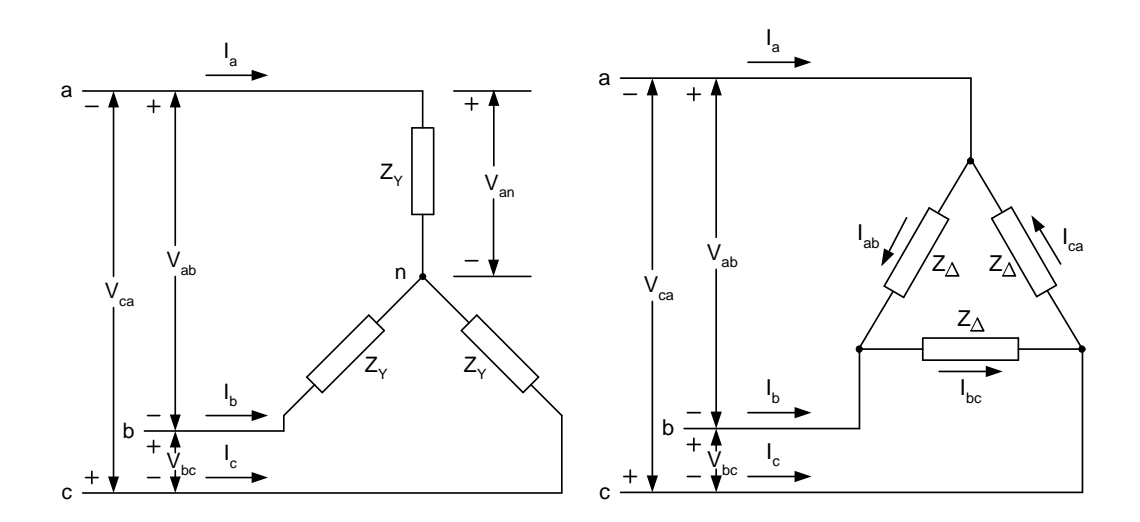


Figure 27: Star (a) and delta (b) connection of a three-phase system

Consider first the star connected system of figure 27(a). The line-to-line voltages can be written in terms of line-to-neutral voltages:

$$v_{ab}(t) = v_{an}(t) - v_{bn}(t) v_{bc}(t) = v_{bn}(t) - v_{cn}(t) v_{ca}(t) = v_{cn}(t) - v_{an}(t)$$
(116)

The zero-sequence component of this set of voltages can be determined with (114):

$$v_{ab}^{0}(t) = \frac{1}{\sqrt{3}} \left(v_{ab}(t) + v_{bc}(t) + v_{ca}(t) \right) = 0$$
(117)

This shows that *line-to-line voltages of a three-phase star connected circuit have no zero-sequence components*. Be aware that the line-to-neutral voltages can have zero-sequence components. When the neutral point is not grounded, it further holds that, due to Kirchhoff's current law:

$$i_a(t) + i_b(t) + i_c(t) = 0$$
 (118)

Consider now the delta-connected system of figure 27(b). The line currents are given as:

$$i_{a}(t) = i_{ab}(t) - i_{ca}(t)$$

 $i_{b}(t) = i_{bc}(t) - i_{ab}(t)$
 $i_{c}(t) = i_{ca}(t) - i_{bc}(t)$
(119)

The zero-sequence component of this set of currents can be determined with (114):

$$i_a^0(t) = \frac{1}{\sqrt{3}} \left(i_a(t) + i_b(t) + i_c(t) \right) = 0$$
 (120)

This shows that *line currents into a three-phase delta-connected circuit have no zero-sequence components*. According to Kirchhoff's voltage law it further holds that:

$$v_{ab}(t) + v_{bc}(t) + v_{ca}(t) = 0 (121)$$

2.4.4 Three-phase transformers

In three-phase transformers, different combinations of the star and delta configurations can be used. The first point that should be noted, is that the current in the secondary winding is equal to the current in the primary winding multiplied by the winding ratio, under the assumption that the relatively small magnetizing current can be neglected. In the same way is the voltage at the secondary winding equal to the voltage at the primary winding multiplied by the winding ratio, under the assumption that the voltage drop across the winding resistance and leakage inductance is negligible. The second point that should be noted is the fact that in a star-delta connected transformers the line-to-line voltages at one side will become line-to-neutral voltages at the other side and that line currents at one side will become phase currents at the other side.

The zero-sequence equivalent circuits of three-phase transformers depend on the connections of the primary and secondary windings. The most common type is the star-delta configuration with a grounded star-point. The zero-sequence circuit of this type of transformer is show in figure 28.

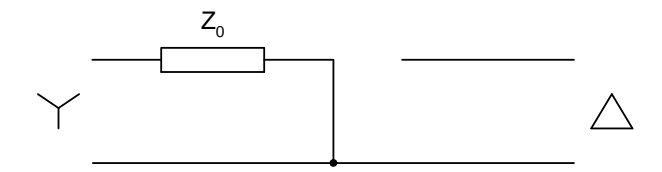


Figure 28: Zero-sequence equivalent circuit of star-delta transformer with grounded star point

It is shown previously that the line-to-line voltages of a star-connected circuit cannot have a zero-sequence component. Therefore, in a star-delta transformer, the line-to-neutral voltages at the delta side of the transformer will have no zero-sequence component, as long as the star side of the transformer is grounded. The transformer will therefore cause no zero-sequence voltage component at the star-side of the transformer.

As the neutral of the star winding is grounded, zero-sequence currents have a path to ground through the star because corresponding induced currents can circulate in the delta winding. The zero-sequence current circulating in the delta magnetically balances the zero-sequence current in the star but cannot flow in the lines connected to the delta.

An ungrounded star winding is a special case, where the impedance between the star point and ground is infinite. The zero-sequence impedance in figure 28 is infinite then, and zero-sequence current cannot flow.

The line currents into a three-phase delta-connected circuit have no zero-sequence components, as is shown previously, and therefore no zero-sequence currents can be transmitted through a delta-delta transformer, although it can sometimes circulate within the delta windings.

The only type of transformer in which zero-sequence currents can be transferred is the star-star transformer with both sides grounded.

Another point that should be mentioned is that there always must be two points that are grounded in a circuit in order to make zero-sequence currents possible.

2.4.5 NSW-park ERAO-II

We will now consider whether zero-sequence voltages or currents can occur in the NSW-park ERAO-II. The zero-sequence network of the park is shown in figure 29

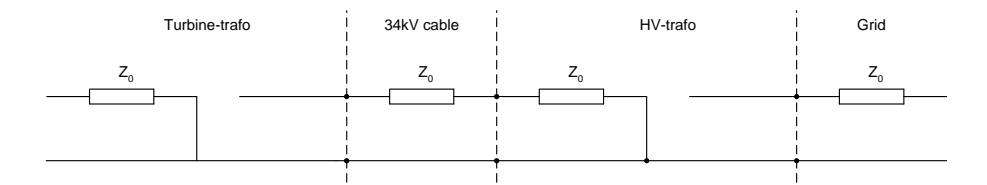


Figure 29: Zero-sequence equivalent network of NSW-park

Consider that, for any reason, the current in the grid will have a zero-sequence component. The grid-side winding of the HV-transformer is delta-connected and therefore the zero-sequence current can not pass to the 34kV cable. For the same reason it can be seen, that zero-sequence currents in the cable can not pass through the turbine transformer to the turbine.

The cable-side winding of the HV-transformer is star connected. Therefore, the line-to-line voltages can not have a zero-sequence component. The cable-side winding of the turbine-transformer is a delta-configuration. Therefore the line currents can not have a zero-sequence component. Thus, the cable does not have zero-sequence components in either the voltage or the current.

The only cause for a zero-sequence current and voltage in the cable, can be a single-phase or two-phase short-circuit from cable to earth. Zero-sequence current can then circulate through the short-circuit and the ground-connection of the HV-transformer. It has already been said, that this zero-sequence current will not pass through the turbine transformer to the wind turbine. Since in the Erao-2 study single-phase or two-phase short-circuits in the cable will not be considered, it is not necessary to include the zero-sequence components in simulations.

3 MODELS OF WIND AND WIND TURBINE

This chapter gives a summary of the models to be used for:

- the wind experienced by the rotor of a single stand alone turbine;
- two types of turbines: constant speed stall (CSS) and variable speed pitch (VSP).

These models are described extensively in the ECN-reports [25] and in [26].

3.1 Wind model

The changes in wind speed experienced by the rotor of a single stand alone turbine are determined by the undisturbed wind speed changes far in front of the turbine and by the properties of the terrain at the location of the turbine. Long term variations (1 or 10 minute average values) are determined by the Weibull distribution of the wind speed. The short term variations, called turbulence, depend strongly on the properties of the location.

To evaluate the effect of wind turbines and wind farms on the grid, the short term variation of the wind has to be known. Since wind speed variation is a statistically determined phenomenon, a wind model will calculate a realisation of the stochastically changing wind speed in time. Furthermore, the wind speed averaged over the turbine rotor has to be determined, including variations caused by the passing of the blades through the inhomogeneous wind field over the rotor area. The inhomogeneous wind field is caused by:

- wind shear (air is being slowed down near the earth's surface, causing a wind speed gradient with height);
- the tower (in front of the tower the air is also slowed down by stagnation).

When a power measurement of a turbine is taken, the effect of the wind field inhomogenity can clearly be seen by regular changes in power with a frequency of the number of blades times the turbine's rotational frequency, often called nP. The wind model aims at a realistic representation of this effect.

Summarizing, three effects will be included in the short term wind model: turbulence, wind shear and tower shade. The resulting wind realisation will be called the rotor effective wind, as opposed to the undisturbed wind.

3.1.1 Longitudinal turbulence model, tower passage and wind shear

The objective is to generate a single point wind speed realisation $\bar{U}+u^{\rm e}(t)$ which gives instantaneous aerodynamic torque values which are statistically equivalent to the values resulting from the logitudinal turbulence. The effect of wind speed variations on the aerodynamic torque is determined by the $C_{\rm p}(\lambda,\theta)$ -curves and the rotor diameter:

$$T_{\mathbf{w}}^{C_{\mathbf{p}}/\bar{U}+u^{\mathbf{e}}}(t) = C_{\mathbf{p}}(\lambda,\theta) \cdot \frac{1}{2}\rho\pi \cdot R^{2}(\bar{U}+u^{\mathbf{e}}(t))^{3}/\Omega$$
, (122)

This implies that the realisation not only depends on the statistical properties of the wind but also on the size and and aerodynamic properties of the turbine rotor. The method makes use of the Auto Power Spectral Density (APSD) of the longitudinal wind speed changes in a single point and is derived in the documentation of the ECN CONTROLTOOL [25]. It is assumed that:

- 1. the APSD is invariant in the rotor plane;
- 2. the effect of distance on the coherence decrement is invariant in the rotor plane;
- 3. the rotor is rigid;
- 4. the rotor speed is constant.

Assumptions 1-3 are sufficiently satisfied, for assumption 4 this is not always true. For variable rotor speed, a statistically equivalent wind speed realisation can be made for the average speed. Figure 30 shows the dependence of the coherence of wind speed variations for different rotor diameters. For a given rotor diameter, the coherence of the variations decreases with the frequency of the changes, i.e. faster changes are more likely to be different at different point in the rotor plane. For a given frequency, the coherence of the variations also decreases for increasing turbine diameter. The figure shows that for rotor diameters larger than 20 m the coherence of variations above 0.3 Hz is practically zero at 10.4 m/s wind speed. At higher wind speeds, the coherence at a given frequency will increase.

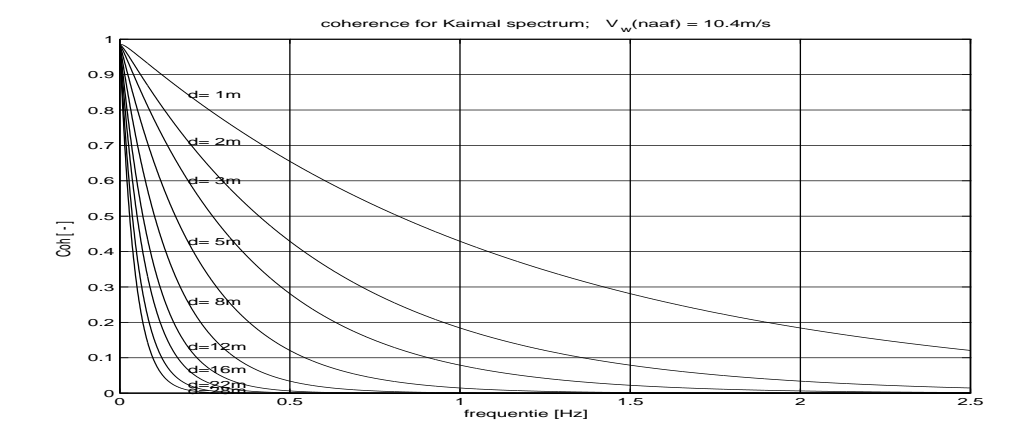


Figure 30: Coherence spectra for turbines of different size

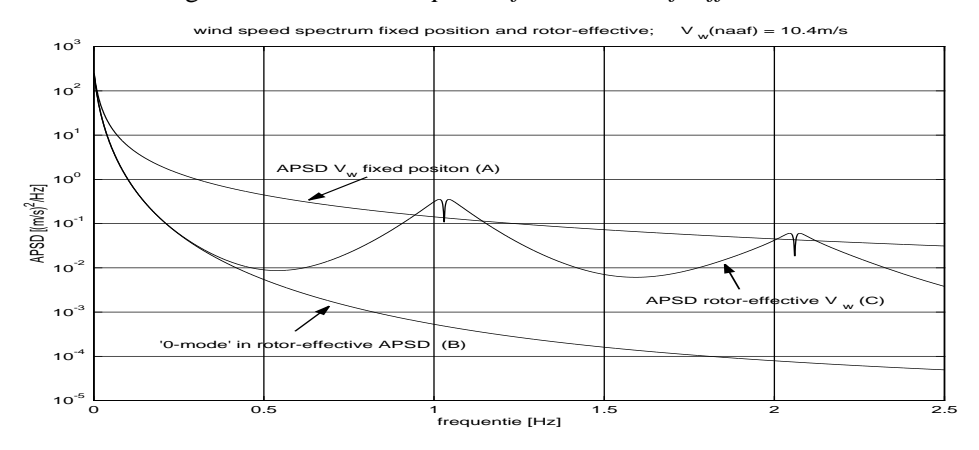


Figure 31: Effect of rotor averaging and rotational sampling on the wind autopower spectra

Figure 31 demonstrates the effect of the rotor dependent statistically equivalent longitudinal turbulence model. Line (A) represents the single point wind speed variations. If the rotor averaging of the turbulence is applied, line (B) spectrum results. The rotor thus acts as a

low pass filter: high frequencies are damped. This rotor effective spectrum is called the '0-mode' spectrum, as opposed to the nBP modes (n=1,2,...; B=number of blades; P=rotational frequency) caused by the sampling of the tower wake and wind shear. Line (C) represents the sum of 0-mode and nBP modes and is referred to as the 'rotor-effective' wind speed.

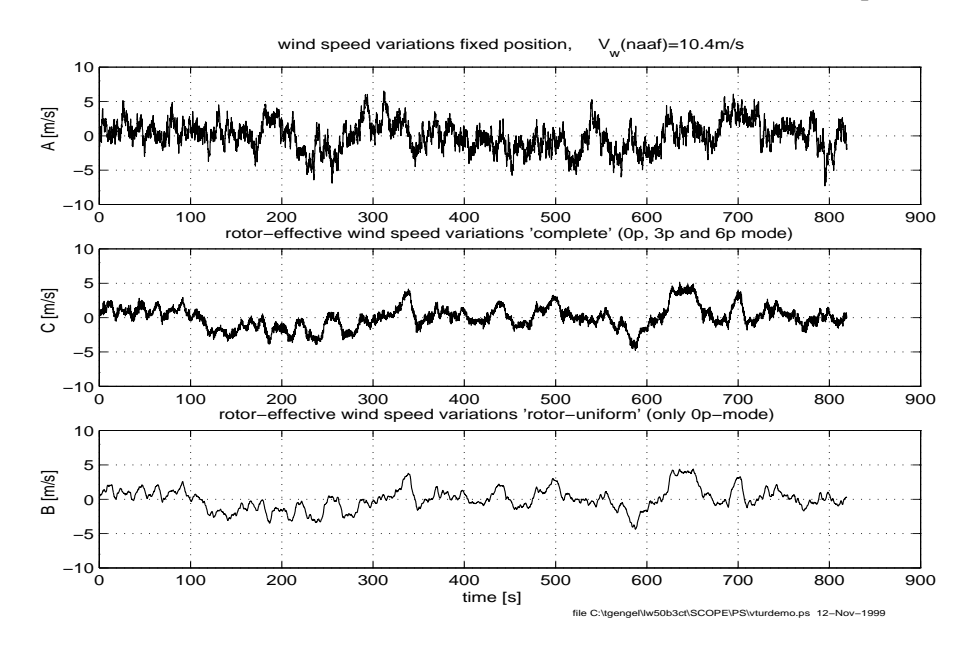


Figure 32: Wind speed variations in a single point (A) and averaged over the turbine rotor (0-mode (B) and complete (C))

3.2 Turbine models

Most large wind turbines, installed for electricity production and connected to a utility grid, are horizontal axis turbines. Four turbine types can be discriminated:

- 1. Constant speed stall controlled;
- 2. Constant speed active stall controlled;
- 3. Constant speed pitch controlled;
- 4. Variable speed pitch controlled.

The majority of the current turbine designs are of type 1 or 4. Type 2 is developed only by a few manufacturers and type 3 only works well with a method to increase the slip of the generator. This option nowadays is abandonned in favour of (partial) variable speed design. In the Erao-2 study only turbine types 1 and 4 will be considered.

The turbine models consists of submodels for:

- aerodynamic behaviour of the rotor;
- rotating mechanical system (drivetrain);
- tower (viz. motion of the tower top);
- control system (power limitation by pitch control, yaw control is not included).

3.2.1 Aerodynamic conversion, rotation and torsion

Figure 33 gives an overview of the aerodynamic and mechanical model. From right to left the following aspects are included in the model:

- axial force F_{ax} and aerodynamic torque T_{ae} on the rotor;
- position of the rotor blades (azimuth Ψ);
- inertia of the blades and hub J_r ;
- gearbox ratio i;
- low and high speed shaft torsion γ ;
- generator inertia J_g and generator speed Ω_g .

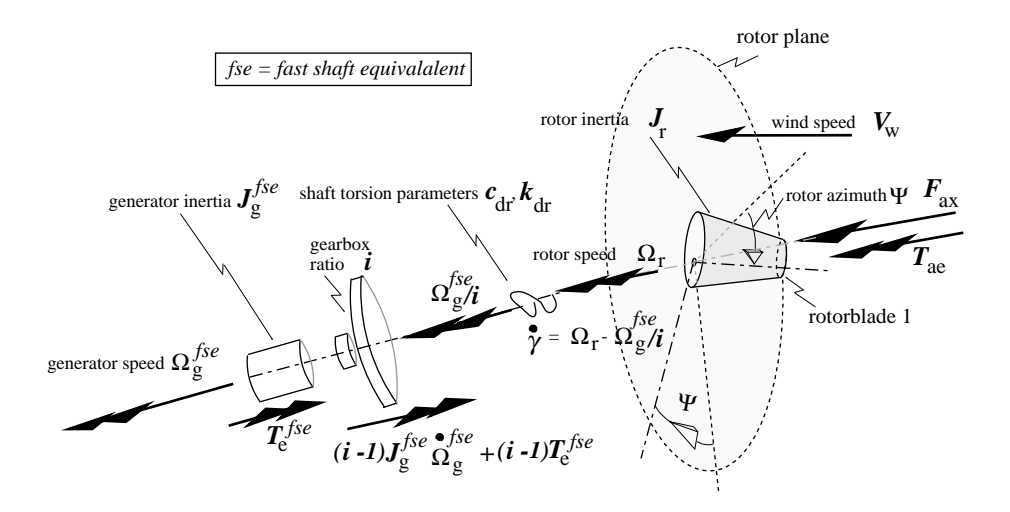


Figure 33: Model of the mechanical system

The aerodynamic conversion model determines the axial force F_{ax} and aerodynamic torque T_{ae} and is based on the quasi-steady state rotor coefficients for power $C_p(\lambda,\theta)$ and axial force (thrust) $C_t(\lambda,\theta)$. For pitch-to-vane turbines a correction for dynamic inflow is added. The rotor characteristics depend on the rotor design and are calculated by an aero-elastic code, for instance the ECN computer programme PHATAS. Figure 34 gives an example of the rotor coefficients of a variable speed turbine as function of the pitch angle θ and the tip speed ratio λ .

The mechanical model for turbine rotor, low and high speed shaft, gearbox and generator rotor consits of a two-mass spring and damper model. The torque of the gearbox and generator on the nacelle is determined, since it interacts with the tower naying.

3.2.2 Tower mechanical model

Figure 35 gives an overview of the forces and moments acting on a turbine tower and the resulting tower top motion. At the far right the thrust F_{ax} from the wind on the rotor is shown. The reaction torque of the gearbox and generator $(i-1)J_g\Omega_g+iT_e$ is the second variable. The rotor speed is represented by Ω_r . The tower top motion is decomposed in two directions:

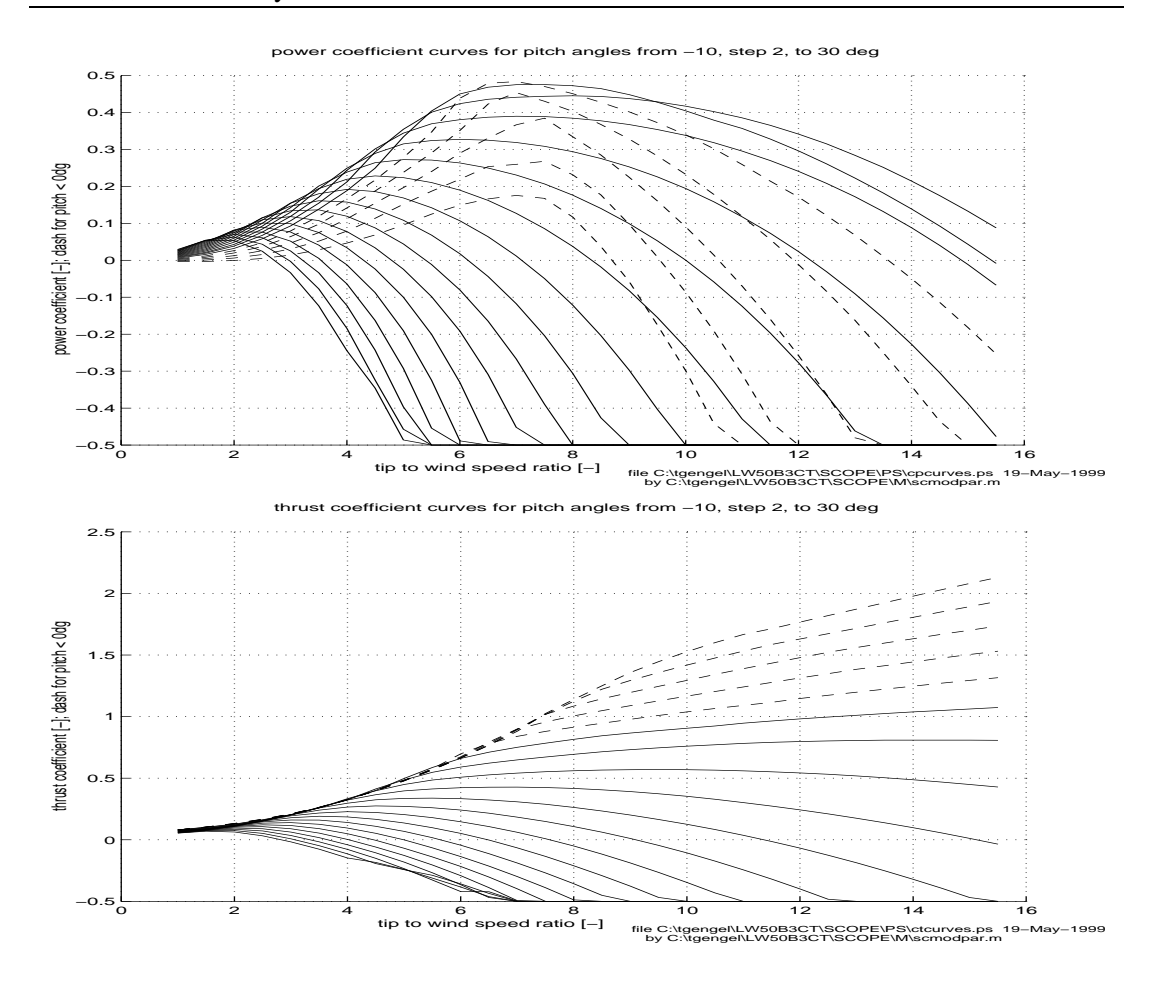


Figure 34: Power and thrust coefficient of a 'pitch to vane' windturbine

in the direction of the wind speed (front-aft motion or 'nodding') x_{nod} , and perpendicular to that direction (sideways motion or 'naying') x_{nay} . The yaw angle and yaw torque are given by α and T_{krui} . The figure includes the effect of waves on the tower, which can be neglected for land based turbines.

The simple tower model consists of two mass-spring-damper models for linear motion (translation): one for nodding and one for naying. This is not sufficient if tower top rotation has to be modelled as well. In that case, a lumped parameter model for rotation is used, consisting of a number of mass-spring-damper-models in series.

3.2.3 Pitch control and electrical torque setpoint

The pitch control algorithm regulates and limits the rotor speed and optimises energy yield under the restriction of only positive tower tilt moments.

The control structure comprises:

- 2 operation modes: partial load and full load
- 2 actuation setpoints: pitch rate and electric torque
- 3 measurements: pitch (reference) angle, rotor speed, electric power

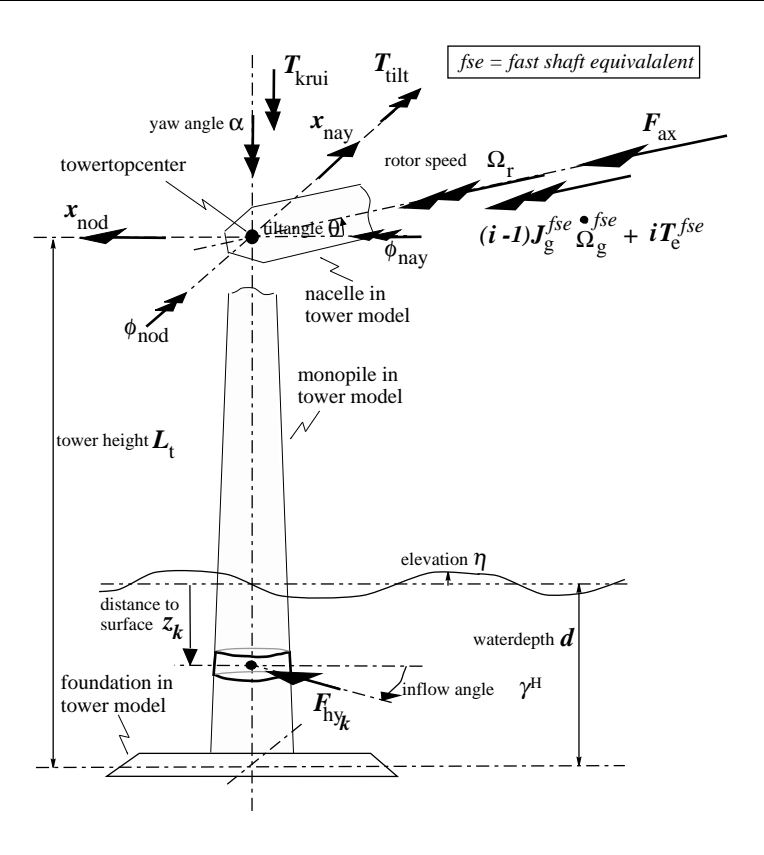


Figure 35: Axissymmetric monopile tower model

The principles of both the pitch control and electric torque control algorithm will be discussed below.

Pitch control algorithm

Start-up is simply realised by moving the pitch angle with constant pitching speed from feathering position towards working position. Shut down is out of the scope, because the overall control system will manage this.

Partial load operation will take over as soon as the measured pitch angle is close to the pitch angle setpoint for partial load operation. This setpoint is dependent of the measured rotor speed and is naturally close to zero. Usually, the pitch angle during partial load operation is related to the theoretical maximum aerodynamic efficiency (maximum power coefficient, C_p), but in practice requirements like noise and thrust loading could also be decisive. Therefore, the rotor speed dependency of the pitch angle setpoint during partial load operation can be manually adjusted to empirical values. The setpoint value is realised by servo control (proportional pitch angle control) using a specific maximum pitching speed. Because of the required small pitch adjustments during partial load operation maximum speed is set to $0.8 \, \mathrm{dg/s}$.

The transition to the full load control algorithm interacts with the electric torque control in order to maximise the energy yield. A transition to partial load will only take place if the measured pitch angle has already reached its working position and the rotor speed has decreased below rated. Reversely, transition from partial load to full load operation is based on a rotor speed threshold level, such that too many transitions are avoided.

During full load control the rotor speed is limited to a maximum value, while rated power production is maintained.

The core is a linear PD control structure, that feeds the low pass filtered rotor speed (propor-

tional part) and acceleration (differential part) back to a setpoint value of the pitching speed. The pitch actuators of each blade will then set the pitch angle simultaneously to a suitable position to regulate the rotor speed between its rated and maximum value. The measured value of the rotor speed is filtered by a cascade filter which consist of a fourth order inverse Chebychev low pass filter (3p effects) and two band notch ellipse filters to reduce collective lead lag effects and tower influences. To deal with the non linear aerodynamic behaviour, some non linear extensions are added to meet satisfactory performance:

- linear controller gains are scheduled dependent on both the actual blade angle and rotor speed; with gain scheduling the linear controller is adapted to the whole operation envelope of the wind turbine;
- an inactivity zone with hysteresis is implemented, to avoid undesired pitch angle adjustments due to small controller corrections caused by noise, tower shadow, rotational sampling effects etc;
- pitching bounds (speed and angle) are incorporated to limit the calculated pitch speed values;
- non linear compensation of the calculated pitching speed is used to cancel foreseen amplification due to 'dynamic inflow effects' (rotor wake effects).

To ensure no excess of maximum rotor speed, a mechanism called 'forced rotor speed limitation' is permitted to overrule the closed loop rotor speed control loop by forcing the pitch angle quickly (3dg/s) -but for as short a period of time as possible- in vane direction. This is only active if the actual rotor speed exceeds a certain safety level and is still accelerating to avoid turbine shut down.

Power production optimisation is incorporated by a mechanism, named 'estimated wind speed feed forward' which adds a non linear control action to the pitching speed setpoint based on the reconstructed value of rotor effective wind speed. The reconstruction is based on filtered measured values of rotor speed, pitch angle, electric power and theoretical aerodynamic properties of the rotor. In case of sufficient bandwidth of electric torque actuation, the power measurement can be replaced by the electric torque setpoint. Estimated rotor speed feed forward results in higher energy yield, less rotor speed fluctuations and smaller pitch actions. From viewpoint of stability 'estimated wind speed feed forward' can be seen as DD feedback control of rotor speed (jerk). For stability reasons and optimal use of this mechanism the following extensions are added:

- non linear scheduling to meet rated power production in the whole operation region;
- 'feed forward' weakening to ensure stability and adjust the amount of power optimisation;
- if rotor speed is below rated level then this optimisation supports only pitch actions in working direction;
- if rotor speed is near maximum rotor speed level then this optimisation supports only pitch actions in vane direction.

A collection of Nyquist plots which cover the turbine operation area assess system stability.

Electric torque setpoint

Electrical torque control is used to determine the power production below rated speed. It is also a valuable actuation port to increase the energy yield around rated conditions if small electrical torque variations (3%) of its rated value are permitted. A mechanism to cross the first bending mode of the tower can also be incorporated.

The electric torque control algorithm generates the torque or power setpoint for the controller of the generator side converter and consists of four operating ranges:

- 1. turbine start-up;
- 2. constant tip-speed-ratio operation (partial load);
- 3. transition between constant tip speed and constant power operation (full load);
- 4. finally constant power operation.

Figure 36 illustrates these operating ranges, best seen in the plots of power and torque against rotor speed. In the torque-wind speed plot, the rectangular area indicates constant power during speed excursions.

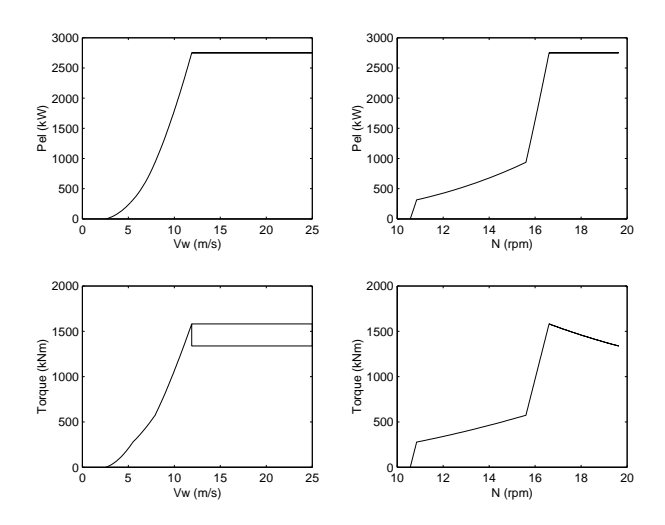


Figure 36: NM92 characteristic curves

If the first bending mode of the tower is situated around its rated speed equivalent, a mechanism has been integrated to cross this point of resonance quickly to avoid excessive tower vibrations (excitation by rotor unbalance). The transition zone from partial load to full load is dynamically implemented. The transition part as shown is valid in case of partial load control. From full load control, the 'constant' power curve limit is extended until the pitch angle is in working position. Mean rated power is guaranteed by additional corrections in full load.

4 DYNAMIC MODELS OF WIND FARMS IN SIMULINK

This chapter lists and explains the four Simulink models of wind farms developed in the Erao-2 project. In this chapter the term phasor is used for the dq0-vector representing voltages, currents or fluxes in the Park reference frame, as discussed in chapter 2. It should not be confused with phasors representing AC quantities with constant angular frequency. The dq0-phasor angular frequency is variable.

In Simulink blocks inputs and outputs and a certain execution order should be defined. The wind turbine has been considered as the starting point. The problems is that not both the voltage and the current can be determined at the wind turbine. It has been assumed that the voltage is determined by the grid voltage. The voltage at the wind turbine terminals can then be defined from the voltage of the grid plus the voltage drop across the cable and transformer impedances. For this reason the grid-side voltage and the turbine-side current has been considered as input for all blocks. Based on these inputs the turbine-side voltage and the grid-side current are determined as outputs.

4.1 Constant speed stall controlled wind farm

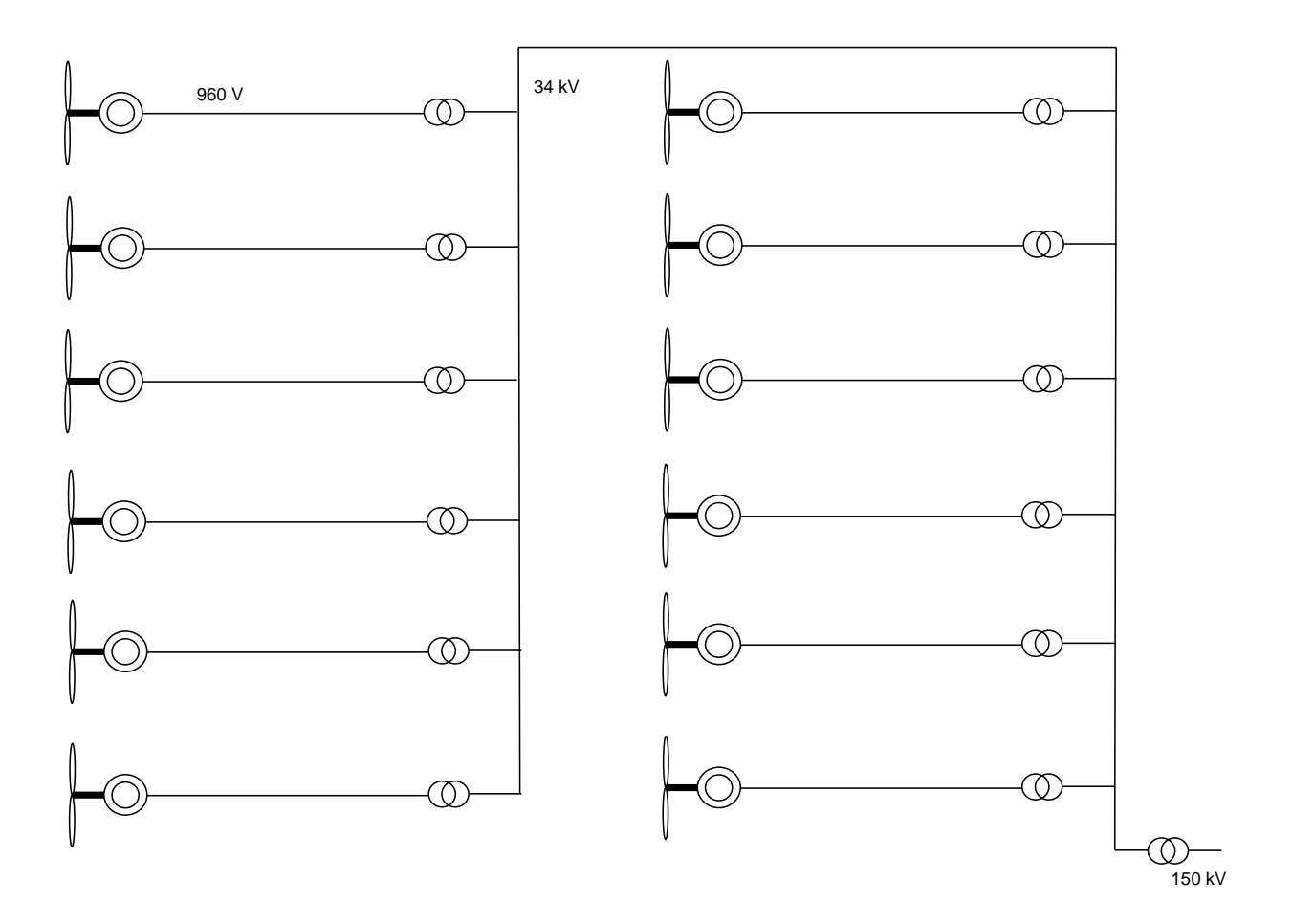


Figure 37: Electrical layout of a string of 12 CSS turbines

The constant speed stall (CSS) controlled wind farm model consists of 12 stall regulated turbines with directly connected induction machines, one string of the Near Shore Wind farm. The

model includes turbine transformers, cables in the wind farm, cable to shore and high voltage transformer in the substation on shore (figure 37). The main window of the Simulink model connects twelve turbines 12 turb + cables through a transformer 34kV/150kV trafo to the 150 kV grid model (figure 38). Separate blocks generate individual wind input for all turbines and plot simulation results.

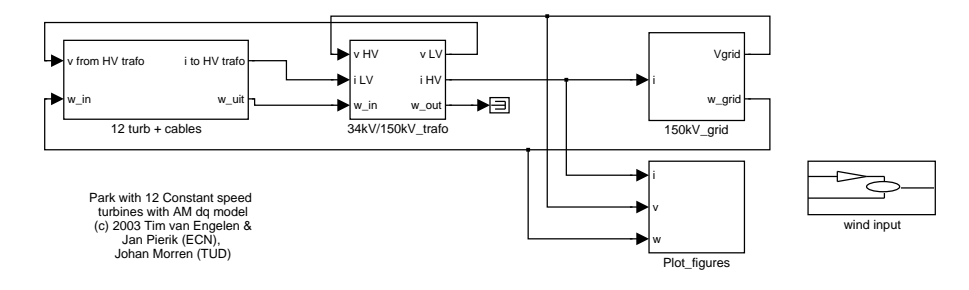


Figure 38: Simulink CSS wind farm model main window

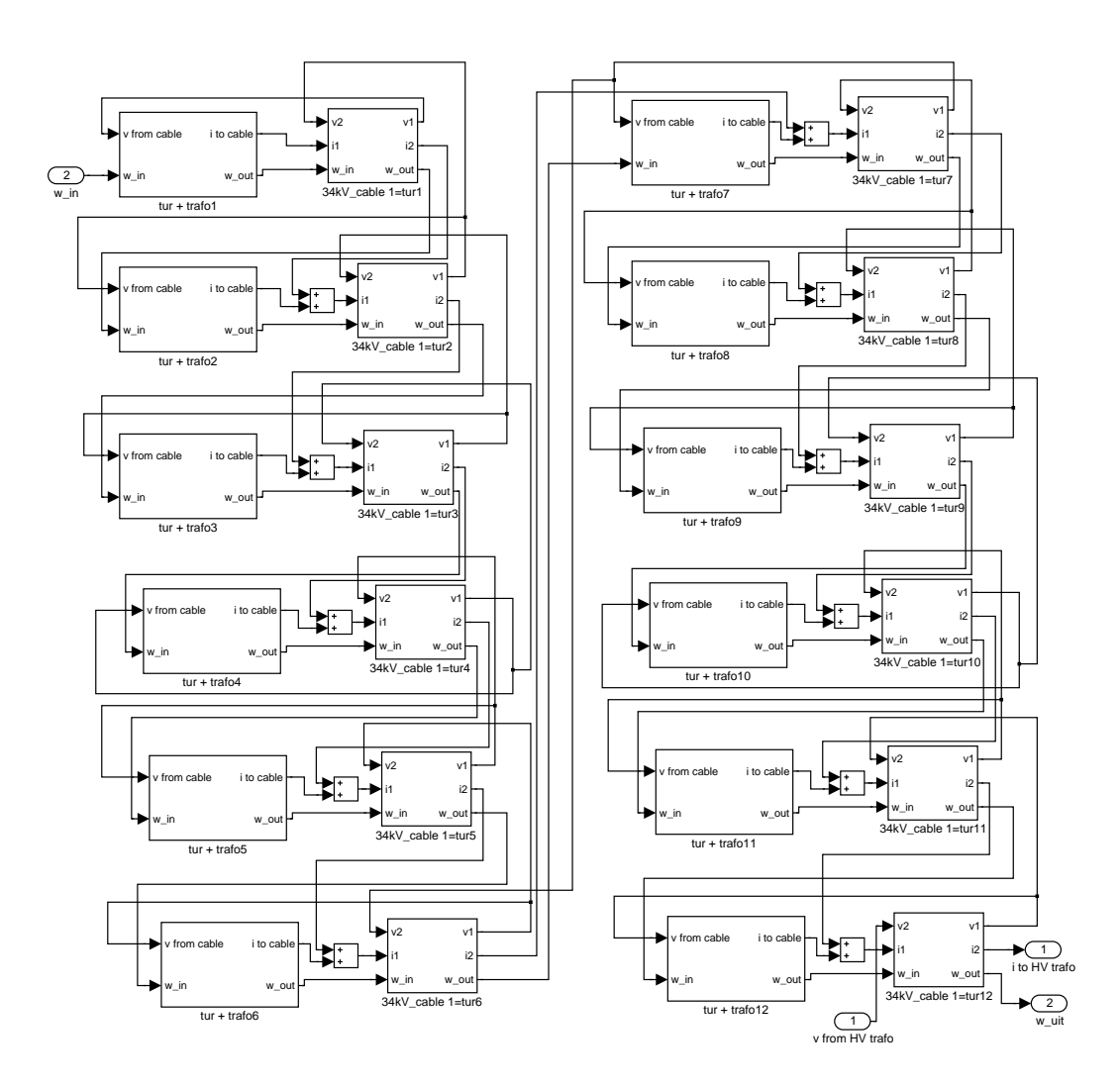


Figure 39: 12 turb + cables: 12 CSS turbines and interconnecting cables

The wind farm block (figure 39) connects 12 turbines and 12 cables. The voltage dq0-phasor at each cable end is input for the turbine and transformer model, the current dq0-phasor is

output. The turbine and transformer model calculates the current phasor, which is returned to the cable model. The turbine current phasor and the current phasor from the cable connecting the other turbines are added before entering the next cable. This is repeated for all 12 turbines and cables.

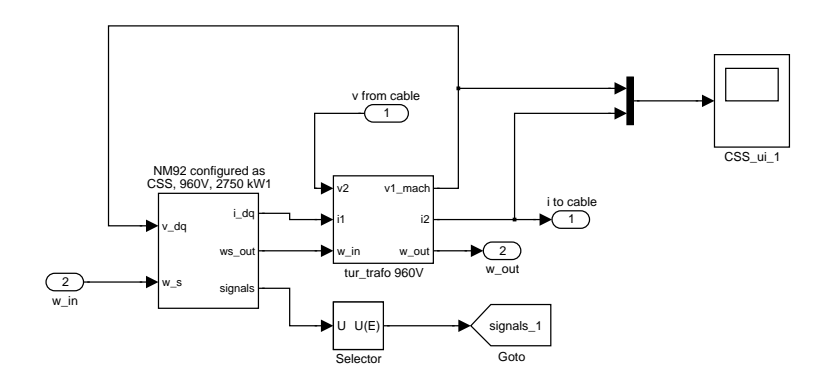


Figure 40: turb + trafo 1: CSS Turbine and 960V/34kV transformer 1

Figure 40 shows the turbine and transformer model, consisting of a NM92 turbine block and a 960V/34kV transformer block. The cable voltage phasor and the current phasor from the turbine are the inputs of the transformer block. The transformer block calculates low voltage side output voltage and high voltage side current. The transformer output voltage is fed to the turbine model, the output current is input to the 34 kV cable.

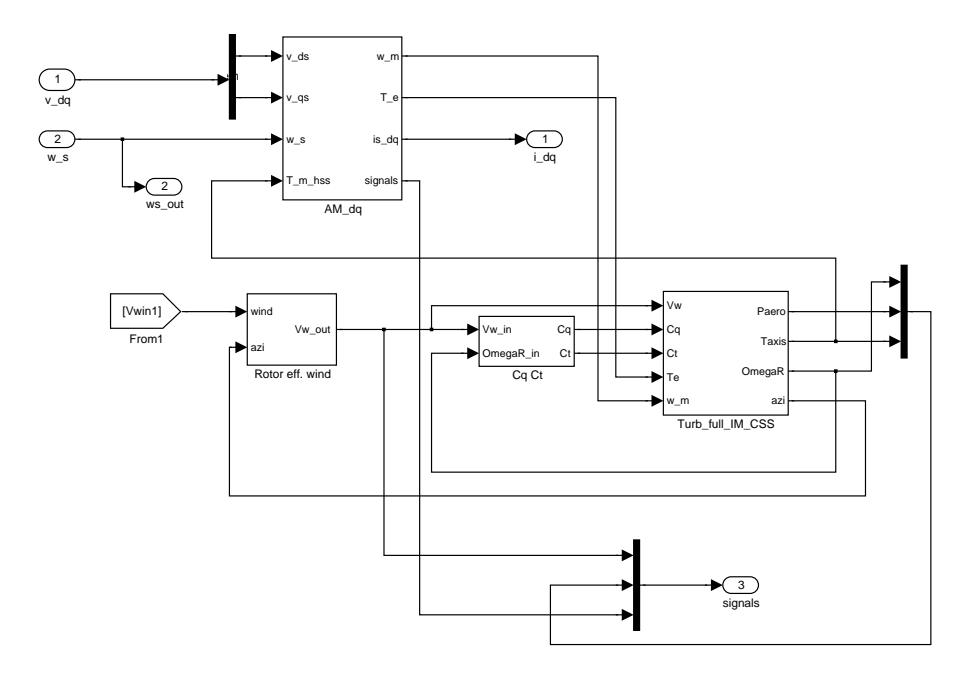


Figure 41: NM92 configured as ...: constant speed stall turbine model

The turbine block consists of the generator model ($AM\ dq$), the calculation of the rotor effective wind ($Rotor\ eff\ wind$), the aerodynamic coefficients (CqCt) and the block containing the mechanical equations of turbine shaft and tower ($Turb\ full\ IM\ CSS$).

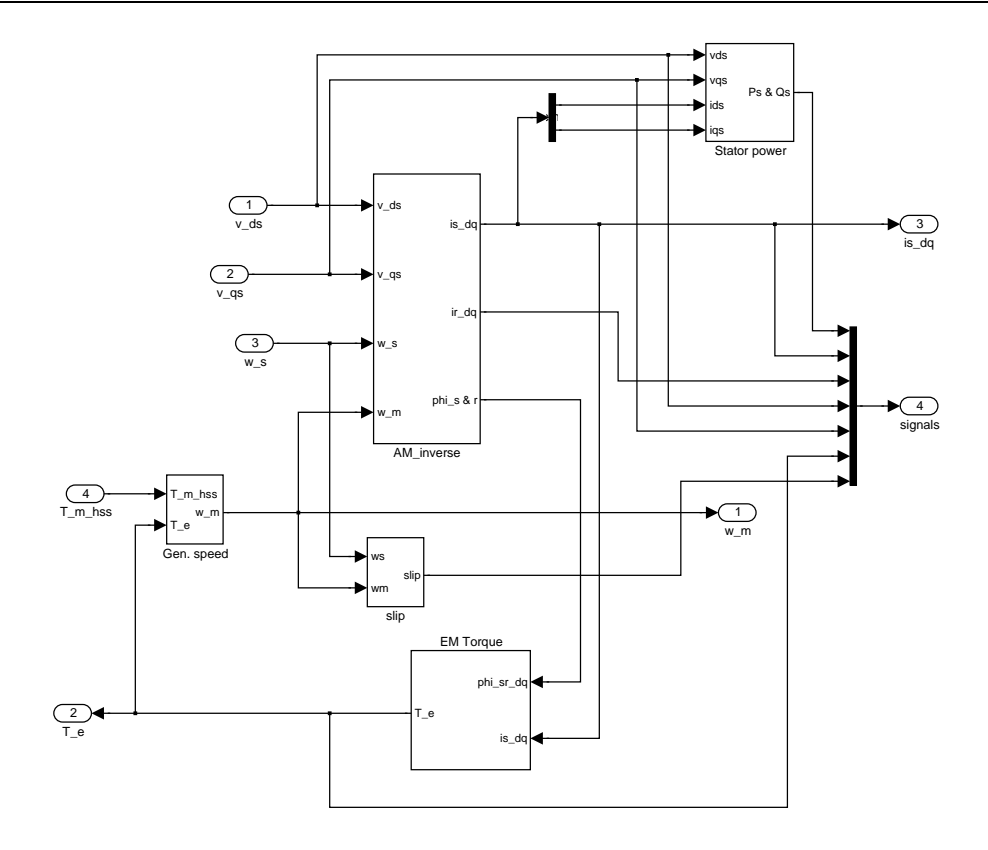


Figure 42: AM dq: induction generator model

The induction machine model (AM dq, figure 42) calculates the stator and rotor current phasors, the electromagnetic torque and the rotor angular speed ω_m . Inputs are the stator voltage phasors, the electrical angular speed ω_s and the mechanical torque.

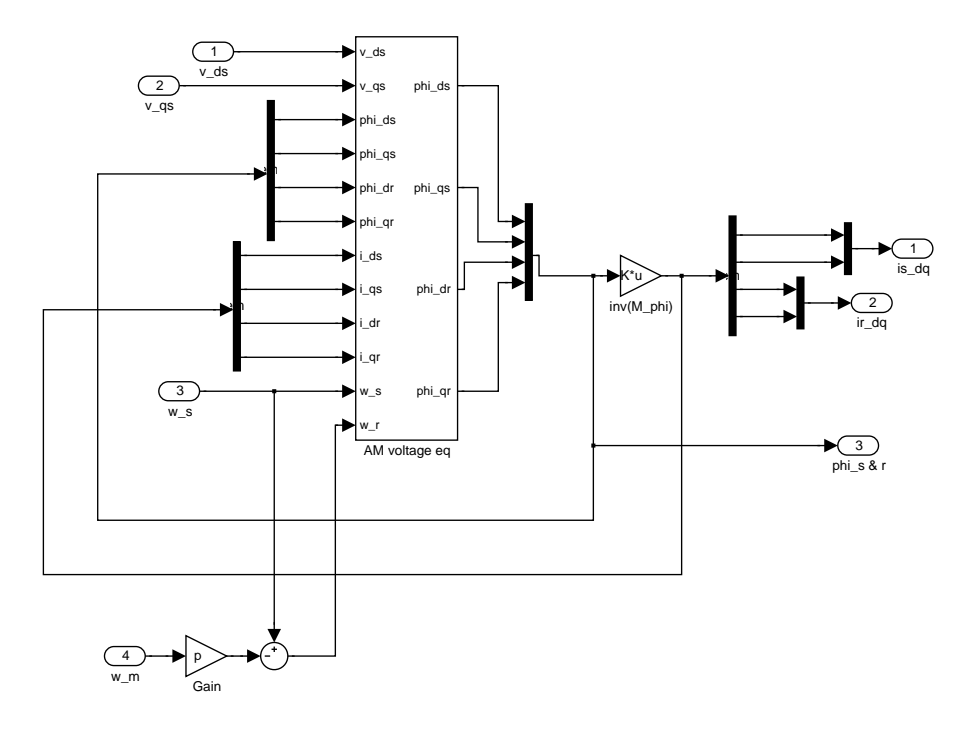
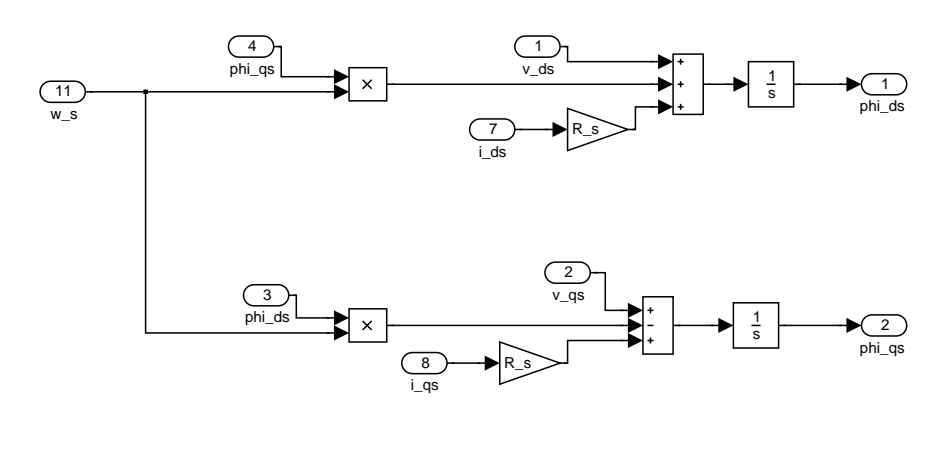


Figure 43: AM inverse: input for the voltage equations



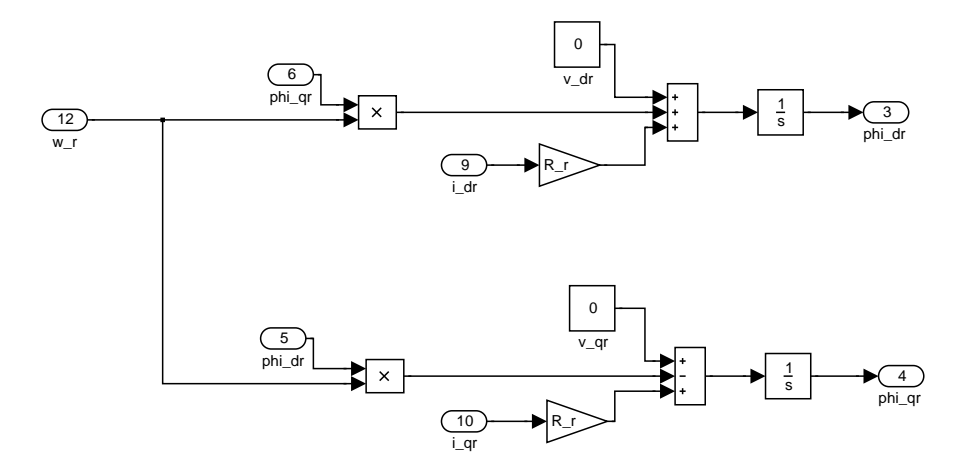


Figure 44: AM voltage eq: induction machine voltage equations

The stator and rotor voltage equations in figure 44 determine the stator and rotor flux phasors $\psi_{sq}+j\psi_{sd}$ and $\psi_{rq}+j\psi_{rd}$ (equation 64 and 65). The current phasors are calculated from the flux phasors in *AM inverse*, figure 43.

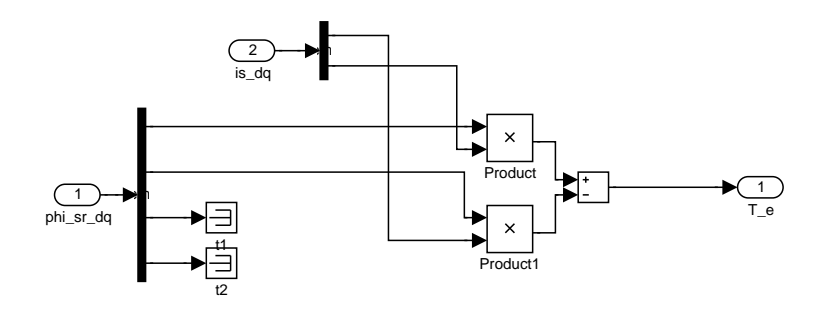


Figure 45: EM torque: calculation of the electromagnetic torque

The electromagnetic torque is calculated from stator flux and stator current (figure 45), followed by the calculation of the induction machine rotor speed (figure 46).

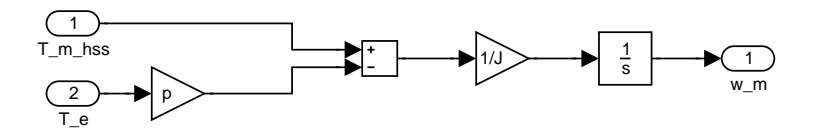


Figure 46: Gen. speed: Induction machine speed

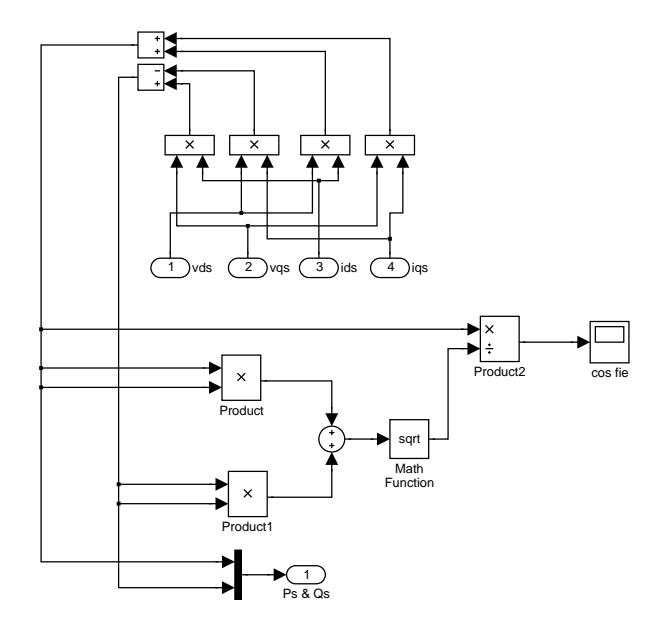


Figure 47: Stator power: Induction machine power and reactive power

Induction machine stator power and reactive power are calculated from the stator voltage and current phasors (figure 47), which completes the induction machine model.

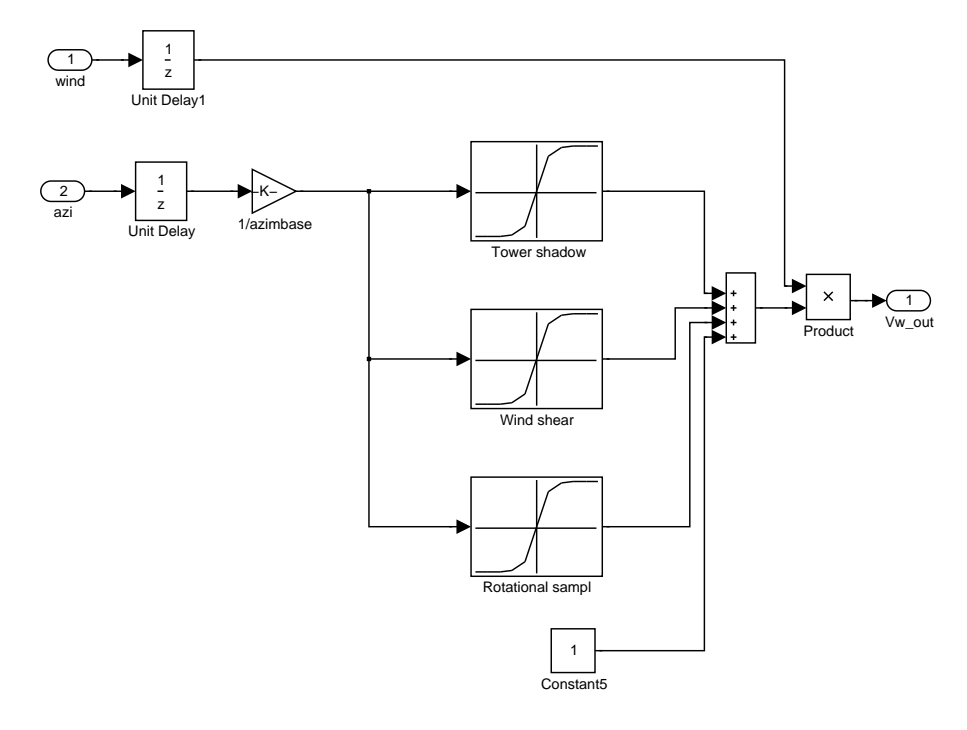


Figure 48: Rotor eff. wind: Rotor effective wind calculation

To calculate the rotor effective wind, tower shadow, wind shear and rotational sampling is taken into account (figure 48). A preprocessor is used to calculate a scaled relation between the azimuth angle and the contributions of tower shadow, wind shear and rotational sampling to the effective turbulence of the specified rotor. In the simulation, the turbulence is scaled with to the instantaneous wind speed.

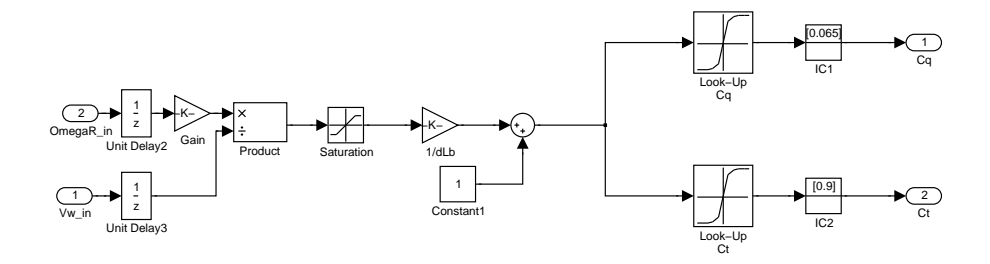


Figure 49: CqCt: Torque and thrust coefficients

The areodynamic torque and thrust coefficients are calculated by look-up tables (figure 49).

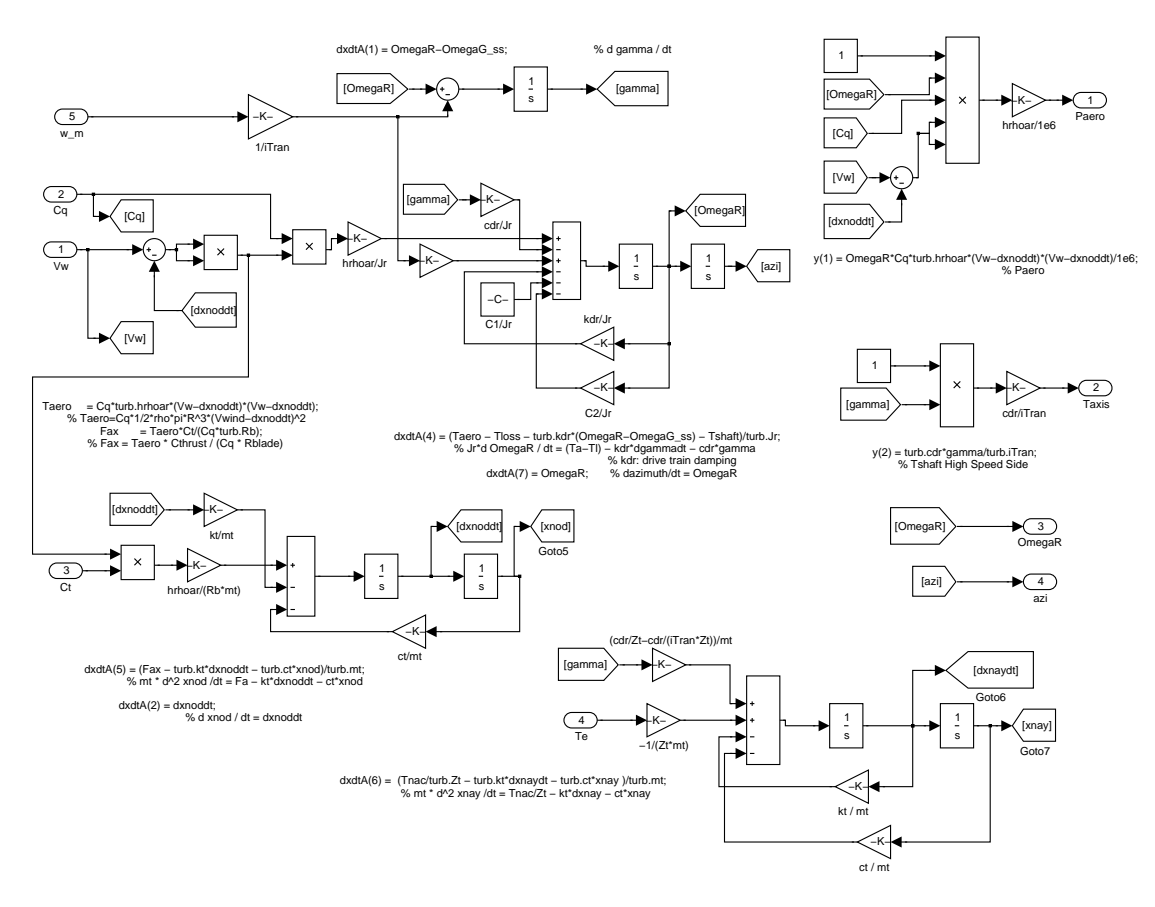


Figure 50: Turb full IM CSS: turbine shaft and tower

The motion of the turbine rotor, shaft and tower is modelled in figure 50. Yaw control is not included in the model.

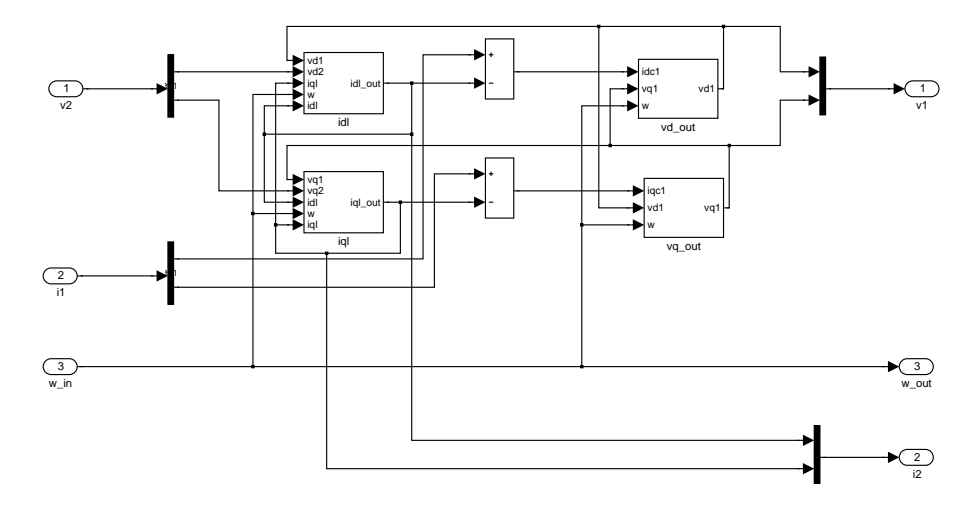


Figure 51: 34kV cable: park cable

The cable model (figure 51) calculates grid side current and turbine side voltage from the input variables turbine side current and grid side voltage. The d-component of the grid side current is determined in figure 52, the d-component of the turbine side voltage is determined in figure 53.

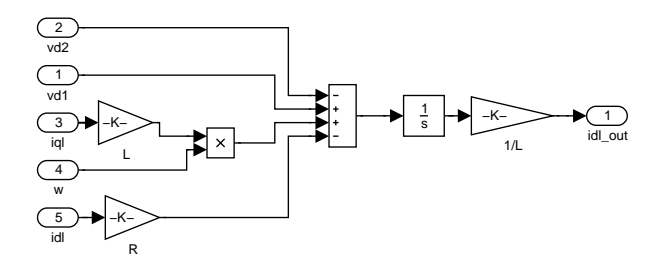


Figure 52: idl: park cable calculation id

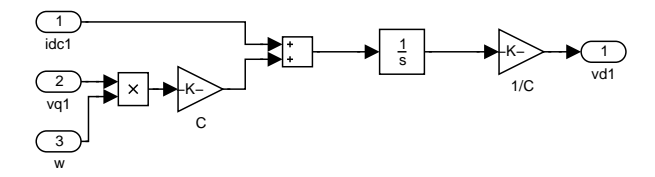


Figure 53: vd out: park cable calculation ud

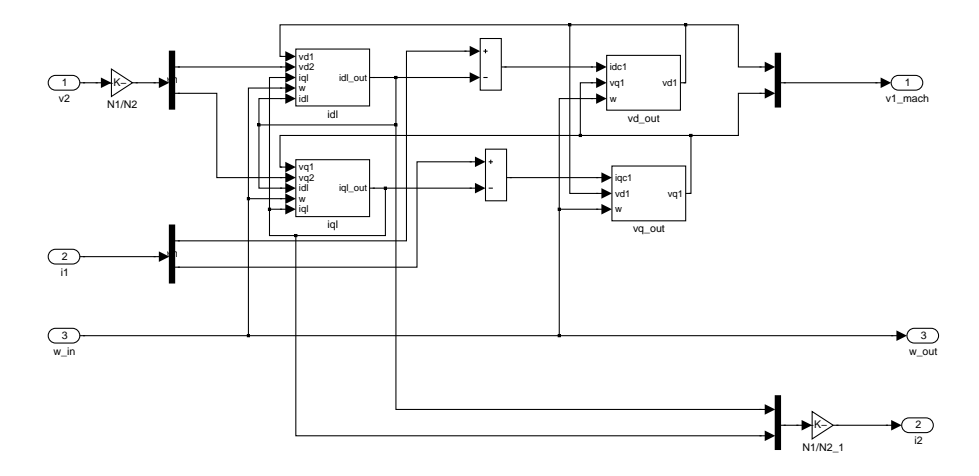


Figure 54: 34kV/150kV trafo: park transformer

The park transformer connects the wind farm to the 150 kV cable to feed the wind power to the substation on land. The magnetizing current of the transformer is neglected and a capacitor has been placed at the primary side of the transformer, as has been explained in section 2.3.2. Therefore, the transformer model is similar to the cable model, see figure 54. The only difference is the winding ratio $\frac{N_1}{N_2}$.

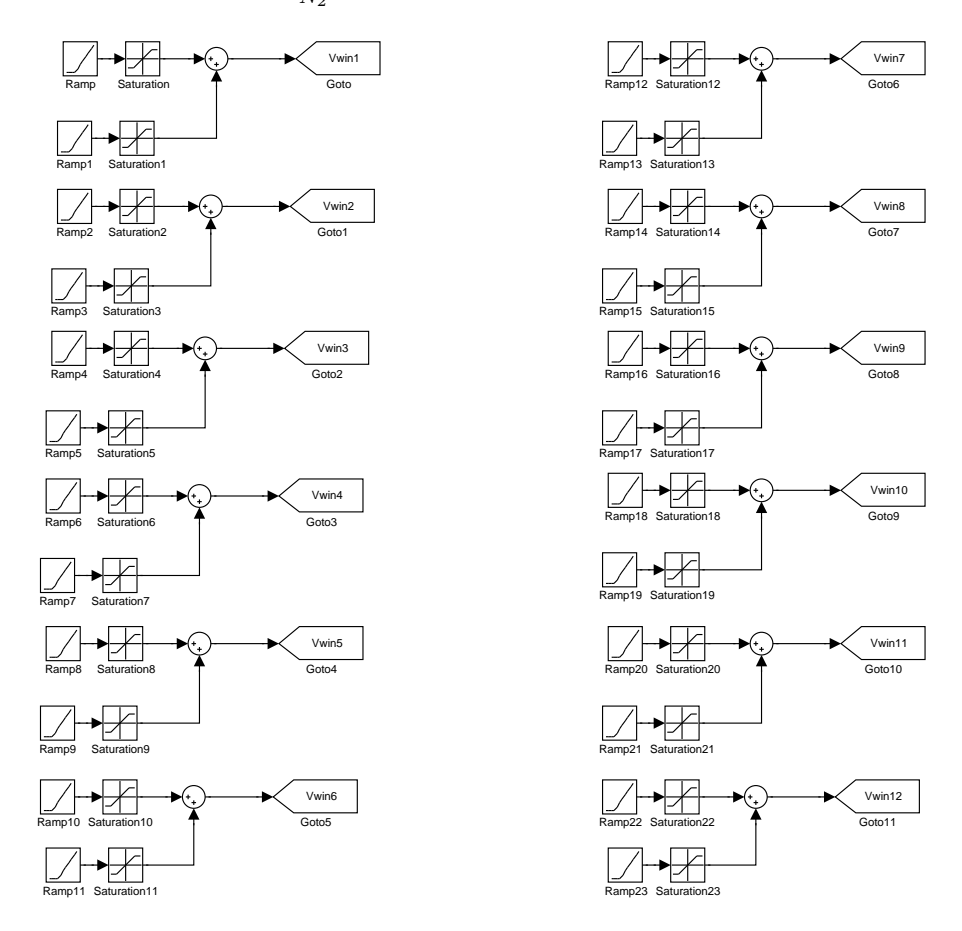


Figure 55: wind input: 0-mode wind input for individual turbines

The wind speed for each turbine is specified separately in the *wind input* block, see figure 55. Aerodynamic effects of the park layout can be included if the individual wind speeds are

calculated by a wind farm aerodynamic code, i.e. *FindFarm*. The grid model used in all wind farm models is described in section 4.5.

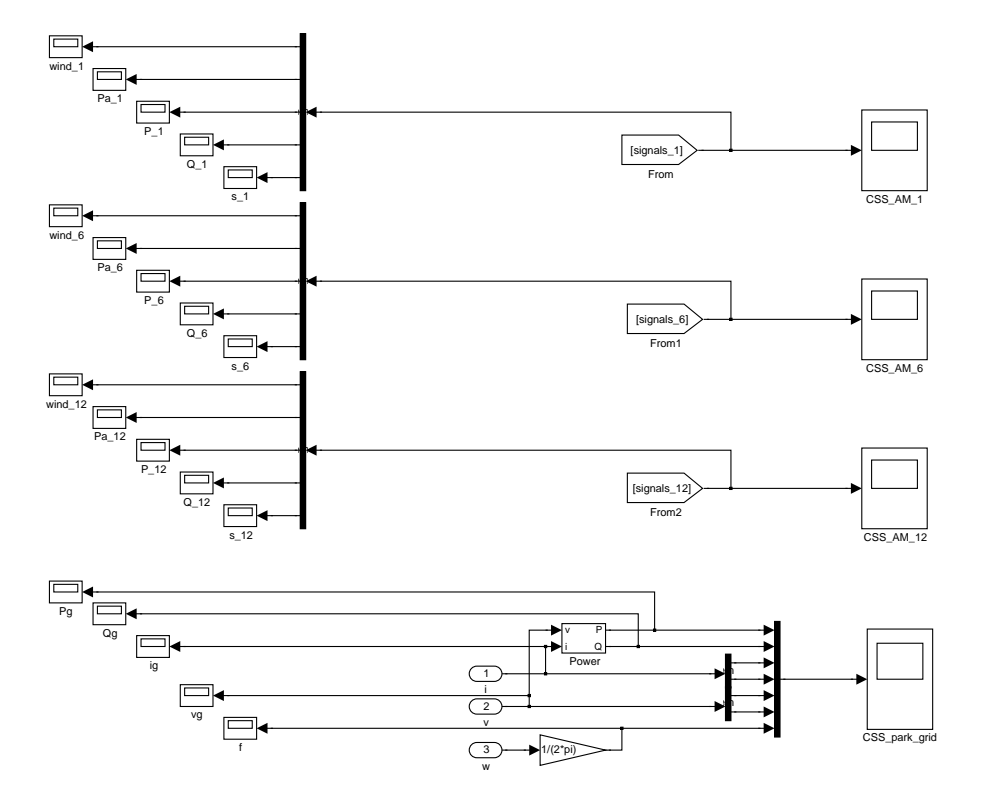


Figure 56: Plot figures: Collection of turbine output variables

A selection of variables is collected for turbines 1, 6 and 12, as well as overall quantities for the whole wind farm, see figure 56.

4.2 Constant speed stall controlled WF with cluster controlled induction machines

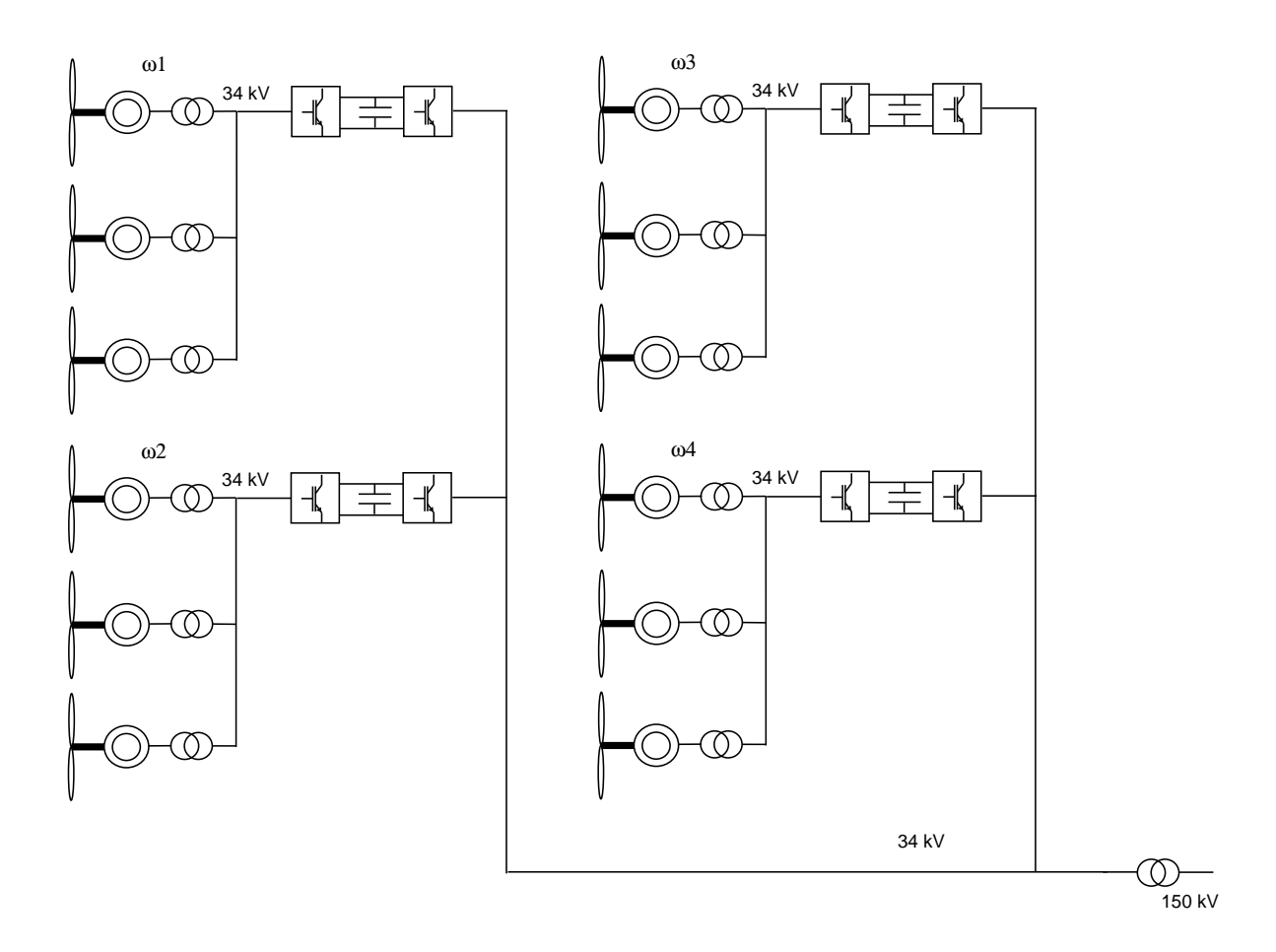


Figure 57: Electrical layout of four strings of 3 cluster controlled turbines

One string of the cluster controlled constant speed stall (CSS-CC) wind farm consists of four clusters of three stall regulated turbines (figure 57). The Simulink farm model consists of only one group of three turbines including turbine transformers, the cluster converter, cables in the wind farm, cable to shore and substation high voltage transformer. The Simulink model connects the cluster through the 34 kV cable and 34kV/150kV transformer to the 150 kV grid model (figure 58). Separate blocks generate individual wind input for all turbines and plot simulation results.

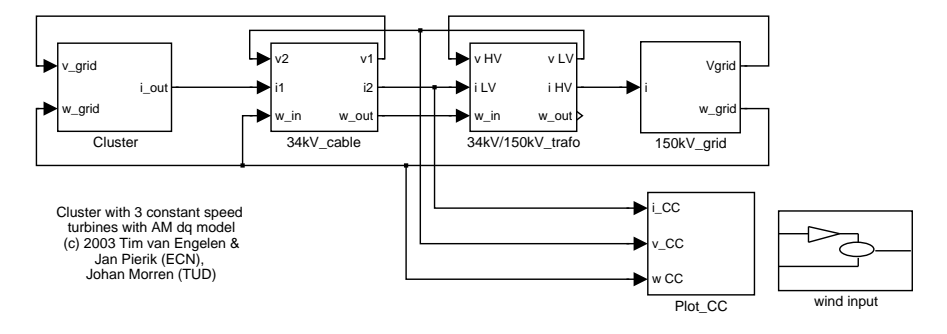


Figure 58: Simulink CC wind farm model: Main

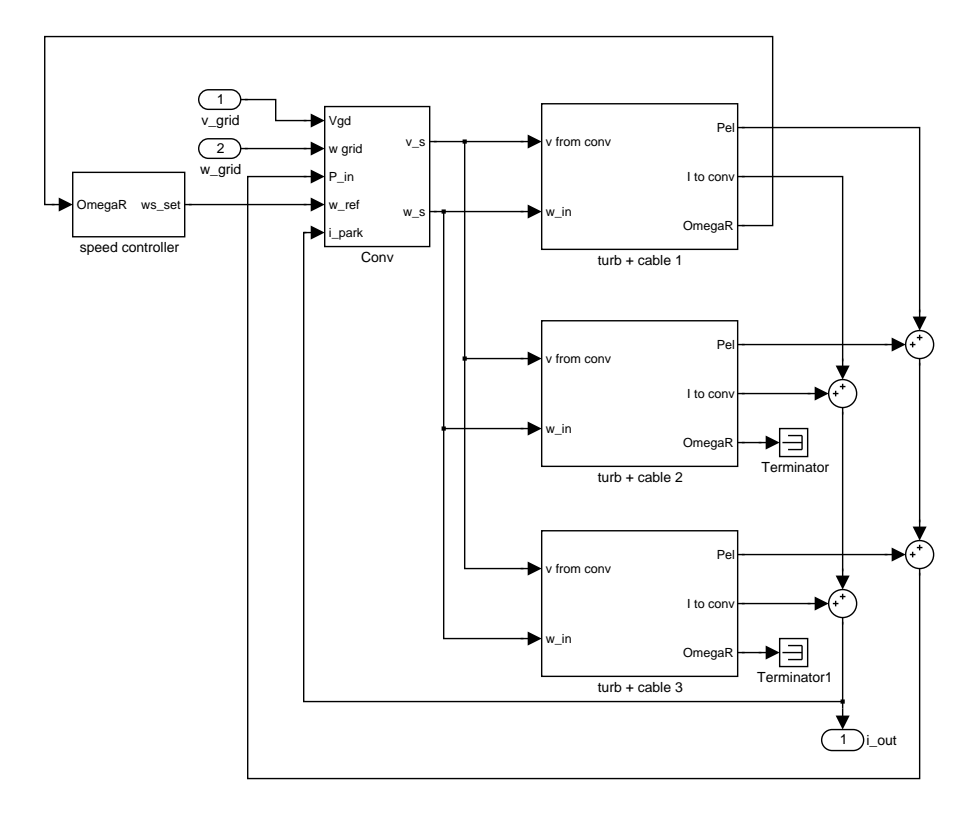


Figure 59: Simulink CC cluster model: cluster

The cluster block (figure 59) connects three turbines plus cables to the cluster converter. The voltage phasor at the turbine side of the cluster converter is input for the turbine plus cable model, the current phasor is output. The sum of the three turbine current phasors is returned to the converter.

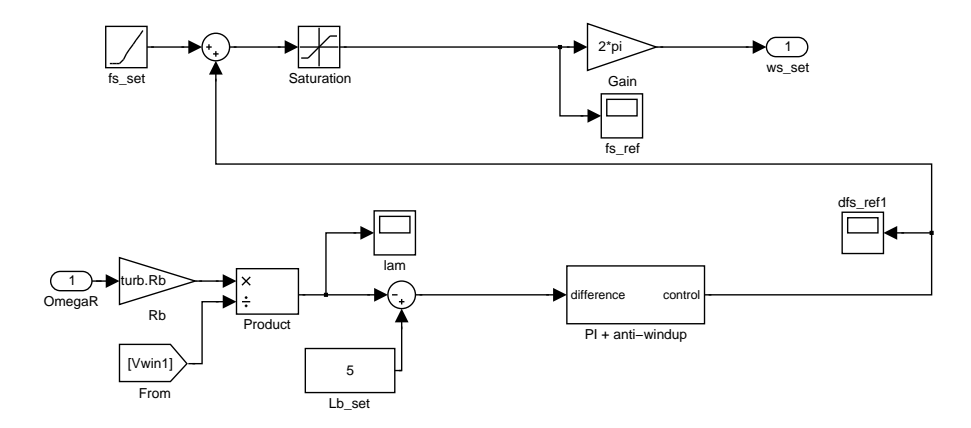


Figure 60: Simulink CC cluster model: speed controller

The speed controller (figure 60) determines the setpoint for the common rotational speed of the turbines in a cluster.

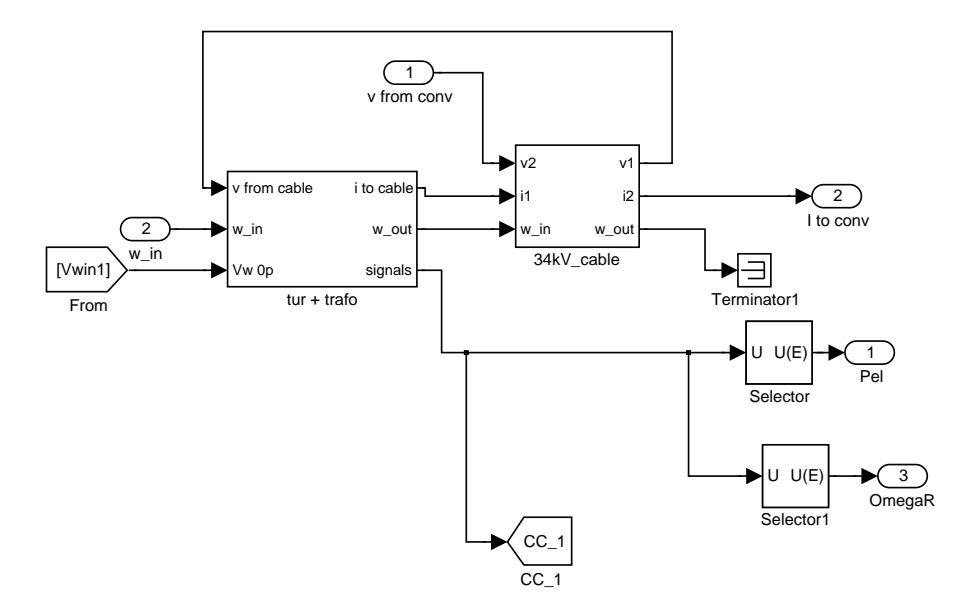


Figure 61: Simulink CC turbine model: turbine + cable

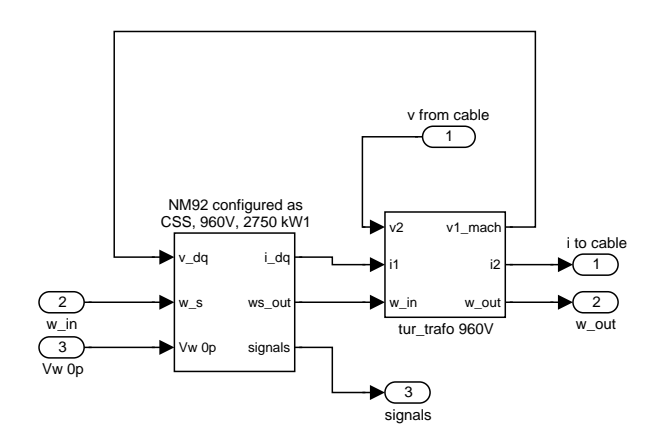


Figure 62: Simulink CC turbine model: tur + trafo

The turbine and transformer model in figure 62 contains the NM92 turbine block and a 960V/34kV transformer block. The cable voltage phasor and the current phasor from the turbine are the inputs of the transformer block. The transformer model calculates the low voltage side voltage phasor and the high voltage side current phasor. The transformer model output voltage phasor is fed to the turbine model, the output current phasor is input to the 34 kV cable model.

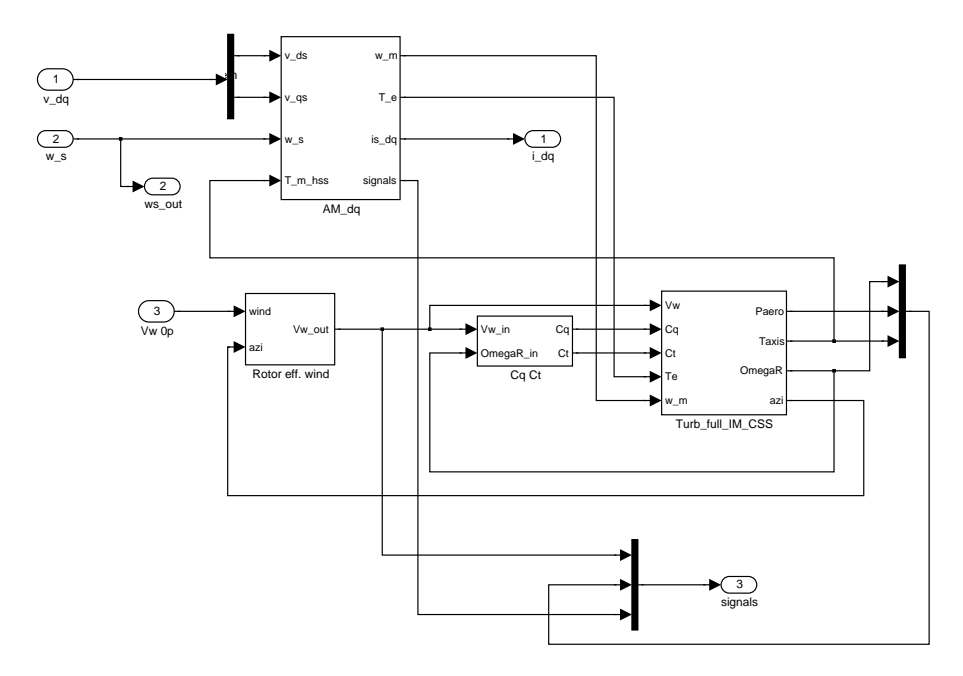


Figure 63: Simulink CC electrical system model: NM92

The turbine model is identical to the turbine model in the CSS wind farm model and consists of the generator model (AM dq), the calculation of the rotor effective wind (Rotor eff wind), the aerodynamic coefficients (CqCt) and the block containing the mechanical equations of turbine shaft and tower (Turb full IM CSS), figure 63). For the description of these blocks is referred to section 4.1.

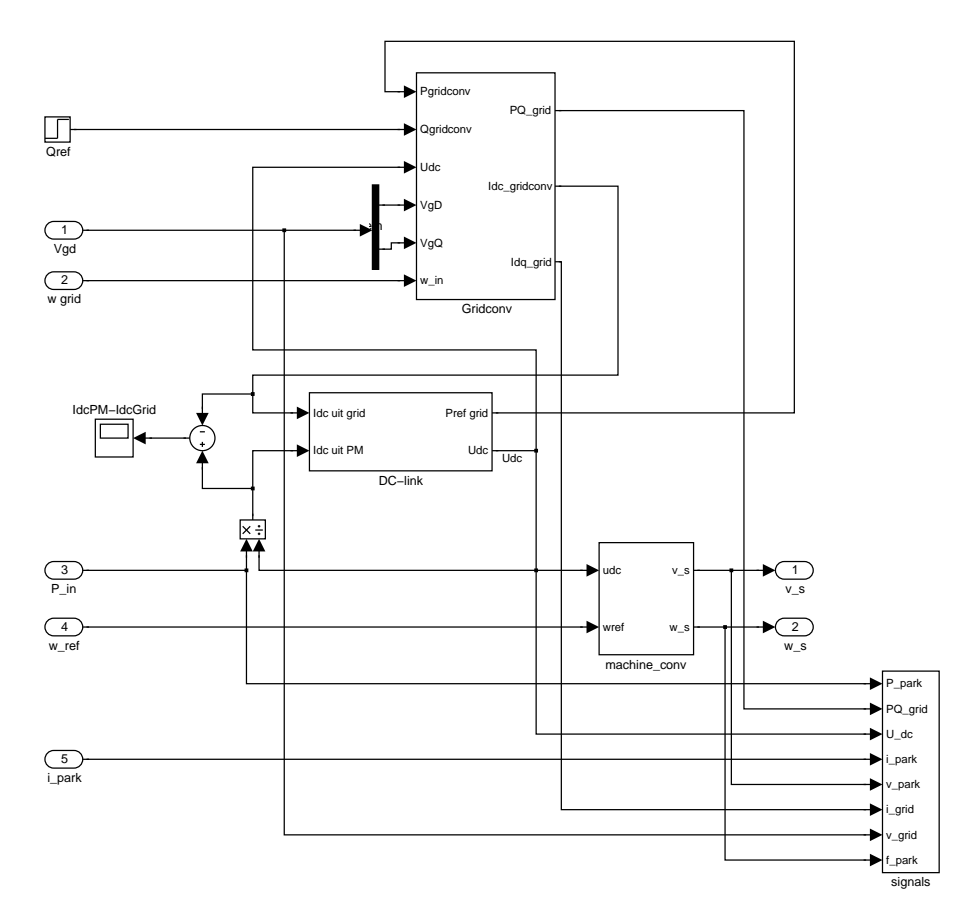


Figure 64: Simulink CC electrical system model: Conv

The cluster converter block in figure 64 connects the grid and machine side converter to the DC link. The inputs of the cluster converter block are the grid voltage phasor, the grid angular frequency, the electrical power and current of all generators connected to the cluster converter and the setpoint for the cluster rotational speed. The outputs are the voltage phasor of the generators and the cluster angular speed.

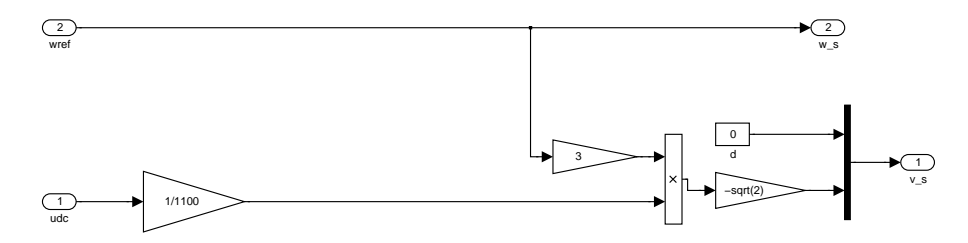


Figure 65: Simulink CC electrical system model: machine conv

The machine side converter (figure 65) determines the stator voltage of the cluster generators. The q-component of this voltage is scaled with the setpoint of the cluster angular speed. The d-component is zero.

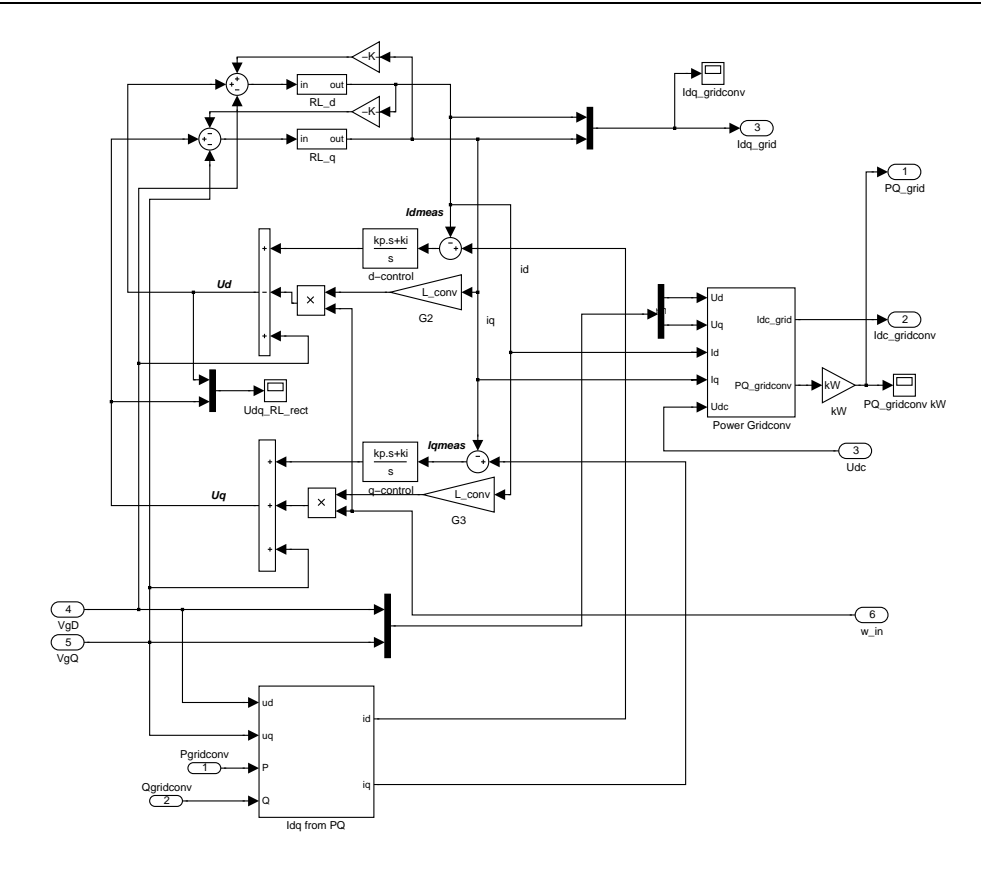


Figure 66: Simulink CC electrical system model: Gridconv

The grid side converter determines the current phasor to the grid by generating a voltage difference over a small RL component between the converter and the grid. The setpoint for the current phasor is calculated from the DC power to the grid that is required to keep the DC link voltage constant and the setpoint for the reactive power to the grid.

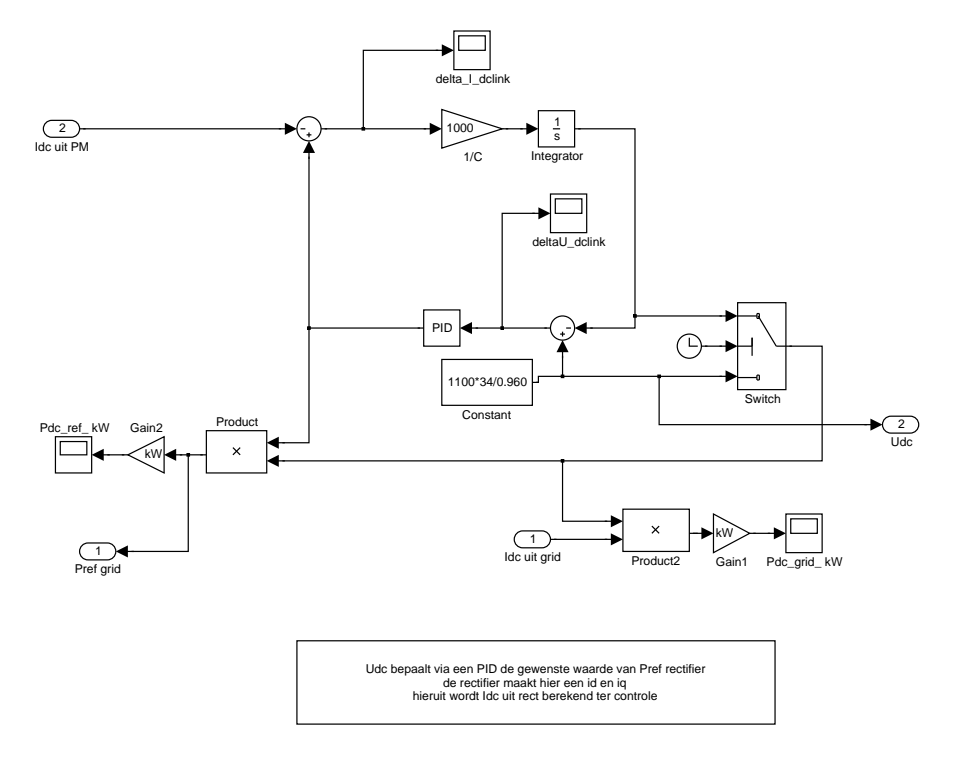


Figure 67: Simulink CC electrical system model: DC-link

In the DC link (figure 67) the DC currents generated by the grid and machine side converter determine the DC voltage and the setpoint for the grid converter power.

The cable and transformer models are identical to those used in the CSS wind farm model, see section 4.1.

4.3 Variable speed pitch controlled WF with doubly fed induction machines

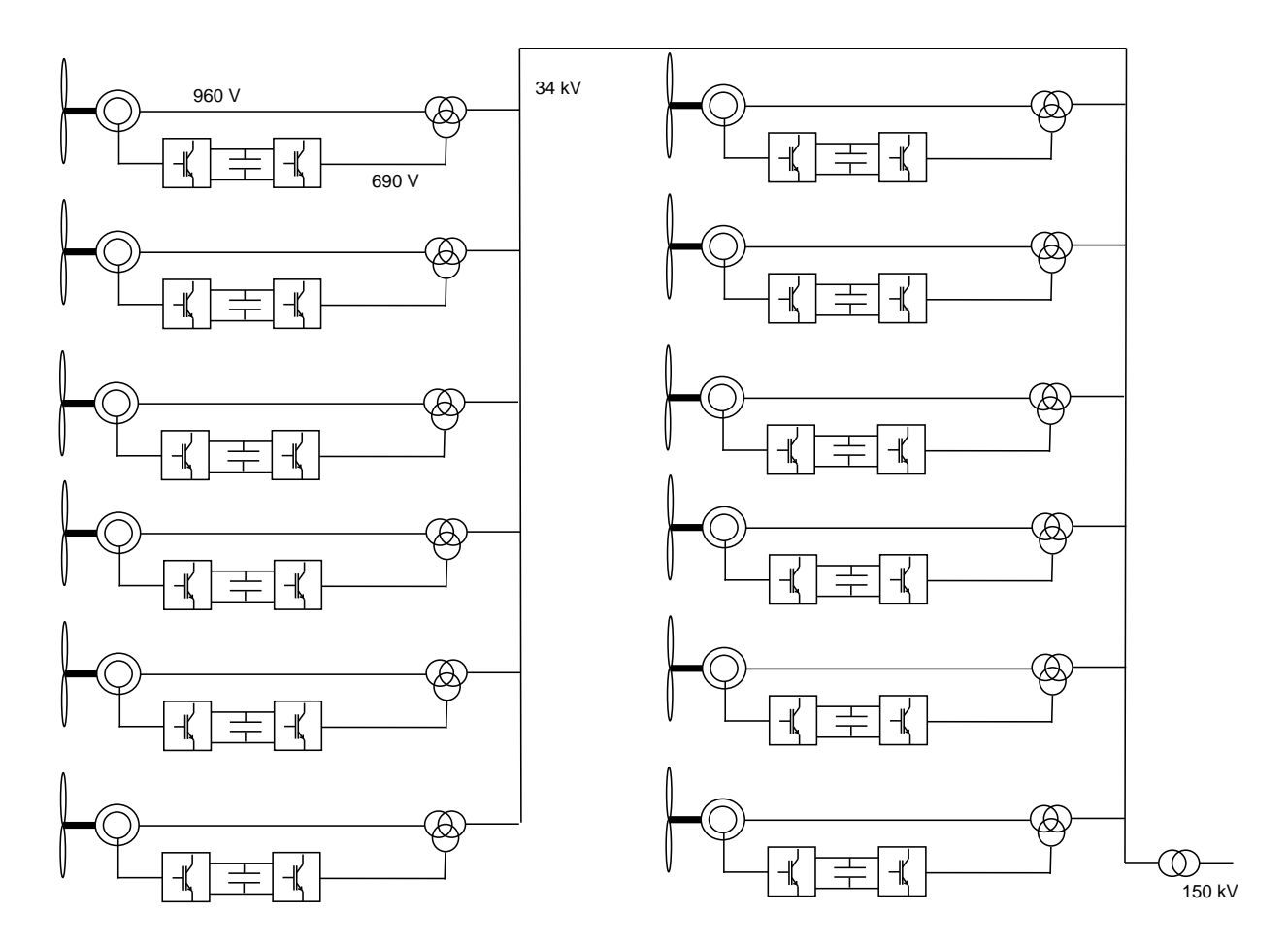


Figure 68: Electrical layout of a string of 12 DFIG turbines

One string in the variable speed pitch controlled wind farm with doubly fed induction machines (VSP-DFIG) contains twelve turbines (figure 68). The Simulink model of this string includes the turbines, the three-winding transformers, the converters connected to the generator rotors, the cables in the wind farm, the cable to shore and the substation high-voltage transformer.

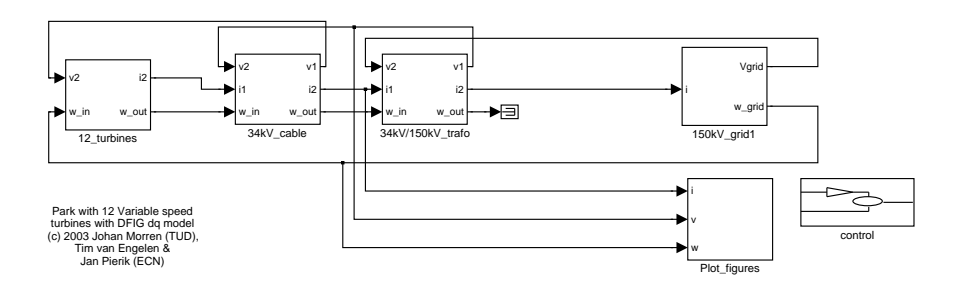


Figure 69: Simulink DFIG wind farm model main window

The Simulink model connects the 12 turbines to a 34 kV cable, a 34kV/150kV transformer and the 150 kV grid model (figure 70). Separate blocks generate individual wind input for all turbines and plot simulation results.

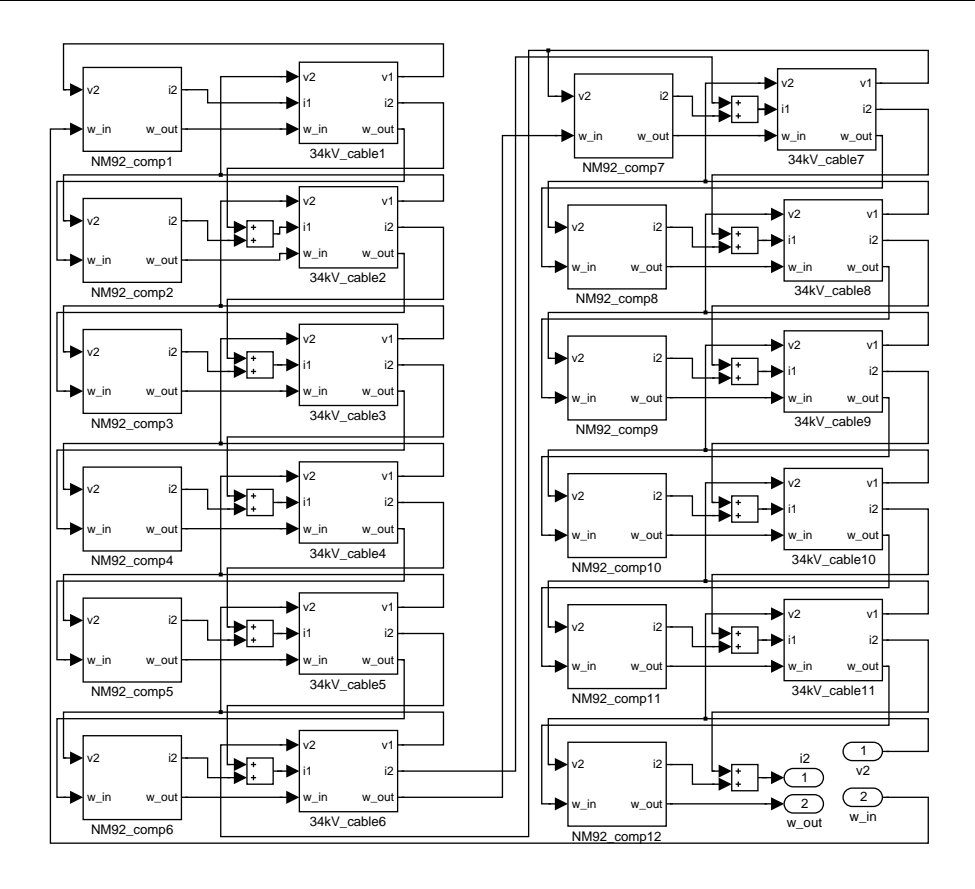


Figure 70: Simulink DFIG wind farm model: 12 turbines

The turbines block (figure 70) connects the 12 turbines and 11 cables in one string of the NSW wind farm. The voltage phasor at each cable-turbine connection is input for the turbine plus transformer model, the current phasor is output. The turbine plus transformer model calculates the current phasor, which is returned to the cable model. The turbine current phasor and the current phasor from the cable connecting the other turbines are added before entering the next cable. This is repeated for all turbines and cables.

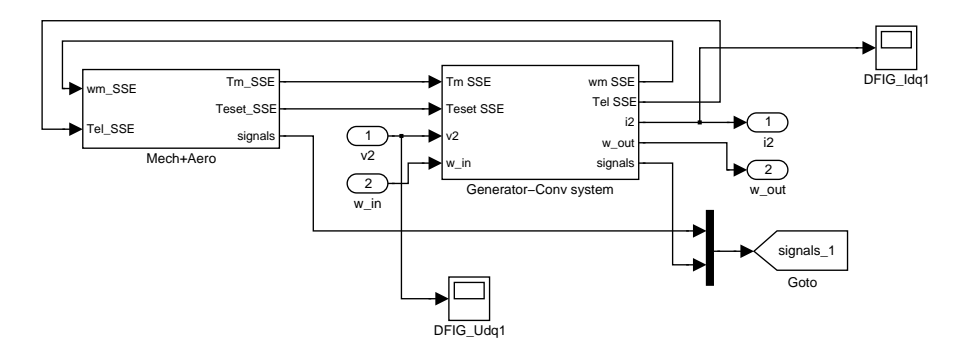


Figure 71: Simulink DFIG turbine model: NM92-comp1

The DFIG turbine model, figure 71), consists of two submodels: a mechanical and aerodynamic part *Mech+Aero* and an electrical part *Generator-Conv system*.

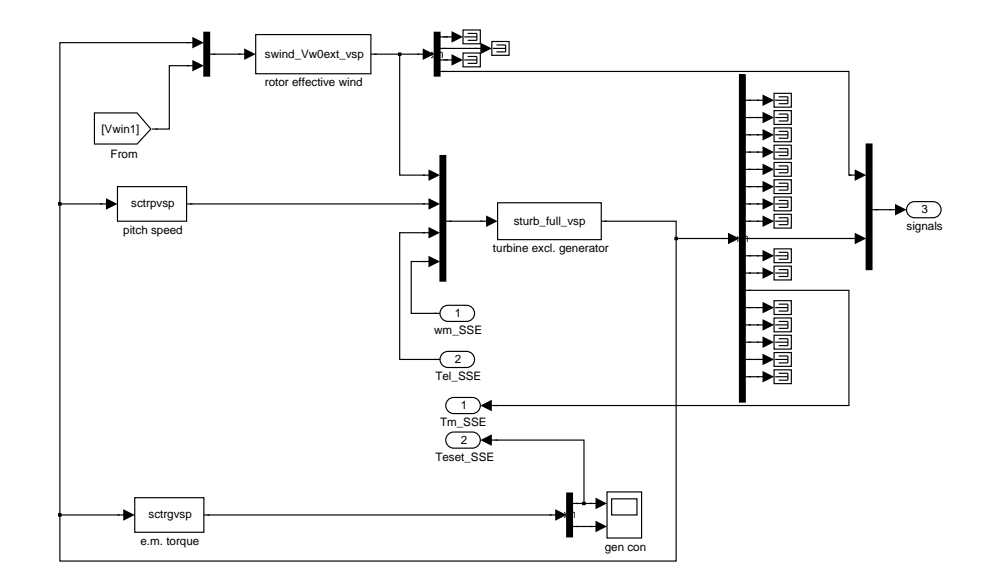


Figure 72: Simulink DFIG turbine model: Mech+Aero

The mechanical and aerodynamic part (Figure 72) consists of four Matlab S-functions, which calculate the rotor effective wind, the pitch control and electromagnetic torque setpoint and the turbine rotor, drive train and tower motion. See chapter 3 for a description.

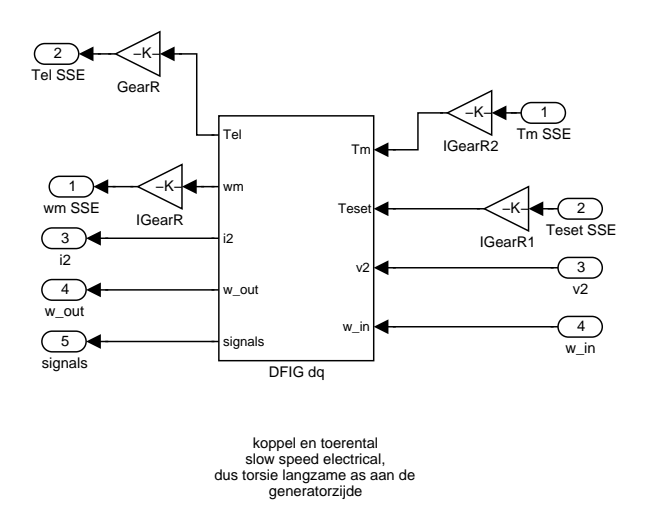


Figure 73: Simulink DFIG electrical system model: Generator-Converter system

The electrical part of the DFIG turbine model in figure 73 contains the models of the 3-winding trafo, the generator and the converter connected to the generator rotor.

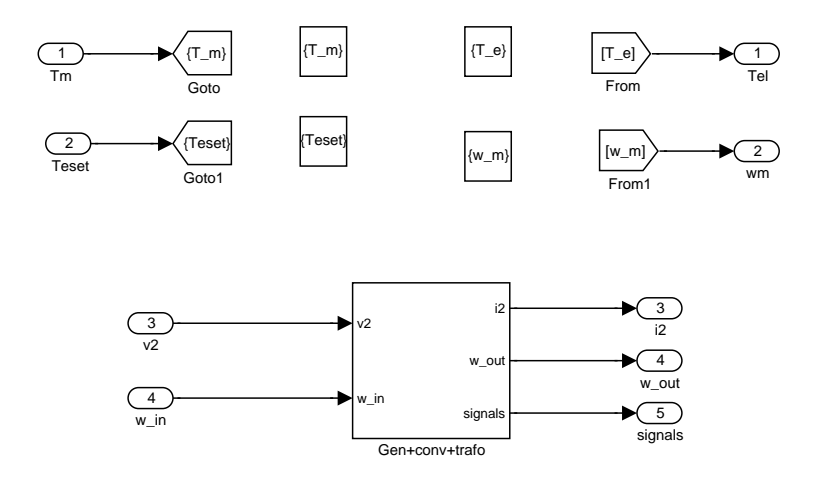


Figure 74: Simulink DFIG electrical system model: DFIG dq

The input variables mechanical torque and electrical torque setpoint in figure 74 are passed to the generator and the torque controller subsystems respectively. The output variables electrical torque and rotational speed are calculated in the generator and the gen+conv subsystems respectively. Other input variables for the Gen-conv-trafo subsystem are the grid voltage phasor and the grid angular frequency. The current phasor into the 34 kV cable is calculated and the grid angular frequency is passed as an output.

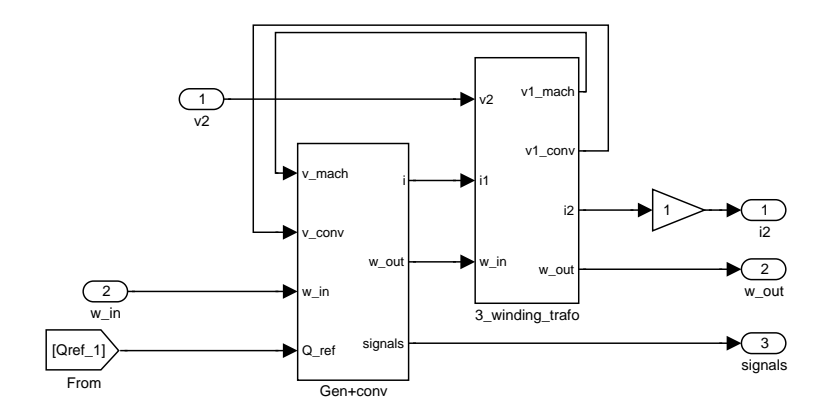


Figure 75: Simulink DFIG electrical system model: Gen+conv+trafo

The three-winding transformer model in figure 75 is almost the same as the two-winding model described in section 4.1. A small inaccuracy is introduced in this way.

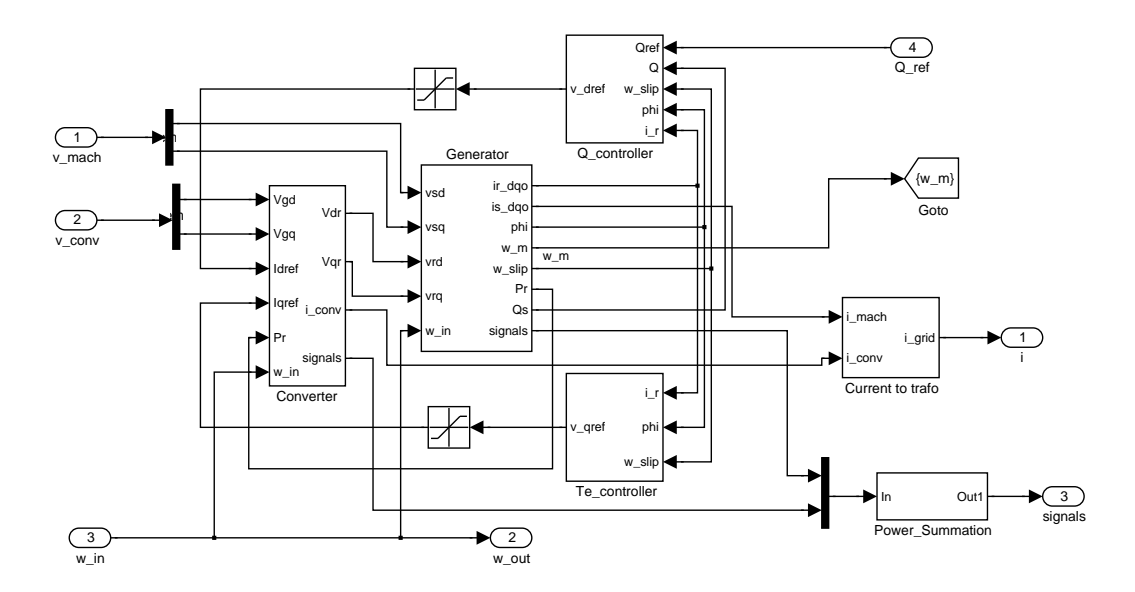


Figure 76: Simulink DFIG electrical system model: Gen+conv

The converter in figure 76 is able to control four quantities:

- by changing the switching of the rotor side converter, the rotor voltage amplitude and phase angle can be controlled;
- on the grid side, the current amplitude and phase angle can be controlled by changing the switching of the grid side converter and thus the voltage at the converter terminals.

The rotor side voltage and phase angle (or the d- and q-component) are determined by two controllers: the reactive power controller determines the d-component and the torque controller sets the q-component. The rotor side converter realises these voltages.

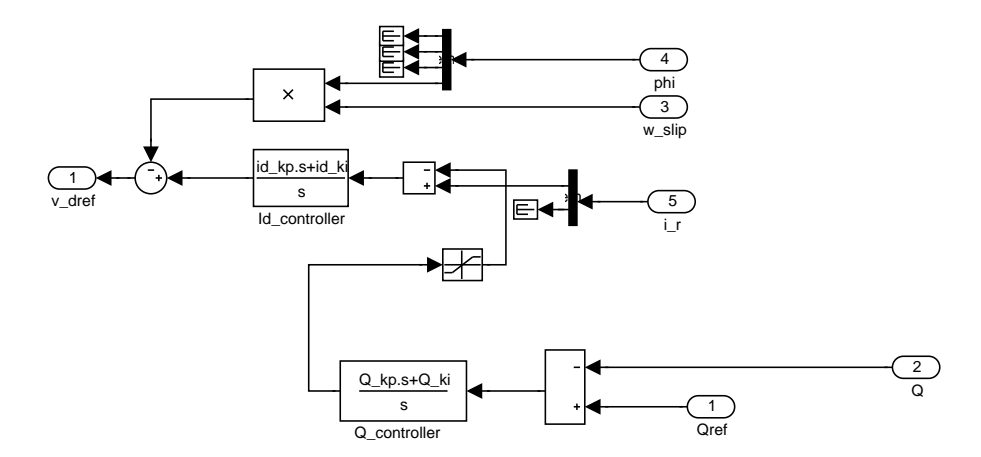


Figure 77: Simulink DFIG electrical system model: Q-controller

The reactive power controller compares the reactive power offset to generate a setpoint for the d-component of the rotor current in figure 77. This setpoint is compared to the actual current value. A second controller generates the setpoint for the d-component of the rotor voltage, corrected for the crossterm $\omega_{slip}\Psi_{rq}$.

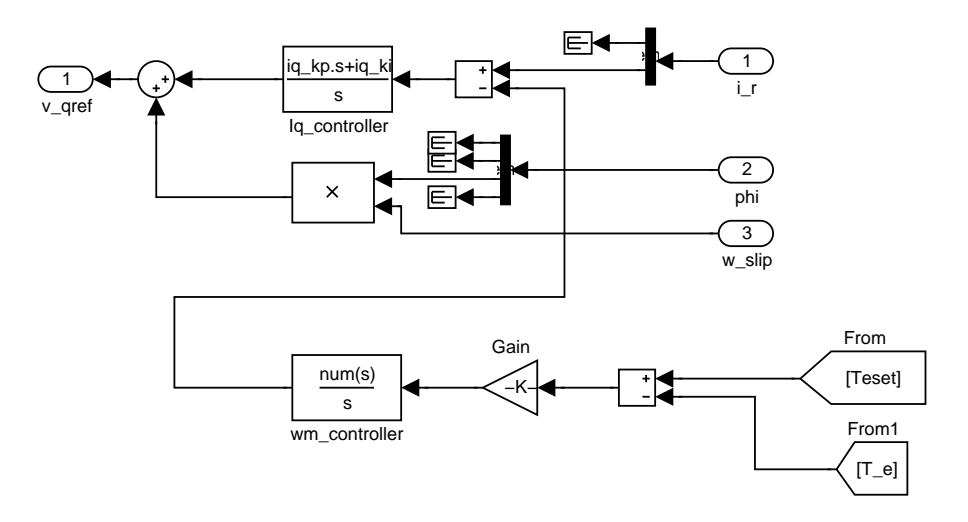


Figure 78: Simulink DFIG electrical system model: Te-controller

The torque controller compares the torque offset to generate a setpoint for the q-component of the rotor current (Figure 78). This setpoint is compared to the actual value. A second controller generates the setpoint for the q-component of the rotor voltage, corrected for the crossterm $\omega_{slip}\Psi_{rd}$.

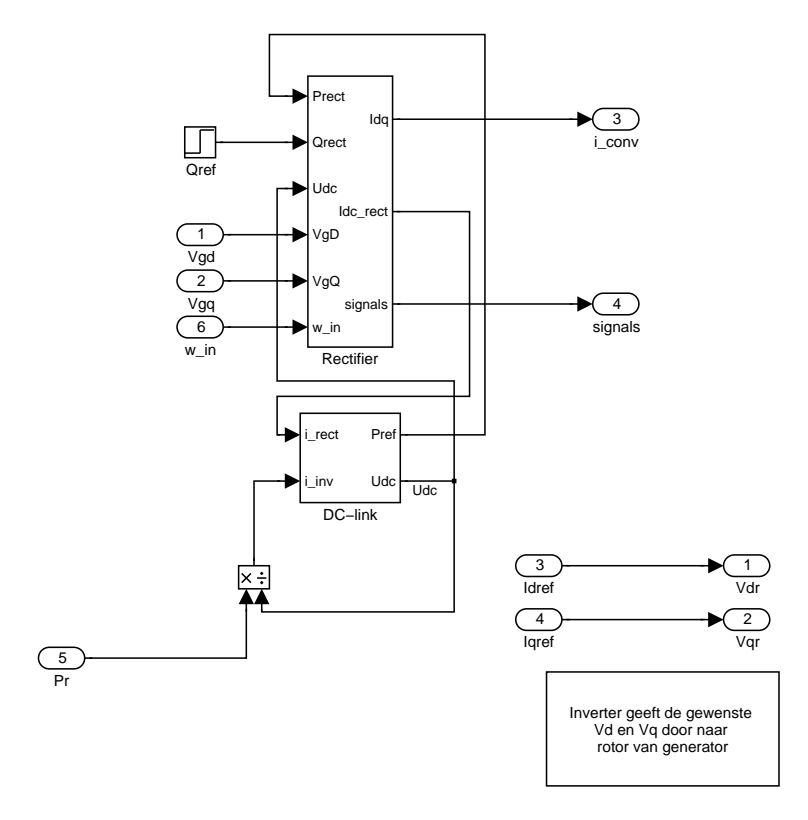


Figure 79: Simulink DFIG electrical system model: Converter

The grid side converter (called rectifier in figure 79) makes the current phasor from the DC link to the grid, based on a reactive power setpoint and the DC voltage. Two controllers in the rectifier block (figure 80) determine d- and q-voltages by comparing the d- and q-current setpoints to the actual d- and q-currents to the grid. The grid current components follow from

the voltage difference over a small impedance between rectifier and grid (figure 80).

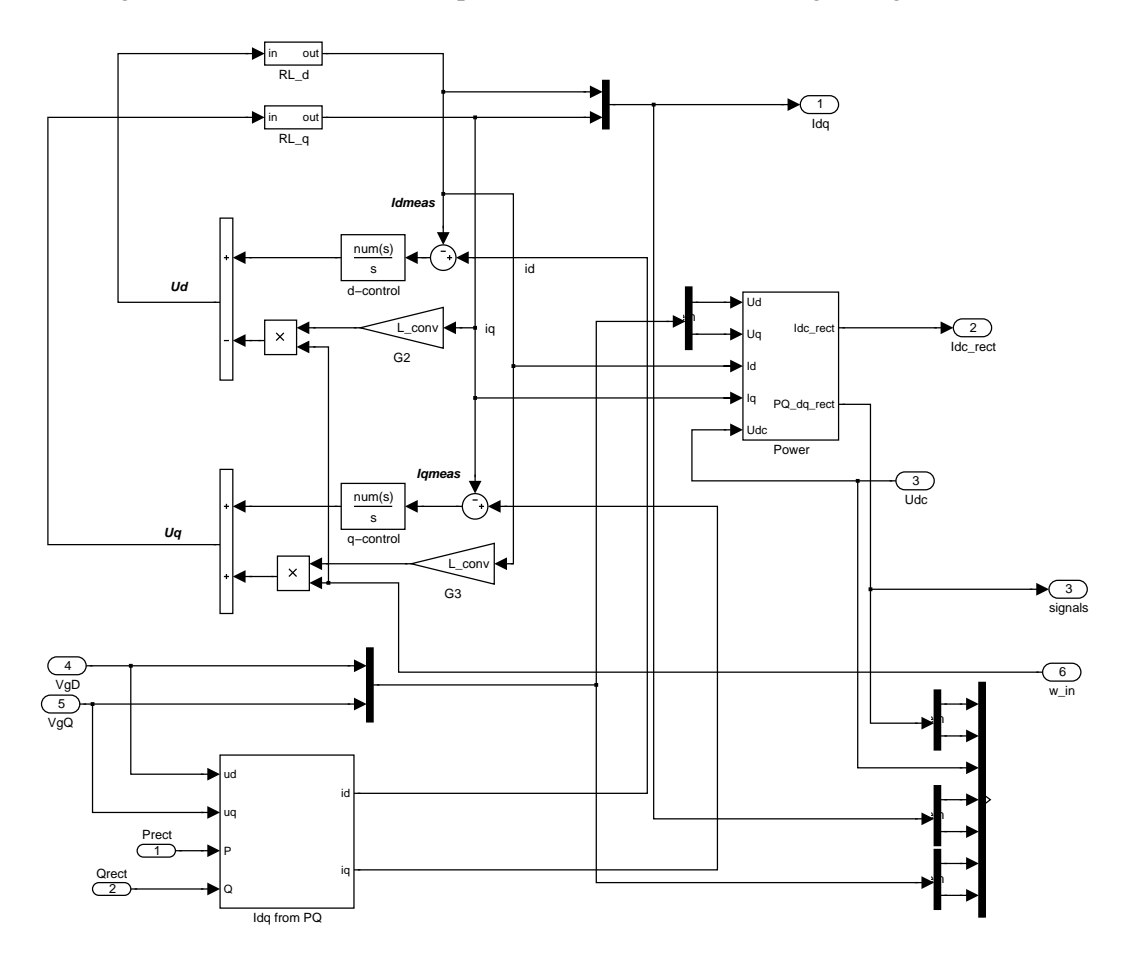


Figure 80: Simulink DFIG electrical system model: Rectifier, grid side converter

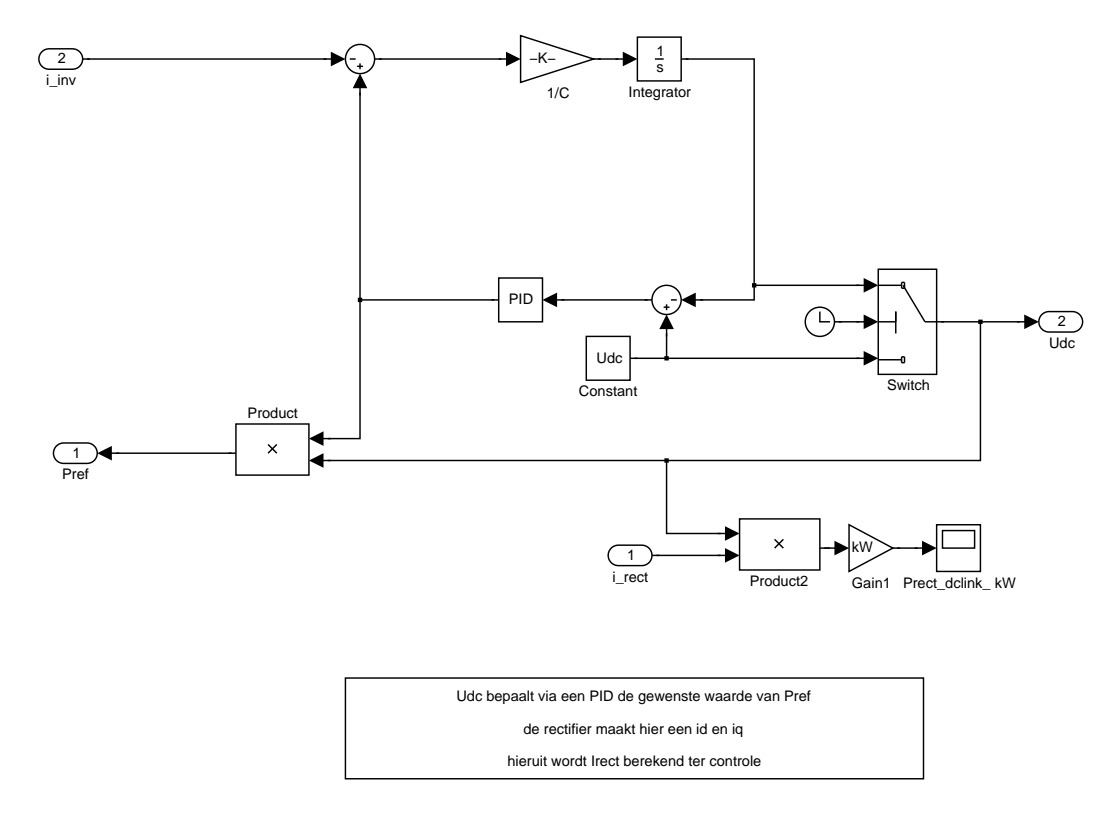


Figure 81: Simulink DFIG electrical system model: DC-link

The DC voltage determines the setpoint for the power to the grid, based on the DC current from the inverter and the actual value of the DC voltage (Figure 81). The setpoint for the power to the grid is fed to the converter to determine the current q-value.

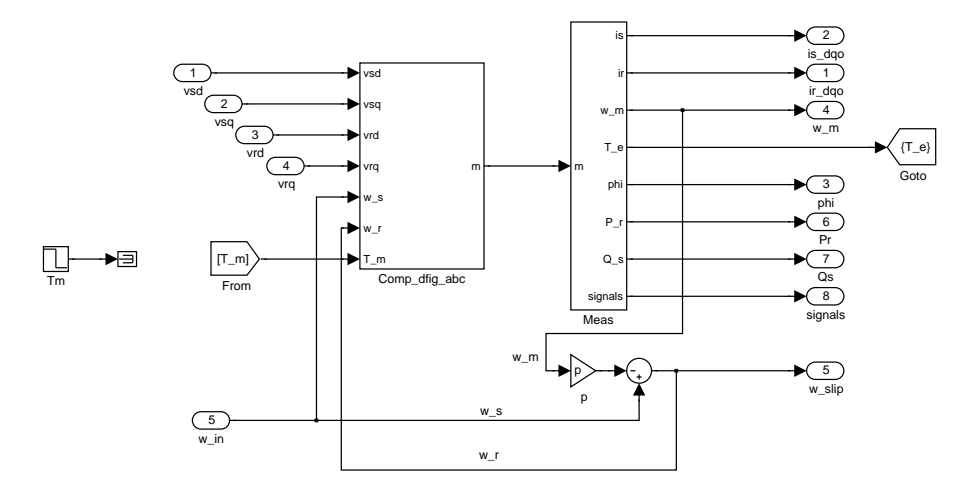


Figure 82: Simulink DFIG electrical system model: Generator

The generator model determines the rotor and stator current phasors based on the rotor and stator voltage phasors, see figure 82. The shaft torque is also an input to the generator model.

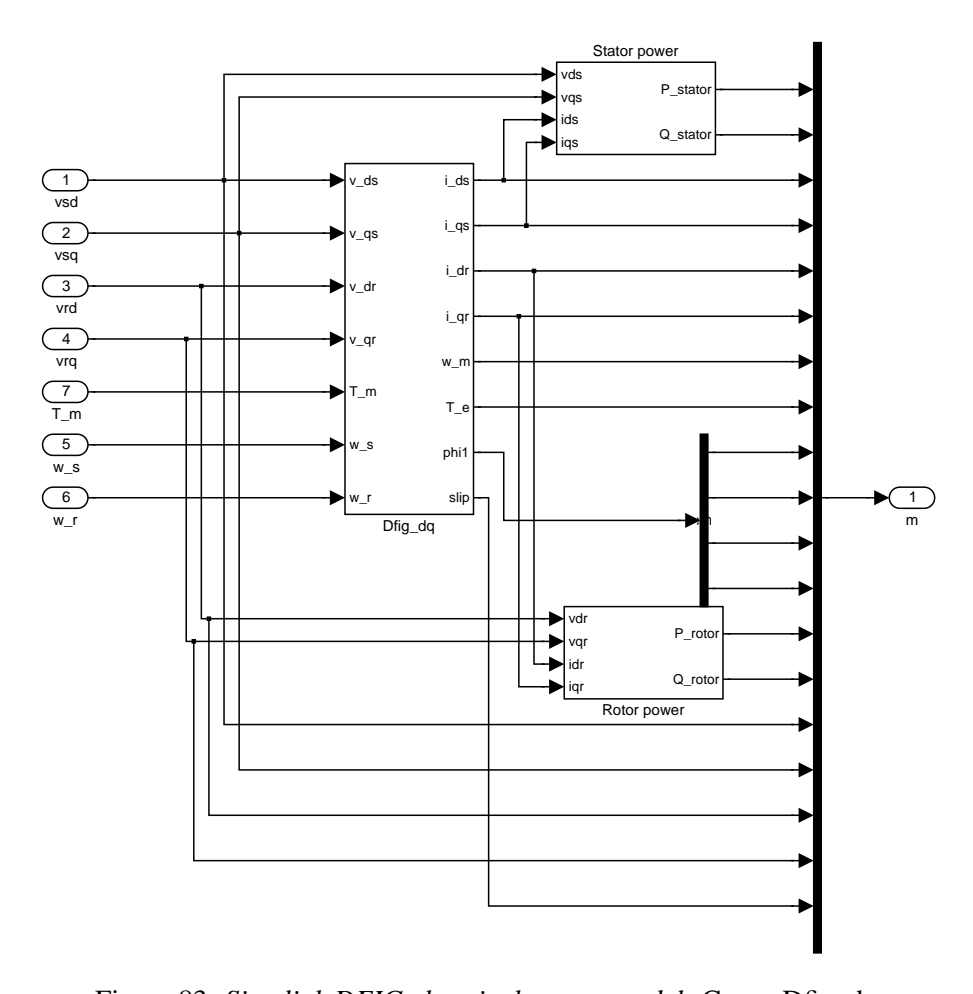


Figure 83: Simulink DFIG electrical system model: Comp-Dfig-abc

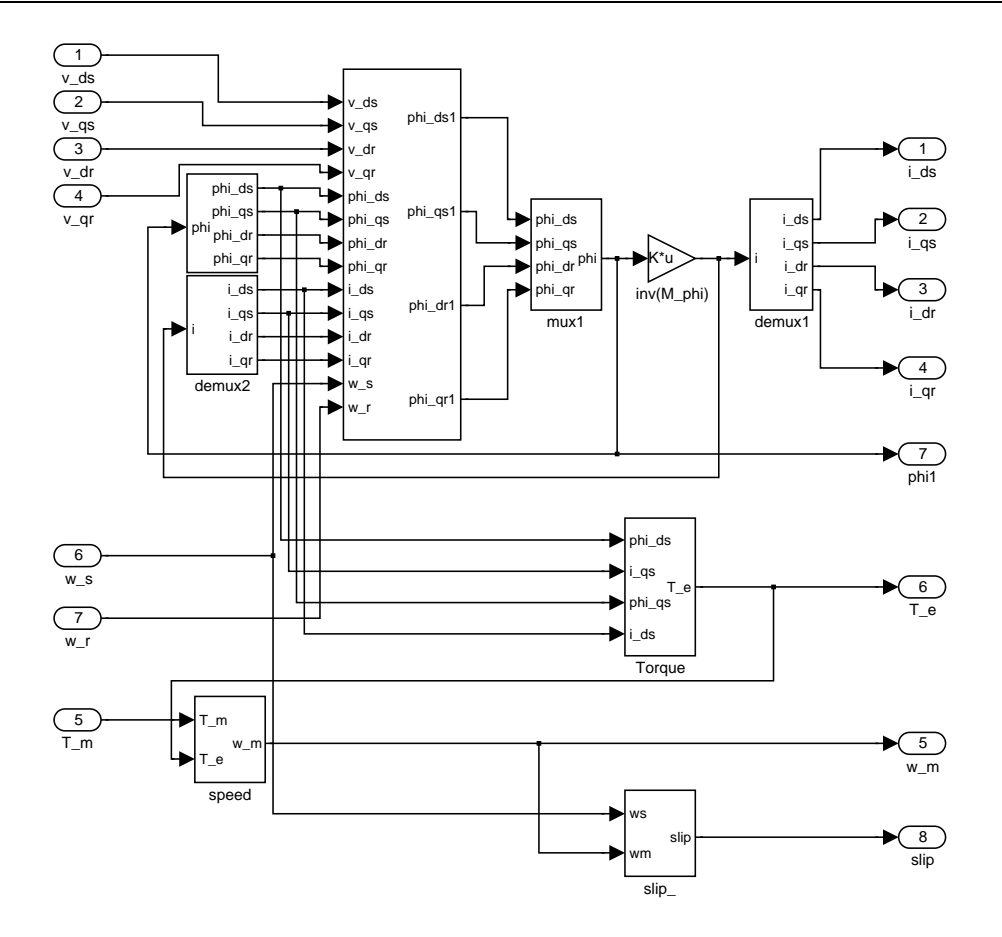


Figure 84: Simulink DFIG electrical system model: Dfig-dq

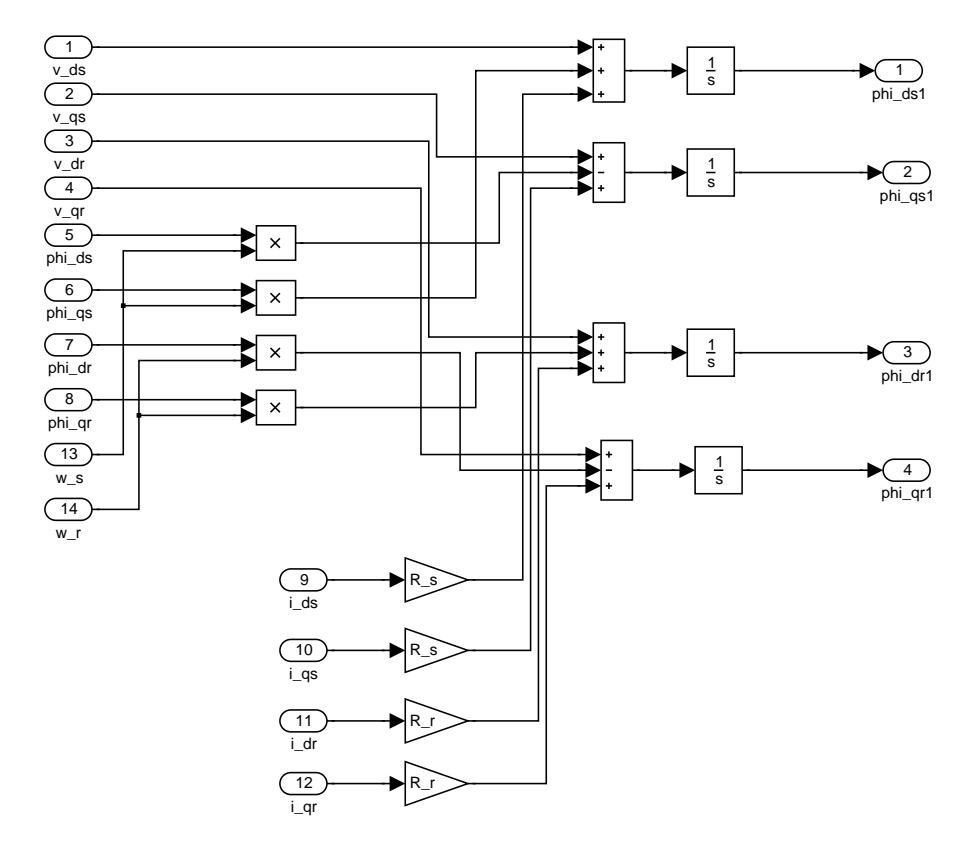


Figure 85: Simulink DFIG electrical system model: Voltage equations

The voltage equations (see equation 33) constituting the generator model are represented by figure 85.

The cable and transformer models are identical to those used in the CSS wind farm model.

4.4 Variable speed pitch controlled WF with permanent magnet machines

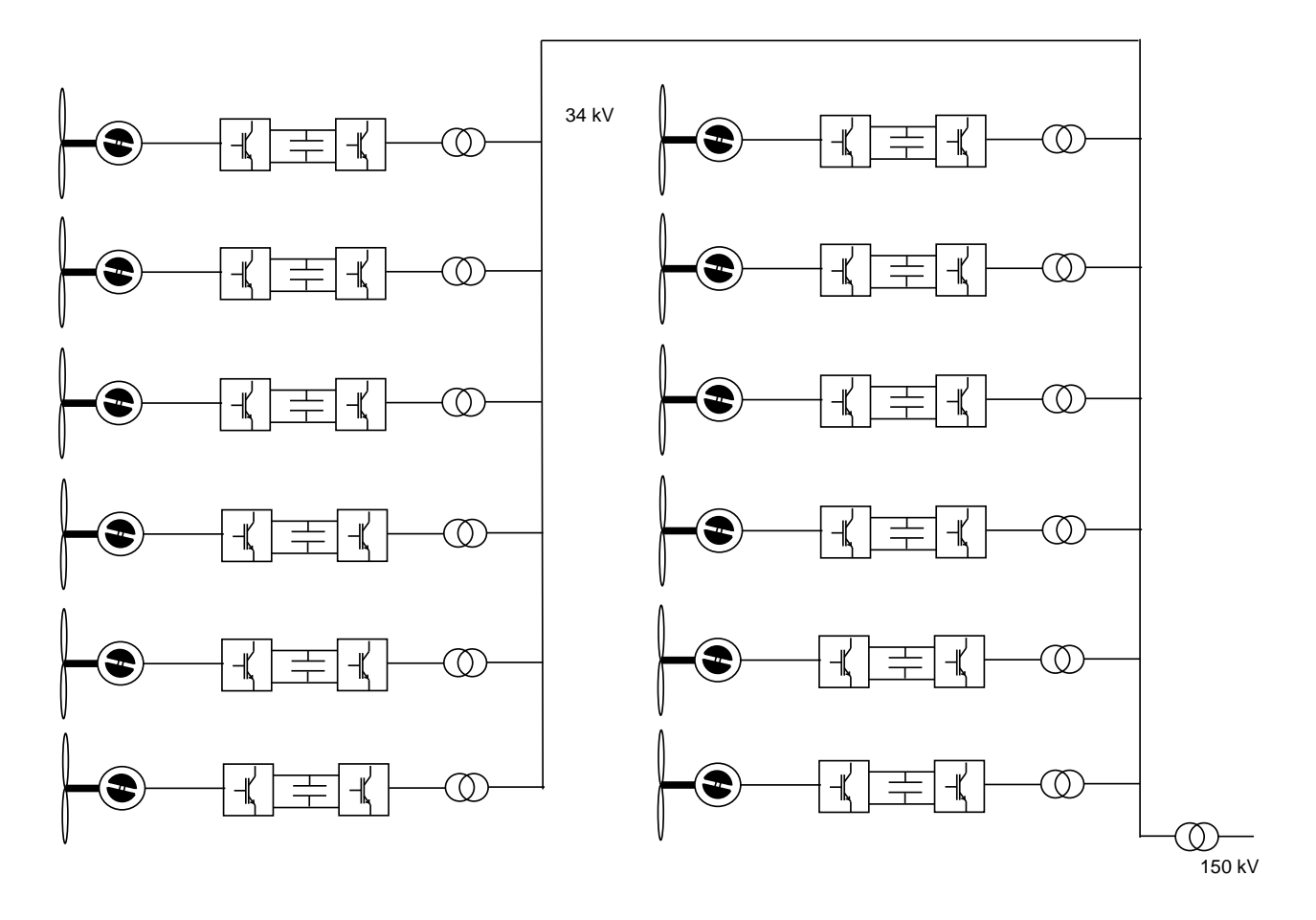


Figure 86: Electrical layout of a string of 12 PM turbines

One string in the variable speed pitch controlled wind farm with permanent magnet machines contains 12 turbines (figure 86). The Simulink model of this string includes the turbines, the transformers, the converters connected to the generator stators, the cables in the wind farm, the cable to shore and the substation high voltage transformer.

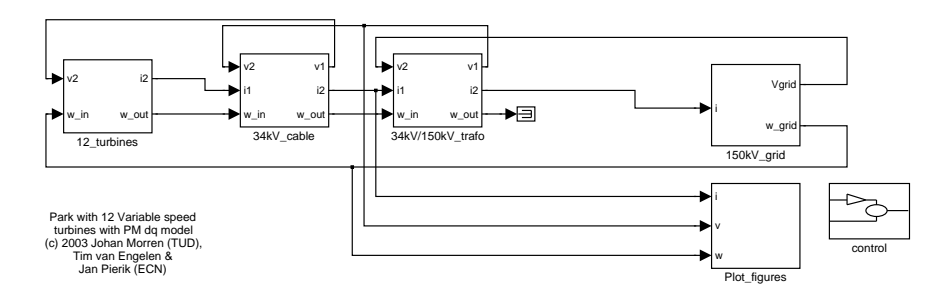


Figure 87: Simulink PM wind farm model: Main window

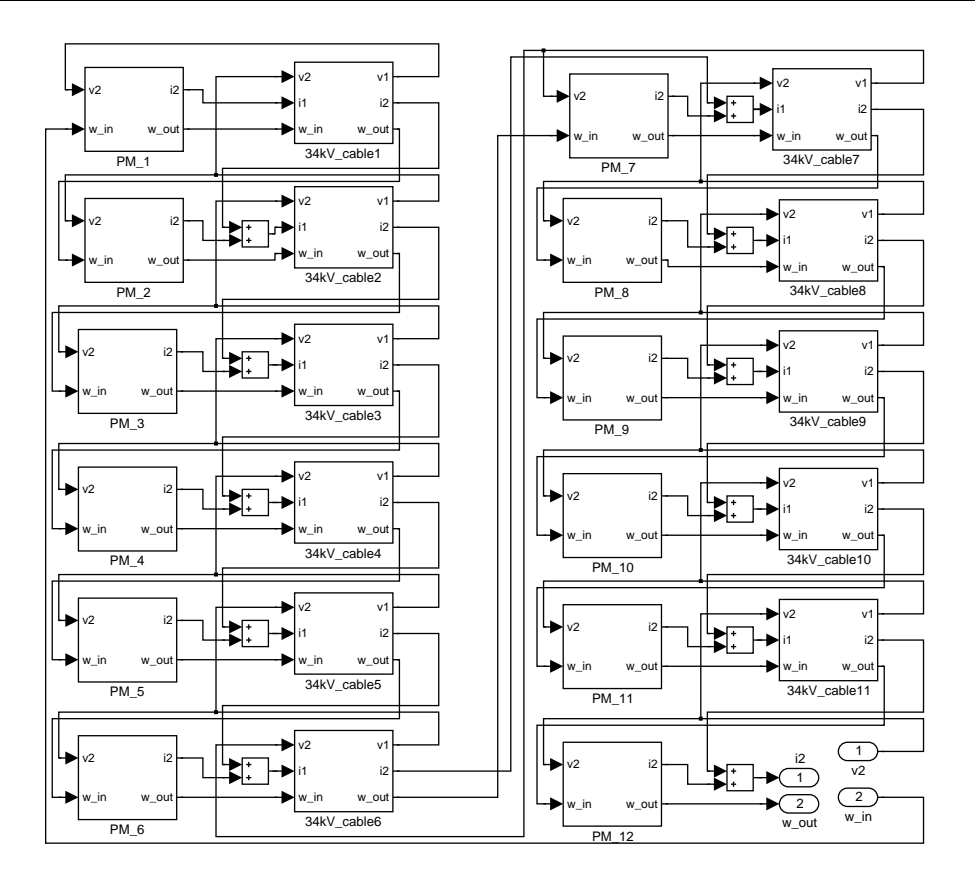


Figure 88: Simulink PM wind farm model: 12 turbines

In figure 88 the twelve variable speed turbines, equipped with permanent magnet generators and the eleven cables in one string are connected. The signal flow is similar to the DFIG model.

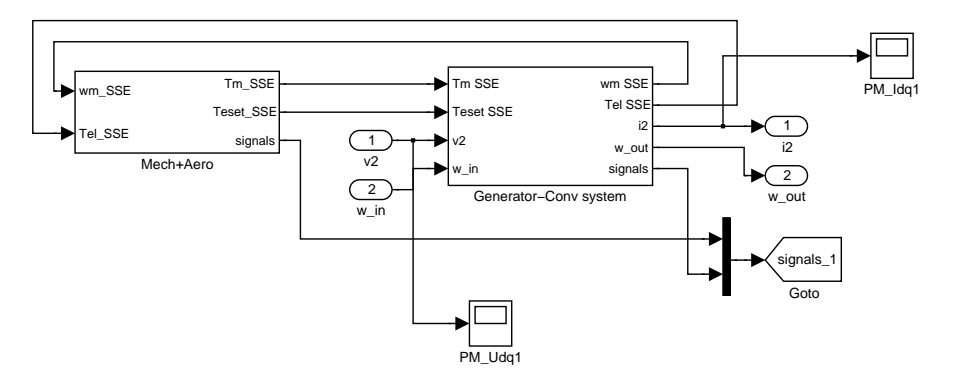


Figure 89: Simulink PM turbine model: PM 1

The PM turbine model (figure 89) consists of two submodels: a mechanical and aerodynamic part *Mech+Aero* and an electrical part *Generator-Converter system*.

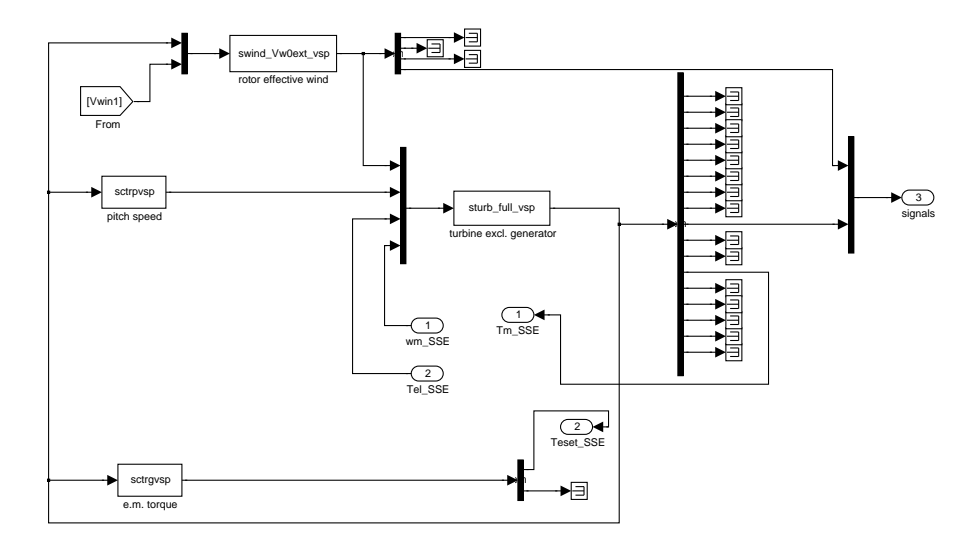


Figure 90: Simulink PM turbine model: Mech + Aero

The mechanical and aerodynamic part (figure 90) is identical to the VSP model of the VSP-DFIG wind farm and consists of four Matlab S-functions, which calculate the rotor effective wind, the pitch control and electromagnetic torque setpoint and the turbine rotor, drive train and tower movement.

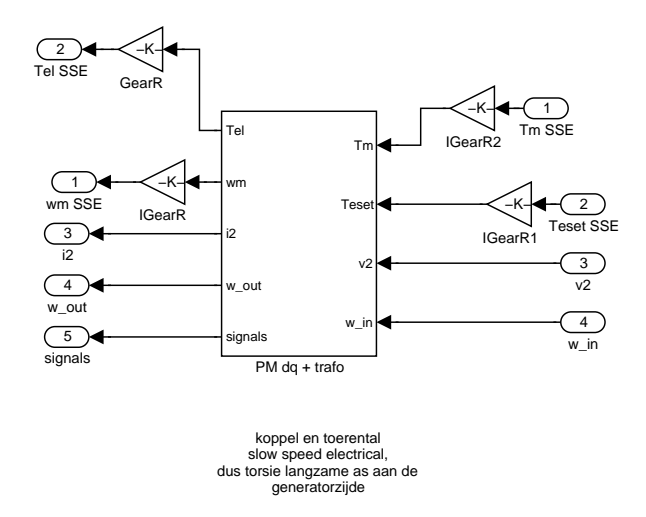


Figure 91: Simulink PM electrical system model: Generator-conv system

The electrical part of the PM turbine model in figure 91 contains the models of the transformer, the generator and the back-to-back converter.

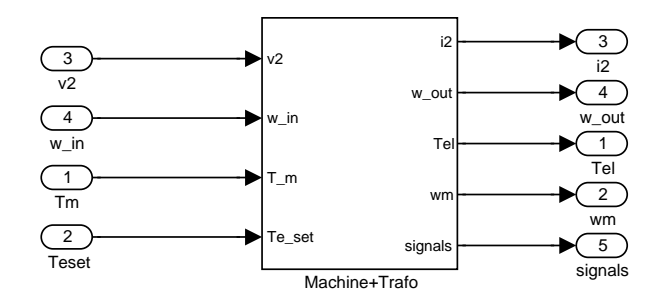


Figure 92: Simulink PM electrical system model: PMdq + trafo

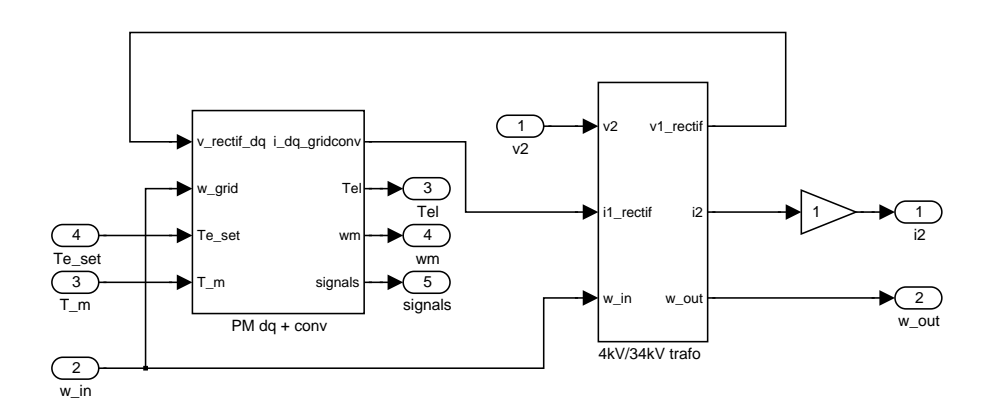


Figure 93: Simulink PM electrical system model: Machine + trafo

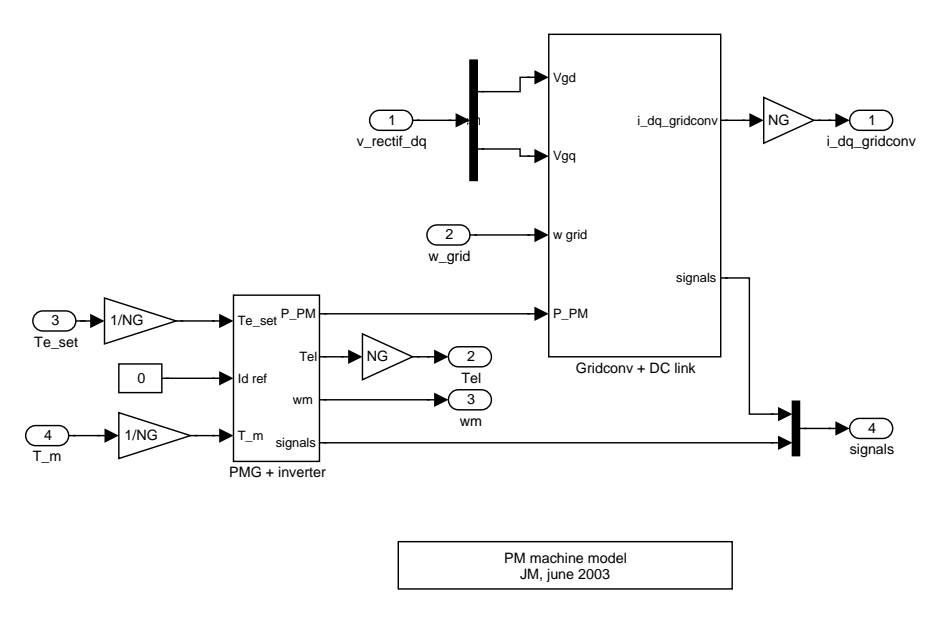


Figure 94: Simulink PM electrical system model: PMdq + conv

The back-to-back converter between PM generator and grid (figure 94) is able to make the voltage phasor at the generator and at the grid side by changing the firing of the generator and grid side converter. These voltages are determined by current setpoints, which depend on the desired reactive power, electromagnetic torque and DC link voltage.

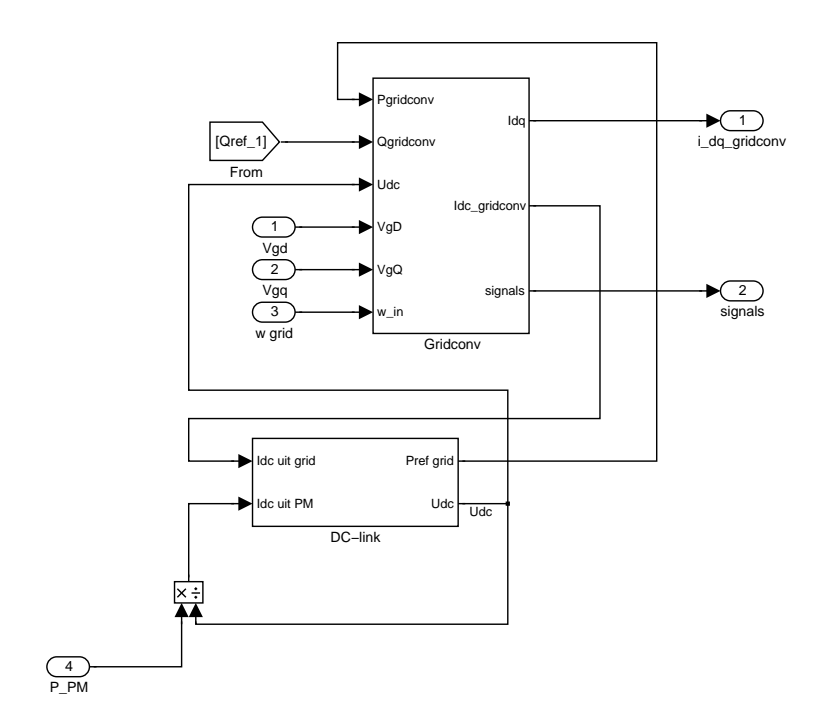


Figure 95: Simulink PM electrical system model: Grid conv + DC link

The grid side converter (called Gridconv in figure 95) determines the d- and q-current from the DC link to the grid, dependent on a reactive power setpoint and the power setpoint calculated in the DC link. Two controllers in the grid converter block (Figure 96) determine d- and q-voltages by comparing the d- and q-current setpoints by the actual d- and q-currents to the grid. The grid current components follow from the voltage difference over a small impedance between rectifier output and grid. This converter operates similar to the grid side converter in the DFIG model.

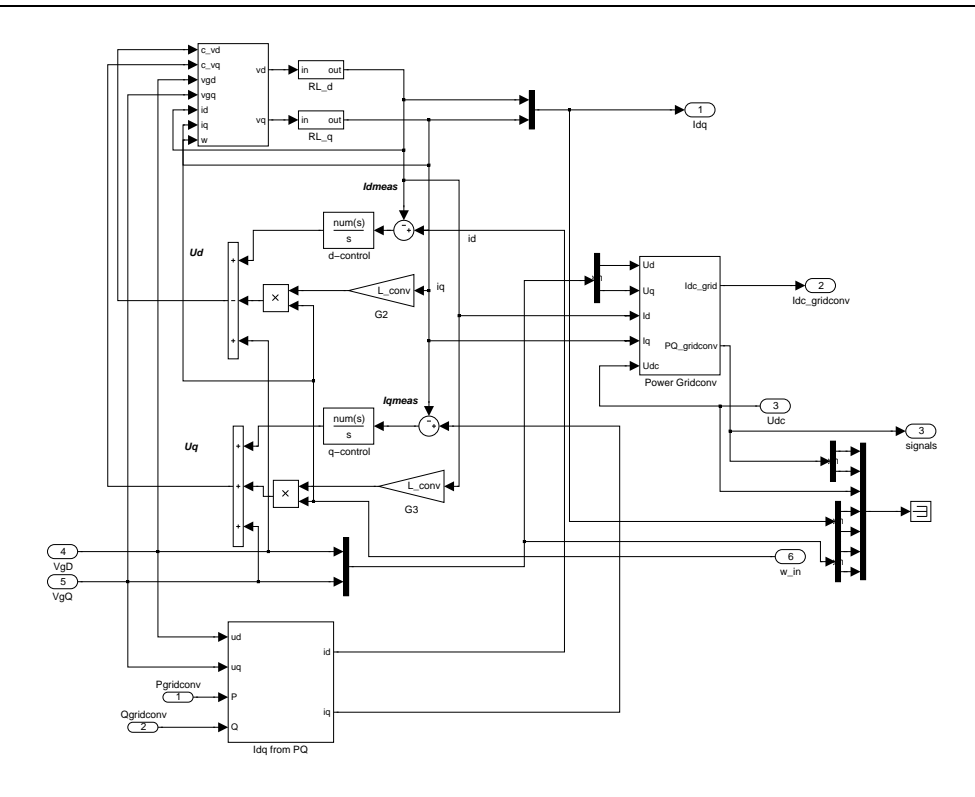


Figure 96: Simulink PM electrical system model: Gridconv

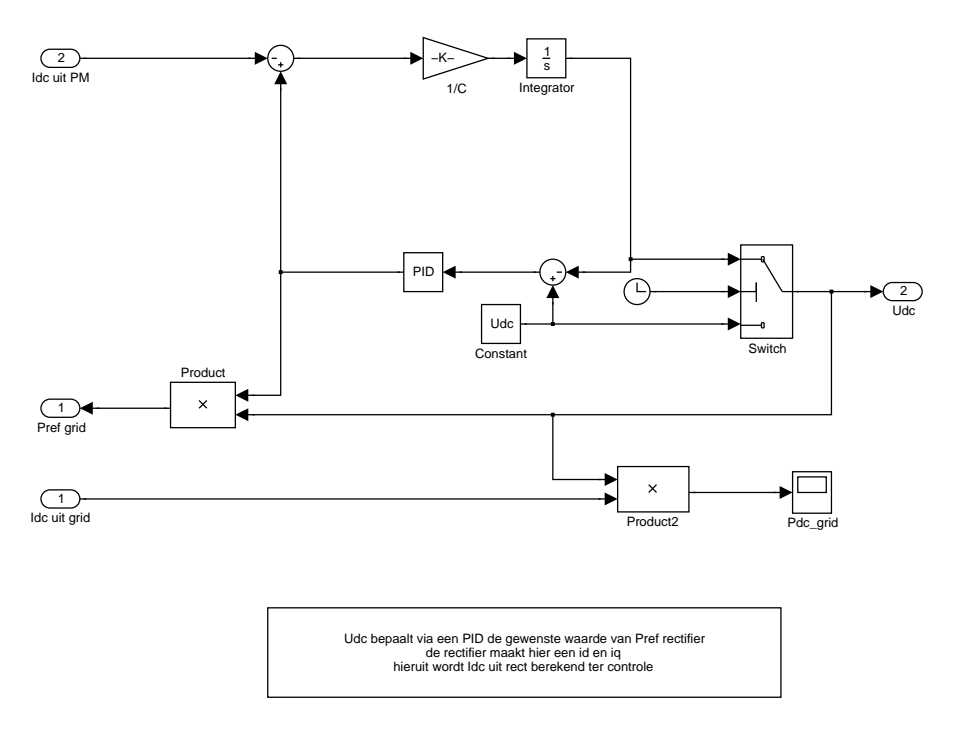


Figure 97: Simulink PM electrical system model: DC link

The DC voltage controller determines the setpoint for the power to the grid, based on the DC current from the inverter and the actual value of the DC voltage (Figure 97). The setpoint for the power to the grid is fed to the rectifier to determine the current d and q values.

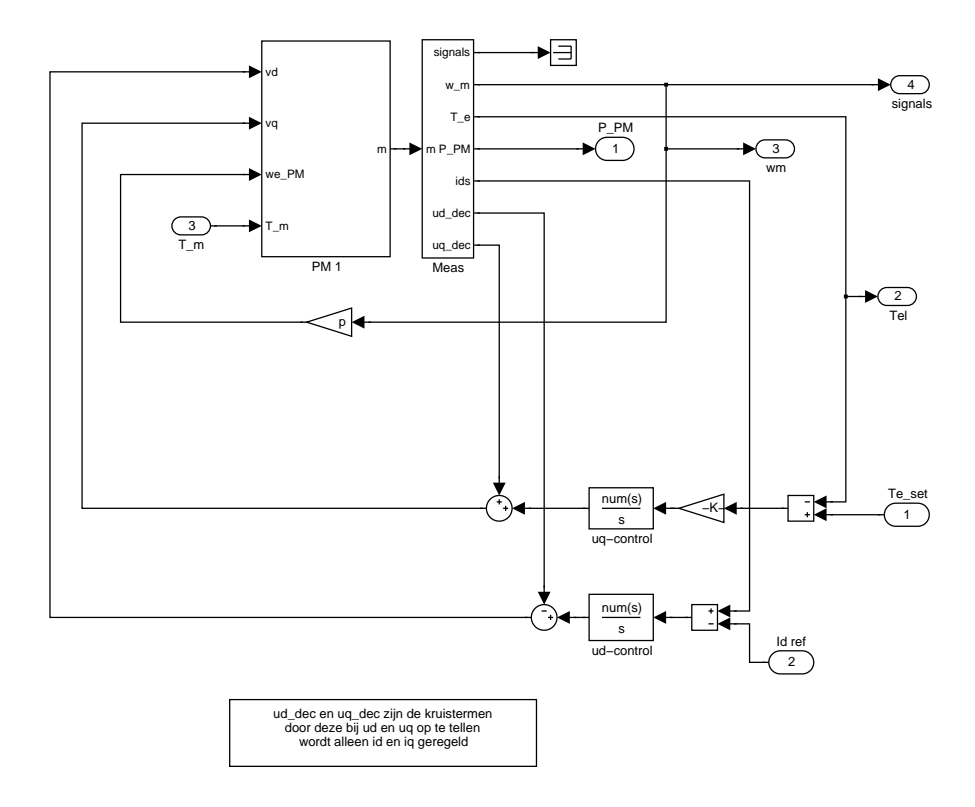


Figure 98: Simulink PM electrical system model: PMG + inverter

The input signals for the PMG and inverter are the setpoints for the electromagnetic torque and the d-component of the stator current (figure 98). The two controllers generate voltages v_q and v_d which are input for the voltage equations of the PM generator model in figures 100 and 101.

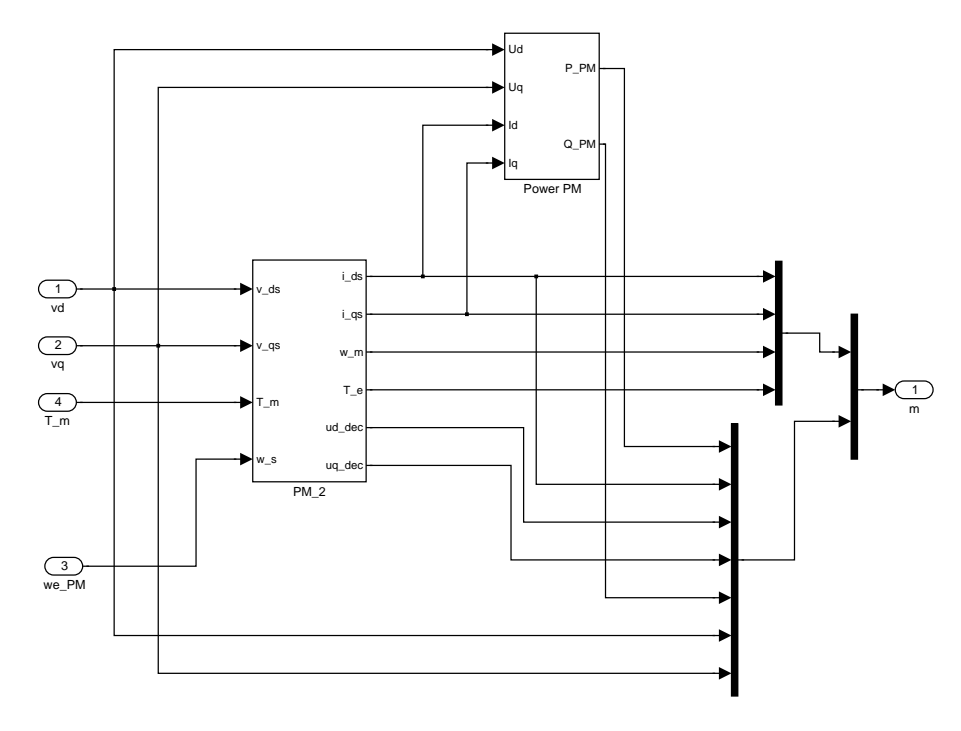


Figure 99: Simulink PM electrical system model: PM1

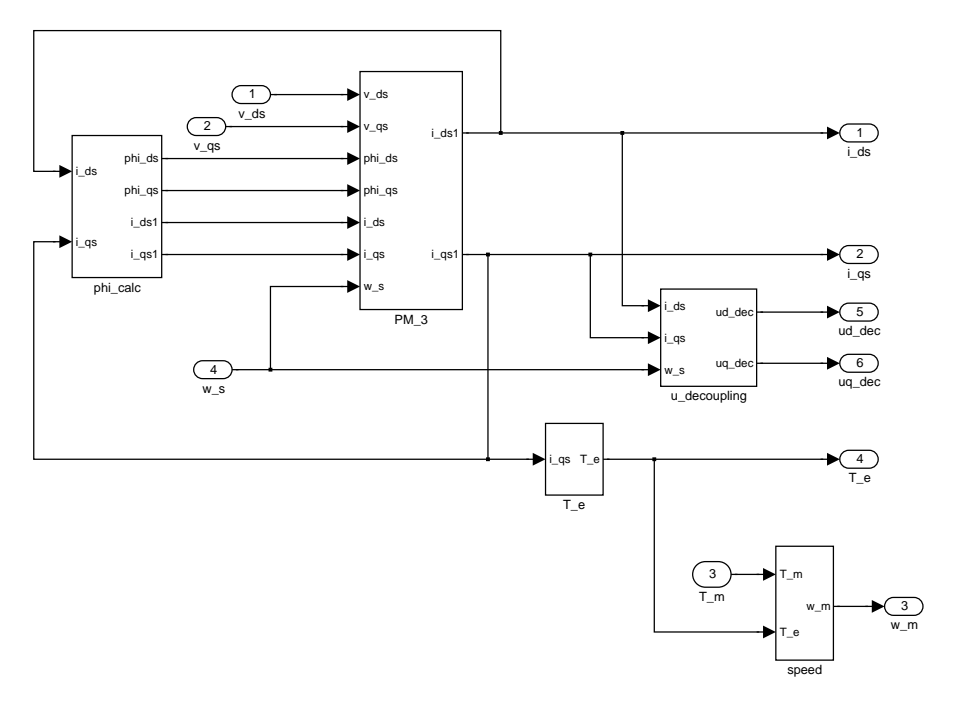


Figure 100: Simulink PM electrical system model: PM2

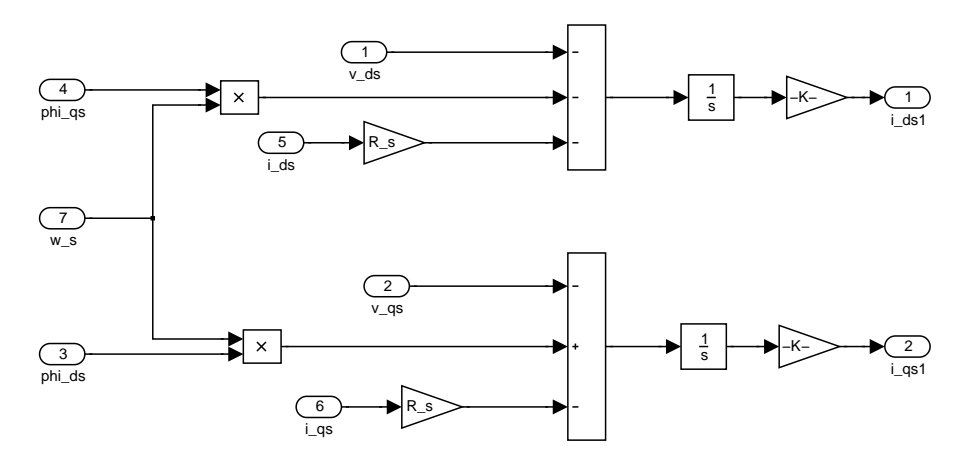


Figure 101: Simulink PM electrical system model: PM3

Figure 101 lists the voltage equation which model the PM generator.

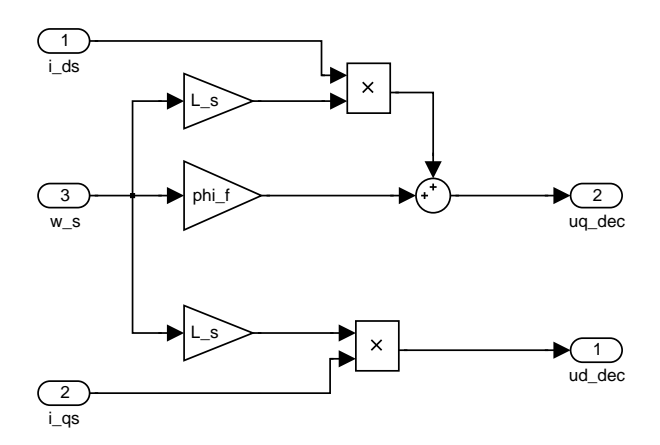


Figure 102: Simulink PM electrical system model: u-decoupling

The setpoint for the voltage phasor is corrected for the cross coupling term $\omega_s\Psi_f$ in figure 102.

4.5 Grid model

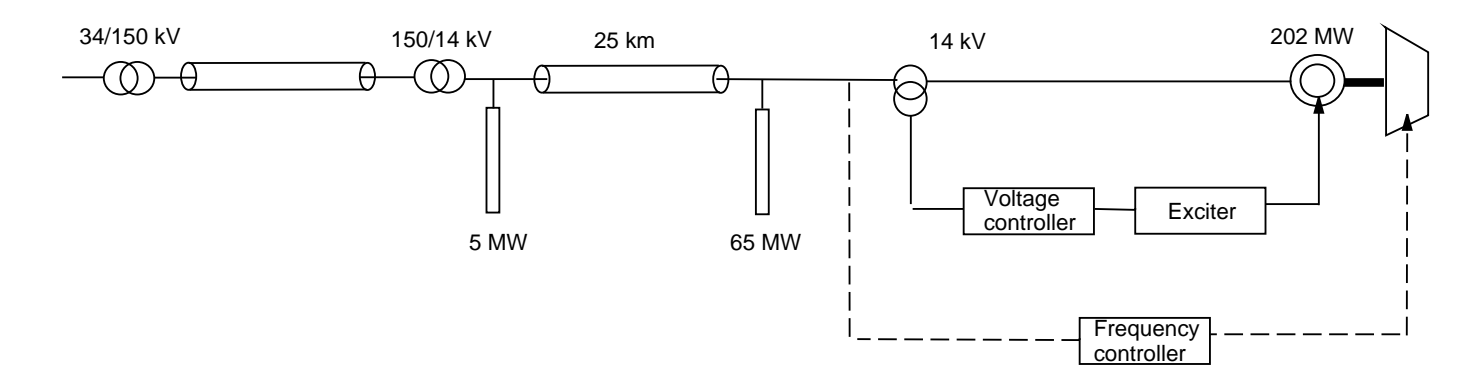


Figure 103: Electrical layout of the equivalent grid model

All wind farm models include a simplified grid model, to simulate the effect of changes in active and reactive wind power as well as changes in consumer power on grid voltage and frequency. The grid model is kept simple: only one large synchronous machine, a transformer, a cable and two consumer loads (figure 103). The synchronous machine controls the grid frequency and the grid voltage.

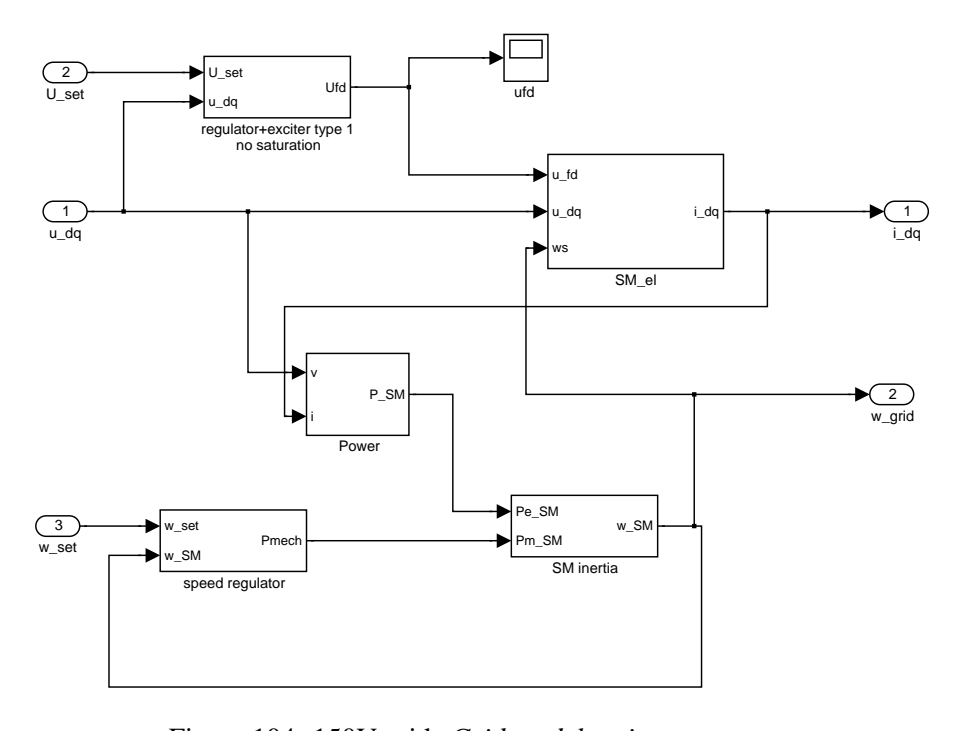


Figure 104: 150V grid: Grid model main components

Figure 104 connects the components of the grid model in Simulink. The voltage equations of the synchronous machine model are evaluated in figure 105. Input variables are the field voltage and the stator voltage phasor. The field current and the stator current phasor are calculated.

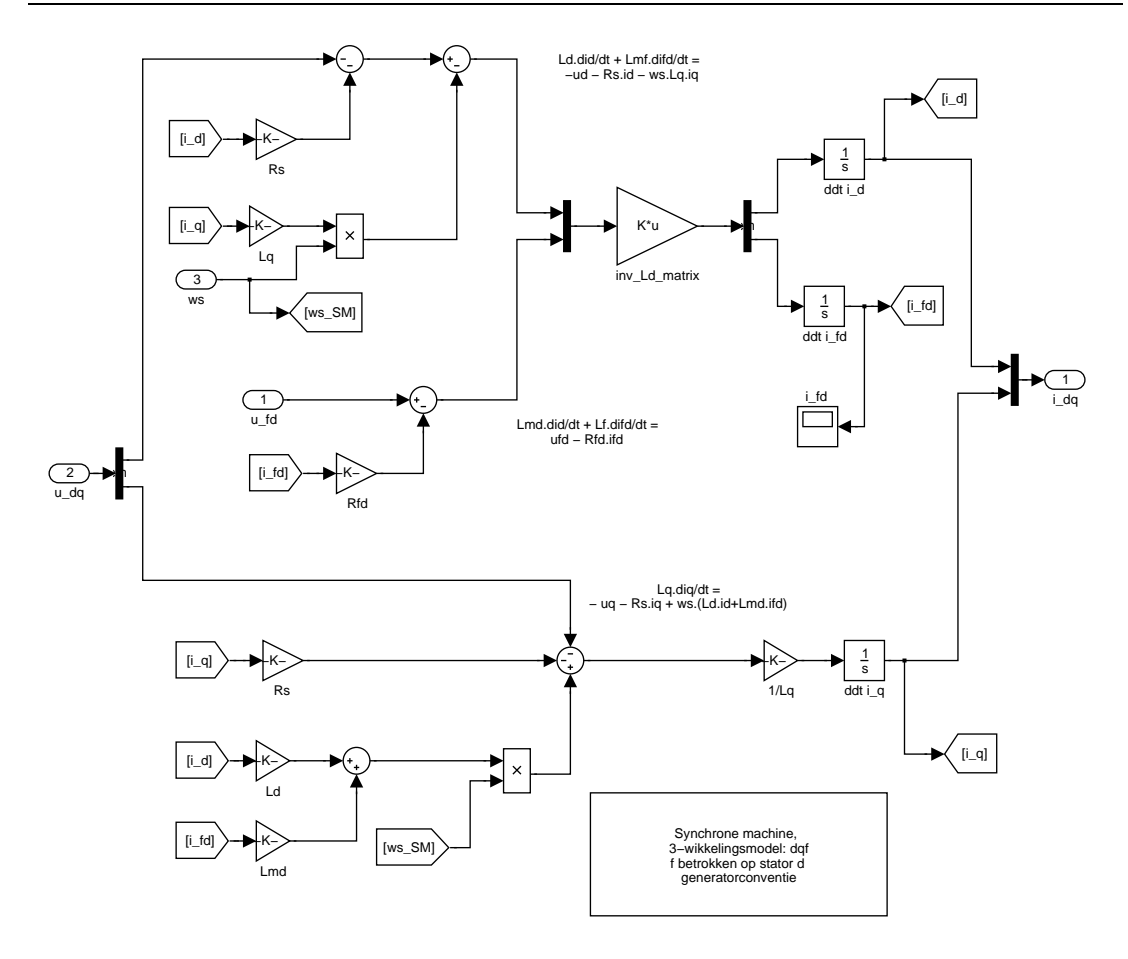


Figure 105: SM el: Synchronous machine voltage equations

The exciter and field regulator model on the synchronous machine (see figure 106) is a type 1 model [1]. It operates on the per unit value of the stator voltage amplitude and generates a per unit value of the field voltage. The parameters have been taken from a SimPowerSystems example and give a satisfactory grid voltage behaviour.

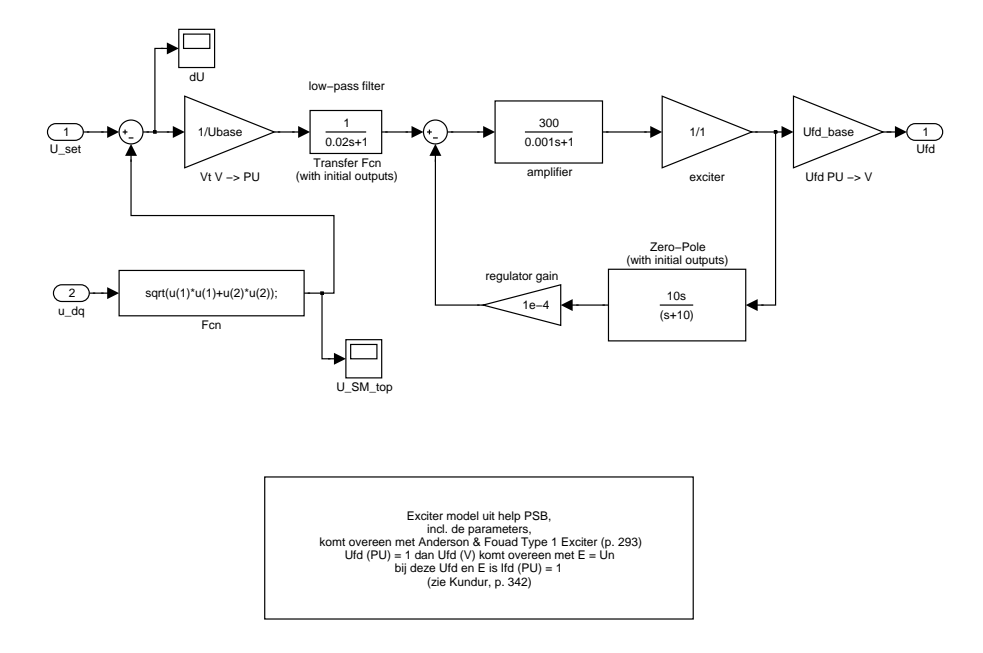


Figure 106: Regulator + exciter type 1: Model for the field voltage control

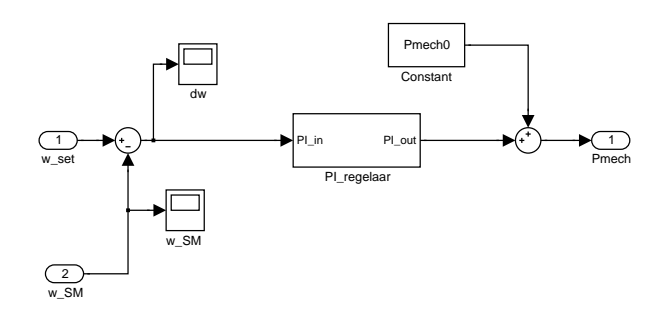


Figure 107: Speed regulator: grid frequency controller

Figure 107 shows the grid frequency controller. The synchronous machine inertia is modelled in figure 108.

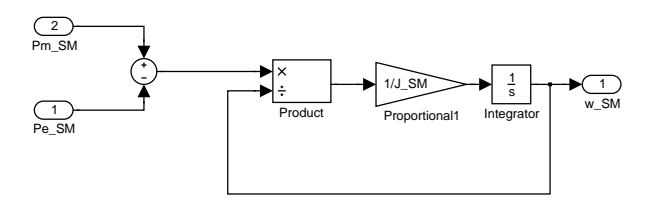


Figure 108: SM inertia: Synchronous machine and consumers equivalent rotating inertia

The cable model presented in the previous sections has been modified to connect the synchronous generator to the wind farm models. Since the wind farm and the synchronous generator both calculate the current phasor and need the voltage phasor as input, the cable model was modified (see figure 109). The equations of both cable models are the same.

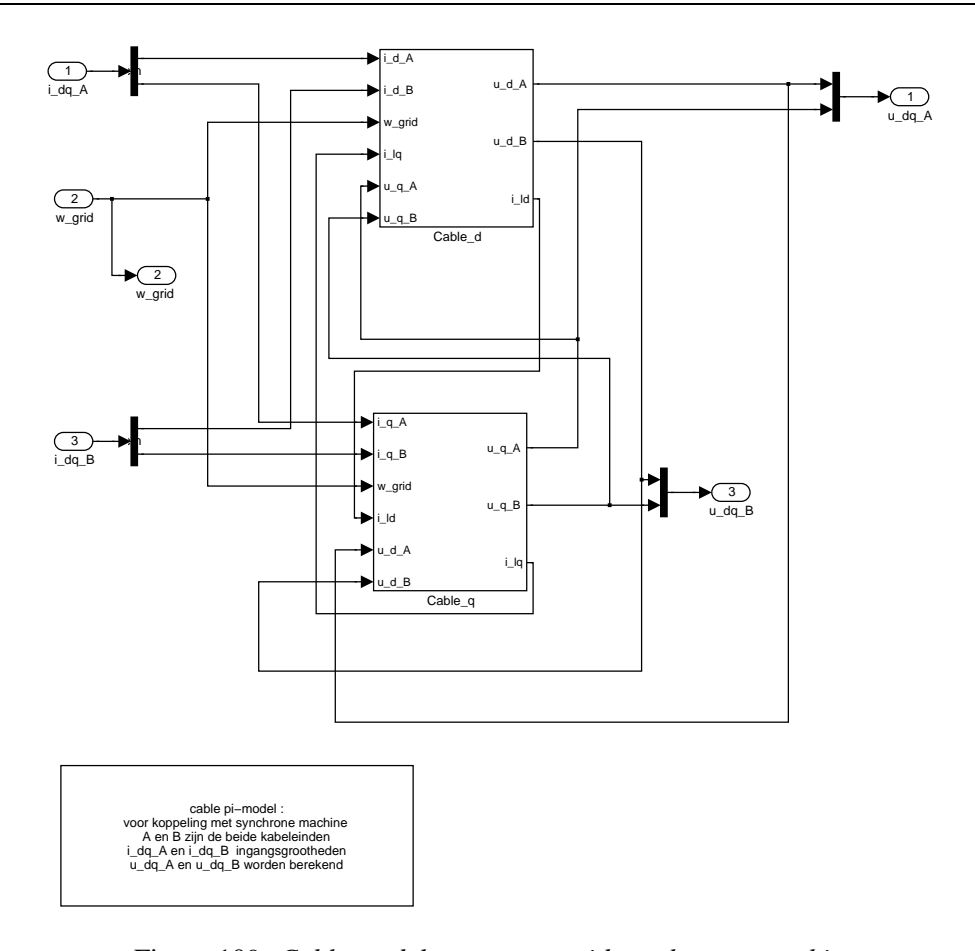


Figure 109: Cable model to connect grid synchonous machine

5 FLICKER METER

5.1 Introduction

Light flicker is the changing intensity of an electric light, caused by voltage variations. The frequency of the variation is important: the annoyance caused by flicker depends on the rate of change. Figure 110 gives the level of voltage changes as function of the frequency of the changes which is just visible by humans. This curve, called the flicker curve, is empirically determined by subjecting persons to light from a 60W lamp fed by a voltage with rectangular variations of different intensity and frequency. The figure shows that the human eye is most sensitive to variations in the range of 1000/60=16.67 Hz and therefore these variations will receive the most weight in a flicker evaluation.

A flicker evaluation is part of the Power Quality assessment of grid connected wind turbines (IEC 61400-21). The evaluation quantifies the voltage amplitude variations caused by a wind turbine and compares them to the levels of the flicker curve.

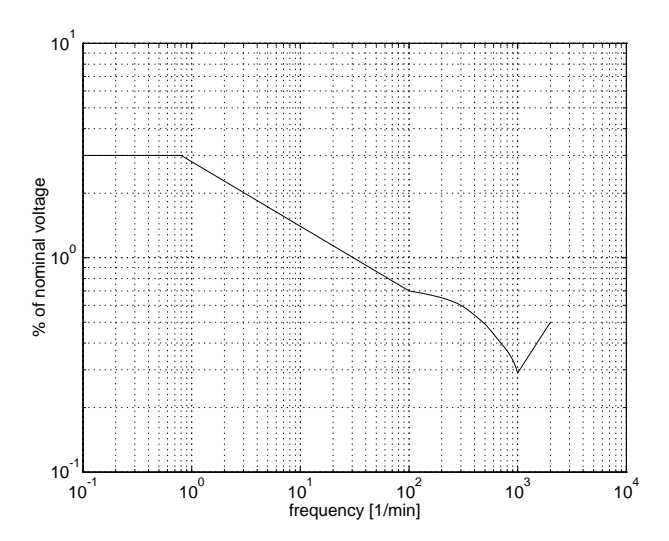


Figure 110: Flicker curve: the level of voltage amplitude variation visible by the human eye

Changes in power and reactive power of wind turbines and switching operations cause flicker. Power fluctuations in the range relevant for flicker (0.5-35Hz) are mainly cased by:

- turbulence;
- wind shear;
- tower shadow;
- yaw misalignment.

For frequencies above 1Hz the blade passing frequency and its multiples dominate the power spectrum and therefore are critical in the assessment of flicker. In constant speed systems, the variations in aerodynamic power are almost instantaneously transmitted to variations in electric power. Figure 111 gives an example of the measured flicker level caused by a constant speed turbine as function of the relative power P/P_{rated} produced by the turbine. The flicker level $P_{st}=1$ if the voltage variations are equal to the level in the flicker curve.

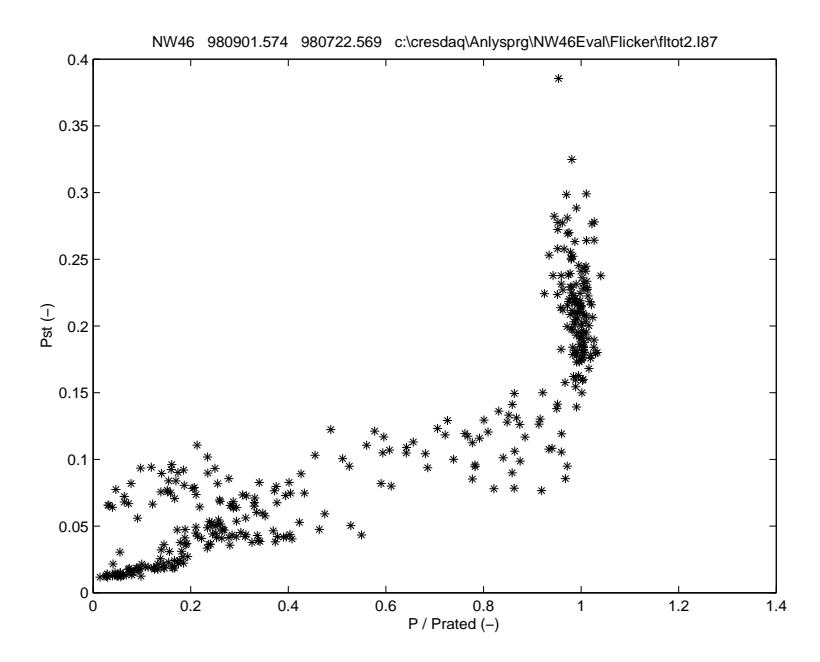


Figure 111: Measured flicker levels P_{st} as function of the relative power for a constant speed turbine

The actual amount of flicker caused by a wind turbine not only depends on the turbine properties but also on the characteristics of the grid at the point of common coupling. A high short circuit ratio will reduce flicker, while nearby producers or loads may increase the flicker level. The aim of a flicker measurement is a test result which is independent of the grid conditions at the test site. To accomplish this, the IEC61400-21 standard [24] specifies a method that uses current and voltage time series measured at the wind turbine terminals to simulate the voltage fluctuations of a fictitious grid with no source of voltage fluctuations other than the wind turbine. Prior to the description of the flicker meter, this method will be summarized.

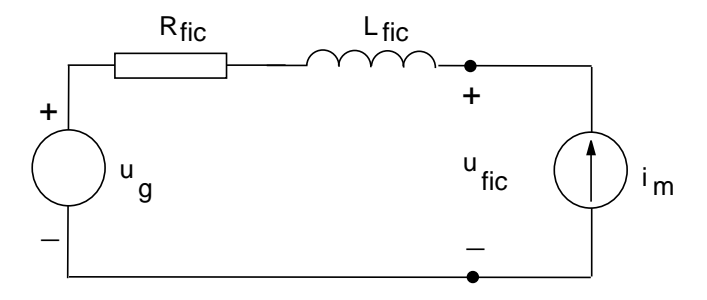


Figure 112: Fictitious grid for flicker evaluation

The fictitious grid is represented by an ideal voltage source with instantaneous voltage u_g and a grid impedance consisting of a resistance R_{fic} in series with an inductance L_{fic} , see figure 112. The wind turbine is represented by a current source i_m . The ideal voltage source will satisfy two criteria:

- ullet the amplitude is constant, i.e. no contribution to the flicker level of the voltage u_{fic} ;
- the instantaneous angle α_m between u_g and i_m is equal to the instantaneous angle between the measured voltage at the PCC and i_m . This ensures that the angle between

 u_{fic} and i_m is practically equal to α_m , since the voltage drop over the grid impedance is small.

For the wind turbine and wind farm models, the PCC voltages u_d and u_q are known and the second requirement can be satisfied by calculating a voltage of amplitude U_n and angle $\angle(u_q, u_d)$. Another option, slightly more time consuming, would be a phase locked loop on the voltage.

The three-phase short circuit power of the fictitious grid is given by:

$$S_{k,fic} = \frac{U_n^2}{\sqrt{R_{fic}^2 + X_{fic}^2}}$$
 (123)

A proper ratio between $S_{k,fic}$ and S_n must be used to assure that the applied flicker meter algorithm or instrument gives short term flicker values P_{st} within the measurement range required in IEC 61000-4-15. As a guide, a ratio of 50 between $S_{k,fic}$ and S_n is suggested in IEC 61400-21. The actual ratio selected will affect the instantaneous flicker level but it will not affect the resulting flicker coefficients as long as it does not bring the flicker meter outside its valid range.

The flicker coefficient $c(\psi_k)$, with ψ_k the fictitious grid impedance angle, for continuous operation of the turbine is determined by:

- measuring the three line currents and the three phase-to-neutral voltages with a sample frequency of 1600 Hz. The cut-off frequency of the measurements shall be at least 400 Hz;
- taking 10 minute time series of instantaneous current and voltage measurements;
- measuring the wind speed simultaneously and determining the 10 minute average.

The flicker coefficient for a 10 minute measurement is determined by:

- calculating the fictitious grid voltage u_{fic} ;
- determining the instantaneous flicker value (perceptability value) $P_{f,fic}$ for the turbine connected to the fictitious grid with a flicker meter;
- determining the short term flicker $P_{st,fic}$ by binning and determination of the 99% percentile value (99% of the instantaneous flicker values are below this value);
- calculating the flicker coefficient:

$$c(\psi_k) = P_{st,fic} \frac{S_{k,fic}}{S_n} \tag{124}$$

The flickermeter has been constructed in Simulink and can be used for both on-line and off-line evaluation. The model consists of the same blocks as the analogue flickermeter which is described in the IEC 60868 and IEC 61000-4-15 standards and is elaborated in section 5.2. The separate bocks are described in section 5.3.

5.2 Flicker meter

The analogue flickermeter as described in IEC 60868 and IEC 61000-4-15 consists of 5 blocks, cf. figure 113:

- 1. input voltage adapter and calibration checking unit;
- 2. square law demodulator;
- 3. weighting filters, squaring and smoothing (electric attenuation);
- 4. weighting filters, squaring and smoothing (human response);
- 5. on-line statistics.

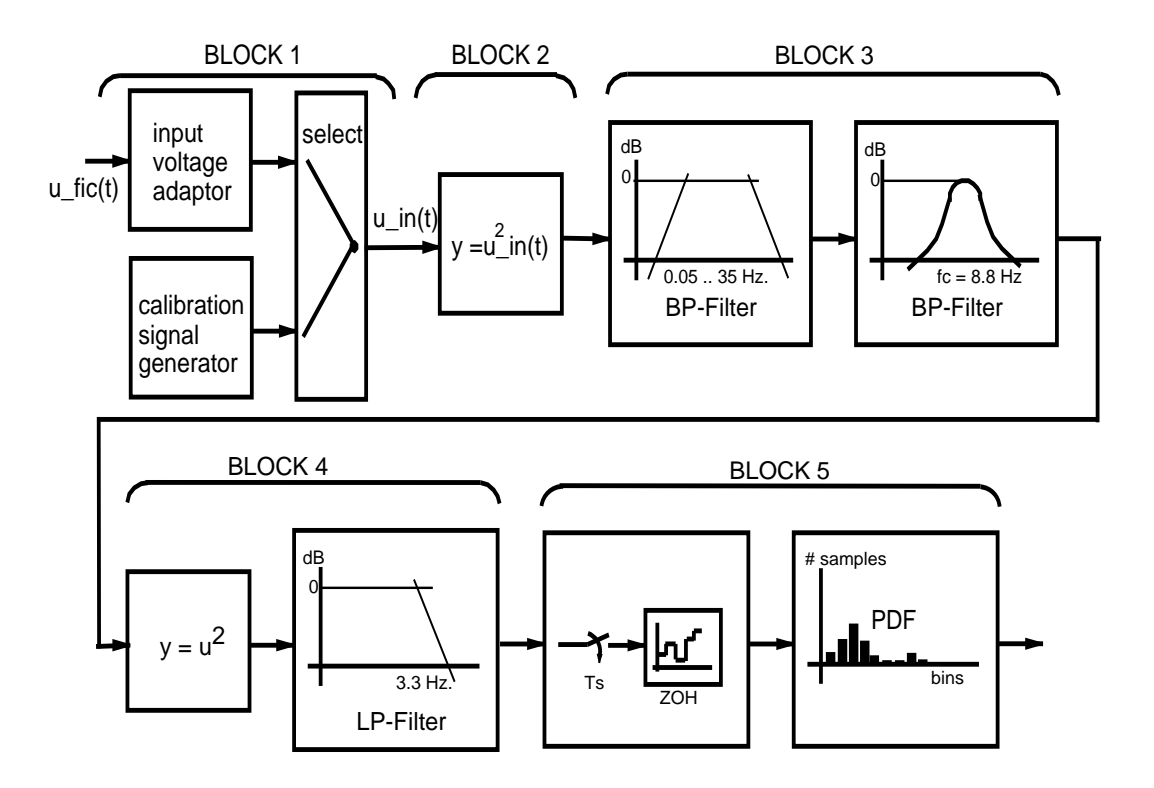


Figure 113: Block scheme of flicker meter

The voltage adaptor in block 1 is not necessary in the simulation model as its purpose is to match the input signal to the limited dynamic range of the analogue flicker meter. The calibration signal generator has been implemented to check the proper operation of the flickermeter. Block 3 eliminates the d.c. and double mains frequency and simulates the response of a coil filament gas filled lamp (60W - 230V). Block 4 simulates the human perception of a flickering lamp. Finally block 5 classifies the perceived flicker level and builds a probablilty density function by binning the measured instantaneous flicker levels.

An extra block, a so-called fictious grid which is also described in the standards, generates the input voltage of block 1 from the measured line currents.

5.3 Implementation in Simulink

This section gives a description of each of the blocks in the flicker meter in figure 113. Figure 114 shows how the flickermeter has been implemented in Simulink.

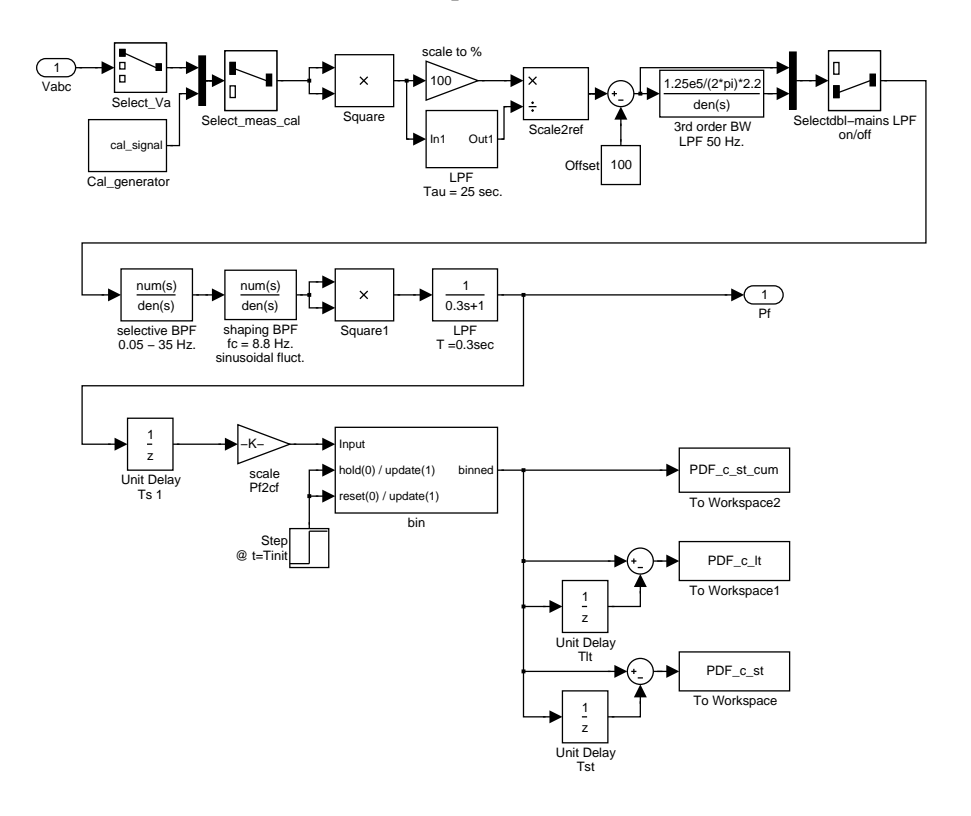


Figure 114: Overview of flicker meter in Simulink

Input selector and calibration signal generator (Block 1)

In this block one of the three line voltages is selected. The calibration signal is a sinewave at grid frequency which is amplitude modulated, as shown in figure 115. The modulated signal is a square-wave of 50/17 Hz with an amplitude equal to 1% of the sinusoidal carrier. This calibration signal, which is prescribed in the standard, should give a unity flicker level output.

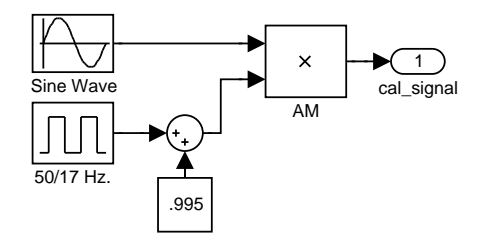


Figure 115: Calibration signal generator in Simulink

Simulation of lamp-eye-brain chain (Blocks 2, 3 and 4)

Block 2 squares the input signal and normalizes the output to unity by dividing it by the low-

pass filtered signal. This first-order filter has a settling time of 60 seconds. In order to speed-up the initial settling of this filter the settling time of the filter can be switched to a 100 times faster rate, as shown in figure 116.

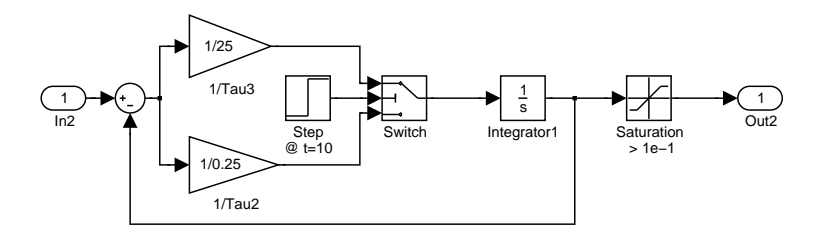


Figure 116: LPF with switching time-constant in Simulink

This block is followed by a second order band-pass filter with a bandwidth from 0.05 Hz to 35 Hz to suppress the d.c. component and double-mains frequency. After this, the signal passes through a shaping band-pass filter centered at 8.8 Hz followed by a square multiplier and a low-pass filter with a time-constant of 300 msec. The output is the instantaneous flicker level $P_f(\psi_k)$.

Yet an extra low-pass filter had to be added to suppress the remaining double-mains frequency signal effectively. For this a third order Butterworth low-pass filter with a cut-off frequency of 50 Hz was chosen. Without this extra filter a flicker-free input signal results in an offset of the output signal $P_f(\psi_k)$ of about 0.8 for 60 Hz mains frequency (and 1.2 for 50 Hz mains frequency). With this extra low pass filter the gain had to be tuned to get a unity flicker level output for the calibration input signal.

Data analysis (Block 5)

To calculate the short-term and long term flicker coefficients $c_{st}(\psi_k)$ and $c_{lt}(\psi_k)$ for a certain grid angle ψ_k , a cumulative probability density function (PDF) over the corresponding periods $T_{st}=60$ sec and $T_{lt}=120$ min has to be built. This PDF is generated as follows: The instantaneous flicker level $P_f(\psi_k)$ is sampled with a sample time T_s of 2.5 msec and then scaled to the short-circuit power of the wind farm, as the instantaneous flicker coefficient $c_f(\psi_k)=P_f(\psi_k)\cdot S_{k,fic}/S_n$, with $S_{k,fic}$ being the grid short-circuit power and S_n the nominal power of the wind turbine.

Then all samples $c_f(\psi_k)$ over a measurement period T_{st} are binned. Therefore each sample is scaled with a factor $No_bins/c_{f,max}(\psi_k)$, with No_bins being the number of bins and $c_{f,max}(\psi_k)$ the maximum expected flicker coefficient. Then the output is mapped to one of the bins by limiting the signal between 1 and No_bins and then generating a vector with a length equal to No_bins . The elements of this vector are zero except for one element with value 1 at the position which corresponds to the instantaneous flicker coefficient (see figure 117). The cumulative sum of this vector, which is updated each period T_s , is the cumulative PDF.

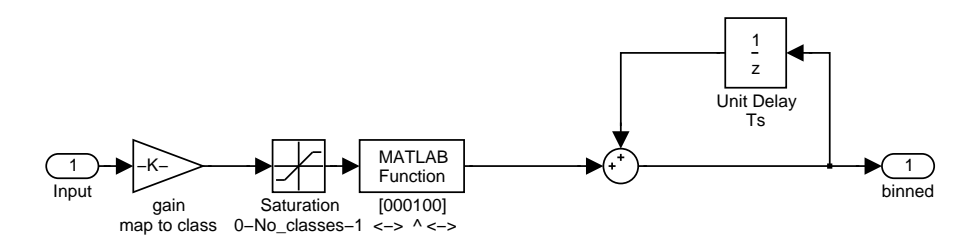


Figure 117: Binning the flicker samples in Simulink

This cumulative PDF and the PDF over each consecutive period T_{st} and T_{lt} as well are written to the MATLAB workspace as "PDF_c_st_cum", "PDF_c_st" and "PDF_c_lt". With these functions the short-term and long-term flicker coefficient $c_{st}(\psi_k)$ and $c_{lt}(\psi_k)$ are determined using M-functions.

Fictious grid

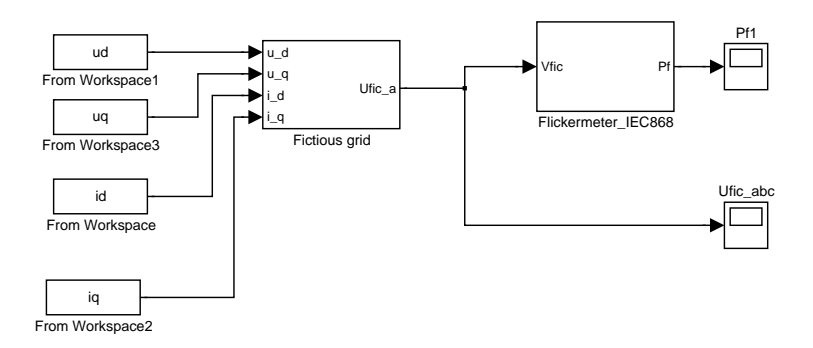


Figure 118: Flicker calculation in Simulink

Figure 118 connects the fictitious grid model to the flicker meter. In the fictitious grid model, see figure 119, the measured line current $i_m(t)$ is injected into a grid consisting of an ideal flicker-free voltage source $u_0(t)$ and a short-circuit impedance $R_{grid} + j\omega L_{grid}$.

The resulting voltage is:

$$u_{fic}(t) = u_0(t) + R_{orid} \cdot i_m(t) + L_{orid} \cdot di_m(t)/dt$$
(125)

 $u_{fic}(t)$ should be calculated for four angles ψ_k of the grid impedance: 30, 50, 70 and 85 degrees, with:

$$\psi_k = \arctan(\omega L_{qrid}/R_{qrid}) \tag{126}$$

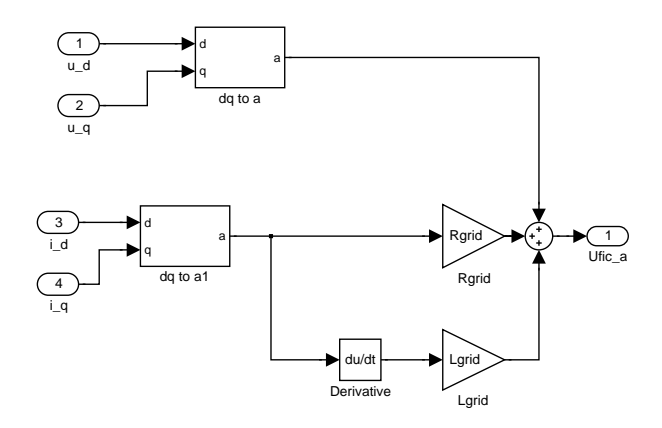


Figure 119: Fictious grid in Simulink

Initialisation

The pre-load function "Init_flicker.m" defines the electrical parameters and sets their values. It sets the input selector in block 1 of the flickermeter: one of the line-voltages Va, Vb or Vc is selected and then either the calibration signal or the selected line-voltage is passed as input signal. The various sample times and measuring times are set, followed by the number of bins and the maximum expected flicker level for the calculation of the PDF.

Post-processing

The function called at simulation stop is "Calc_flicker.m". In this function the flicker coefficients $c_{st}(\psi_k)$ and $c_{lt}(\psi_k)$ are calculated. For $c_{st}(\psi_k)$ this is done by calculating the cumulative probability $p[x < c_{st,i}(\psi_k)]$ using PDF_c_st with $c_{st,i}(\psi_k)$ increasing from 0 up to the maximum expected flicker coefficient. The result $c_{st}(\psi_k)$ is the minimum value of $c_{st,i}(\psi_k)$ for which this probability is equal to or higher than 99%.

5.4 Testing the flicker meter in Simulink

In this section the response of the simulated flicker meter to a calibration signal and a load step in a simulated test circuit are presented. Secondly, the on-line calculation of the voltage change factor for two types of input signals is demonstrated.

5.4.1 Response to calibration input signal

The calibration signal is a 50 Hz sine wave that is amplitude modulated with a symmetrical square wave signal, as illustrated in figure 115. Figure 120 shows a detail of the calibration signal that is switched on and off around t=12 sec and t=16 sec. The period before t=10 sec is not shown as this is used for stabilizing the flicker meter output signal. The response of the flicker meter to the calibration signal is shown in figure 121: as required it generates a value of oscillating around an instantaneous flicker value of 1.

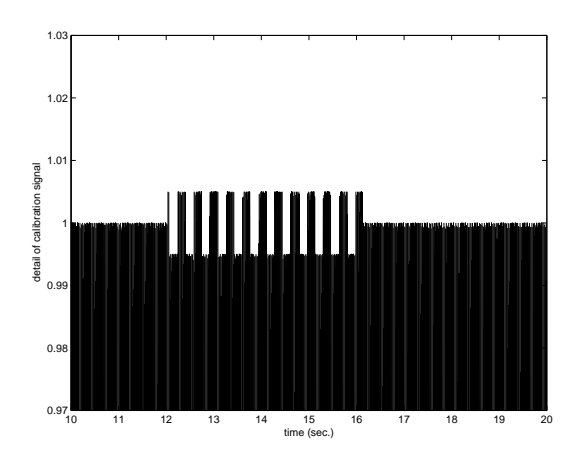


Figure 120: Amplitude modulated calibration signal

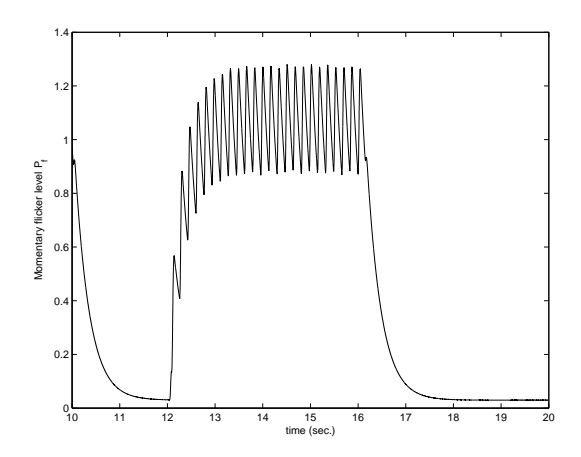


Figure 121: Response of the flicker meter to the calibration signal

5.4.2 Response to modulated grid voltage and load step

The flicker meter has been tested using the circuit in figure 122, where components of the Power Systems Blockset simulate an electrical network during switching operations. The flicker source in this network is the amplitude modulated "3-Phase programmable Voltage Source". The amplitude of the modulated signal is 0.25 p.u. and the frequency is 8.8 Hz. The modulation starts at t=12 sec and ends at t=15 sec. Subsequently a 50 kW load step is generated by closing the "3-Phase Breaker" at t = 18 sec and reopening it at t=19 sec. The measured line currents are injected into the fictious grid with a short-circuit impedance chosen equal to 25 MVA with an angle of 30 degrees. The flicker level for the measured input current $i_m(t)$ is small as the short-circuit power of the fictious grid is relatively high.

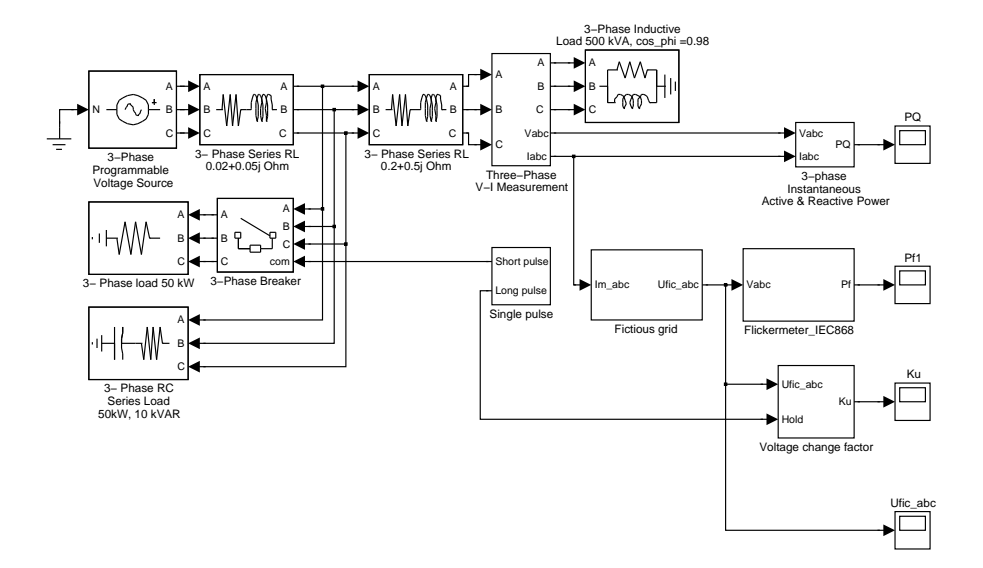


Figure 122: Test circuit with flicker meter

Figure 123 shows the response $u_{fic}(t)$ of the fictious grid for the line voltage U_a . Figure 124 shows the calculated instantaneous flicker $P_f(\psi_k)$.

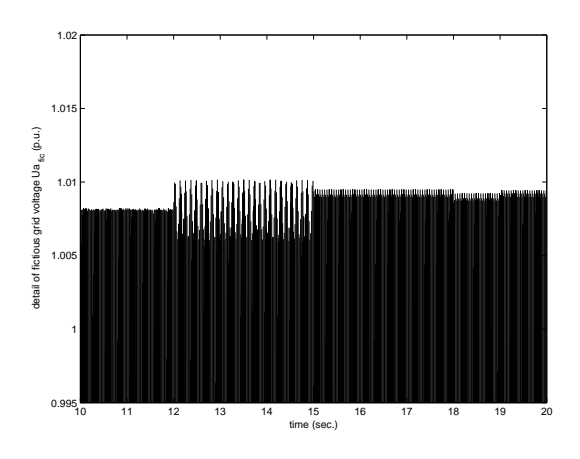


Figure 123: Output voltage of the fictious grid

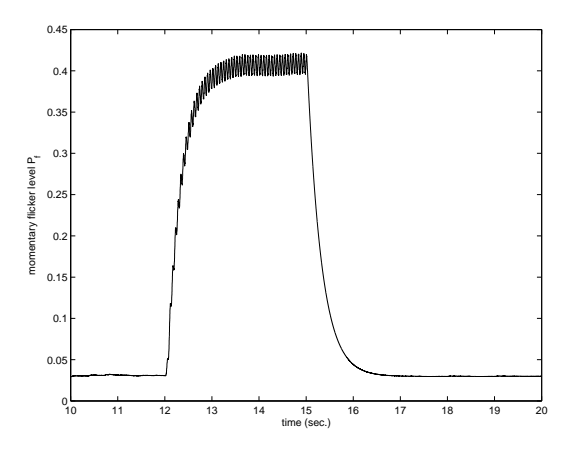


Figure 124: Response of instantaneous flicker level

Figure 125 shows the cumulative probability density function of the flicker coefficient at t=18 sec for the input signal of figure 123.

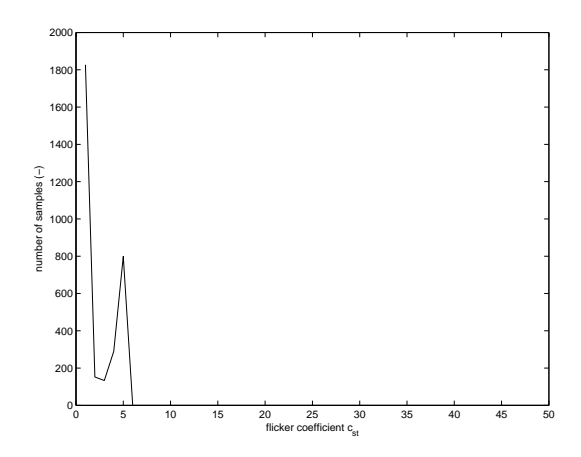


Figure 125: Cumulative probability density function

Calculation of the flicker step factor and voltage change factor

The flicker step factor and voltage change factor are calculated for the output voltage in figure 123. The flicker step factor $k_f(\psi_k)$ is calculated as:

$$k_f(\psi_k) = \frac{1}{36} \cdot \frac{S_{k,fic}}{S_n} \cdot P_{st}(\psi_k)$$
 (127)

The voltage change factor $k_U(\psi_k)$ is calculated as:

$$k_U(\psi_k) = \sqrt{3} \cdot \frac{S_{k,fic}}{S_n} \cdot \frac{U_{fic,max} - U_{fic,min}}{U_n}$$
 (128)

with $U_{fic,max}$, $U_{fic,max}$ and U_n being the maximum, minimum and nominal one period RMS voltage on the fictious grid during the switching operation. For the calculation of $U_{fic,max}$ and $U_{fic,min}$ over a certain measurement period of time a separate block has been defined, which is shown in figure 126.

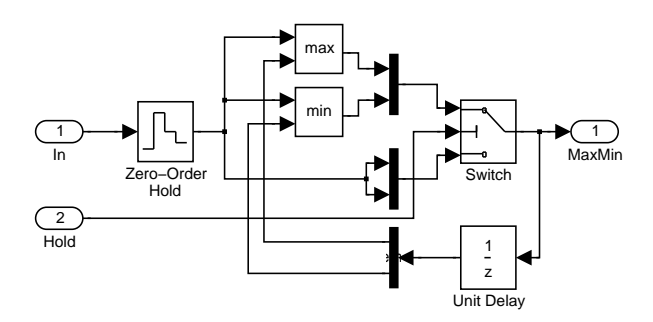


Figure 126: Calculation of minimum and maximum voltage

Figure 127 shows the response of the voltage change factor $k_U(\psi_k)$ for all three line voltages for the simulated load step at t=18 sec. It shows that the load decrease at t=19 sec contributes

most to $k_U(\psi_k)$. Further the voltage change differs for the three line voltages, depending on the timing of the switching operation.

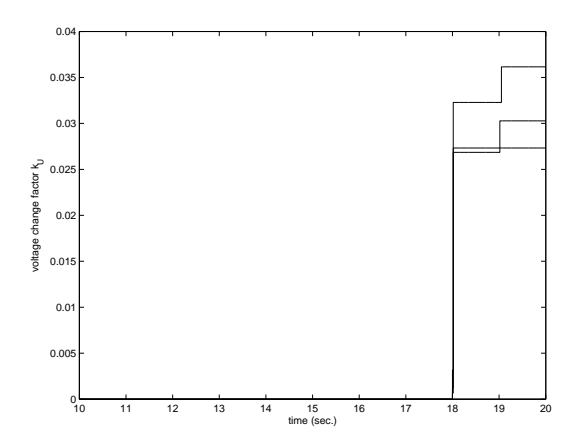


Figure 127: Calculated voltage change factor

5.5 Conclusion

A flicker meter has been build in Simulink by implementing the blocks of the flicker meter in IEC 60868 and IEC 61000-4-15. The response of the flicker meter was tested by applying a calibration signal as well as a simulated grid response. The results demonstrated proper operation.

6 CONCLUSIONS AND REMARKS

6.1 Conclusions

- Dynamic models of offshore wind farms have been developed based on individual turbine models. The models include aerodynamic aspects and mechanical details of the turbines, the electrical system of the turbine, the cable connections inside the farm and the connection to the substation on shore. These models present a powerful tool for the investigation of wind farm dynamics and wind farm-grid interaction and for the development of wind farm controllers.
- 2. The electrical systems modelled in the wind farms are (1) the directly coupled induction generator (IG), (2) the cluster coupled induction generator (CC), (3) the doubly-fed induction generator (DFIG) and (4) the permanent magnet generator with full converter (PM). The turbines modelled in the wind farms are (1) the constant speed stall turbine (CSS) and (2) the variable speed pitch turbine (VSP).
- 3. A simplified grid model has been included to enable simulation of wind farm-grid interaction.
- 4. All electrical models, including the models of cables, transformers and the grid model, are based on the Park transformation to increase computational speed in quasi steady-state conditions.
- 5. A model of the flicker meter has been developed and tested.
- 6. All models have been implemented in Simulink to ensure full control over the details by the user and to have a powerfull graphical interface. Simulink makes modification and extension of the wind farm models very easy and efficient.
- 7. The wind farm models can be used to develop wind farm control, investigate dynamic interaction within the farm and between wind farm and grid and also to study wind farm response to wind gusts and grid faults. These applications are demonstrated in a number of case studies in Volume 2 of this report.

6.2 Remarks

- 1. Dynamic models of wind farms based on individual turbines are large and complicated. The number of state variables is high and some of the time constants are small, leading to a relatively long simulation time. For the incorporation of dynamic models of (a number of) wind farms in models of national grids, the complexity of the wind farm models has to be reduced. Aggregated wind farm models, in which all turbines are represented by some kind of equivalent model are more suitable for this purpose. However, aggregated models loose the wide range of applicability of the wind farms based on individual turbines.
- 2. Simulink appears to be less suitable for very large models with many (thousand or more) state variables. Computation of the steady state becomes very time consuming and the simulation time for normal runs increases more than proportional. The exact cause needs to be discussed with Mathworks, the developer of Simulink.
- 3. With regard to simulation speed the choice of dq0-variables proved successful. The current bottleneck is not the simulation speed of the electrical part any more but of the

mechanical and control part of the variable speed turbine model. This submodel has to be increased in speed before comfortable full scale farm simulations can be made for variable speed systems. The variable speed turbine in the current version is still programmed as an S-function in Matlab. Conversion to Simulink blocks will probably reduce CPU time.

- 4. In the current Simulink implementation the 0-component, which is only relevant under specific asymmetrical conditions is not implemented. Since short circuit calculations are increasingly relevant and asymmetrical short circuit have a high probability of occurrence, it is recommended to include it in the next version.
- 5. Now that the model development has reached a certain level of completion, model validation is a high priority task. A database with turbine and wind farm measurement is currently being set up in IEA Annex XXI: Wind Farm Models for Power System Studies. This database will serve as the basis for the validation process, executed in the Erao-3 project, which has recently been started.

For the conclusions and recommendations from the case studies is referred to Volume 2 of this report.

REFERENCES

- [1] P.M. Anderson and A.A. Fouad. *Power System Control and Stability*. Iowa State Univ. Press, Iowa, 1977.
- [2] J.C. Das. *Power System Analysis Short Circuit Load Flow and Harmonics*. Marcel Dekker, Inc., New York, 2002.
- [3] C.L. Fortescue. Method of symmetrical coordinates applied to the solutions of polyphase networks. *Trans. of AIEE, Vol. 37*, pages 1027–1140, 1918.
- [4] J.J. Grainger and Jr. W.J. Stevenson. *Power System Analysis*. McGraw-Hill, New York, 1994.
- [5] L. Harnefors and H.-P. Nee. Model-based current control of ac machines using the internal model control method. *IEEE Trans. Ind. Appl., Vol. 34, No. 1*, pages 133–141, 1998.
- [6] S.A. Herman and J.T.G. Pierik. Locaties en opwekkosten 6000 MW offshore windenergie. Technical Report ECN-CX- -03-086, ECN, 2003.
- [7] C.P.J. Jansen and R.A.C.T de Groot. Aansluiting van 6000 MW offshore windvermogen op het Nederlandse elektriciteitsnet, Deel 2: Net op land. Technical Report 40330050-TDC 03-37074B, Kema, 2003.
- [8] The Mathworks. *Using Matlab/Simulink/Simpower*. The Mathworks, Natick MA, 2001.
- [9] N. Mohan, T.M. Undeland, and W.P. Robbins. *Power Electronics Converters, Applications and Design*. John Wiley & Sons, New York, 1995.
- [10] J. Morren, S.W.H. de Haan, P. Bauer, and J.T.G. Pierik. Comparison of complete and reduced models of a wind turbine using doubly-fed induction generator. In *10th European Conference on Power Electronics and Applications (EPE 2003)*, Toulouse, 2003.
- [11] J. Morren, S.W.H. de Haan, and J.A. Ferreira. Model reduction and control of electronic interfaces of voltage dip proof DG units. In 2004 IEEE Power Engineering Society (PES) General Meeting, Denver, 6- 10 June 2004. to be published.
- [12] E.ON Netz. Ergänzede Netzanschlussregeln für Windenergieanlagen. Technical report, E.ON Netz, 2001.
- [13] C.-H. Ong. *Dynamic Simulation of Electric Machinery using Matlab/Simulink*. Prentice Hall, Upper Saddle River, 1998.
- [14] R. Ottersten. *On control of Back-to-Back Converters and Sensorless Induction Machine Drives*. Technical Report no. 450, Chalmers University, Goteborg, Sweden, 2003. Ph.D. thesis.
- [15] G.C. Paap. Symmetrical components in the time domain and their application to power network calculations. *IEEE Trans. Power Systems, Vol. 15, No. 2*, pages 522–528, 2000.
- [16] R. Pena, J.C. Clare, and G.M. Asher. Doubly fed induction generator using back-to-back pwm converters and its application to variable-speed wind-energy generation. In *IEEE Proc.-Electr. Power Appl, Vol. 143*, *No. 3*, pages 231–241. 1996.

- [17] A. Petersson. Analysis, Modelling and Control of Doubly-Fed Induction Generators for Wind Turbines, Licentiate thesis. Technical Report 464L, Chalmers University, Goteborg, Sweden, 2003.
- [18] J.T.G. Pierik, M.E.C. Damen, P. Bauer, and S.W.H. Electrical and control aspects of offshore wind farms, Phase 1: Steady state electrical design and economic modeling, Vol. 1: Project results. Technical Report ECN-CX-01-083, ECN Wind Energy, 2001.
- [19] J.T.G. Pierik, J.C. Montero Quiros, T.G. van Engelen, D. Winkelaar, and R. Sancho Chaves. Costa Rica grid feed-in study: Effect of wind power on grid frequency. Technical Report ECN-CX-03-080, ECN, 2003.
- [20] I. Schiemenz and M. Stiebler. Control of a permanent magnet synchronous generator used in a variable speed wind energy system. In *IEEE Electric Machines and Drives Conference*, *IEMDC 2001*, pages 872–877, 2001.
- [21] S. Skogestad and I. Postlethwaite. *Multivariable feedback control*. Wiley, Chichester, 1996.
- [22] J.G. Slootweg. Wind power modelling and impact on power system dynamics. Technical Report ISBN 90-9017239-4, T.U. Delft, 2003. PhD Thesis.
- [23] J.G. Slootweg, H. Polinder, and W.L. Kling. Dynamic modelling of a wind turbine with doubly fed induction generator. In *2001 IEEE Power Engineering Society Summer meeting*, pages 644–649, 2001.
- [24] TC88. IEC61400-21, Ed. 1: Measurement and assessment of power quality of grid connected wind turbines. Technical Report IEC61400-21, IEC-TC88, 1999-11-12. Draft.
- [25] T.G. van Engelen, E.L. van der Hooft, and P. Schaak. Ontwerpgereedschappen voor de regeling van windturbines. Technical report.
- [26] T.G van Engelen and E.J. Wiggelinkhuizen. ECN design tool for control development; revised points of departure; status report. Technical report, ECN, 2002.
- [27] P.D. Ziogas, E.P. Wiechmann, and V.R. Stefanoviæ. A computer aided analysis and design approach for static voltage source inverters. *IEEE Trans. on Ind. Appl*, *Vol. 21, No. 5*, pages 1234–1241, 185.

A SUMMARY OF ERAO I PROJECT

The aim of the ERAO project "Electrical and Control Aspects of Offshore Wind Farms" Phase 1 "Steady state electrical design, power performance and economic modeling" has been to investigate the electrical concepts for the interconnection of offshore wind turbines and the transportation of the electric power to the high voltage grid. The project started with an inventory of architectures to collect the electric power from individual wind turbines in an offshore wind farm and transmit this power to an on-shore high-voltage grid node. The inventory included constant speed options, individual variable speed, cluster variable speed and park variable speed options using AC as well as mixed AC-DC-AC modes. Steady state electrical models have been developed for all electrical components in the architectures to calculate load flow and electrical losses. Based on these models, the EeFarm computer program (Electrical and Economic wind FARm Model) has been developed. The EeFarm program has been used in a case study to compare 13 electrical architectures. The electrical parameters voltage, current, active and reactive power have been calculated in all system nodes. Based on the aerodynamic performance of the chosen wind turbine, the electrical losses have been calculated over the entire range of operation of the wind farm. From budget prices obtained from manufacturers, the investment costs of the electrical systems and the contribution to the costs per kWh have been determined.

In the case study two wind farm sizes (100 and 500 MW) and two distances to shore (20 and 60 km) have been investigated. In the constant speed concepts C1 and C2 the wind turbines in the farm are connected by AC and the cable to shore is AC as well. These systems have the smallest number of main components, only transformers and cables. The case study has shown that the systems C1 (string layout) and C2 (star layout), operating on AC only, have the lowest contribution of the electrical system to the price per kWh for both farm sizes and distances to shore. For the 100 and 500 MW farm at 20 km and the 500 MW farm at 60 km, the C1 system also gives the lowest electrical losses.

In those cases where a DC connection is required (longer distance to shore or avoidance of grid stability problems), the PV1 configuration with an HVDC Light or Plus connection is the best alternative. For the investigated distances and park sizes this currently increases the investment costs and contribution of the electrical system to the price per kWh by a factor 2 or more, but this may reduce at longer distances to shore and by price reduction of the converters and more experience is gained with this new technology. The electrical losses of concepts C1 and PV1 are of the same order of magnitude.

The options with individual turbine speed control, IV1 and IV2, although more expensive than the constant speed systems C1 and C2, should not be discarded based on the ERAO case study only. The reason is that they may be preferred by a large number of turbine manufacturers (due to their potential in load reduction and increased controllability) and have a potentially better aerodynamic performance, which was not taken into account in the ERAO case study.

Conclusion: In the analyses of the electrical system options for future developments three architectures should be compared: constant speed (C1-C2), individual variable speed (IV1-IV2) and park variable speed (PV1-PV2). An important criterion should be the dynamic performance of the wind farm, internally as well as with respect to the grid. These are the subjects of the phases 2 and 3 of the ERAO project.

B CONTRIBUTIONS TO INTERNATIONAL CONFERENCES

- **B.1** Nordic Wind Power Conference 2004
- B.2 4th International Workshop on Large Scale Integration of Wind Power and Transmission Networks for Offshore Wind Farms

B.3 EPE 2003 Toulouse

.

	Date: June 2004	Report No.: ECN-C04-050	
Title	Erao II, Volume 1: Dynamic models for wind farms		
Author	J.T.G. Pierik, J. Morren, E.J. Wiggelinkhuizen, S.H.W. de Haan,		
	T.G. van Engelen, J. Bozelie		
Principal(s)	Novem, Ministry of Economic Affairs		
ECN project number	7.4336		
Principal's order number	2020-01-13-10-001		
Programmes	DEN		

Abstract

In The Netherlands offshore wind power is on the brink of implementation. Specific plans exist for two offshore wind farms of about 100 MW, located 12 and 25 km from the coast of the province of North Holland. The effects of the incorporation of 6000 MW offshore wind power in the Dutch high voltage grid are currently investigated. Only the steady state behaviour has been considered, thus far resulting in suggestions for grid reinforcement. This investigation needs to be complemented by a study on the dynamic interaction of wind power and grid. Tools for this investigation, viz. dynamic models of wind farms including all relevant electrical components, have been developed in the Erao-2 project. This report describes the wind farm dynamic models (Volume 1) and demonstrates their use in a number of case studies (Volume 2). Special concern exists about wind farm behaviour during extreme wind speed changes and abnormal grid conditions (voltage and frequency dips); these may cause complete wind farms to shut down instantaneously. Assisting grid voltage and frequency control is also an issue. In the case studies the models have been used to compare four types of wind farms: (1) constant speed stall with directly coupled induction generators and (2) with cluster control, (3) variable speed with doubly fed induction generator and (4) with permanent magnet generator. The case studies compare normal dynamic behaviour, flicker contribution and responses to grid faults. Wind farm control has been developed to support the grid frequency and voltage.

Keywords

wind farm models, wind farm dynamics, electrical systems, fault ride through, grid support

Authorization	Name	Signature	Date
Checked	E.J. Wiggelinkhuizen		
Approved	L.W.M.M. Rademakers		
Authorised	H.J.M. Beurskens		

1

Dynamic models of wind farms for grid-integration studies

Case study results

Jan Pierik[⋄], Johan Morren[♠], Sjoerd de Haan[♠],
Tim van Engelen[⋄], Edwin Wiggelinkhuizen[⋄], Jan Bozelie
[⋄]Energy research Centre of the Netherlands (ECN)
[♠]Delft University of Technology (TUD)

e-mail: pierik@ecn.nl

Abstract – In The Netherlands offshore wind power is on the brink of implementation. Specific plans exist for two offshore wind farms of about 100 MW, located 12 and 25 km from the coast of the province of North Holland. The effects of the incorporation of 6000 MW offshore wind power in the Dutch high voltage grid are currently investigated. Until now only the steady state behaviour is considered, resulting in suggestions for grid reinforcement. This investigation will be complemented by a study on the dynamic interaction of wind power and grid. Tools for this investigation, viz. dynamic models of wind farms including all relevant electrical components, have recently been developed.

This paper gives an overview of wind farm dynamic models and concentrates on their use in a case study. Special concern exists about wind farm behaviour during extreme wind speed changes and abnormal grid conditions (voltage and frequency dips); these may cause complete wind farms to shut down instantaneously. Assisting grid voltage and frequency control is also an issue. In a case study the models will be used to calculate the flicker contribution of a wind farm, simulate responses to grid faults and develop wind farm control.

Index Terms – wind farm models, wind farm dynamics, electrical systems, fault ride through.

I. INTRODUCTION

Offshore wind farms have to be large to be economical and with the increase of the contribution of wind energy to the electric power production, the interaction between the wind farms and the grid will be an important aspect in the planning of the farms [1]. It is essential to ensure that the grid is capable of staying within the operational limits of frequency and voltage for all foreseen combinations of wind power production and consumer loads [8]. A second aspect is to ensure appropriate transient and small signal stability of the grid [10]. Adequate grid control plays an important role but the electrical control and protection of large wind farms is also of increasing importance.

Large wind farms are a source of fluctuating power and sometimes of reactive power as well. Secondly, the response of wind farms to voltage and frequency dips is a cause for worry: the farm will shut down immediately. The dip itself is a sign of a serious grid control problem, and the problem may become worse if wind power shuts down on

a large scale. For conventional power stations the required behaviour during a grid dip is to stay in operation and supply (reactive) power. This behaviour is prescribed in grid codes. It is likely that large offshore wind farms have to follow these rules also. In Germany, operator E.On Netz already requires specific behaviour of wind farms during dips [5]. Depending on the type of wind turbine, viz. constant or variable speed, and the design of the turbine and wind farm control, a wind farm will have more or less problems to comply with these rules.

In order to investigate the dynamic interaction of wind farms and the electrical grid, dynamic models of wind farms are needed. Dynamic models of wind turbines and wind farms will be of great help in the design and evaluation of the behaviour of wind power during normal grid operation as well as during grid faults. Dynamic models of wind farms, including the relevant electrical components and sections of the grid, are not readily available however. The Erao-2 project has been started to develop these models and to demonstrate their use by designing controllers to cope with grid code requirements.

The dynamic models of turbines and wind farms developed in the Erao-2 project include the following components:

Electrical:

induction generator; doubly-fed induction generator; permanent magnet generator; voltage source converter; transformer; cable;

Mechanical and aerodynamic:

turbine rotor; mechanical drive train; tower; rotor effective wind;

Control:

converter controller; wind turbine pitch controller; overall wind farm controller.

To represent the interaction between the wind farm and the grid, a simplified grid model is used, based on the following component models:

Grid model components:

synchronous generator; frequency and voltage controller. consumer load; transformer; cable.

An important aspect of dynamic models for power system studies is computational speed. Electrical transients have very small time constants, resulting in small time steps and long computation time. In Erao-2 special attention has been paid to computational speed. An important increase in speed can be realised by the use of the dq0 transformation (also known as Park transformation). This transformation is mainly used in electrical machine theory, in Erao-2 models it is applied to all electrical components.

This paper can only give an overview of the models. For a detailed description is referred to [4], [12], [11] and [9]. The main characteristics of the electrical models are:

- all electrical components are modelled in dq0 coordinates;
- AC-DC-AC converters are modelled by controlled voltage sources;
- the models are implemented in Simulink.

The electrical component models have only been validated partially, viz. by comparing abc-models with switching converters to dq0-models with controlled voltage source converters [2], [3]. For extensive testing and validation the Erao-3 project has been started, which takes part in the IEA Annex XXI (Dynamic models of Wind Farms for Power System Studies). This Annex is a joint effort of eight countries to set up a data base of wind farm measurements and to use these measurements for validation of dynamic models. The participating countries are Norway (Coordinator), Sweden, Finland, Denmark, USA, England, Portugal and the Netherlands. Observing countries are Canada and Ireland.

II. CASE STUDY

The models developed in the Erao-2 project are used in a case study based on the lay-out of the Near Shore Wind Farm (NSWF): 36 variable speed wind tubines of 2.75 MW, connected in three strings of 12 turbines. The NSWF will be equiped with Doubly Fed Induction Generators (DFIG). In the case study this farm is compared to hypothetical wind farms of the same lay-out with Cluster Control (multiple induction generators on a single AC-DC-AC converter), Permanent Magnet Generators and directly connected induction generators. For each of the four types, normal operation, flicker, response to frequency and voltage dips, and (if technically feasible) frequency and voltage support are simulated (Table 1). In this paper, the some of the results for the Cluster Control option will be given.

Figure 1 shows the layout of one string of the Near Shore Wind Farm (NSWF) in cluster controlled mode. The string is divided into four clusters of three wind turbines on an

AC-DC-AC converter. The converters are connected by 34 kV submarine cables to a 34/150 kV transformer station on shore.

Table 1: Erao-2 case study simulations

	CSS ¹	VSP-DFIG ²	VSP-PM ³	CC-CSS ⁴
Normal operation	X	X	X	X
Flicker	X	X	X	X
Frequency dip	X	X	X	X
Voltage dip	X	X	X	X
Frequency support	-	X	X	X
Voltage support	-	X	X	X

- ¹ Constant Speed Stall
- 2 Variable Speed Pitch Doubly Fed Induction Generator
- ³ Variable Speed Pitch Permanent Magnet generator
- 4 Cluster Controlled Constant Speed Stall

For power limitation of a cluster controlled wind turbine stall or pitch control can be chosen. Both options are technically feasible, in this case study stall control is chosen. The turbine rotational speed is dictated by the frequency of the turbine side AC-DC converter. The effect of rotational speed variation on the aerodynamic power is illustrated in figure 2 by plotting the power-wind speed curves of the stall turbine at frequencies of 20-60 Hz (0.53-1.59 rad/s low speed shaft rotational speed). At 60 Hz the wind speed at which the turbine rotor stalls exceeds the rated wind speed and the rated power of the turbine is exceeded. Therefore, 50 Hz will be the upper speed limit for the cluster controlled stall turbines.

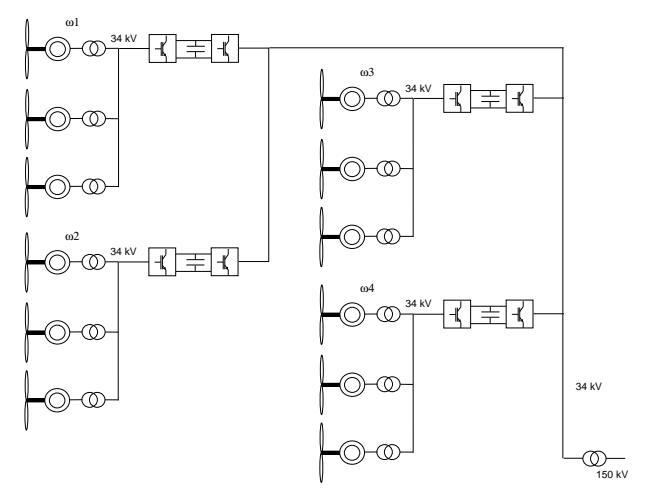


Figure 1: Electrical layout of four clusters of 3 turbines

At low wind speed, below rated rotational speed can increase aerodynamic efficiency compared to constant speed operation: the 20, 30 and 40 Hz curves are above the 50 Hz power curve. At high wind speed a low rotational speed reduces the aerodynamic efficiency compared to constant speed operation. Pitch control can compensate this effect.

Speed control of a cluster will be based on measured wind speed(s). In the simulations, the wind speed at turbine 1 has been chosen, but a different choice may be more efficient. Speed control aims at constant lambda operation for

this wind speed, limited by the 50 Hz barrier.

Since the instantaneous wind speeds at the individual turbines in a cluster will differ, there will always be a mismatch, leading to lower overall aerodynamic efficiency compared to individual variable speed. This reduction in energy yield has been estimated at 1.4% [6]. Maybe this is compensated by a reduction in cost of the electrical system.

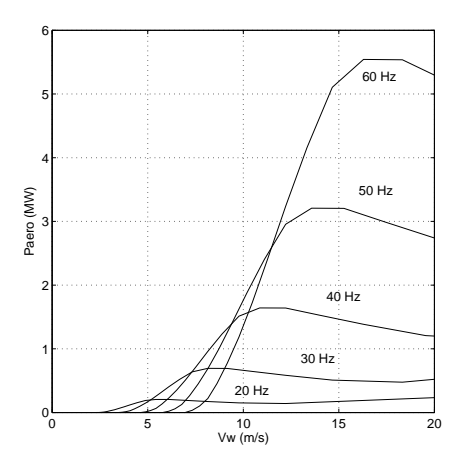


Figure 2: Steady state power curves of a stall controlled turbine

When the frequency in the stator of the induction machine is reduced, the amplitude of the stator voltage is reduced proportional to this frequency. The decrease in frequency would otherwise lead to above rated currents and the activation of the thermal protection. Figure 3 illustrates the combined effect of reduced frequency and voltage: the power-slip and torque-slip curves are similar in shape at 50Hz-960V and 40Hz-768V, only the pull-out power is reduced. The reactive power consumption is reduced as well.

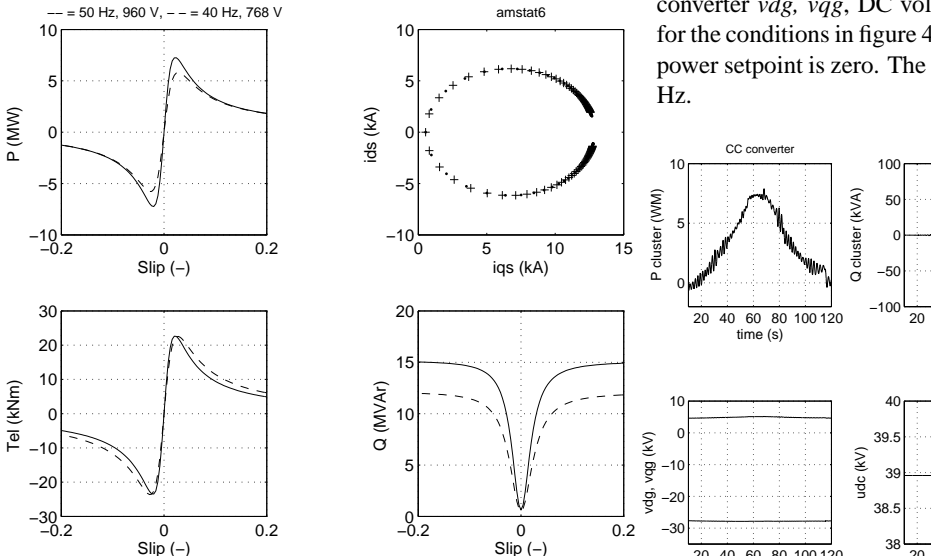


Figure 3: Steady state power *P*, current *vw1*, *Ids*, *Iqs*, torque *Tel* and reactive power *Q* for an induction machine operating at 50Hz-960V and 40Hz-768V

A. Normal Operation

The Simulink model which is used in the case study consists of the model of a cluster of 3 turbines including transformers connected to a single AC-DC-AC converter, the 34 kV cable, the 34kV-150 kV transformer and a simplified grid model (a large synchronous generator with frequency and voltage control, transformer, cables and two consumer loads). Figure 4 demonstrates normal operation of the cluster. A gust from 4 to 15 m/s passes the turbines with a small delay: vwI, vw2 and vw3. Below rated wind speed, the turbine speed controller maintains a tip speed ratio of 5 with respect to vw1. Rotor speed vw1, vw2 and vw3 follow the changing wind speed vw1, resulting in similar aerodynamic power and slip variations vw2, vw3, vw

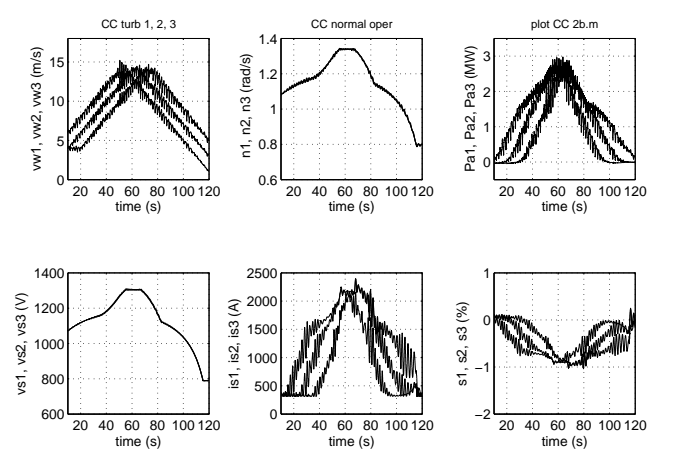


Figure 4: Cluster control, normal operation, turbines 1, 2 and 3

Figure 5 gives cluster power P and cluster reactive power Q, d and q current to the grid idg, iqg, d and q grid voltage at the converter vdg, vqg, DC voltage udc and cluster frequency f for the conditions in figure 4. The grid side converter reactive power setpoint is zero. The cluster frequency is limited to 50 Hz.

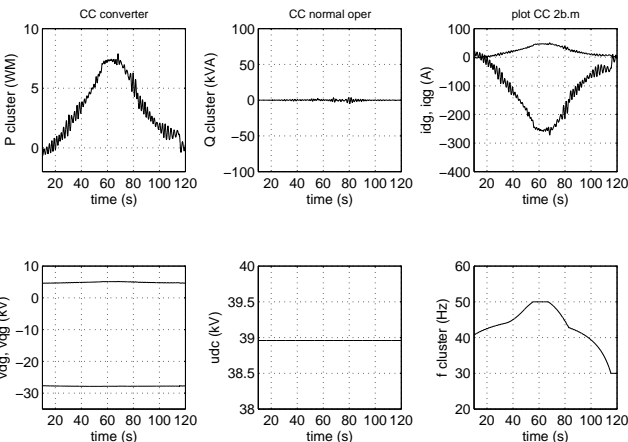


Figure 5: Cluster control, normal operation, converter values

Figure 6 gives the response of the grid to the changes in wind power. The synchronous machine power *Psm* is reduced, the total consumer load *Pcons* remains constant. The frequency deviations *freq* are small and there is not much voltage controller action *Vexc* either.

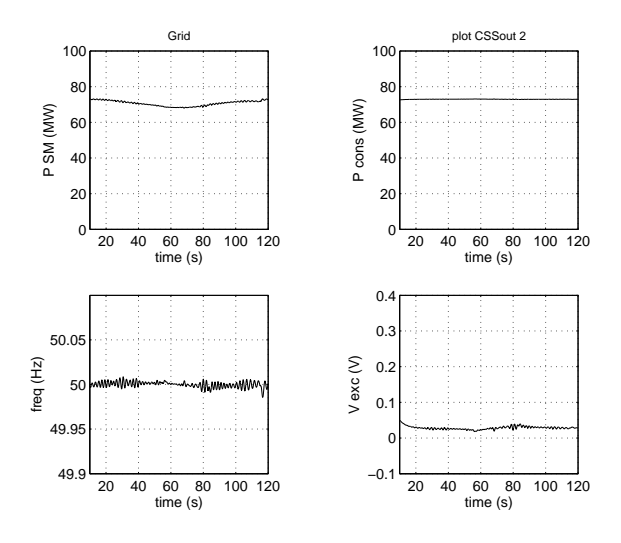


Figure 6: Cluster control, normal operation, grid values

B. Flicker

The currents and voltages calculated for the cluster in the previous section have been used to calculate instantaneous flicker values. The short circuit power for the flicker calculation is 50 times the rated power of the cluster and a fictitious grid angle of 30° has been chosen. The sample frequency in the calculation was 400 Hz. The instantaneous flicker values have been binned during intervals of 6 s. The binned instantaneous flicker values for the cluster are plotted in figure 7.

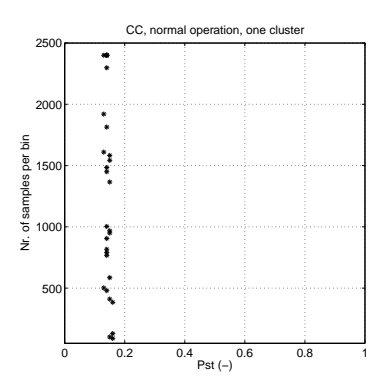


Figure 7: Binned instantaneous flicker values for three cluster controlled turbines

The flicker level for a variable speed turbine is expected to be lower than for a constant speed turbine, if the turbine control is well tuned. Cluster control is a special case of variable speed operation, turbines in a cluster will speed up and down and wind power variations are not immediately transfered to the grid. The 99 percentile level in figure 7, sometimes used to classify flicker, is below the level calculated for the constant speed stall wind farm under the same external conditions.

C. Frequency Dip

A grid frequency dip is simulated by a change of the frequency setpoint of the synchronous machine in the grid model. At t=10 s the setpoint is decreased to 45 Hz and at 20 s it is changed to the normal value of 50 Hz (figure 8). This dip is significantly larger than any expected dip in a large grid, in magnitude as well as rate, since grid frequency changes take time and corrective action will be taken before this level is reached. The 5 Hz dip was chosen to demonstate the cluster behaviour more clearly.

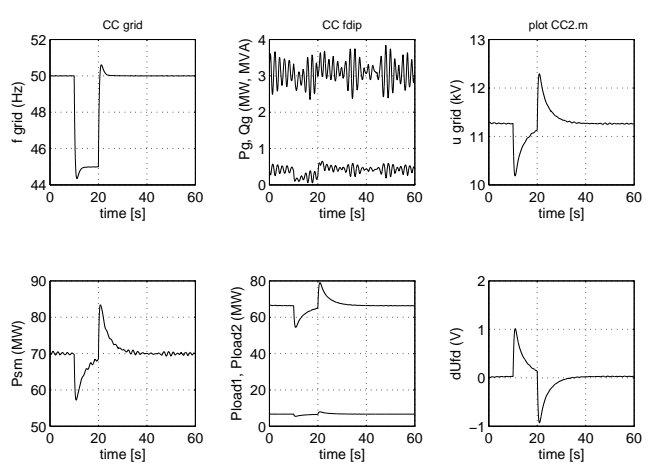


Figure 8: Response of cluster controlled turbines to a 10% frequency dip: Grid variables

The total consumer load *Pload1* plus *Pload2* is 73 MW, which is supplied partly by the synchronous machine and partly by the wind turbine cluster (figure 8). The frequency dip causes a voltage dip *u grid*, which is counteracted by the synchronous machine voltage controller *dUfd*. The initial voltage dip is of the same magnitude as the frequency dip: about 10%.

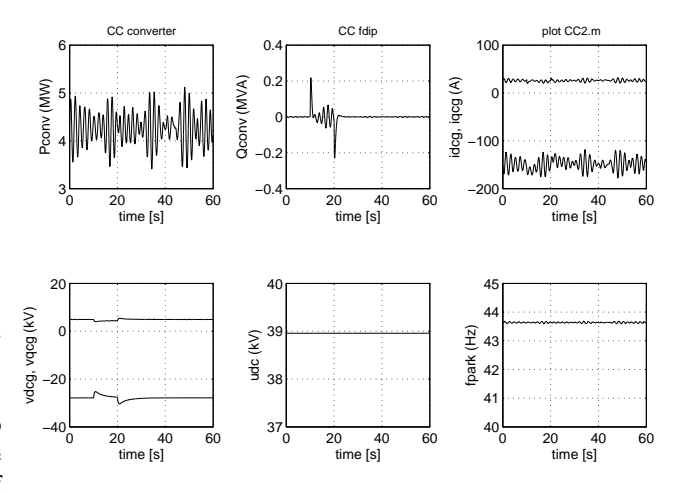


Figure 9: Response of cluster controlled turbines to a 10% frequency dip: converter variables

The grid side converter voltages vdcg and vqcg follow the grid voltage dip (figure 9). The grid side converter d-component of the current idcg remains almost constant, the

q-current *iqcg* becomes more negative. The grid side converter power *Pconv* and reactive power *Qconv* are not affected by the frequency dip and corresponding voltage dip. The DC voltage *udc* shows no effect either.

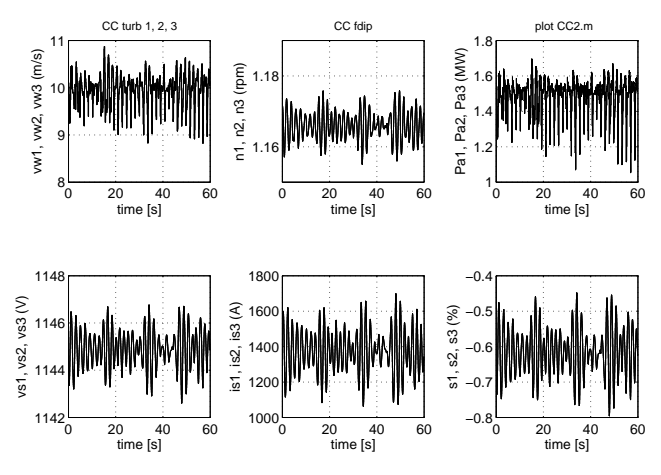


Figure 10: Response of cluster controlled turbines to a 10% frequency dip: turbine variables

The converter effectively decouples the turbines and the grid. In spite of the frequency dip, the turbines operates as if no grid dip occurs (figure 10): aerodynamic powers *Pa1*, *Pa2* and *Pa3*, stator currents *is1*, *is2*, *is3* and voltages *vs1*, *vs2*, *vs3* and turbine speed *n1*, *n2*, *n3* follow the changes in rotor effective wind speed.

D. Voltage Dip

A 30% voltage dip is applied to the grid side voltage of the cluster converter during 10 seconds (vconv, figure 13). The simulation does not include the grid model in order to realise a well defined voltage dip without oscillations in either voltage or frequency. Only the parameters of the first turbine are shown; since all turbines have similar wind speed, similar behaviour of the other turbines is expected. The rotor effective wind speed Vw is about 15 m/s, the turbine then operates at rated power Pa (see figure 11). The electrical variables in the next figures are per unit values.

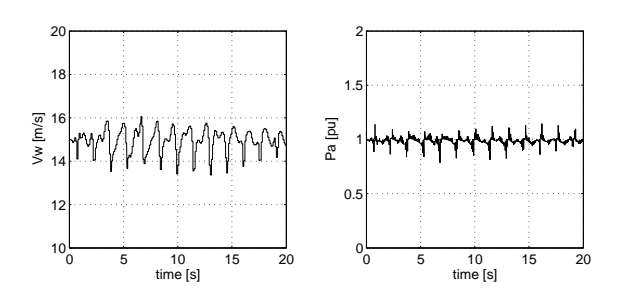


Figure 11: Response of cluster controlled turbines to a 30% - 10s voltage dip: rotor effective wind speed and aerodynamic power

At 15 m/s the turbine is kept at rated speed (equivalent to 50 Hz) by the speed controller: the slip *slip* is unchanged (see figure 12). The turbine aerodynamic power is not affected

by the voltage dip, for a stall controlled turbine it only depends on wind speed and rotor speed. The grid side converter power Pconv will decrease due to the voltage dip (see figure 13). The power difference between turbine side converter and grid side converter will lead to an increase of the grid side converter current iconv to keep the DC-link voltage constant. The current increases is limited by the current rating of the converter, and the DC-link voltage udc will also increase. To overcome this problem, a resistance is connected parallel to the dc-link capacitor. The resistance is connected via a chopper. When the DC-link voltage reaches a threshold, the chopper opens and the energy surplus is dissipated in the resistance. The duty-ratio of the chopper is determined by the difference between the actual DC-link voltage and the preferred DC-link voltage. The results show that a 30% voltage dip is no problem for the cluster controllers.

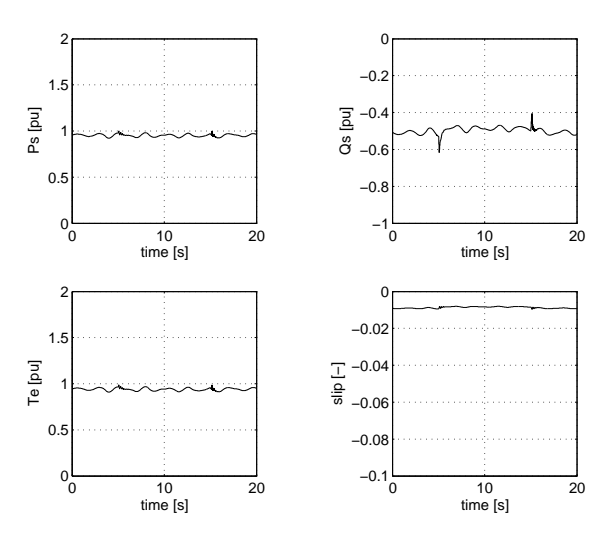


Figure 12: Response of cluster controlled turbines to a 30% - 10s voltage dip: active power, reactive power, electric torque and slip

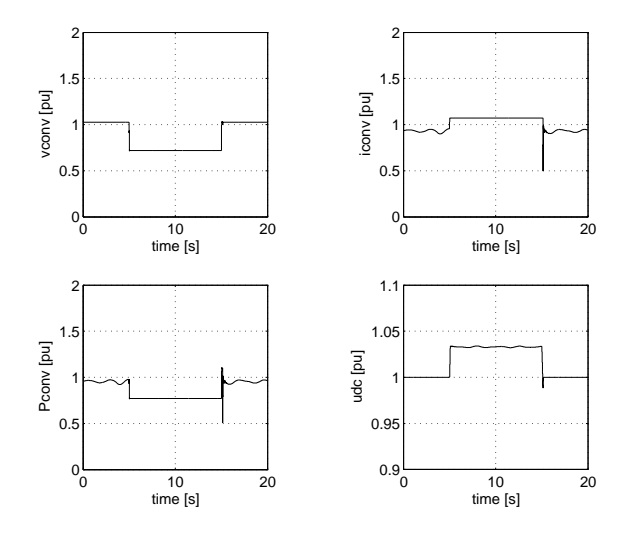


Figure 13: Response of cluster controlled turbines to a 30% - 10s voltage dip: AC voltage, current and active power of grid-side converter, DC-link voltage

III. CONCLUSIONS

Dynamic wind farm models based on individual turbine models have been developed in Simulink. Detailed models of the turbine mechanical and electrical system and of the grid are used. The models include constant speed stall and variable speed pitch turbines. Four types of turbine electrical systems have been modelled, based on doubly fed induction generators, permanent magnet generators, directly coupled and cluster controlled induction generators. These models present a powerful tool for the investigation of wind farm dynamics and wind farm-grid interaction and for the development of wind farm control.

The models have been used to develop electrical system control and to investigate system responses to grid faults. In this paper, results for the cluster controlled wind farm have been presented. The results show that grid faults do not present a problem for the cluster controlled turbine.

With regard to simulation speed the choice of dq0 variables proved successful. The current bottleneck is not the simulation speed of the electrical part any more but of the mechanical and control part of the variable speed turbine model. This submodel has to be increased in speed before comfortable full scale farm simulations can be made for variable speed systems.

Model validation now has a high priority. A database with turbine and wind farm measurement is currently being set up in IEA Annex XXI: Wind Farm Models for Power System Studies. This database will serve as the basis for the validation process.

ACKNOWLEDGMENT

Erao-2 is a continuation of the Erao-1 project, in which a steady state (load flow) and economic model for offshore wind farms has been developed [7]. The Erao projects are funded by the Dutch Agency for Energy and Environment (NOVEM) and the Ministry of Economic Affairs of the Netherlands.

REFERENCES

- [1] C.P.J. Jansen and R.A.C.T de Groot. Aansluiting van 6000 MW offshore windvermogen op het Nederlandse elektriciteitsnet, Deel 2: Net op land. Technical Report 40330050-TDC 03-37074B, Kema, 2003.
- [2] J. Morren, S.W.H. de Haan, P. Bauer, and J.T.G. Pierik. Comparison of complete and reduced models of a wind turbine using doubly-fed induction generator. In 10th European Conference on Power Electronics and Applications (EPE 2003), Toulouse, 2003.
- [3] J. Morren, S.W.H. de Haan, and J.A. Ferreira. Model reduction and control of electronic interfaces of voltage dip proof DG units. In 2004 IEEE Power Engineering Society (PES) General Meeting, Denver, 6-10 June 2004. to be published.

- [4] J. Morren, J.T.G. Pierik, S.W.H. de Haan, and J. Bozelie. Fast dynamic models of offshore wind farms for power system studies. In 4th International workshop on large-scale integration of wind power and transmission networks for offshore wind farms, Billund, 20-21 October 2003.
- [5] E.ON Netz. Ergänzede Netzanschlussregeln für Windenergieanlagen. Technical report, E.ON Netz, 2001.
- [6] I. Nusimovich, S.W.H. de Haan, and J.G. Slootweg. Comparison of the energy yield of wind turbines with individual ac/dc/ac converters and wind turbines connected to a common ac/dc/ac converter. In EPE-PEMC, Dubrovnik, 2002.
- [7] J.T.G. Pierik, M.E.C. Damen, P. Bauer, and S.W.H. Damen. Electrical and control aspects of offshore wind farms, phase 1: Steady state electrical design and economic modeling, Vol. 1: Project results. Technical Report ECN-CX-01-083, ECN Wind Energy, 2001.
- [8] J.T.G. Pierik, J.C. Montero Quiros, T.G. van Engelen, D. Winkelaar, and R. Sancho Chaves. Costa Rica grid feed-in study: Effect of wind power on grid frequency. Technical Report ECN-CX-03-080, ECN, 2003.
- [9] J.T.G. Pierik, J. Morren, E.J. Wiggelinkhuizen, S.H.W. de Haan, T.G. van Engelen, and J. Bozelie. Electrical and control aspects of offshore wind turbines II (Erao-2). Volume 1: Dynamic models of wind farms. Technical Report ECN-CX- -04-018, ECN, 2004. to be published.
- [10] H. Slootweg. Wind power modelling and impact on power system dynamics. Technical Report ISBN 90-9017239-4, T.U. Delft, 2003.
- [11] E.L van der Hooft, P. Schaak, and T.G. van Engelen. Wind turbine control algorithms. Technical Report ECN-C-03-111, ECN, 2003.
- [12] T.G. van Engelen, E.L. van der Hooft, and P. Schaak. Ontwerpgereedschappen voor de regeling van windturbines. Technical report.

Fast Dynamic Models of Offshore Wind Farms for Power System Studies

J. Morren, J.T.G. Pierik, S.W.H. de Haan and J. Bozelie

Abstract--In this contribution dynamic wind farm models suitable for fast simulation of power system studies are presented.

While deriving the models, special attention has been paid to increasing the computational speed of the simulation program. An important increase in speed is realised by the use of the $dq\theta$ transformation (Park transformation) not only for the generator but also for all other electrical components. The Park transformation is common use in electrical machine models, but not in the modelling of other electrical components.

A description is given of the way in which models of basic electrical components can be transformed from the abc reference frame to the $dq\theta$ reference frame. The results are demonstrated in a case study of a wind farm consisting of a string of wind turbines with doubly-fed induction generator.

Index Terms—Dynamic modelling, Park Transformation, Wind Energy

I. INTRODUCTION

tendency to increase the amount of electricity generated Afrom wind can be observed [1]. As the penetration of wind turbines in electrical power systems will increase, they may begin to influence overall power system operation [2]. The behaviour of wind turbines with respect to their interaction with the grid is therefore studied at different places [3]-[5]. In order to facilitate the investigation of the impact of a wind farm on the dynamics of the power system, an adequate model of the wind turbines is required. Although personal computers become faster and faster, computational speed is still one of the limiting factors in (dynamic) simulation of power systems. One of the problems is the complexity of the models that limits the computational speed. When reduced models are used simulation of complex systems like wind farms can be done much faster, but the results may be less accurate [6].

The Park transformation (some-times called Blondel-Park transformation) is well-known from its use in electrical machinery. The electrical signals are transformed to a

stationary rotating reference frame. As this stationary frame is chosen to rotate with the grid frequency, all voltages and currents in the dq0 reference frame are constant in steady state situations. Therefore, modelling in the dq0 reference frame is expected to increase the simulation speed significantly, as a variable step-size simulation program can apply a large time step during quasi steady-state phenomena. An example is shown in Fig. 1 where the inrush currents of a three-phase induction machine are shown in the abc and dq0 reference system respectively. The time step that can be applied without introducing significant errors will be much large in the case of the dq0 reference system.

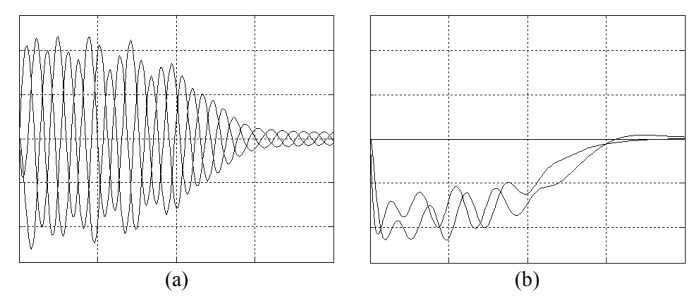


Fig. 1. Inrush current of induction machine in the abc (a) and $dq\theta$ (b) reference system

In a research project on the grid integration of large wind farms, dynamic models have been derived for: electrical generators (induction generator, doubly-fed induction generator, permanent magnet generator), power electronic converters, transformers, cables, turbine rotor, mechanical drive train and rotor effective wind. All models of electrical components are in the $dq\theta$ reference frame.

In this contribution a description will be given of the way in which models of different electrical components in the $dq\theta$ reference frame can be obtained. The model derivation will be shown for two basic components: a three-phase RL line segment and the three-phase shunt capacitance. The simulation results of different models are compared, in order to show the validity of the $dq\theta$ -model. Afterwards wind models and the turbine models are given. These models are used in a case study that is performed to demonstrate the effectiveness of the proposed modelling method.

II. PARK TRANSFORMATION

In the study of power systems, mathematical transformations are often used to decouple variables, to facilitate the solution of difficult equations with time-varying coefficients, or to refer all variables to a common reference

This research is partially funded by Novem within the Program Renewable Energy in The Netherlands 2001, and by Senter within the Program IOP-EMVT.

J. Morren and S. W. H. de Haan are with the Electrical Power Processing unit of the Delft University of Technology. Mekelweg 4, 2628CD Delft, The Netherlands. J.Morren@its.tudelft.nl

J. T. G. Pierik is with Energy research Centre of the Netherlands, section Wind Energy, P.O. Box 1, 1755 ZG Petten, The Netherlands

J. Bozelie was with NEG-Micon NL.

frame [7]. Probably the most well-known, is the method of symmetrical components, developed by Fortescue. This transformation is mostly used in it's time-independent form and applied to phasors, when it is used in electrical power system studies [8]. Another commonly-used transformation is the Park transformation, which is well-known from the modelling of electrical machines. The Park transformation is instantaneous and can be applied to arbitrary three-phase time-dependent signals.

For $\theta_d = \omega_d t + \varphi$, with ω_d the angular velocity of the signals that should be transformed, t the time and φ the initial angle, the Park transformation is given by:

$$\begin{bmatrix} \mathbf{x}_{dq0} \end{bmatrix} = \begin{bmatrix} \mathbf{T}_{dq0} (\theta_d) \end{bmatrix} \cdot \begin{bmatrix} \mathbf{x}_{abc} \end{bmatrix}$$
 (1)

with:

and with the $dq\theta$ transformation matrix $\mathbf{T}_{dq\theta}$ defined as:

$$\begin{bmatrix} \mathbf{T}_{dq0} \end{bmatrix} = \sqrt{\frac{2}{3}} \begin{bmatrix} \cos\theta_d & \cos\left(\theta_d - \frac{2\pi}{3}\right) & \cos\left(\theta_d + \frac{2\pi}{3}\right) \\ -\sin\theta_d & -\sin\left(\theta_d - \frac{2\pi}{3}\right) & -\sin\left(\theta_d + \frac{2\pi}{3}\right) \\ \frac{1}{\sqrt{2}} & \frac{1}{\sqrt{2}} & \frac{1}{\sqrt{2}} \end{bmatrix}$$
(3)

and its inverse given by:

$$\left[\mathbf{T}_{dq0}\right]^{-1} = \sqrt{\frac{2}{3}} \begin{bmatrix} \cos\theta_d & -\sin\theta_d & \frac{1}{\sqrt{2}} \\ \cos\left(\theta_d - \frac{2\pi}{3}\right) & -\sin\left(\theta_d - \frac{2\pi}{3}\right) & \frac{1}{\sqrt{2}} \\ \cos\left(\theta_d + \frac{2\pi}{3}\right) & -\sin\left(\theta_d + \frac{2\pi}{3}\right) & \frac{1}{\sqrt{2}} \end{bmatrix}$$
 (4)

The positive q-axis is defined as leading the positive d-axis by $\pi/2$, as can be seen from Fig. 2.

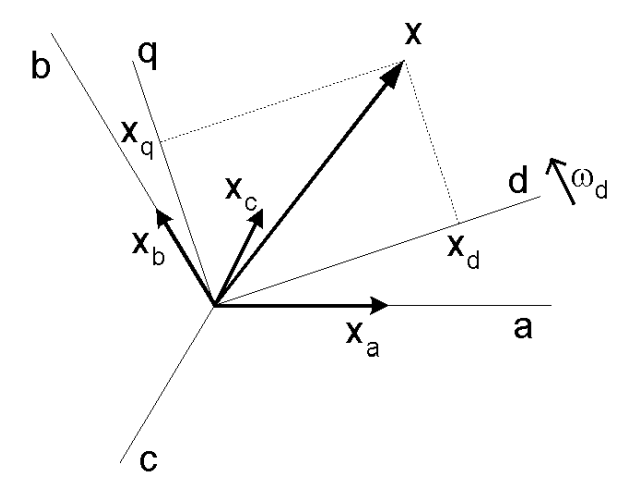


Fig. 2. Relationship between abc and dq quantities

Some additional properties of the Park transformation can be derived. As the transformation is orthogonal, it holds that:

$$\left[\mathbf{T}_{dq0}(\theta_d)\right] \cdot \left[\mathbf{T}_{dq0}(\theta_d)\right]^{-1} = \left[\mathbf{T}_{dq0}(\theta_d)\right] \cdot \left[\mathbf{T}_{dq0}(\theta_d)\right]^T = \left[\mathbf{I}\right] \tag{5}$$

The transformations of (3) and (4) are unitary, as is shown in (5) and conserves power as is shown in (6). Note that by replacing the factor $\sqrt{2/3}$ by a factor 2/3 in (3) and (4) the transformation will be amplitude-invariant, implying that the length of the current and voltage vectors in both abc and dq0 reference frame are the same. This amplitude-invariant transformation is mostly used in modelling of electrical machines [8].

The voltages and currents in the $dq\theta$ reference frame are constant in steady-state situations. Be aware that also non-fundamental harmonics are correctly transformed as x_a , x_b and x_c are time signals, including all harmonics. In steady state a non-fundamental frequency component with frequency ω_h will appear as a sinusoidal signal with frequency $(\omega_h - \omega_p)$ in the $dq\theta$ domain. The highest frequency that can be represented accurately in the $dq\theta$ frame depends on the time step that is used.

With (5) it can be shown that the Park transformation conserves power [9]:

$$p(t) = [\mathbf{v}_{abc}]^{T} \cdot [\mathbf{i}_{abc}]$$

$$= [[\mathbf{T}_{dq0}(\theta_{d})]^{-1}[\mathbf{v}_{dq0}]]^{T} \cdot [\mathbf{T}_{dq0}(\theta_{d})]^{-1}[\mathbf{i}_{dq0}]$$

$$= [\mathbf{v}_{dq0}]^{T}[[\mathbf{T}_{dq0}(\theta_{d})]^{-1}]^{T} \cdot [\mathbf{T}_{dq0}(\theta_{d})]^{-1}[\mathbf{i}_{dq0}]$$

$$= [\mathbf{v}_{dq0}]^{T}[\mathbf{T}_{dq0}(\theta_{d})] \cdot [\mathbf{T}_{dq0}(\theta_{d})]^{-1}[\mathbf{i}_{dq0}]$$

$$= [\mathbf{v}_{dq0}]^{T} \cdot [\mathbf{i}_{dq0}]$$
(6)

The Park transformation is often used in control loops, as it offers the possibility of decoupled control between active and reactive power. Be aware however that active and reactive power cannot directly be related to the d and the q axis component. These components are just a representation. The instantaneous active and reactive power can be obtained directly from the voltages and currents in the dq0 reference system [10]:

$$p = v_d i_d + v_q i_q$$

$$q = v_a i_d - v_d i_q$$
(7)

III. MODEL DERIVATION

A. Introduction

In this section the $dq\theta$ models of basic components (capacitance, inductance, resistance) are obtained. With the models of these basic components all further models, such as transformers, machines and cables, can be obtained. The derivation of the basic model starts by defining the voltage drop of the a-phase. The a-phase equation is then transformed to a $dq\theta$ equation with (3). The b and c phase equations are written as a function of the a-phase and the zero-sequence

component, in order to eliminate them. After some mathematical manipulations, the models in the d, q and θ phase can be obtained. First the $dq\theta$ equations for a three-phase series RL line with a ground return will be given and afterwards the $dq\theta$ equations of shunt capacitances will be derived.

B. Series RL

In this section the $dq\theta$ equations for a three-phase series RL line with ground return, shown in Fig. 3, will be presented. The equations for the line can be obtained by considering the resistive and inductive drops of the respective phase equations. The send end voltage with respect to local ground for line a is given by:

$$v_{a1} = R_a i_a + L_a \frac{di_a}{dt} + L_{ab} \frac{di_b}{dt} + L_{ac} \frac{di_c}{dt} + L_{ag} \frac{di_g}{dt} + v_{a2} + v_{g21}$$
 (8)

With $v_{g2l}=v_{g2}-v_{gl}$. Using the relation $i_g=-(i_a+i_b+i_c)$, the voltage drops across the three phases of the line can be expressed in matrix form as:

$$[\mathbf{v}_{1,abc}] - [\mathbf{v}_{2,abc}] = [\mathbf{R}] [\mathbf{i}_{abc}] + \frac{d}{dt} [\mathbf{L}] [\mathbf{i}_{abc}]$$
 (9)

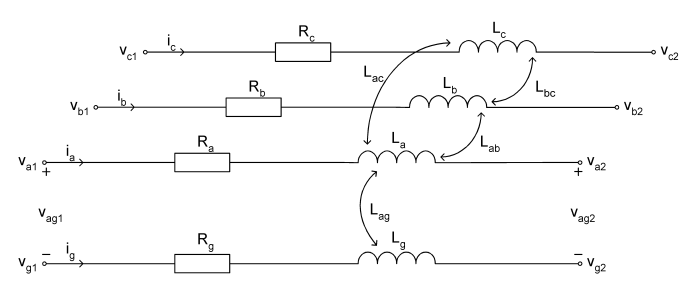


Fig. 3. Three-phase RL line with ground return

For a uniformly transposed line, $R_a=R_b=R_c$, $L_{ab}=L_{bc}=L_{ca}$, and $L_{ag}=L_{bg}=L_{cg}$. Letting $L_s=L_a+L_g-2L_{ag}$, $L_m=L_{ab}+L_g-2L_{ag}=L_s-L_a+L_{ab}$, $R_s=R_a+R_g$, and $R_m=R_g$, the resistance and inductance matrices are given by:

$$\begin{bmatrix} \mathbf{R} \end{bmatrix} = \begin{bmatrix} R_s & R_m & R_m \\ R_m & R_s & R_m \\ R_m & R_m & R_s \end{bmatrix} \text{ and } \begin{bmatrix} \mathbf{L} \end{bmatrix} = \begin{bmatrix} L_s & L_m & L_m \\ L_m & L_s & L_m \\ L_m & L_m & L_s \end{bmatrix}$$

The equation of the voltage drop across the ground path is:

$$v_{g21} = v_{g2} - v_{g1} = -R_g i_g - L_g \frac{di_g}{dt} - L_{ag} \frac{di_a}{dt} - L_{bg} \frac{di_b}{dt}$$

$$-L_{cg} \frac{di_c}{dt}$$

$$= R_g (i_a + i_b + i_c) + (L_g - L_{ag}) \frac{di_a}{dt} + (L_g - L_{bg}) \frac{di_b}{dt}$$

$$+ (L_g - L_{cg}) \frac{di_c}{dt}$$
(10)

The $dq\theta$ equations for the uniformly transposed line can be obtained by considering the resistive and inductive drops of the a-phase equations. The resistive drop in the a-phase is given by:

$$R_a i_a + R_m (i_b + i_c) \tag{11}$$

Substituting $i_o = (i_a + i_b + i_c)/3$ to eliminate i_b and i_c , we obtain:

$$\left(R_{s}-R_{m}\right)i_{a}+3R_{m}i_{0}\tag{12}$$

Expressing i_a in terms of the dq0 currents, the resistive drop in the a-phase becomes:

$$(R_s - R_m)(i_d \cos \theta_d - i_a \sin \theta_d + i_0) + 3R_m i_0 \tag{13}$$

Similarly, for the inductive drop in the a-phase, we have:

$$L_{s} \frac{di_{a}}{dt} + L_{m} \frac{d(i_{b} + i_{c})}{dt} \tag{14}$$

Eliminating i_b and i_c :

$$\left(L_{s}-L_{m}\right)\frac{di_{a}}{dt}+3L_{m}\frac{di_{0}}{dt}\tag{15}$$

Using the inverse $dq\theta$ transform of (4) to express i_a in terms of the $dq\theta$ currents, the inductive drop in the a-phase becomes:

$$(L_s - L_m) \frac{d}{dt} (i_d \cos \theta_d - i_q \sin \theta_d + i_0) + 3L_m \frac{di_0}{dt}$$
(16)

Knowing that for x=x(t):

$$\frac{d}{dt}\sin x = \cos x \frac{dx}{dt} \quad and \quad \frac{d}{dt}\cos x = -\sin x \frac{dx}{dt}$$
 (17)

Eq. (16) can be written as:

$$\left(L_{s} - L_{m}\right) \left[-i_{d} \sin \theta_{d} \frac{d\theta_{d}}{dt} + \cos \theta_{d} \frac{di_{d}}{dt} - i_{q} \cos \theta_{d} \frac{d\theta_{d}}{dt} - \sin \theta_{d} \frac{di_{q}}{dt} + \frac{di_{0}}{dt}\right] + 3L_{m} \frac{di_{0}}{dt} \tag{18}$$

The dq0-transform can also be applied to the voltage difference $\Delta v_a = v_{al} - v_{a2}$, resulting in:

$$\Delta v_d \cos \theta_d - \Delta v_q \sin \theta_d + \Delta v_0 \tag{19}$$

Combining (13), (18), and (19), Eq. (8) can be written as:

$$\Delta v_{d} \cos \theta_{d} - \Delta v_{q} \sin \theta_{d} + \Delta v_{0} = (R_{s} - R_{m})(i_{d} \cos \theta_{d} - i_{q} \sin \theta_{d} + i_{0}) + 3R_{m}i_{0} + (L_{s} - L_{m})\left[-i_{d} \sin \theta_{d} \frac{d\theta_{d}}{dt} + \cos \theta_{d} \frac{di_{d}}{dt} - i_{q} \cos \theta_{d} \frac{d\theta_{d}}{dt} - \sin \theta_{d} \frac{di_{q}}{dt} + \frac{di_{0}}{dt}\right] + 3L_{m} \frac{di_{0}}{dt}$$

$$(20)$$

By equating the coefficients of the $\cos \theta_d$, $\sin \theta_d$, and constant terms, we obtain:

$$\Delta v_{d} = (R_{s} - R_{m})i_{d} + (L_{s} - L_{m})\frac{di_{d}}{dt} - (L_{s} - L_{m})i_{q}\frac{d\theta_{d}}{dt}$$

$$\Delta v_{q} = (R_{s} - R_{m})i_{q} + (L_{s} - L_{m})\frac{di_{q}}{dt} + (L_{s} - L_{m})i_{d}\frac{d\theta_{d}}{dt}$$

$$\Delta v_{0} = (R_{s} + 2R_{m})i_{0} + (L_{s} + 2L_{m})\frac{di_{0}}{dt}$$
(21)

When the mutual inductances between the phases and between phase to ground are zero, that is $L_{ab}=L_{bc}=L_{ca}=0$ and $L_{ag}=L_{bg}=L_{cg}=0$, then $L_s=L_a+L_g$, and $L_m=L_{ab}+L_g$. With $\omega_d=d\theta_d/dt$ the final result is:

$$\Delta v_{d} = R_{a}i_{d} + L_{a}\frac{di_{d}}{dt} - \omega L_{a}i_{q}$$

$$\Delta v_{q} = R_{a}i_{q} + L_{a}\frac{di_{q}}{dt} + \omega L_{a}i_{d}$$

$$\Delta v_{0} = \left(R_{a} + 3R_{g}\right)i_{0} + \left(L_{a} + 3L_{g}\right)\frac{di_{0}}{dt}$$
(22)

The resulting equivalent dq0 circuits are shown in Fig. 4.

C. Shunt C

In the same way as is done for the series line inductances and resistances, equations for shunt capacitances can be obtained. A line with shunt capacitances is shown in Fig. 5. Besides the phase to neutral capacitance of the phases, also the mutual capacitances between the phases have been shown.

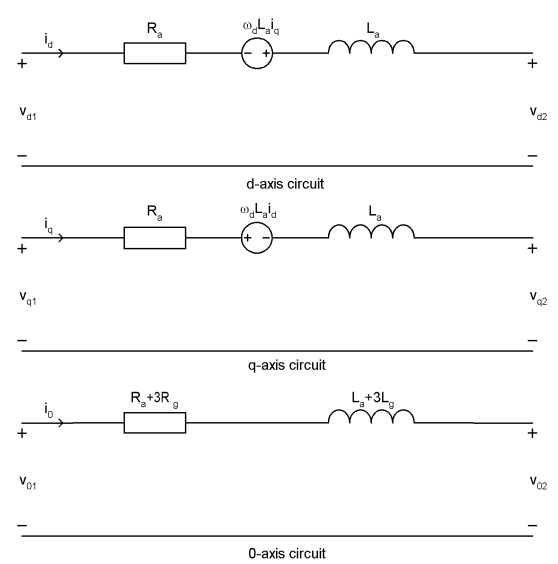


Fig. 4. Equivalent $dq\theta$ circuit of a series RL line

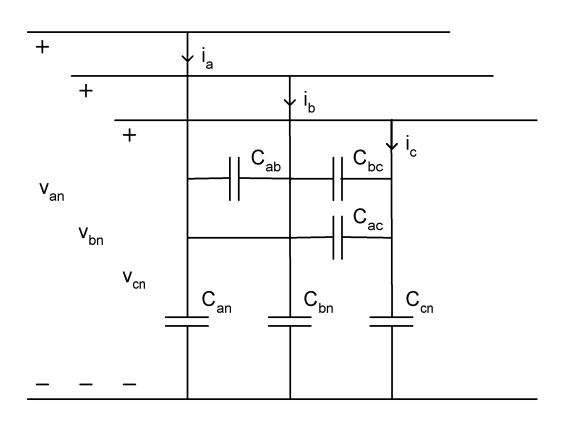


Fig. 5. Shunt capacitances of a three-phase line

Let $C_{ab} = C_{bc} = C_{ca} = C_{m}$, $C_{an} = C_{bn} = C_{cn}$, and $C_s = C_{an} + 2 C_{ab}$. The equation of the *a*-phase current in Fig. 5 may be expressed as:

$$i_{a} = C_{an} \frac{d}{dt} v_{an} + C_{ab} \frac{d}{dt} (v_{an} - v_{bn}) + C_{ac} \frac{d}{dt} (v_{an} - v_{cn})$$
 (23)

$$i_{a} = \left(C_{an} + C_{ab} + C_{ac}\right) \frac{dv_{an}}{dt} - C_{m} \frac{dv_{bn}}{dt} - C_{m} \frac{dv_{cn}}{dt}$$
 (24)

Exchanging the *b* and *c* phase voltages with $v_0 = (v_{an} + v_{bn} + v_{cn})/3$ gives:

$$i_a = \left(C_s + C_m\right) \frac{dv_{an}}{dt} - 3C_m \frac{dv_0}{dt} \tag{25}$$

Applying the dq0 transformation to the current and the voltage of the a-phase we obtain:

$$i_d \cos \theta_d - i_a \sin \theta_d + i_0 =$$

$$\left(C_{s}+C_{m}\right)\frac{d}{dt}\left(v_{d}\cos\theta_{d}-v_{q}\sin\theta_{d}+v_{0}\right)-3C_{m}\frac{dv_{0}}{dt}\tag{26}$$

In analogy to (16) - (21), by equating the coefficients of the $\cos \theta_d$, $\sin \theta_d$, and constant terms, the following set of equations is obtained for the dq0 currents:

$$i_{d} = (C_{s} + C_{m}) \frac{dv_{d}}{dt} - (C_{s} + C_{m})v_{q} \frac{d\theta_{d}}{dt}$$

$$i_{q} = (C_{s} + C_{m}) \frac{dv_{q}}{dt} + (C_{s} + C_{m})v_{d} \frac{d\theta_{d}}{dt}$$

$$i_{0} = (C_{s} - 2C_{m}) \frac{dv_{0}}{dt}$$

$$(27)$$

When the mutual capacitances between the phases are zero, that is $C_{ab}=C_{bc}=C_{ca}=0$, then $C_{m}=0$ and $C_{s}=C_{an}$. With $\omega=d\theta_{d}/dt$ the final result is:

$$i_{d} = C \frac{dv_{d}}{dt} - \omega C v_{q}$$

$$i_{q} = C \frac{dv_{q}}{dt} + \omega C v_{d}$$

$$i_{0} = C \frac{dv_{0}}{dt}$$
(28)

The resulting equivalent $dq\theta$ circuits are shown in Fig. 6.

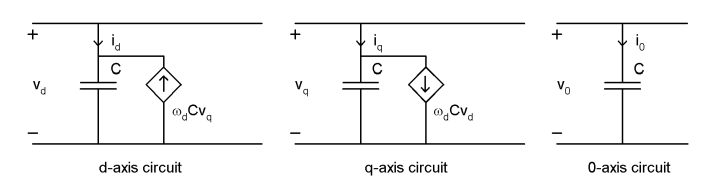


Fig. 6. Equivalent $dq\theta$ circuits of shunt capacitances of a three-phase line

D. Summary

The equations for the series resistor, series inductor, and shunt capacitor are derived in the previous sections. The voltage-current relationships for the basic components are summarised in table I. For clearness the models have been derived bases on the phase equations. It is also possible to transfer complete sets of differential equations at once. Equations to obtain this can be found in the appendix.

TABLE I. VOLTAGE-CURRENT RELATIONSHIP IN DQ0 REFERENCE FRAME FOR BASIC COMPONENTS

Three-phase resistor	$R\left[\mathbf{i}_{dq0}\right] = \left[\mathbf{u}_{dq0}\right]$
Three-phase inductor	$L\frac{d}{dt}\left[\mathbf{i}_{dq0}\right] + \omega_p \cdot y \cdot \left[\mathbf{i}_{dq0}\right] = \left[\mathbf{u}_{dq0}\right]$
Three-phase capacitor	$C\frac{d}{dt}\left[\mathbf{u}_{dq0}\right] + \omega_p \cdot y \cdot \left[\mathbf{u}_{dq0}\right] = \left[\mathbf{i}_{dq0}\right]$

IV. COMPARISON

It should be shown, that the models in a dg0 reference frame give correct simulation results. The best solution would be to compare the simulation results with measurements. As this was not possible at the moment, some simulation results have been compared to results of simulations with well-known and accepted models in the normally used abc reference frame [11]. Both the responses to slow and fast dynamic phenomena have been compared. Therefore, the response of a doubly-fed induction machine to a step in the mechanical torque (slow dynamics) and to a dip in the grid voltage (fast dynamics) have been considered. The response of the rotor current of the machine to a step in the mechanical torque is shown in Fig. 7 and the resonse to a dip in the grid voltage in Fig. 8. A difference in the responses in the abc and in the $dq\theta$ reference frame cannot be observed in these figures. One should be aware, that the high rotor currents, caused by the dip, might destroy the converter, if no measures are taken [12], [13].

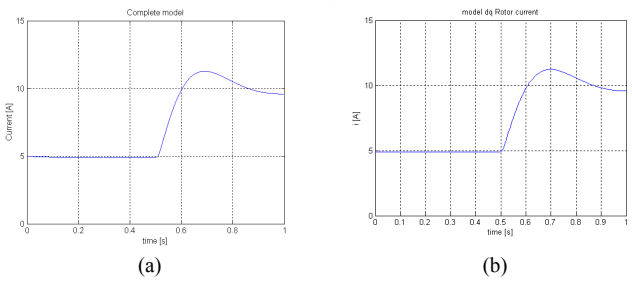


Fig. 7. Response of rotor current to step in mechanical torque for *abc*-model (a) and $dq\theta$ model (b)

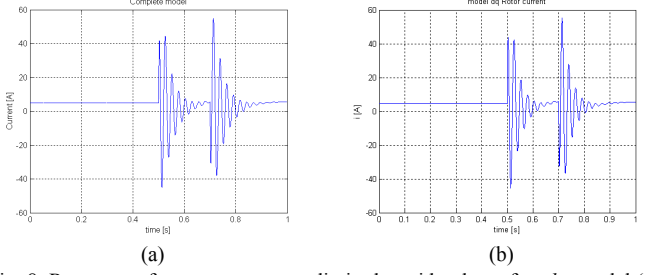


Fig. 8. Response of rotor current to a dip in the grid voltage for *abc*-model (a) and $dq\theta$ model (b)

In the abc-model, the switching operation of the power electronic converters is not taken into consideration. A comparison has been made between the behaviour of a converter in the dq0 reference frame and a complete IGBT-converter that also takes into account the switching operation of all switches. The IGBT converter that has been used is obtained from the SimPower Systems Blockset of Matlab. Again the behaviour during a dip in the grid voltage has been simulated. The d-axis current of the converter is shown for both models in Fig. 9. It can be seen that except the high-frequency 'noise' due to the switching operation of the IGBT converter, the response to the dip is almost the same. The response depends more on the parameters of the converter controller, then on the type of model.

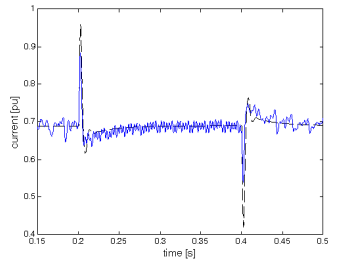


Fig. 9. Response of *d*-axis converter current to dip in the grid voltage for reference IGBT model (solid line) and *dq0* model (dashed line)

V. CASE STUDY SIMULATIONS

A. Introduction

A case study will demonstrate the effectiveness of the proposed modelling method. All simulations have been done in Simulink®, a toolbox extension of Matlab that is widely used in dynamic simulation. The Near Shore Wind park (NSW park) that is planned to be built in the North Sea about 12 kilometres from the Dutch coast will be used as a case study. The wind farm will consist of 36 turbines with a 2.75 MVA doubly-fed induction generator. The park layout is shown in Fig. 10. For convenience only one string of 12 turbines is simulated. Each of the turbines is connected to the 34kV grid by a three-winding transformer with a nominal power of 2.5MW. This transformer has a 960V winding connected to the stator and a 690V winding to the rotor winding via a frequency converter. The wind farm is connected to the 150kV grid via a transformer with a nominal power of 125MVA.

To simulate the dynamics of a wind farms not only models of the electrical system are required, but also dynamic models of the wind and the wind turbine including generator. The main goal of this paper is to show the possibilities of using the dq0 transformation for the modelling of wind farms. Therefore, the description of the wind and turbine models will be limited. In this section a short description of the wind model and the turbine model will be given. More information on the modelling of these parts can be found in literature [14].

B. Wind model

To evaluate the dynamic behaviour of wind turbines and wind farms, the short-term variation of the wind has to be known. Since wind speed variation is a statistically determined phenomenon, a wind model is needed that will calculate a realisation of the stochastically changing wind speed in time. Furthermore, the wind speed averaged over the turbine rotor has to be determined, including variations caused by the passing of the blades through the inhomogeneous wind field over the rotor area. This inhomogeneous wind field is caused by wind shear and the tower [14].

When a power measurement of a turbine is observed, the effect of the wind field inhomogenity can clearly be seen by regular changes in power with a frequency of the number of blades times the turbine's rotational frequency, often called nP. The wind model aims at a realistic representation of this effect.

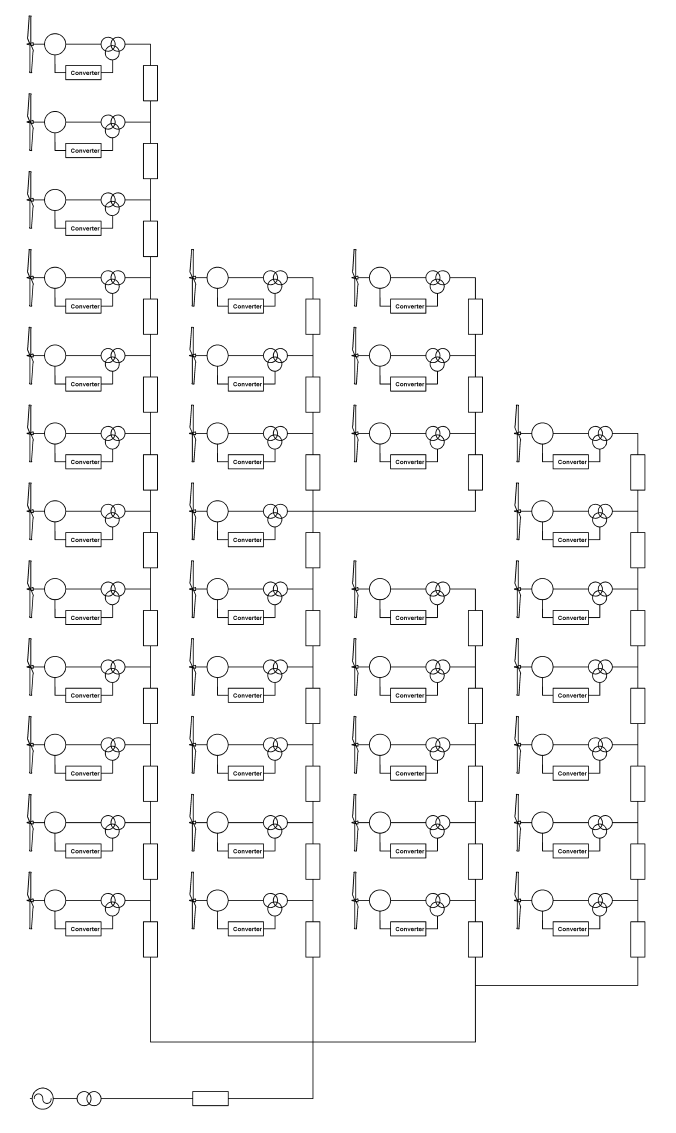


Fig. 10. NSW park layout

The objective of wind modelling in these type of problems is to generate a single point wind speed realisation, which gives instantaneous aerodynamic torque values that are statistically equivalent to the values resulting from the longitudinal turbulence. The effect of wind speed variations on the aerodynamic torque is determined by the $C_p(\lambda,pitch$ angle) curves and the rotor diameter. This implies that a realisation not only depends on the statistical properties of the wind but also on the size and aerodynamic properties of the turbine rotor. The method makes use of the Auto Power Spectral Density (APSD) of the longitudinal wind speed changes in a single point [15].

C. Turbine model

The turbine model used consists of sub-models for:

- aerodynamic behaviour of the rotor;
- rotating mechanical system (drive-train);
- tower (viz. motion of the tower top);
- electrical system (generator, power electronic converter);
- power limitation by pitch control or stall;

The mechanical model for turbine rotor, low and highspeed shaft, gearbox and generator rotor consists of a twomass spring and damper model. The torque of the gearbox and generator on the nacelle is determined, since it interacts with the tower naying.

The simple tower model consists of a mass-spring-damper model for the translation of the tower top in two directions: front-aft (nodding) and sideways (naying). This is not sufficient if tower top rotation has to be modelled as well. In that case, a lumped parameter model for rotation is used, consisting of a number of mass-spring-damper models in series.

The variable speed turbine includes two control loops: the turbine aerodynamic power is limited by pitch control and the electrical power is controlled to maximise energy production (optimal-lambda control). This requires additional component models (sensor and actuator models) and the design of two controllers. How to design controllers for wind turbines, can be found in [15] and will not be presented here.

D. Generator model

Modelling of a doubly-fed induction generator is well-known [7], [11], [16], [17]. The model of the induction machine is based on the fifth-order two-axis representation. A synchronously rotating dq reference frame is used with the direct d-axis oriented along the stator flux position. In this way, decoupled control between the electrical torque and the rotor excitation current is obtained. This reference frame is rotating with the same speed as the stator voltage. When modelling the DFIG, the generator convention will be used, which means that the currents are outputs and that real power and reactive power have a positive sign when they are fed into the grid. Using the generator convention, the following set of equations results:

$$v_{ds} = -R_{s}i_{ds} - \omega_{s}\psi_{qs} + \frac{d\psi_{ds}}{dt}$$

$$v_{qs} = -R_{s}i_{qs} + \omega_{s}\psi_{ds} + \frac{d\psi_{qs}}{dt}$$

$$v_{dr} = -R_{r}i_{dr} - \omega_{r}\psi_{qr} + \frac{d\psi_{dr}}{dt}$$

$$v_{qr} = -R_{r}i_{qr} + \omega_{r}\psi_{dr} + \frac{d\psi_{qr}}{dt}$$

$$(29)$$

with v the voltage [V], R the resistance $[\Omega]$, i the current [A], ω_s and ω_r the stator and rotor electrical angular velocity [rad/s] respectively and ψ the flux linkage [Vs]. The indices d and q indicate the direct and quadrature axis components of the reference frame and s and r indicate stator and rotor quantities respectively. All quantities are functions of time.

A converter is used to connect the rotor circuit of the DFIG to the grid, whereas the stator circuit is connected to the grid directly. The converter must be able to transfer energy in both directions. The grid-side converter has to control the DC-link voltage, regardless of the magnitude and direction of the rotor power and the rotor-side converter has to control the rotor currents. For the converter model it is assumed that the

converters are ideal. It assumed that they exactly make the reference voltage signal that is set by the controller. It has been shown in [11] that such a model gives good simulation results.

E. Simulation results

The response of one string of the wind farm to a gust in the wind speed has been simulated. The gusts in the wind speed are important for the grid behaviour of the park, as the gust in wind speed will lead to a gust in the output power of the park and will thus cause fluctuations in the voltage at the connection point. The reactive power settings of the turbines are kept constant during the simulation.

The gust is assumed to cross with a certain speed through the string. The turbines are affected one after another by the gust. It is assumed that the gust will affect first the turbine with the largest distance to shore, and it will come closer and closer to the shore, affecting each turbine. It is assumed that the time between affecting two turbines will be 5 seconds. The rotor effective wind speed at the first turbine that experiences the gust is shown in Fig. 11. The wind speed before the gust is about 5 m/s. The wind speed increases to 20 m/s during the gust.

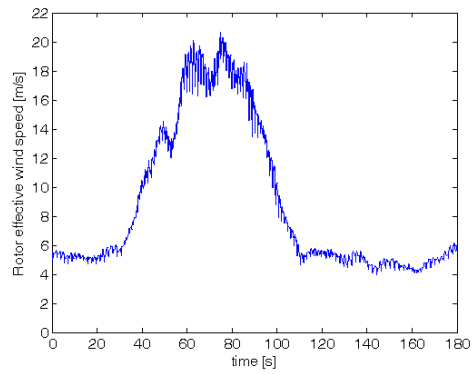


Fig. 11. Gust in wind speed

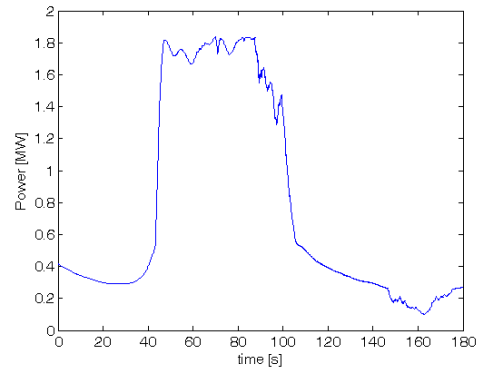


Fig. 12. Output power of first wind turbine

The increasing wind speed will cause an increasing output power of the turbine. The output power of the first turbine is shown in Fig. 12. The output power of the sixth and twelfth turbine are shown in Fig. 13 and Fig. 14 respectively.

The output power of the whole first string of the wind farm is shown in Fig. 15. The large changes in output power of the wind farm will also affect the voltage of the 150kV grid at the point of connection. The voltage at the park side of the 150kV

transformer is shown in Fig. 16. Be aware that the change in output voltage of the wind farm shown in Fig. 16, is only due to one string. The resulting change in output voltage due to the whole park will be somewhat higher, but it is to be expected that it will meet the grid requirements. The doubly-fed induction generators used in this simulation offer the possibility to control the reactive power output. It should be investigated whether or not it is possible to decrease the voltage fluctuations by controlling the reactive power output of the turbines.

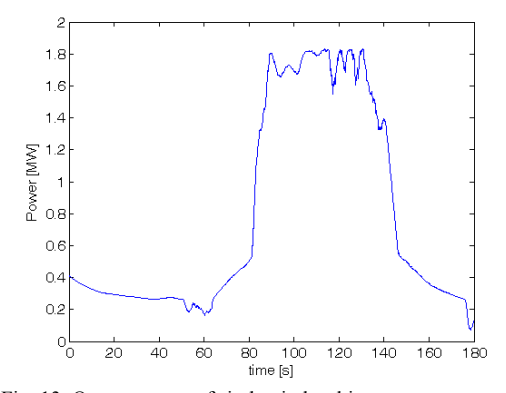


Fig. 13. Output power of sixth wind turbine

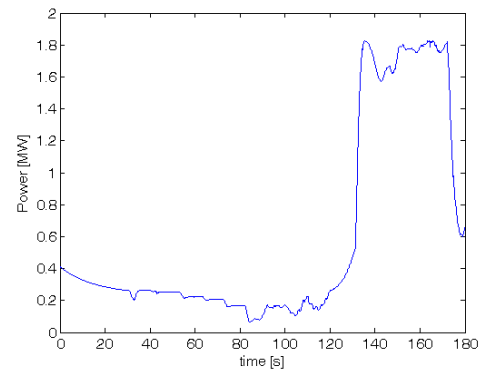


Fig. 14. Output power of twelfth wind turbine

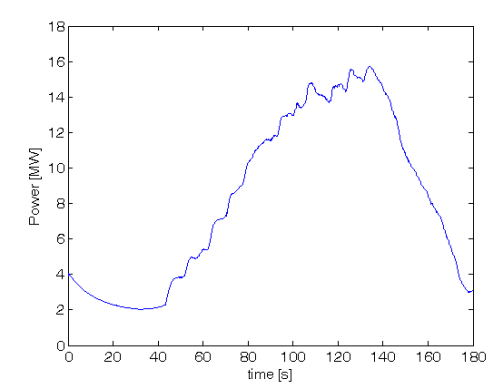


Fig. 15. Output power of one string of the wind farm

After completion of the wind farm models based on four different electrical systems (direct coupled induction machine, doubly fed induction machine, permanent magnet generator and cluster-controlled induction machine), the next step is to investigate the impact of wind turbines or wind farms on the grid and to improve the interaction between wind farms (turbines) and the grid by control of the electrical system.

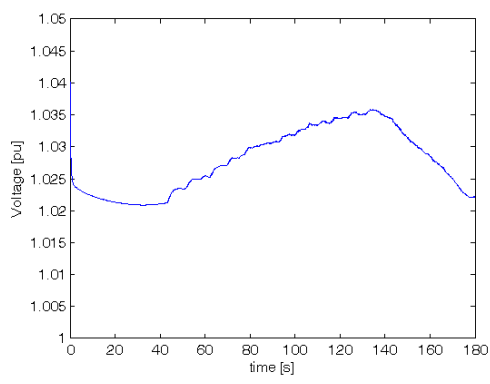


Fig. 16. Output voltage of wind farm

VI. SUMMARY

In this contribution it has been shown, that the Park transformation can be used to translate models of all electrical components of a wind farm from the abc reference frame to models in the $dq\theta$ reference frame. A description and some examples have been given of the methods to derive the $dq\theta$ models. A case study simulation showed the use of the models to evaluate the impact of wind farms on the electricity grid.

VII. APPENDIX

Voltages and currents of electrical systems are often given as a set of differential equations. A short description will be given of how these complete sets of equations can be transformed to the dq0 reference system. The derivative of a vector in the abc reference system is given by:

$$\frac{d}{dt} \left[\mathbf{x}_{abc} \right] = \frac{d}{dt} \left[\left[\mathbf{T}_{dq0} \left(\boldsymbol{\theta}_{d} \right) \right]^{-1} \cdot \left[\mathbf{x}_{dq0} \right] \right]$$
(30)

With the chain-rule for derivatives:

$$\frac{d}{dt} \left[\mathbf{x}_{dq0} \right] = \left[\mathbf{T}_{dq0} \left(\theta_d \right) \right] \cdot \frac{d}{dt} \left[\mathbf{x}_{abc} \right] + \left(\frac{d}{dt} \left[\mathbf{T}_{dq0} \left(\theta_d \right) \right] \right) \cdot \left[\mathbf{x}_{abc} \right]$$
(31)

$$[\mathbf{T}_{dq0}(\theta_d)] \cdot \frac{d}{dt} [\mathbf{x}_{abc}] = \frac{d}{dt} [\mathbf{x}_{dq0}] - \left(\frac{d}{dt} [\mathbf{T}_{dq0}(\theta_d)] \right) \cdot [\mathbf{T}_{dq0}(\theta_d)]^{-1} \cdot [\mathbf{x}_{dq0}]$$
(32)

$$[\mathbf{T}_{dq0}(\theta_d)] \cdot \frac{d}{dt} [\mathbf{x}_{abc}] = \frac{d}{dt} [\mathbf{x}_{dq0}] - \omega_d \cdot \frac{1}{\omega_d}$$

$$\left(\frac{d}{dt} [\mathbf{T}_{dq0}(\theta_d)] \right) \cdot [\mathbf{T}_{dq0}(\theta_d)]^{-1} \cdot [\mathbf{x}_{dq0}]$$
(33)

With (17) and knowing that $\omega_d = d\theta_d/dt$ the following result is obtained:

$$\left(\frac{d}{dt}\left[\mathbf{T}_{dq0}(\theta_d)\right]\right) \cdot \left[\mathbf{T}_{dq0}(\theta_d)\right]^{-1} = \omega_d \cdot \begin{bmatrix} 0 & -1 & 0 \\ 1 & 0 & 0 \\ 0 & 0 & 0 \end{bmatrix}$$
(34)

And it can easily be seen that:

$$\left[\mathbf{T}_{dq0}(\theta_d)\right] \cdot \frac{d}{dt} \left[\mathbf{x}_{abc}\right] = \frac{d}{dt} \left[\mathbf{x}_{dq0}\right] + \omega_d \cdot y \cdot \left[\mathbf{x}_{dq0}\right]$$
(35)

with y given by:

$$y = \frac{1}{\omega_d} \cdot \left(\frac{d}{dt} \left[\mathbf{T}_{dq0} (\theta_d) \right] \right) \cdot \left[\mathbf{T}_{dq0} (\theta_d) \right]^{-1} = \begin{bmatrix} 0 & -1 & 0 \\ 1 & 0 & 0 \\ 0 & 0 & 0 \end{bmatrix}$$
(36)

It can be seen from (36) that differential equations will cause a cross-relation between the d and the q axis.

VIII. REFERENCES

- [1] J.G. Slootweg, H. Polinder, W.L. Kling, "Dynamic Modelling of a Wind Turbine with Doubly Fed Induction Generator", in *Proc. 2001 IEEE Power Engineering Society Summer meeting*, pp. 644-649.
- [2] J.G. Slootweg, W.L. Kling, "Modeling of large wind farms in power system simulations", in *Proc. 2002 IEEE Power Engineering Society Summer meeting*, pp. 503-508.
- [3] P. Sorensen, A. Hansen, L. Janosi, J. Bech, B. Bak-Jensen, Simulation of Interaction between Wind Farm and Power System, Report Risoe-R-1281 (EN), Risoe National Laboratory, Roskilde, Denmark, December 2001.
- [4] V. Akhimatov, H. Knudsen, A. H. Nielsen, J.K. Pedersen, N.K. Poulsen, "Modelling and transient stability of large wind farms", *International Journal of Electrical Power & Energy Systems*, Vol. 25, No. 2, Feb. 2003, pp. 123-144.
- [5] J.G. Slootweg, S.W.H. de Haan, H. Polinder, and W.L. Kling, "General model for representing variable speed wind turbines in power system dynamics simulations", *IEEE Trans. Power Systems*, Vol. 18, No. 1, pp. 144-151, Feb. 2003.
- [6] V. Akhimatov, "Modelling of variable-speed wind turbines with doubly-fed induction generators in short-term stability investigations", in: Proc. 3rd Int. Workshop on Transmission Networks for Offshore Wind Farms, April 11-12, 2002, Stockholm, Sweden.
- [7] C.-H. Ong, Dynamic Simulation of Electric Machinery using Matlab/Simulink, Upper Saddle River: Prentice Hall, 1998.
- [8] G.C. Paap, "Symmetrical Components in the Time Domain and Their Application to Power Network Calculations", IEEE Trans. Power Systems, Vol. 15, No. 2, pp. 522-528, May 2000.
- [9] B Bachmann, H. Wiesmann, "Advanced Modeling of Electromagnetic Transients in Power Systems", in Proc. Modelica Workshop, 23-24 Oct. 2000, Lund, Sweden pp. 93-97.
- [10] H. Akagi, Y. Kanazawa, A. Nabae, "Instantaneous Reactive Power Compensators Comprising Switching Devices Without Energy Storage Components", IEEE Trans. Ind. Appl., Vol 20, pp. 625, 1984.
- [11] J. Morren, S.W.H. de Haan, P. Bauer, J.T.G. Pierik, J. Bozelie, "Comparison of complete and reduced models of a wind turbine with Doubly-Fed Induction Generator" in *Proc.* 10th European conference on Power Electronics and applications (EPE), Toulouse, France, 2 4 September 2003.
- [12] A. Dittrich and A Stoev, "Grid Voltage Fault Proof Doubly-Fed Induction Generator System", in Proc. 10th European conference on Power Electronics and applications (EPE), Toulouse, France, 2 – 4 September 2003.
- [13] I. Serban, F. Blaabjerg, I. Boldea, Z. Chen, "A Study of the Doubly-Fed Wind Power Generator Under Power System Faults", in *Proc.* 10th European conference on Power Electronics and applications (EPE), Toulouse, France, 2 4 September 2003.
- 14] L.L. Freris, Wind Energy conversion systems, Upper Saddle River: Prentice Hall, 1990.
- [15] T.G. van Engelen, E.L. van der Hooft and P. Schaak: Ontwerpgereedschappen voor de Regeling van Windturbines, ECN Report (in preparation)
- [16] R. Pena, J.C. Clare, G.M. Asher, "Doubly fed induction generator using back-to-back PWM converters and its application to variable-speed wind-energy generation", *IEE Proc.-Electr. Power Appl.*, Vol. 143, No. 3, pp. 231-241, May 1996.
- [17] A. Petersson, Analysis, Modelling and Control of Doubly-Fed Induction Generators for Wind Turbines, Licentiate thesis, Technical report no. 464L, Chalmers University, Göteborg, Sweden, 2003.

Comparison of complete and reduced models of a wind turbine using Doubly-Fed Induction Generator

J. Morren¹⁾, S.W.H. de Haan¹⁾, P. Bauer¹⁾, J.T.G. Pierik²⁾

1) Electrical Power Processing, Delft University of Technology Mekelweg 4, 2628 CD Delft, The Netherlands

2) ECN, Petten, The Netherlands

J.Morren@its.tudelft.nl

http://ee.its.tudelft.nl/epp/

Keywords

Adjustable speed generation systems, Modelling, Renewable energy systems

Abstract

Wind turbines equipped with a Doubly-Fed Induction Generator are increasingly popular in the power range above 1 MW. For power system stability studies it is desirable to apply reduced models of the machine and the converter in order to limit the computation time. Several reduced models have been developed and compared with each other. With respect to the generator, models with and without transient terms in the fluxes have been compared. With respect to the converter, models with and without PWM operation have been used. The whole system has been modelled both in abc coordinates and in a rotating d-q reference frame. Especially a model with transient flux terms and without PWM operation, which has been modelled in the d-q reference frame has shown to be accurate and fast.

Introduction

One of the most important contemporary wind turbines is a wind turbine equipped with a Doubly-Fed Induction Generator (DFIG), shown in Fig. 1, with a voltage source converter feeding the rotor circuit. Compared to variable speed wind turbines with the converter connected to the stator, one of the major advantages of the doubly-fed induction generator is the fact that the converter in the DFIG scheme only needs to handle the rotor power. This rotor power is around 25% of the total generator power, depending on the speed range that is allowed [1].

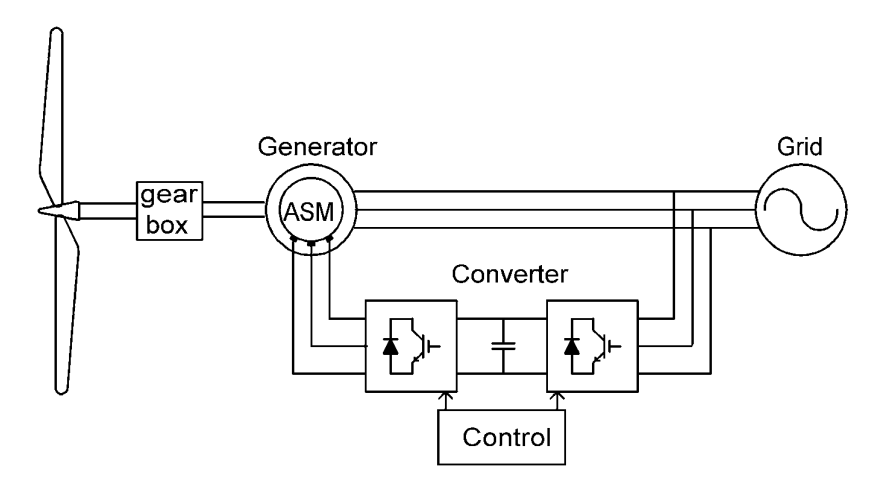


Fig. 1. Doubly-fed induction generator with voltage source converter

A tendency to increase the amount of electricity generated from wind can be observed [2]. As the penetration of wind turbines in electrical power systems will increase, they may begin to influence overall power system operation [3]. The behaviour of wind turbines with respect to their interaction with the grid is therefore studied at different places [3], [4], [5]. To facilitate the investigation of the impact of a wind farm on the dynamics of the power system to which it is connected, an adequate model of the wind turbines is required. Although personal computers become faster and faster, computational speed is still one of the limiting factors in (dynamic) simulation of power systems. One of the problems is the complexity of the models that limits the computational speed. When reduced models are used simulation can be done much faster, but the results may be less accurate [1].

In this contribution a number of different models (from detailed complete models to simple reduced models) for the doubly-fed induction generator with back-to-back converter have been developed and compared to each other. With respect to the generator, models with and without transient terms in the fluxes have been compared. With respect to the converter, models with and without PWM operation have been modelled. The whole system has been modelled both in abc coordinates and in a rotating d-q reference frame. It will be shown that accurate models can be developed, which can be simulated very fast.

Modelling and control

Modelling the generator

A d-q reference frame is chosen to model the doubly-fed induction generator. This so-called Park Transformation is used to transform the stator quantities of a synchronous machine onto a d-q reference frame that is fixed to the rotor [6]. Its use is not limited to synchronous machines however. Other quantities can be chosen as a reference as well. The d-q reference frame is obtained from the rectangular α - β reference frame by the inverse Park-transformation:

$$\begin{bmatrix} x_{d} \\ x_{q} \end{bmatrix} = C_{\text{rot}}^{-1} (\theta) \begin{bmatrix} x_{\alpha} \\ x_{\beta} \end{bmatrix} \text{ with } C_{\text{rot}} (\theta) = \begin{bmatrix} \cos \theta & -\sin \theta \\ \sin \theta & \cos \theta \end{bmatrix} \text{ and } C_{\text{rot}}^{-1} (\theta) = C_{\text{rot}} (-\theta)$$
 (1)

The α - β reference frame is obtained from the 3-phase abc system with the Clarke transformation:

$$\begin{bmatrix} x_{\alpha} \\ x_{\beta} \\ x_{0} \end{bmatrix} = C_{\alpha\beta0,abc} \begin{bmatrix} x_{a} \\ x_{b} \\ x_{c} \end{bmatrix} \text{ with } C_{\alpha\beta0,abc} = \sqrt{\frac{2}{3}} \begin{bmatrix} 1 & -\frac{1}{2} & -\frac{1}{2} \\ 0 & \frac{\sqrt{3}}{2} & -\frac{\sqrt{3}}{2} \\ \frac{1}{\sqrt{2}} & \frac{1}{\sqrt{2}} & \frac{1}{\sqrt{2}} \end{bmatrix}$$
 (2)

The model that is obtained is well known and can be found in literature [2], [6]. The generator convention will be used, which means that the currents are outputs instead of inputs and real power and reactive power have a positive sign when they are fed into the grid. Using the generator convention, the following set of equations results:

$$v_{ds} = -R_s i_{ds} - \omega_s \psi_{qs} + \frac{d\psi_{ds}}{dt}$$

$$v_{qs} = -R_s i_{qs} + \omega_s \psi_{ds} + \frac{d\psi_{qs}}{dt}$$

$$v_{dr} = -R_r i_{dr} - \omega_r \psi_{qr} + \frac{d\psi_{dr}}{dt}$$

$$v_{qr} = -R_r i_{qr} + \omega_r \psi_{dr} + \frac{d\psi_{qr}}{dt}$$

$$(3)$$

with v the voltage [V], R the resistance $[\Omega]$, i the current [A], ω_s and ω_r the stator and rotor electrical angular velocity [rad/s] respectively and ψ the flux linkage [Vs]. The indices d and q indicate the

direct and quadrature axis components of the reference frame and s and r indicate stator and rotor quantities respectively. All quantities in (3) are functions of time. The flux linkages in (3) can be calculated using the following set of equations:

$$\psi_{ds} = -(L_{s} + L_{m})i_{ds} - L_{m}i_{dr}
\psi_{qs} = -(L_{s} + L_{m})i_{qs} - L_{m}i_{qr}
\psi_{dr} = -(L_{r} + L_{m})i_{dr} - L_{m}i_{ds}
\psi_{as} = -(L_{r} + L_{m})i_{as} - L_{m}i_{as}$$
(4)

with L_m the mutual inductance [H] and L_s and L_r the stator and rotor leakage inductance [H] respectively.

Sometimes the transients in the fluxes, represented by the last terms in equation (3), are neglected. The most important reasons to do this have to do with the computation speed during simulations. Another reason is that taking into account the rotor transients would require detailed modelling of the converter [2]. When the transients are neglected, the following set of equations can be derived:

$$v_{ds} = -R_{s}i_{ds} + \omega_{s}((L_{s} + L_{m})i_{qs} + L_{m}i_{qr})$$

$$v_{qs} = -R_{s}i_{qs} - \omega_{s}((L_{s} + L_{m})i_{ds} + L_{m}i_{dr})$$

$$v_{dr} = -R_{r}i_{dr} + \omega_{r}((L_{r} + L_{m})i_{qr} + L_{m}i_{qs})$$

$$v_{qr} = -R_{r}i_{qr} - \omega_{r}((L_{r} + L_{m})i_{dr} + L_{m}i_{ds})$$
(5)

The electrical angular velocity of the rotor, ω_r , can be determined as:

$$\omega_r = \omega_s - p\omega_m \tag{6}$$

with p the number of pole pairs [-] and ω_m the mechanical angular velocity [rad/s], which is given by:

$$\frac{d\omega_m}{dt} = \frac{1}{J} (T_m - T_e) \tag{7}$$

with J the inertia of the rotor [kg·m²] and T_m and T_e the mechanical and electrical torque [Nm] respectively. The mechanical torque is generated by the wind turbine and depends on the wind speed. The electrical torque is given by:

$$T_e = p\left(\psi_{dr}i_{qs} - \psi_{qr}i_{ds}\right) \tag{8}$$

The power invariant d-q transformation has been used. If the amplitude-invariant transformation is used, (8) should be multiplied by a factor 3/2.

A synchronously rotating d-q reference frame is used with the direct d-axis oriented along the stator flux vector position. In this way a decoupled control between the electrical torque and the rotor excitation current is obtained. This reference frame is rotating with the same speed as the stator voltage and assuming that the stator resistance is negligible, i.e, $R_s \ll \omega_s(L_s + L_m)$, the angle of the stator flux vector can be calculated as:

$$\theta_s = \int \omega_s dt \tag{9}$$

The reference frame of the rotor is rotating with the electrical frequency of the rotor ω_r . The angle of the rotor can be obtained as:

$$\theta_r = \int \omega_r dt = \int \omega_s - p\omega_m dt \tag{10}$$

The angles θ_s and θ_r can be used for the Park-transformation of the stator and the rotor quantities respectively.

With the scaling factors used in (1) and (2) the active power delivered by the stator is given by:

$$P_s = v_{ds}i_{ds} + v_{as}i_{as} \tag{11}$$

and the reactive power by

$$Q_s = v_{as}i_{ds} - v_{ds}i_{as} \tag{12}$$

When the amplitude invariant transformation was used, (11) and (12) should be multiplied by a factor 3/2. Due to the chosen reference frame, ψ_{qs} and v_{ds} are zero. Therefore the reactive power and the active power delivered by the stator can be written as:

$$P_s = v_{qs}i_{qs} = v_{qs} \left(\frac{L_m}{L_r + L_m}\right)i_{qr} \tag{13}$$

and

$$Q_{s} = v_{as}i_{ds} = \omega_{s} \left(-(L_{s} + L_{m})i_{ds} - L_{m}i_{dr} \right) i_{ds}$$
(14)

As the stator current is equal to the supply current, it can be assumed that it is constant. The reactive power is then proportional to the direct component of the rotor current i_{dr} .

Control of the generator

The electrical and mechanical dynamics of a wind turbine are in different time scales. The electrical dynamics are much faster than the mechanical. Therefore, it is possible to control the machine in a cascade structure, as shown in Fig. 2. The fast electrical dynamics can be controlled in an inner loop and a speed controller can be added in a much slower outer loop.

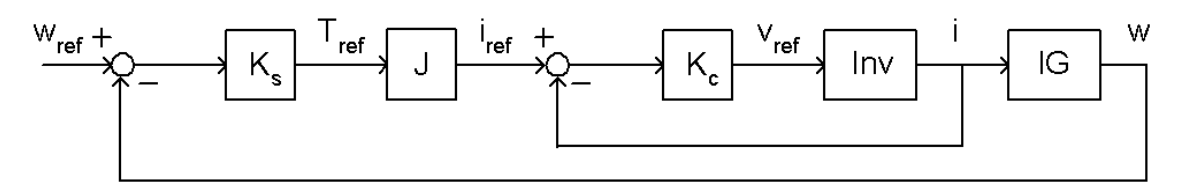


Fig. 2. Cascade control; IG=Induction Generator, Inv=Inverter, K_c=current controller, J=inertia of turbine, K_s=speed controller

The internal model control (IMC) principle [7] has been used to design the controllers. The idea behind internal model control is to reduce the error between the system G(s), and the model of the system $\hat{G}(s)$ by a transfer function K(s). In Fig. 3 the principle is shown for the current controller. One common way of choosing the transfer function K(s) is [8]:

$$K(s) = \left(\frac{\alpha}{s+\alpha}\right)^n G^{-1}(s) \tag{15}$$

where n should be at least one larger than the number of zero's of $\hat{G}(s)$, so that K(s) becomes proper. The parameter α is a design parameter that is equal to the closed loop bandwidth of the system. The system G(s) should be minimum phase, i.e. it shouldn't contain right half-plane zeros, as these will become unstable under feedback. The controller C(s), inside the dashed line in Fig. 3, becomes [8]:

$$C(s) = \left(1 - K(s)\hat{G}(s)\right)^{-1}K(s) \tag{16}$$

For a first order system, n=1 is sufficient and the controller becomes then a PI controller. With (16) and $\hat{G}(s) = G(s)$ the controller becomes [8]:

$$C(s) = k_p + \frac{k_i}{s} = \frac{\alpha}{s} G^{-1}(s)$$
 (17)

Where k_p is the proportional gain and k_i is the integral gain. The closed loop system with ideal parameters become:

$$G_{cl}(s) = G(s)K(s) = \frac{\alpha}{s + \alpha}$$
(18)

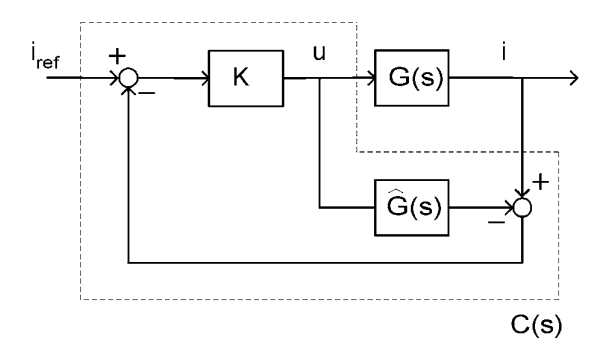


Fig. 3. Internal Model Control (IMC)

The voltage equations of the rotor are given in (3) as:

$$v_{dr} = -R_r i_{dr} - \omega_r \psi_{qr} + \frac{d\psi_{dr}}{dt}$$

$$v_{qr} = -R_r i_{qr} + \omega_r \psi_{dr} + \frac{d\psi_{qr}}{dt}$$
(19)

Since the stator flux is almost fixed to the stator voltage, it is practically constant. This implies that the derivative of the stator flux and of the stator magnetising current are close to zero, and can be neglected [9], [10]. Equation (19) can then be written as:

$$v_{dr} = -R_r i_{dr} - L_r \frac{di_{dr}}{dt} - \omega_r \psi_{qr}$$

$$v_{qr} = -R_r i_{qr} - L_r \frac{di_{qr}}{dt} + \omega_r \psi_{dr}$$
(20)

The last term in both equations causes a cross-relation between the two current components. Reference voltages to obtain the desired currents can be written as [9]:

$$v_{dr}^{*} = v_{dr}^{'} - \omega_{r} \psi_{qr} v_{qr}^{*} = v_{qr}^{'} + \omega_{r} \psi_{dr}$$
(21)

with

$$v'_{dr} = -R_r i_{dr} - L_r \frac{di_{dr}}{dt}$$

$$v'_{qr} = -R_r i_{qr} - L_r \frac{di_{qr}}{dt}$$
(22)

The i_{dr} and i_{qr} errors are processed by a PI controller to give v_{dr} and v_{qr} respectively. To ensure good tracking of these currents, the cross-related flux terms are added to v_{dr} and v_{qr} to obtain the reference voltages. Treating $\omega_r \Psi_{dr}$ and $\omega_r \Psi_{qr}$ as a disturbance, the transfer function from the rotor voltage v_{dr} to the rotor current i_{dr} and from the rotor voltage v_{qr} to the rotor current i_{qr} is given by:

$$G(s) = \frac{1}{L_{\nu}s + R_{\nu}} \tag{23}$$

Using the IMC, the current controllers become:

$$C(s) = k_p + \frac{k_i}{s} = \frac{\alpha_c}{s} G^{-1}(s)$$
(24)

Where α_c is the bandwidth of the current control loop, k_p is the proportional gain and k_i is the integral gain. The two gains become [10]:

$$k_p = \alpha_c L_r, \quad k_i = \alpha_c R_r \tag{25}$$

The rotational speed is given by (7) as:

$$\frac{d\omega_m}{dt} = \frac{1}{I} (T_m - T_e) \tag{26}$$

It is assumed that the current controller is much faster than the speed controller. The electrical torque is than $T_e = T_{e,ref}$. The reference torque is set to:

$$T_{e,ref} = T_{e,ref'} - B_a \omega_m \tag{27}$$

where B_a is an "active damping torque" [10]. The transfer function from rotational speed to electrical torque becomes now:

$$G_s(s) = \frac{1}{J_{S} + B_a} \tag{28}$$

Using again the internal model control method, the following gains of the controller are obtained:

$$k_{ps} = \alpha_s J, \quad k_{is} = \alpha_s B_a$$
 (29)

Where α_s is the desired closed-loop bandwidth of the speed controller. When B_a is chosen to be $B_a = J\alpha_s$ changes in the mechanical torque are damped with the same time constant as the bandwidth of the speed control loop [10].

Modelling the converter

A three-phase AC-AC converter is normally used to connect the rotor circuit of the DFIG to the grid, whereas the stator circuit is connected to the grid directly. The converter that will be used must be able to transfer energy in both directions, i.e. it must be able to work as a rectifier and as an inverter. When the generator operates in sub-synchronous mode the converter will transfer energy to the rotor, while it is extracting energy from the rotor when the generator operates in super-synchronous mode [1]. The converter connected to the grid has to control the DC-link voltage, regardless of the magnitude and direction of the rotor power. As modelling and control of voltage source converters is well known, no description will be given here. A detailed description, related to the converter of a DFIG can be found in [9].

Compared models

Four different models of a doubly-fed induction generator and converter have been developed and compared to each other. A short description of the different models will be given here. The generator system consist of two components namely the generator itself and the converter in the rotor circuit. Two different machine models have been used. The first is a 5th order model, including all transient flux terms, based on the equations (3) and (4). From now on this model is referred to as the complete model. The second model is a reduced model, based on (5) in which the transient flux terms in the stator and rotor circuit are not taken into consideration. This last machine model is often used in power system stability studies [2]. From now on this model is referred to as reduced model.

A number of models have been developed for the converter. In the first model the PWM operation of the converter is modelled, which means that the output voltages have a pulsating character. The instantaneous DC-link currents are derived from the power balance in the converter, so they still reflect the switching nature of the converter and are pulsating too. In the second model the converter is modelled as a controllable three-phase sinusoidal voltage source, where amplitude, frequency and

phase of the output voltages can be controlled independently and on both sides (rotor side and grid side). In this model both converter parts can be considered as power amplifiers that convert the input control voltages (normally used to obtain the PWM signals) directly to output ac waveforms that are set to the grid and the rotor. The DC-link currents are again derived from the power balance in the converter. In this model the DC-link currents are constant in steady state.

The generator has internally been modelled in a d-q reference frame, based on (3) and (4). Transformations from d-q to abc coordinates have been used to connect them with the converter and the grid, which are both modelled in abc coordinates. When all signals in the time domain are sinusoidal, the signals in the d-q frame are constant. Therefore, complete modelling in d-q domain is expected to increase the simulation speed significantly, because the variable step-size simulation program can apply a large time step during quasi steady state phenomena. To verify this, a model has been developed that is based completely on d-q signals. Also the converter and the grid are modelled in the d-q reference frame. The d-q model of the machine is given in (3) and (4). An example of a converter model in the d-q reference frame can be found in [11].

Results

A number of different models have been obtained in Simulink[®]. Simulink[®] is a toolbox extension of Matlab that is widely used in dynamic simulation. Some results of four different models will be shown. The first model (A) is the benchmark, consisting of a complete machine model (based on (3) and (4)) and a converter model including PWM. Model B uses the complete machine model of (3) and (4) and the sinusoidal converter model. Model C uses the reduced machine model based on (5) and the same converter model as B. Model D is completely modelled in the d-q reference frame. The generator is again based on (3) and (4) and the converter model is based on sinusoidal operation. The four different models are schematically shown in Fig. 4. The sub-plots a, b, c and d, correspond with the models A, B, C and D respectively.

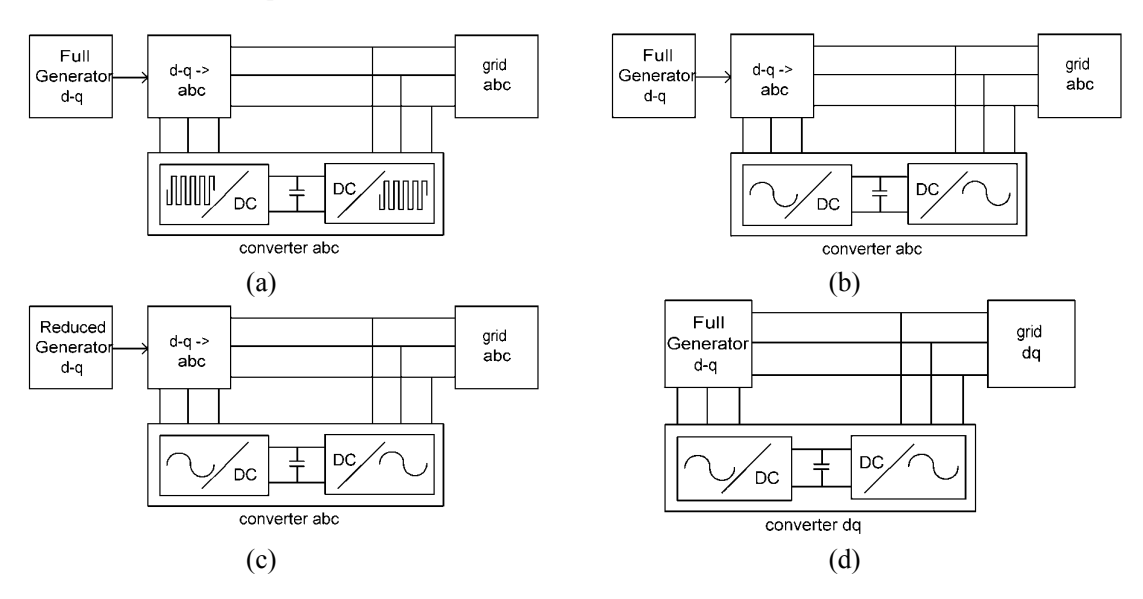


Fig. 4. Four models used for the simulations

The four models have been compared for a number of events. The level of detailing that is needed in a model, to obtain reliable simulation results, might depend on the event that is investigated. Especially the time scale of the events might be important. The models have therefore been compared for two important events with different time scales. The first is a change in the wind speed, which causes a change in the mechanical torque. Fig. 5 shows, for the different models, the rotor current i_{qr} and the rotational speed ω_m of the machine for a step in the mechanical torque. The second event is a dip in the

grid voltage. Voltage dips cause large problems for this type of generators, and the generator might be easily destructed [1], [10]. The dip in the grid voltage will result in a fast increasing large current in the stator windings of the DFIG. Because of the magnetic coupling between stator and rotor a large current will also flow in the rotor circuit and will lead to destruction of the converter. To analyse this behaviour it's important to have a model of the Doubly-Fed Induction Generator that desibes the fast dynamic events that occur during the grid dip accurately. Fig. 6 shows the rotor current i_{qr} and the rotational speed ω_m of the machine for a dip of 30% in the grid voltage.

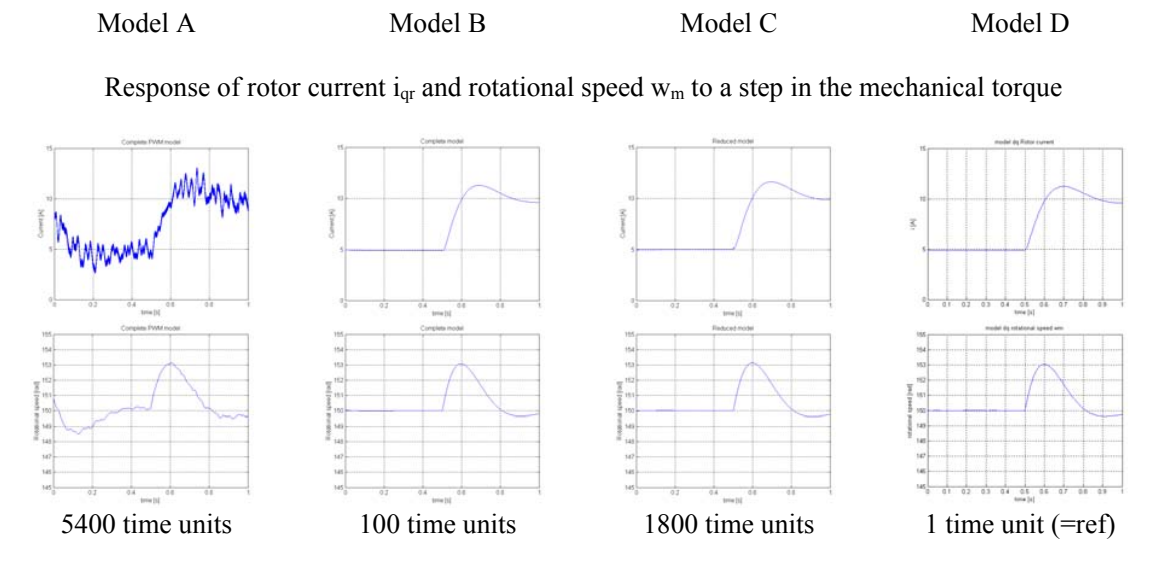


Fig. 5. Response to a step in the mechanical torque for model A, B, C and D. Upper row: response of rotor current i_{qr} to the step. Second row: response of rotational speed w_m to the step. On the lower row the relative computation time is indicated with respect to the fastest model

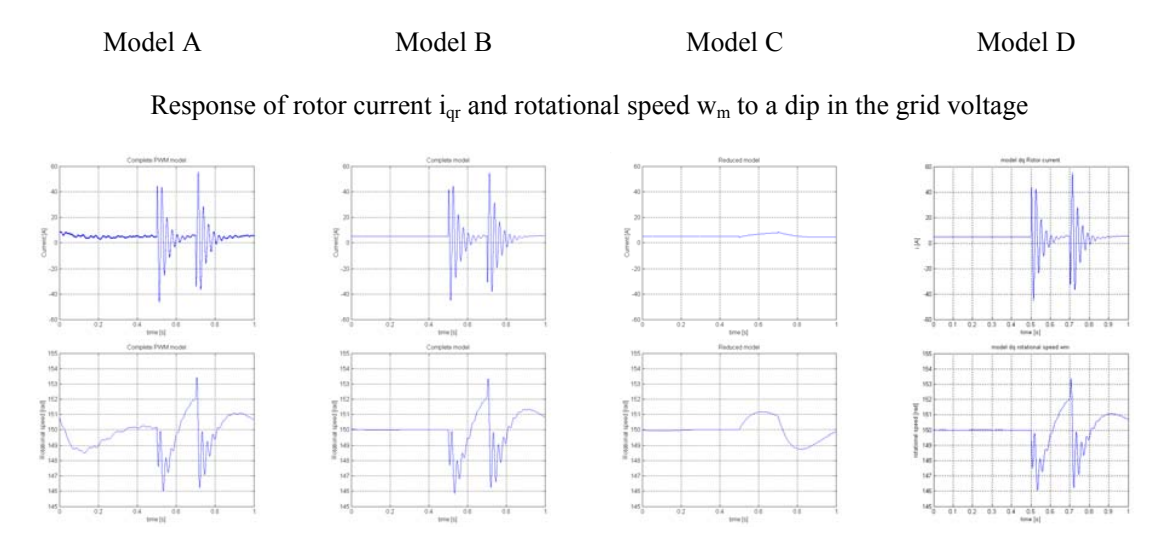


Fig. 6. Response of rotor current i_{qr} and rotational speed w_m to a 30% dip in the grid voltage

In Fig. 5 also the time is shown that it takes to simulate the different models. The simulation of the different models is related to that of the fastest model (D), which is set to 1 (about 50 times faster than real time on a 2 GHz personal computer). As can be seen, the simulation results of model B show a good similarity with the benchmark model A. During the first 0.4 seconds the signals of model A are slightly different from the other models. This is due to the fact that not all signals of model A had reached steady state yet, when the plot was started. Further there is a high-frequency ripple in model A

due to the PWM operation of the converter. In most simulation cases, this ripple is of no importance and model B can be used. The reduced machine model (model C) gives bad results when fast transients play a role (voltage dip) and also has a simulation time that is much longer than that of the models B and D. This long simulation time is due to method in which machine models are constructed in Simulink®. The derivative terms of the complete model appear in Simulink® as integrators. These integrators interrupt a loop in the model. For the reduced order model, the loop doesn't contain these integrators. The model then contains algebraic loops and therefore the model becomes difficult to simulate. Model D, which is made completely in the d-q reference frame, behaves almost exactly equal to model B. Again the only difference with model A is the high-frequency ripple. As model D can be simulated about 100 times faster than model B and about 5000 times faster than model A, it will be a very powerful tool for simulation of the impact of a wind farm on the dynamics of the power system to which it is connected.

Conclusion

For power system stability studies of power systems including wind turbines it is desirable to apply reduced models of the turbines in order to limit the computation time. One of the most important contemporary wind turbines is a wind turbine equipped with a doubly-fed induction generator (DFIG) with a voltage source converter feeding the rotor circuit. Four different Simulink® models of a DFIG (with different complexity) have been developed and simulated. The four models consist of a model including a converter with full PWM operation and a generator model that models all transient phenomena (model A), a model with a sinusoidal converter model and the same generator model as the previous model (model B), a model with the same converter model as the previous model, but with transient phenomena in the generator neglected (model C) and a model with sinusoidal converter model and including all transient phenomena in the generator which has been modelled completely in a rotating d-q reference frame (model D).

The models have been compared for 2 events, i.e. a step in the reference torque and a dip in the grid voltage. As soon as fast transients play a role, the behaviour of the reduced (transient phenomena neglected) machine model (model C) is completely different from the behaviour of the complete (including all transient phenomena) machine model. The model including PWM operation shows much more higher frequency components, as could be expected. The model including the complete machine parameters and a converter with only sinusoidal operation (model B) shows accurate simulation results and can be simulated much faster than the model including full PWM operation (model A). The model that is made completely in d-q coordinates (model D) shows far the best results. Its behaviour is equal to that of the complete model with sinusoidal operation, but it can be simulated 100 times faster. The only difference with the model including PWM operation, is a high-frequency ripple, which isn't important in most cases. Therefore, this model might be a valuable tool for power system studies including wind farms.

References

- [1] V. Akhimatov, "Modelling of variable-speed wind turbines with doubly-fed induction generators in short-term stability investigations", in: *Proc.* 3rd Int. Workshop on Transmission Networks for Offshore Wind Farms, April 11-12, 2002, Stockholm, Sweden.
- J.G. Slootweg, H. Polinder, W.L. Kling, "Dynamic Modelling of a Wind Turbine with Doubly Fed Induction Generator", in *Proc. 2001 IEEE Power Engineering Society Summer meeting*, pp. 644-649.
- [3] J.G. Slootweg, W.L. Kling, "Modeling of large wind farms in power system simulations", in *Proc. 2002 IEEE Power Engineering Society Summer meeting*, pp. 503-508.

- [4] V. Akhimatov, H. Knudsen, A. H. Nielsen, J.K. Pedersen, N.K. Poulsen, "Modelling and transient stability of large wind farms", *International Journal of Electrical Power & Energy Systems*, Vol. 25, No. 2, Feb. 2003, pp. 123-144.
- [5] P. Sorensen, A. Hansen, L. Janosi, J. Bech, B. Bak-Jensen, *Simulation of Interaction between Wind Farm and Power System*, Report Risoe-R-1281 (EN), Risoe National Laboratory, Roskilde, Denmark, December 2001.
- [6] C.-H. Ong, *Dynamic Simulation of Electric Machinery using Matlab/Simulink*, Upper Saddle River: Prentice Hall, 1998.
- [7] S. Skogestad, I. Postlethwaite, *Multivariable feedback control*, Chicester: Wiley, 1996.
- [8] L. Harnefors, H.-P. Nee, "Model-Based current control of AC Machines using the Internal Model Control Method", *IEEE Trans. Industry Applications*, Vol. 34, No. 1, pp. 133-141, Jan./Feb. 1998.
- [9] R. Pena, J.C. Clare, G.M. Asher, "Doubly fed induction generator using back-to-back PWM converters and its application to variable-speed wind-energy generation", *IEE Proc.-Electr. Power Appl.*, Vol. 143, No. 3, pp. 231-241, May 1996.
- [10] A. Petersson, *Analysis, Modelling and Control of Doubly-Fed Induction Generators for Wind Turbines*, Licentiate thesis, Technical report no. 464L, Chalmers University, Göteborg, Sweden, 2003.
- [11] S.-B. Han, N.-S. Choi, C.-T. Rim, G.-H. Cho, "Modeling and Analysis of Static and Dynamic Characteristics of a Buck-Type Three-phase PWM Rectifier by Circuit DQ Transformation", *IEEE Trans. on Power Electronics*, Vol. 13, No. 2, March 1998, pp. 323-336.